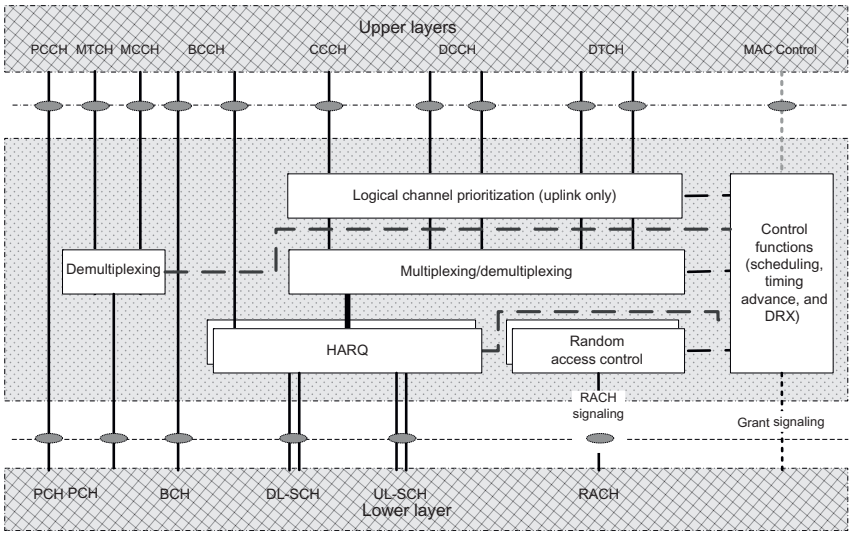


FIGURE 8.3

LTE UE MAC sublayer functions and services [1].

prioritization entity, a random access control entity, and a controller which performs various control functions, such as scheduling, timing advance maintenance, and discontinuous reception (DRX). The HARQ entity is responsible for downlink/uplink HARQ operations. The transmit HARQ operation includes transmission and retransmission of transport blocks, and receiving and processing of acknowledgment/negative-acknowledgment (ACK/NACK) signaling. The receive HARQ operation includes reception of transport blocks, combining of the received data and generation of ACK/NACK signaling. In order to enable continuous transmission while previous transport blocks are being decoded, up to eight HARQ processes in parallel are used to support a multi-process stop-and-wait HARQ protocol, which implies that in each HARQ process, upon transmission of a transport block, the transmitter stops further transmissions and waits for feedback from the receiver. When a NACK is received, or when a certain time period elapses without receiving any feedback, the transmitter retransmits the transport block. Each HARQ process is responsible for a separate stop-and-wait operation and manages a separate buffer.

In general, HARQ protocols can be categorized as synchronous or asynchronous, and the retransmissions in each case can be adaptive or non-adaptive. In a synchronous HARQ scheme, the retransmission(s) for each process occur at predefined time intervals relative to the initial transmission time. In this method, there is no need to signal information, such as the HARQ process number, as this can be inferred from the transmission timing. In contrast, in an asynchronous HARQ scheme, the retransmissions can occur at any time relative to the initial

Petitioners' Exhibit 1021
Nokia of America Corp., et al. v. KT Corporation, et al.
Case No. IPR2025-00036; U.S. Patent No. 11,627,631
Page 357 of 1122

transmission, thus additional signaling is required so that the receiver can correctly associate each retransmission with the corresponding initial transmission. The synchronous HARQ schemes have the advantage of reducing the signaling overhead, whereas asynchronous HARQ schemes allow more flexibility in scheduling. In an adaptive HARQ scheme, transmission attributes, such as the modulation, coding, and resource allocation can be changed at each retransmission in response to variations in the channel conditions. In a non-adaptive HARQ scheme, the retransmissions are performed without explicit signaling of new transmission attributes, i.e., either the same transmission format is reused or the attributes are deterministically changed. The adaptive HARQ schemes offer higher scheduling gains at the expense of increased signaling overhead. In LTE/LTE-Advanced, asynchronous adaptive HARQ is used for the downlink and synchronous HARQ for the uplink. In the uplink, the retransmissions may be either adaptive or nonadaptive depending on the signaling of new transmission attributes.

In the multiplexing and demultiplexing entity, data from several logical channels is multiplexed or demultiplexed to/from one transport channel. The multiplexing entity generates MAC PDUs from MAC SDUs when radio resources are available for a new transmission based on the decisions of the logical channel prioritization entity. The demultiplexing entity reassembles the MAC SDUs from MAC PDUs and distributes them to the appropriate RLC entities.

The logical channel prioritization entity prioritizes the data from logical channels and decides the amount and the source of data that should be included in each MAC PDU. The decisions are sent to the multiplexing/demultiplexing entity. The random access control entity is responsible for controlling the random access procedure. The controller entity is also responsible for a number of functions including DRX, scheduling procedure, and maintaining the uplink timing alignment.

To support priority handling, multiple logical channels, where each logical channel has its own RLC entity, are multiplexed into one transport channel by the MAC sublayer. At the receiver, the MAC sublayer performs the corresponding demultiplexing and forwards the RLC SDUs to their respective RLC entity for in-sequence delivery and other RLC functions. The demultiplexing function at the receiver is enabled through addition of a MAC header, shown in Figure 8.2. There is a subheader in the MAC header associated with each RLC PDU. The subheader further contains the logical channel ID (LCID) from which the RLC PDU was originated, and the length of the PDU in octets.

In addition to multiplexing functions, the MAC sublayer can also include MAC control elements (CEs) in the transport blocks transmitted via the transport channels. A MAC control element is used for in-band control signaling, such as timing advance commands and random access response (RAR) message. The control elements are identified with reserved values in the LCID field, where the LCID value indicates the type of control information. The MAC multiplexing functions were extended to handle multiple component carriers in the case of carrier aggregation. The basic principle of carrier aggregation is independent processing of the component carriers in the physical layer, including control signaling,

Petitioners' Exhibit 1021
Nokia of America Corp., et al. v. KT Corporation, et al.
Case No. IPR2025-00036; U.S. Patent No. 11,627,631
Page 358 of 1122

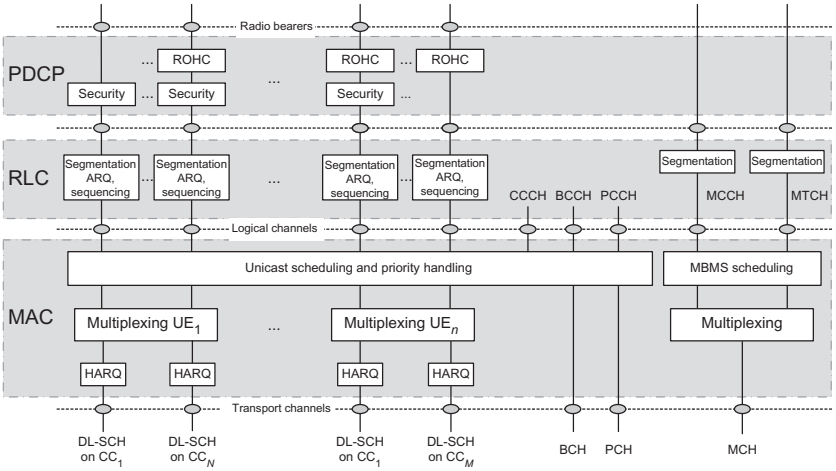


FIGURE 8.4

LTE Layer 2 structure with carrier aggregation support in the downlink [8].

scheduling, and HARQ retransmissions, while carrier aggregation is invisible to the RLC and PDCP. Carrier aggregation is therefore mainly seen in the MAC sublayer, where the logical channels, including any MAC control elements, are multiplexed to one or two transport blocks per component carrier with each component carrier having its own HARQ entity (see Figures 8.4 and 8.5).

The E-UTRA defines one MAC entity in the UE and one MAC entity in the eNB. These MAC entities control the following transport channels: BCH; DL-SCH; PCH; UL-SCH; and RACH. The exact functions performed by the MAC entities are different in the UE and the eNB. As shown in Figures 8.4 and 8.5, the MAC sublayer provides services, such as data transfer and radio resource allocation, to the upper layers. The physical layer provides the MAC sublayer with data transfer services, signaling of HARQ feedback, signaling of scheduling request, and measurements. The access to the data transfer services is through the use of transport channels. The characteristics of a transport channel are defined by its transport format which specifies the physical layer processing to be applied to the transport channel, such as channel coding and interleaving, and any other service-specific rate matching.

8.2 Logical and transport channel mapping

The LTE MAC sublayer provides data transfer services to the RLC sublayer through logical channels. Figures 8.6 and 8.7 depict classification of logical and transport channels in LTE, respectively. Each logical channel type is defined by the type of information which is transferred. The logical channels are generally classified into two groups: (1) control channels (for the transfer of control-plane

Petitioners' Exhibit 1021
Nokia of America Corp., et al. v. KT Corporation, et al.
Case No. IPR2025-00036; U.S. Patent No. 11,627,631
Page 359 of 1122

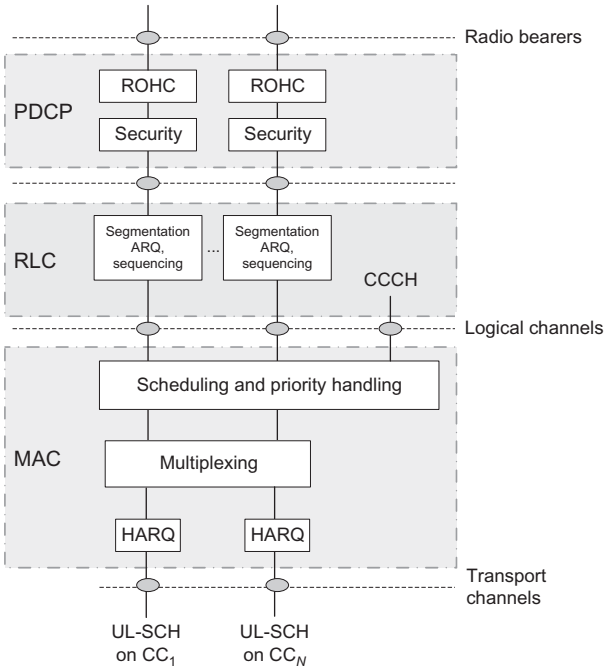


FIGURE 8.5

LTE Layer 2 structure with carrier aggregation support in the uplink [8].

information); and (2) traffic channels (for the transfer of user-plane information), as shown in Figure 8.6.

The control channels are exclusively used for transfer of control-plane information. The control channels supported by MAC can be classified as follows (Figure 8.6):

- Broadcast Control Channel (BCCH): A downlink channel for broadcasting system control information.
- Paging Control Channel (PCCH): A downlink channel that transfers paging information and system information (SI) change notifications. This channel is used for paging when the network does not know the location of the UE.
- Common Control Channel (CCCH): A logical channel for transmitting control information between UEs and eNBs. This channel is used for UEs having no RRC connection with the network.
- Multicast Control Channel (MCCH): A point-to-multipoint downlink channel used for transmitting multimedia broadcast multicast service (MBMS) control information from the network to the UE, for one or several multicast traffic channels. This channel is only used by UEs that are subscribed to MBMS.

Petitioners' Exhibit 1021
Nokia of America Corp., et al. v. KT Corporation, et al.
Case No. IPR2025-00036; U.S. Patent No. 11,627,631
Page 360 of 1122

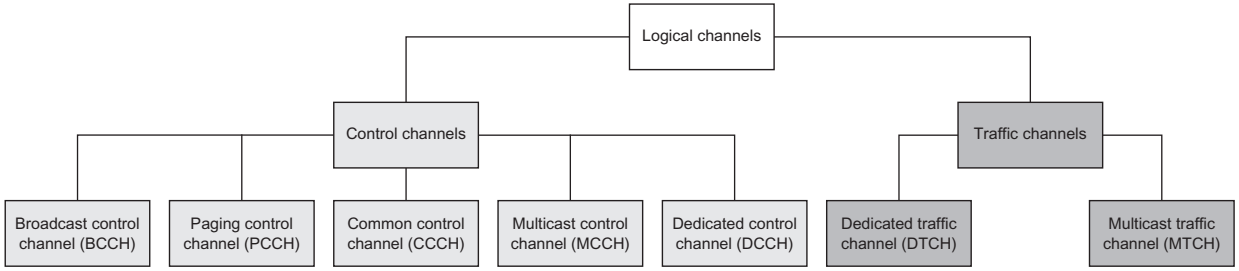


FIGURE 8.6

Classification of LTE logical channels [8].

Petitioners' Exhibit 1021
Nokia of America Corp., et al. v. KT Corporation, et al.
Case No. IPR2025-00036; U.S. Patent No. 11,627,631
Page 361 of 1122

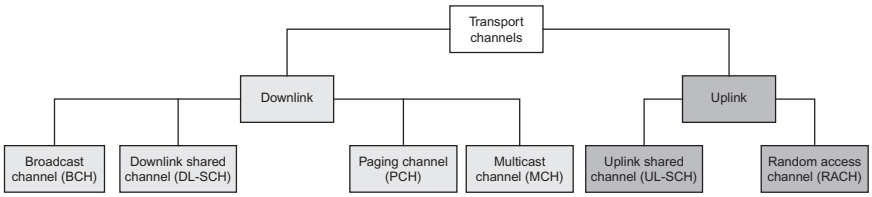


FIGURE 8.7

Classification of LTE transport channels [8].

- Dedicated Control Channel (DCCH): A point-to-point bi-directional channel that transmits dedicated control information between a UE and the network. It is used by UEs that have already established RRC connection.

The traffic channels are exclusively used for the transfer of user-plane information. The traffic channels supported by MAC can be classified as follows (as shown in Figure 8.6):

- Dedicated Traffic Channel (DTCH): A point-to-point bi-directional channel dedicated to a single UE for the transfer of user information.
- Multicast Traffic Channel (MTCH): A point-to-multipoint downlink channel for transmitting traffic data from the network to the UE. This channel is only used by UEs that receive MBMS.

As shown in Figure 8.7, downlink transport channels can be classified as follows:

- Broadcast Channel (BCH) that is characterized by a fixed, predefined transport format and is required to be broadcast in the entire coverage area of the cell.
- Downlink Shared Channel (DL-SCH) that is characterized by support for HARQ, support for dynamic link adaptation by varying the modulation, coding, and transmit power, possibility for broadcast in the entire cell, possibility to use beamforming, support for both dynamic and semi-static resource allocation, support for UE DRX to enable power saving, and support for MBMS transmission.
- Paging Channel (PCH) that is characterized by support for UE DRX in order to enable power saving, requirement for broadcast in the entire coverage area of the cell, mapped to physical resources which can also be used dynamically for traffic or other control channels.
- Multicast Channel (MCH), which is required to be broadcast in the entire coverage area of the cell, and is characterized by support for macro-diversity combining of MBMS transmission on multiple cells, and support for semi-static resource allocation.

The uplink transport channels are classified as follows (Figure 8.7):

- Uplink Shared Channel (UL-SCH), which is characterized by the possibility to use beamforming, support for dynamic link adaptation by varying the transmit

Petitioners' Exhibit 1021
Nokia of America Corp., et al. v. KT Corporation, et al.
Case No. IPR2025-00036; U.S. Patent No. 11,627,631
Page 362 of 1122

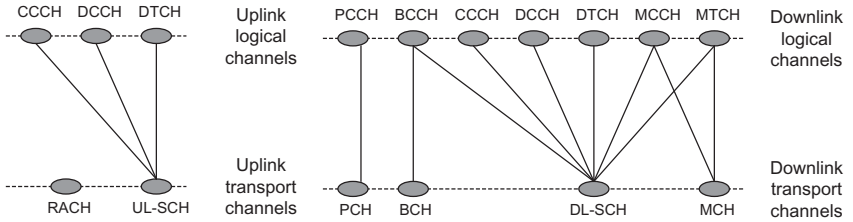


FIGURE 8.8

Mapping of logical to transport channels in the downlink and uplink [8].

power and MCS, support for HARQ, and support for both dynamic and semi-static resource allocation.

- Random Access Channel (RACH) that is characterized by limited control information and collision risk.

The mapping of logical channels to transport channels depends on the multiplexing that is configured by the RRC sublayer (see Figure 8.8) [4].

8.3 Downlink/uplink data transfer

The resource allocation on DL-SCH and UL-SCH is performed by the eNB scheduler. In the downlink, the allocation information pertaining to the physical downlink shared channel (PDSCH) within the same subframe is carried on the physical downlink control channel (PDCCH). The UE may be addressed using different radio network temporary identifiers (RNTIs). During normal operation, either cell radio network temporary identifier (C-RNTI) or semi-persistent scheduling (SPS) C-RNTI may be used depending on whether the transmission is dynamically scheduled, or is periodic with a predefined scheduling pattern. During the RACH procedure, DL-SCH transmissions may also be scheduled using the random access RNTI (RA-RNTI) or the temporary C-RNTI. Furthermore, if the system information is being transmitted via DL-SCH, then the SI-RNTI is utilized. The allocation information that is sent on the PDCCH using various downlink control information (DCI) formats includes resource block allocation, MCS, and HARQ information. Only one HARQ process may be scheduled in any subframe corresponding to either one or two transport blocks [10–12].

The allocation of the uplink grant is managed by the eNB. The allocation information is carried in the PDCCH. Similar to the downlink, the uplink transmissions can be identified using different RNTIs. For normal operation, either C-RNTI or SPS-C-RNTI may be used depending on the scheduling type. During the contention resolution (part of RACH procedure), temporary C-RNTI may be used to address a UE. The allocation information for the uplink is sent using a single DCI format that includes the allocated resource blocks, MCS, HARQ information, and whether frequency hopping is enabled.

Petitioners' Exhibit 1021
Nokia of America Corp., et al. v. KT Corporation, et al.
Case No. IPR2025-00036; U.S. Patent No. 11,627,631
Page 363 of 1122

The BCCH is a downlink logical channel that carries system information. The MAC sublayer maps the BCCH channel to BCH and DL-SCH transport channels. When mapped to BCH, BCCH broadcasts a master information block (MIB). The MIB carries essential parts of the system information that are necessary for initial system acquisition, such as system bandwidth, system frame number (SFN), and physical hybrid-ARQ indicator channel (PHICH) configuration information. The periodicity of MIB transmission is 40 ms. The remaining parts of the system information are transmitted in the form of system information blocks (SIBs), which are sent via BCCH and are mapped to DL-SCH. The SIBs are sent via system information messages, which can contain multiple SIBs. The system information messages are recognized on the DL-SCH by SI-RNTI. The system information message transmission is scheduled at regular intervals as specified in SIB1, which is transmitted on DL-SCH every 80 ms [10–12].

All SIBs are carried on the BCCH and are mapped to DL-SCH. The BCCH carries SIB1 that is mapped to the SI message 1 (SI-1), whereas other SIBs are mapped to other system information messages. The SI messages are identified by SI-RNTI, which has a predefined value of *0xFFFF*. The SIB1 is always transmitted with a period of 80 ms and contains the scheduling and multiplexing information of other SIBs. A broadcast HARQ process is utilized for all system information transmissions such that ACK/NACK feedback is not required. The redundancy version of a received downlink assignment in a specific TTI is determined by $RV_k = \lceil (3k/2) \rceil \bmod 4$ where k depends on the type of SI message. For the SIB1 message $k = (\mathrm{SFN}/2) \bmod 4$. For all other SI messages $k = l \bmod 4|_{l=0,1,\ldots,N_{\mathrm{SW}}-1}$ where l denotes the subframe number within the SI window, which has a duration defined by N_{SW}. The SI window is defined in SIB1 and specifies the starting point and time duration during which the SIs will be transmitted [11].

The paging control channel is a logical channel that is mapped by the MAC sublayer to the paging transport channel, which is transmitted on DL-SCH. For PCH, a unique radio network paging identifier with a value of *0xFFFE* is signaled in the PDCCH allocation message. Multiple UEs may be paged simultaneously using a single paging allocation with the UE identity indicated within the paging message.

8.3.1 HARQ principles

While the ARQ error control mechanism is simple and provides high transmission reliability, the throughput of ARQ schemes drops rapidly with increasing channel error rates and the ARQ latency, due to retransmissions, could be excessively high and intolerable for some delay-sensitive applications. Systems using forward error correction (FEC), on the other hand, can maintain constant throughput regardless of channel error rate. However, FEC schemes have some drawbacks. High reliability is hard to achieve with FEC and requires the use of long and powerful error correction codes that increase the complexity of implementation [10–12]. The drawbacks of ARQ and FEC can be overcome, if the two error control schemes are properly combined.

Petitioners' Exhibit 1021
Nokia of America Corp., et al. v. KT Corporation, et al.
Case No. IPR2025-00036; U.S. Patent No. 11,627,631
Page 364 of 1122

In order to achieve increased throughput and lower latency in packet transmission, the HARQ scheme was designed to combine the ARQ error control mechanism and FEC coding. A HARQ system consists of an FEC subsystem contained in an ARQ system. In this approach, the average number of retransmissions is reduced by using FEC through correction of the error patterns that occur more frequently; however, when the less frequent error patterns are detected, the receiver requests a retransmission where each retransmission carries the same or some redundant information to help the packet detection. The HARQ uses FEC to correct a subset of errors at the receiver and relies on error detection to detect the remaining errors. Most practical HARQ schemes utilize CRC codes for error detection and convolutional or turbo codes for error correction. The HARQ schemes are typically classified into three groups depending on the content of subsequent retransmissions, as follows [10–12]:

1. Type I HARQ: In type I HARQ schemes, the same data packet is transmitted in all the retransmissions. Soft combining may be used to improve the reliability. This type of HARQ is also referred to as chase combining (CC) where the blocks of data along with the CRC code are encoded using a FEC encoder before transmission. If the receiver is unable to correctly decode the data block, a retransmission is requested. When a retransmitted coded block is received, it is combined with the previously received block corresponding to the same information bits (using for example maximal ratio combining method) and fed to the decoder. Since each retransmission is an identical replica of the original transmission, the received E_b/N_0, i.e., the energy per information bit divided by the noise spectral power density, increases per each retransmission, improving the likelihood of correct decoding. In chase combining HARQ, the redundancy version of the encoded bits is not changed from one transmission to the next; therefore, the puncturing pattern remains the same. The receiver uses the current and all previous HARQ transmissions of the data block in order to decode the information bits. The process continues until either the information bits are correctly decoded and pass the CRC test, or the maximum number of HARQ retransmissions is reached. When the maximum number of retransmissions is reached, the MAC sublayer resets the process and continues with fresh transmission of the same data block.

   A number of parallel channels for HARQ can help improve the throughput as one process is awaiting an acknowlegment; another process can utilize the channel and transmit other subpackets. Figure 8.9 illustrates the operation of the chase combining HARQ scheme and how the retransmission of the same coded bits changes the combined energy per bit E_b while maintaining the effective code rate intact.
2. Type II HARQ: In the original type II HARQ scheme, an alternate parity/user data retransmission scheme is used. With proper choice of the channel encoder, the user information may also be recovered by parity bits. However, most type II algorithms adopt an incremental parity retransmission scheme, in which only additional parity bits are sent in subsequent retransmissions.

Petitioners' Exhibit 1021
Nokia of America Corp., et al. v. KT Corporation, et al.
Case No. IPR2025-00036; U.S. Patent No. 11,627,631
Page 365 of 1122

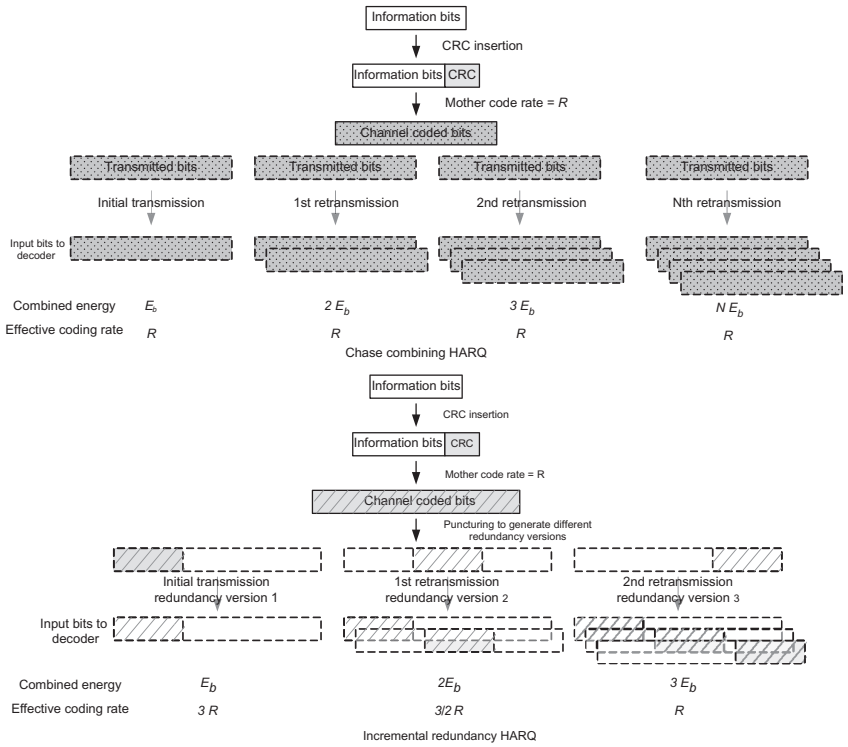


FIGURE 8.9

Illustration of the chase combining (CC) and incremental redundancy (IR) HARQ schemes [12].

Therefore, after each retransmission, a richer set of parity bits is available at the receiver, improving the probability of reliable decoding. In incremental schemes, however, information cannot be recovered from parity bits alone.

In an incremental redundancy HARQ scheme, a number of coded bits with increasing redundancy, where each represents the same set of input bits, are generated and transmitted to the receiver, when a retransmission, is requested to assist the receiver with the decoding of the information bits. The receiver combines each retransmission with the previously received bits belonging to the same packet. Since each retransmission carries additional parity bits, the effective code rate is lowered by each retransmission, as shown in Figure 8.9. The incremental redundancy is based on a low-rate code and the different redundancy versions are generated by puncturing the channel coder output. In the example shown in Figure 8.9, the basic code rate is R and 1/3 of the coded bits are transmitted in each retransmission. Aside from increasing the received signal to noise ratio E_b/N_0 by each retransmission due to combining, there is

Petitioners' Exhibit 1021
Nokia of America Corp., et al. v. KT Corporation, et al.
Case No. IPR2025-00036; U.S. Patent No. 11,627,631
Page 366 of 1122

a coding gain[1] attained as result of each retransmission. It must be noted that chase combining is a special case of incremental redundancy HARQ where the retransmissions are identical copies of the original coded bits.

3. Type III HARQ: In a type III HARQ scheme, both user data and complementary parity bits are included in every retransmission. The type III HARQ schemes are less efficient than incremental redundancy schemes due to repeated transmission of user data bits. Also in this case, after every retransmission, a richer set of parity bits is available at the receiver, improving the probability of reliable decoding. Moreover, by adopting combining techniques, reliability may be further improved. In a type III incremental scheme, information can be recovered from every transmission. In a self-decodable HARQ retransmission scheme, the user data may be recovered from every single transmission.

8.3.2 Downlink HARQ timing and signaling protocols

LTE uses an adaptive asynchronous HARQ scheme in the downlink. Therefore, the retransmissions are scheduled in the same way as new transmissions, i.e., the transmission/retransmissions may occur at any time and at an arbitrary frequency location over the downlink bandwidth. The use of asynchronous and adaptive HARQ in the LTE downlink was partially motivated by the desire to avoid scheduling conflicts with transmission of SI, multicast, and broadcast content over single frequency network (MBSFN) subframes. Instead of dropping a retransmission that otherwise would have collided with MBSFN subframes or SI, the eNB can schedule the retransmission in time and/or frequency to avoid the overlap in resources. The HARQ scheme applies to the data transmissions on PDSCH, where the ACKs are received via the physical uplink control channel (PUCCH) or physical uplink shared channel (PUSCH). There is one HARQ entity at the UE for each serving cell. There are multiple serving cells and multiple HARQ entities when the UE supports carrier aggregation [12].

Soft combining is supported through transmission of an explicit new data indicator (NDI) flag, toggled for each new transport block. In addition to the NDI, HARQ-related downlink control signaling consists of the HARQ process number (3 bits for FDD, 4 bits for TDD) and the redundancy version (2 bits), both explicitly signaled in the scheduling assignment for each downlink transmission. Downlink spatial multiplexing implies transmission of two transport blocks in parallel on a component carrier. In this case, it is possible to retransmit only one of the transport blocks, since error occurrences in transmission of the transport blocks are typically uncorrelated; thus each transport block has separate new data and redundancy version indicators. However, there is no need to signal the process number separately, given that each HARQ process consists of two sub-processes in

[1]The coding gain is defined as the difference between E_b/N_0 required to achieve a given bit error rate (BER) in a coded system and the E_b/N_0 required to achieve the same BER in an uncoded system.

Petitioners' Exhibit 1021
Nokia of America Corp., et al. v. KT Corporation, et al.
Case No. IPR2025-00036; U.S. Patent No. 11,627,631
Page 367 of 1122

the case of spatial multiplexing, once the process number for the first transport block is known, the process number for the second transport block is derived implicitly. Transmissions on downlink component carriers are acknowledged independently. On each component carrier, transport blocks are acknowledged by transmitting one or two bits on the uplink. In the absence of spatial multiplexing, there is only a single transport block within a TTI and consequently only a single acknowledgment bit is required. However, in the case of spatial multiplexing, there are two transport blocks per TTI, each requiring its own HARQ feedback. The total number of bits required for HARQ acknowledgments depends on the number of component carriers and the transmission mode of each component carrier. Since downlink component carriers are scheduled separately using the PDCCH, the HARQ process numbers are signaled independently for each component carrier. It is obvious that the terminal is not expected to transmit a HARQ acknowledgement in response to transmission of system information, paging messages, and other broadcast information. Therefore, HARQ feedback is only sent in the uplink for unicast transmission [12].

LTE utilizes incremental-redundancy HARQ with a 1/3 turbo encoder used for FEC. The transport block CRC is used to detect errors. The receiver only receives different punctured versions of the same turbo-encoded data; each of these retransmissions is self-decodable. Thus, it falls into the category of a type III HARQ described earlier. The maximum number of retransmissions is limited to four, with an initial coding rate of 1/2 or 3/4. The maximum number of simultaneous downlink HARQ processes (number of PDSCH transmissions) is limited to eight for FDD mode, as specified in [7].

8.3.3 Uplink HARQ timing and signaling protocols

The operation of the LTE uplink HARQ protocol is different from the downlink counterpart. The choice of uplink HARQ protocol was made by taking into consideration the lower overhead of a synchronous non-adaptive scheme compared to an asynchronous adaptive scheme. As a result, uplink retransmissions always occur at fixed intervals. In the case of FDD mode, the uplink retransmissions occur eight subframes after the previous transmission attempt for the same HARQ process. The set of resource blocks used for the retransmission on each component carrier are identical to the initial transmission. The control signaling required in the downlink for an uplink retransmission is a HARQ feedback, which is transmitted on PHICH. In the case of a NACK on PHICH, the data is retransmitted. Spatial multiplexing is handled in the same way as in the downlink where two transport blocks are concurrently transmitted in the uplink, each with its own MCS and NDI, but sharing the same HARQ process number. The two transport blocks are individually acknowledged, thus two bits of information are needed in the downlink to acknowledge an uplink transmission when spatial multiplexing is utilized. The uplink carrier aggregation is another example where multiple ACKs/NACKS are required, i.e., one or two ACK/NACK bits per uplink component

Petitioners' Exhibit 1021
Nokia of America Corp., et al. v. KT Corporation, et al.
Case No. IPR2025-00036; U.S. Patent No. 11,627,631
Page 368 of 1122

carrier. In the TDD mode, the uplink transmissions in different subframes may need to be acknowledged in the same downlink subframe. Thus, multiple PHICHs may be needed as each PHICH is capable of transmitting one bit of HARQ feedback. Each of the PHICHs is transmitted on the same downlink component carrier that was used to schedule the initial uplink transmission. Despite the fact that the default mode of operation for the uplink is synchronous, non-adaptive HARQ, it is also possible to operate the uplink HARQ in a synchronous, adaptive mode, where the resource block set and MCS for the retransmissions are changed according to the transmission conditions. Although non-adaptive retransmissions are typically used, due to their very low downlink control signaling overhead, adaptive retransmissions are sometimes useful in order to avoid the uplink frequency resource fragmentation or to avoid collisions with random access allocated resources. A UE is scheduled for an initial transmission in subframe n and if the transmission is not correctly received, a retransmission is required in subframe $n + 8$ in FDD mode (the TDD retransmission timing depends on the subframe configuration). With non-adaptive HARQ, the retransmissions occupy the same part of the uplink spectrum as the initial transmission. In this case, the spectrum may be fragmented, which limits the bandwidth available for other terminals, unless the other terminal is capable of multi-cluster transmission (LTE Rel-10 and onward UEs). Example HARQ operation and timing in the uplink for an FDD and TDD system are shown in Figures 8.10 and 8.11, respectively.

Figure 8.12 depicts an example uplink HARQ process using adaptive and non-adaptive schemes to better understand this operation. In the adaptive case, the

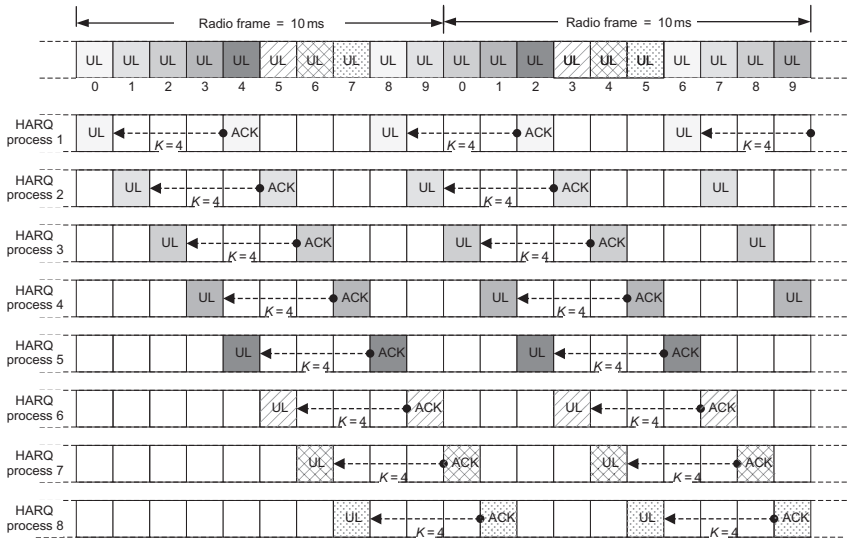


FIGURE 8.10

Example uplink HARQ timing for an FDD system [10].

Petitioners' Exhibit 1021
Nokia of America Corp., et al. v. KT Corporation, et al.
Case No. IPR2025-00036; U.S. Patent No. 11,627,631
Page 369 of 1122

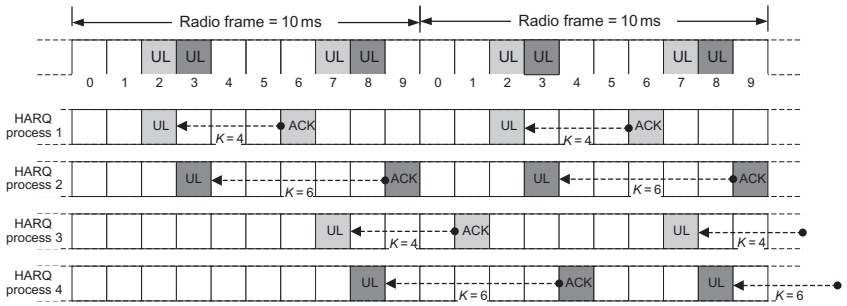


FIGURE 8.11

Example uplink HARQ timing for a TDD system with subframe configuration 1 [10].

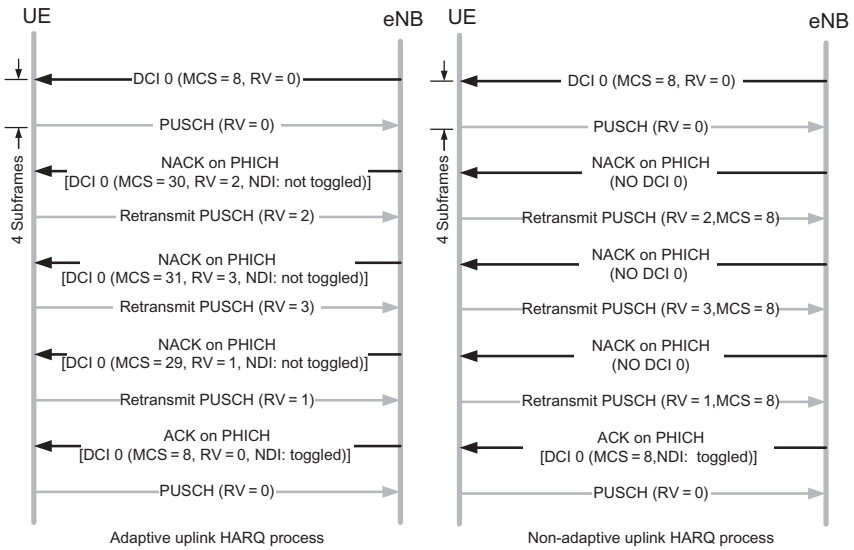


FIGURE 8.12

Illustration of example adaptive and non-adaptive uplink HARQ processes [21].

main idea is that each uplink retransmission uses a different redundancy version (RV) and the RV is determined by DCI format 0 (i.e., uplink grant). In the case of non-adaptive uplink HARQ, each uplink retransmission uses a different RV and the RV is determined by a predefined sequence specified in [1]. An important question is how the UE determines whether it is supposed to use adaptive retransmission or non-adaptive retransmission. The UE uses adaptive retransmission if it detects DCI format 0 and NDI is not toggled. In this case, the UE ignores HARQ feedback in PHICH and it retransmits based on DCI format 0 information. The

Petitioners' Exhibit 1021
Nokia of America Corp., et al. v. KT Corporation, et al.
Case No. IPR2025-00036; U.S. Patent No. 11,627,631
Page 370 of 1122

UE determines that it is supposed to use non-adaptive retransmission when it receives negative HARQ feedback in PHICH and does not receive DCI format 0.

The adaptive and non-adaptive HARQ schemes can be supported by having the terminal save the content of its transmission buffer until it receives an NDI on PDCCH. The decision on whether the data in the transmission buffer should be retransmitted is made based on the NDI included in the uplink scheduling grant which is sent in the PDCCH. The NDI is toggled for each new transmission. If the NDI is toggled, the terminal flushes the transmission buffer and transmits a new data packet. However, if the NDI does not indicate transmission of a new transport block, the previous transport block is retransmitted. The negative HARQ ACK on PHICH could instead be seen as a single-bit scheduling grant for retransmissions, where the set of bits to transmit and all the resource information are known from the previous transmission attempt [12].

The NDI is explicitly transmitted in the uplink grant. However, unlike the downlink case, the redundancy version is not explicitly signaled for each retransmission and cannot be inferred from a single-bit HARQ feedback on PHICH. Instead, given that the uplink HARQ protocol is synchronous, the redundancy version follows a predefined pattern, starting with zero when the initial transmission is scheduled by PDCCH. Whenever a retransmission is requested by sending a NACK on PHICH, the next redundancy version in the sequence is used. However, if a retransmission is explicitly scheduled by PDCCH overriding PHICH, there is a possibility that a different redundancy version may be used. Uplink grants for retransmissions use the same format as normal grants (for initial transmissions). The transport block size is already known from the initial transmission and cannot change between retransmission attempts.

The uplink HARQ retransmissions are associated with the HARQ feedback as seen by the UE on PHICH and the uplink grant sent in PDCCH. The information in the uplink grant takes precedence over retransmissions. The UE adheres to the following rules:

1. If the HARQ feedback is an ACK and no grant is detected for the HARQ process on PDCCH, then the UE maintains the data in its soft buffer until the PDCCH grant indicates whether the previous transmission was successful.
2. If the HARQ feedback is a NACK and no PDCCH grant is detected for the HARQ process, then the UE retransmits using the same PUSCH resources as the last transmission. The redundancy version used follows a known sequence.
3. If the PDCCH indicates a new transmission on PDCCH for a specific HARQ process, then regardless of HARQ feedback on PHICH, it is treated as a new transmission. Any data in the soft buffer is flushed.
4. If the PDCCH indicates a retransmission for a specific HARQ process, then irrespective of HARQ feedback, the UE performs a retransmission according to the parameters on the PDCCH.

In the case of carrier aggregation, if cross-carrier scheduling is not used and each uplink component carrier is scheduled on its corresponding downlink component carrier, the uplink component carriers are not associated with the same

Petitioners' Exhibit 1021
Nokia of America Corp., et al. v. KT Corporation, et al.
Case No. IPR2025-00036; U.S. Patent No. 11,627,631
Page 371 of 1122

PHICH resource. However, when cross-carrier scheduling is utilized, transmissions on multiple uplink component carriers may need to be acknowledged on a single downlink component carrier. In order to avoid PHICH collisions, the scheduler ensures that different reference signal phase rotations (cyclic shifts) or different resource block starting positions are used for different uplink component carriers. For semi-persistent scheduling, the reference signal phase rotation is always set to zero, since the semi-persistent scheduling is only supported on the primary component carrier. If multiple component carriers are scheduled for uplink data transmission in a subframe, there will be one or two (with spatial multiplexing) PHICHs transmitted per uplink component carrier. In general, LTE transmits the PHICH on the same component carrier that was used for the uplink grant, scheduling the corresponding uplink data transmission. Thus, a terminal is only required to monitor the component carriers that include uplink scheduling grants (especially as the PDCCH may override PHICH to support adaptive retransmissions in some cases), which helps to reduce the terminal's power consumption [10–12].

The transmission of HARQ feedback in the uplink in response to PDSCH transmissions is illustrated in Figure 8.13 for an FDD system. The data on PDSCH is transmitted to the terminal in subframe n and received by the terminal after the propagation delay in subframe n. The terminal attempts to decode the received signal, using soft combining of previous retransmissions, and then it transmits a HARQ ACK/NACK in uplink subframe $n + 4$. It must be noted that the start of an uplink subframe at the terminal is offset by the timing advance relative to the start of the corresponding downlink subframe at the terminal. Upon reception of the HARQ feedback, the eNB can transmit new data or retransmit the previous data in subframe $n + 8$. Thus, the HARQ round-trip time (RTT) is 8 ms for an FDD system.

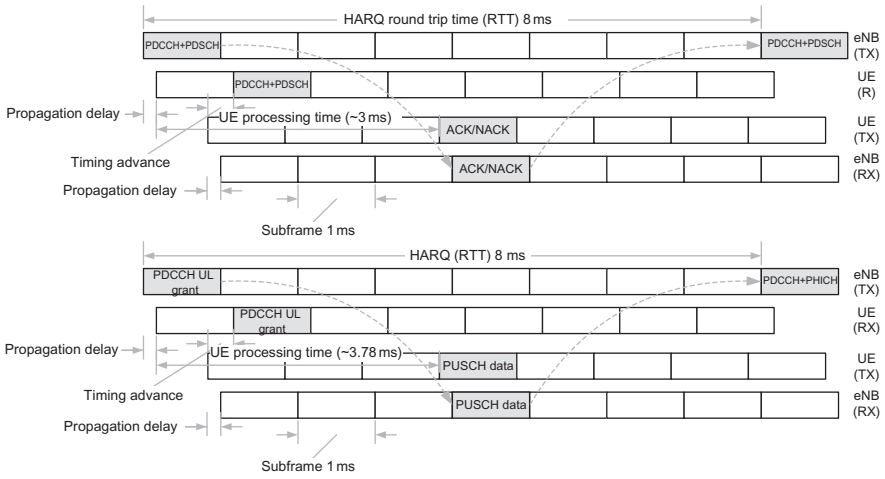


FIGURE 8.13

Example timing diagram for downlink and uplink HARQ schemes (FDD mode) [11].

Petitioners' Exhibit 1021
Nokia of America Corp., et al. v. KT Corporation, et al.
Case No. IPR2025-00036; U.S. Patent No. 11,627,631
Page 372 of 1122

In practice, the UE processing time depends on the value of the timing advance (to compensate variable propagation delay), or alternatively on its distance to the base station. Since the UE is required to operate at any distance up to the maximum cell radius of 100 km (corresponding to 0.67 ms) supported by the standard, the UE is designed for the worst-case scenario. That means UE baseband processing time is approximately 2.3 ms. For the eNB, the baseband processing time is 3 ms [11].

In LTE TDD, the time association between the data transmission and the ACK/NACK cannot be maintained due to the variable numbers of downlink and uplink subframes being present in a frame. The uplink and downlink delay between data and ACK/NACK is dependent on the TDD subframe configuration. Therefore, a fixed delay between a transmission and the HARQ ACK/NACK is not possible in LTE TDD. In TDD mode, the delay between the transmission and the HARQ ACK/NACK depends on both TDD subframe configuration and the subframe in which the data was transmitted. A fixed delay cannot be assured as subframes are allocated to downlink and uplink depending on the subframe configuration. As an example, in subframe configuration 1 (see Table 8.1), there are a number of downlink subframes whose nearest uplink subframe (four or more subframes apart) is seven subframes apart.

Table 8.1 shows the HARQ ACK/NACK timing delays for the downlink and uplink of a TDD system assuming the initial data transmission occurred in subframe n, i.e., the transmission of ACK/NACK occurs in subframe $n + k$. It can be noticed that the delays are dependent on the configuration and the subframe in which the original data transmission has occurred. For example, in configuration 1, the delay from the eNB side can range from four to six subframes, while the delays from the UE side can be from four to seven subframes. As a result, the delay for transmission of ACK/NACK can range from four to seven subframes for the downlink HARQ and from four to thirteen subframes for the uplink HARQ. The higher number in the uplink case is due to the larger downlink asymmetry in the configuration. Therefore, in TDD systems, the acknowledgment of a transport block in subframe n is transmitted in subframe $n + k$, where $k \geq 4$ and is selected such that $n + k$ is an uplink subframe when the acknowledgment is transmitted from the terminal on PUCCH or PUSCH, and a downlink subframe when the acknowledgment is transmitted from the eNB on PHICH. The value of k depends on the downlink−uplink subframe configuration, as shown in Table 8.1 for downlink and uplink transmissions.

In FDD systems, multiple HARQ processes can be activated in both downlink and uplink directions. Due to the fixed timing associations between the original and the retransmission on the uplink, the maximum number of HARQ processes has been set to eight. However, in TDD systems, due to the variable delays experienced with respect to ACK/NACK arrivals as well as the retransmissions, the number of HARQ processes is dependent on the configuration. The maximum number of HARQ processes allowed per configuration for downlink and uplink is given in Table 8.1. Typically, the retransmissions can be scheduled four subframes (or more) after the reception of a NACK message. In LTE TDD, the numbers of downlink and uplink subframes in a frame are not equal. For instance, configurations 0−5 have more downlink subframes compared to uplink subframes. Consequently, data

Petitioners' Exhibit 1021
Nokia of America Corp., et al. v. KT Corporation, et al.
Case No. IPR2025-00036; U.S. Patent No. 11,627,631
Page 373 of 1122

Table 8.1 Number of HARQ Processes and Timing for Different TDD Configurations [12]

Subframe Configuration (DL:UL)	Downlink Subframe Number										Uplink Subframe Number										Number of Processes	
	0	1	2	3	4	5	6	7	8	9	0	1	2	3	4	5	6	7	8	9	Uplink	Downlink
0 (2:3)	4	6	–	–	–	4	6	–	–	–	–	–	4	7	6	–	–	4	7	6	7	4
1 (3:2)	7	6	–	–	4	7	6	–	–	4	–	–	4	6	–	–	–	4	6	–	4	7
2 (4:1)	7	6	–	4	8	7	6	–	4	8	–	–	6	–	–	–	–	6	–	–	2	10
3 (7:3)	4	11	–	–	–	7	6	6	5	5	–	–	6	6	6	–	–	–	–	–	3	9
4 (8:2)	12	11	–	–	8	7	7	6	5	4	–	–	6	6	–	–	–	–	–	–	2	12
5 (9:1)	12	11	–	9	8	7	6	5	4	13	–	–	6	–	–	–	–	–	–	–	1	15
6 (5:5)	7	7	–	–	–	7	7	–	–	5	–	–	4	6	6	–	–	4	7	–	6	6

Petitioners' Exhibit 1021
Nokia of America Corp., et al. v. KT Corporation, et al.
Case No. IPR2025-00036; U.S. Patent No. 11,627,631
Page 374 of 1122

transmission from multiple downlink subframes needs to be acknowledged in a certain uplink subframe and vice versa for certain cases for the uplink data transmission.

The transmission of multiple ACK/NACK messages in uplink or downlink subframes is a unique feature of LTE TDD compared with FDD due to the above-mentioned limitation. Two methods have been specified in the standard to deal with this issue: ACK/NACK bundling and ACK/NACK multiplexing. For the eNB, transmission of separate ACK/NACKs is not a major problem as the eNB is not power constrained and can send multiple ACK/NACKs in a subframe. This method, where separate ACK/NACKs are sent in the same subframe for transmissions in different subframes, is called ACK/NACK multiplexing. Thus, in the downlink ACK/NACK transmission, it is by default ACK/NACK multiplexing. However, in the uplink, the UEs might be power constrained depending on their location within the cell. For UEs which are not constrained by power and coverage, multiple PUCCH messages relating to each HARQ process can be generated, i.e., separate ACK/NACK messages can be sent. For coverage-limited UEs, ACK/NACK bundling is used since fewer bits need to be sent in this case. Multiplexing implies that independent ACKs/NACKs for each of the received transport blocks are sent to the eNB, which allows independent retransmission of erroneous transport blocks. However, it also suggests that multiple bits need to be transmitted from the terminal, which may limit the uplink coverage. This is the motivation for the bundling mechanism.

Bundling of ACKs/NACKs implies that the outcome of the decoding of downlink transport blocks from multiple downlink subframes can be combined into a single HARQ feedback transmitted in the uplink [12]. A logical AND operation on all ACK/NACK messages is typically performed and the result is sent. For example, in TDD subframe configuration 1, the transmissions in subframes 0 and 1 are acknowledged in subframe 7. A logical AND of these messages is performed and sent. This implies that both transport blocks will be retransmitted by the eNB as it does not have the individual acknowledgment status of the downlink transmissions. This is a disadvantage of ACK/NACK bundling as more retransmissions than necessary might be sent. The main advantage of the ACK/NACK bundling method is the fact that the limited power resources of a UE will now be used only in a fewer resource blocks as compared to a larger number of resource blocks. This can improve the uplink coverage of the UE since there will be more power per resource block that will be available to the UE in the case of ACK/NACK bundling [12].

In order to transmit on the UL-SCH the UE must have a valid uplink grant (except for non-adaptive HARQ retransmissions) which it may receive dynamically on the PDCCH or in an RAR message. To perform requested transmissions, the MAC sublayer receives HARQ information from lower layers. When the physical layer is configured for uplink spatial multiplexing, the MAC sublayer can receive up to two grants (one per HARQ process) for the same TTI from lower layers [1].

At a given TTI, if an uplink grant is indicated for the TTI, the HARQ entity identifies the HARQ processes for which a transmission should occur. It also routes the received HARQ feedback (ACK/NACK information), modulation and

Petitioners' Exhibit 1021
Nokia of America Corp., et al. v. KT Corporation, et al.
Case No. IPR2025-00036; U.S. Patent No. 11,627,631
Page 375 of 1122

coding, and resource allocation information (conveyed by the physical layer) to the appropriate HARQ processes. When TTI bundling is configured, the parameter *TTI_BUNDLE_SIZE* provides the number of TTIs of a TTI bundle. The TTI bundling operation relies on the HARQ entity for invoking the same HARQ process for each transmission that is part of the same bundle. Within a bundle, HARQ retransmissions are non-adaptive and triggered without waiting for feedback from previous transmissions according to the *TTI_BUNDLE_SIZE*. The HARQ feedback of a bundle is only received for the last TTI of the bundle (i.e., the TTI corresponding to *TTI_BUNDLE_SIZE*), regardless of a transmission in that TTI (e.g., when a measurement gap occurs). A retransmission of a TTI bundle is also a TTI bundle. TTI bundling is not supported when the UE is configured with one or more secondary cells (SCells) with configured uplink [1].

Each HARQ process in the uplink maintains a state variable *CURRENT_TX_NB*, which indicates the number of transmissions that have taken place for the MAC PDU currently in the buffer, and a state variable *HARQ_FEEDBACK*, which indicates the HARQ feedback for the MAC PDU currently in the buffer. When the HARQ process is established, *CURRENT_TX_NB* set to zero. The sequence of redundancy versions is 0, 2, 3, and 1 (Figure 8.12). The variable *CURRENT_IRV* is an index to the sequence of redundancy versions. This variable is updated in modulo 4. New transmissions are performed on the resource and with the MCS indicated on PDCCH or RAR message. Adaptive retransmissions are performed on the resource and, if provided, with the MCS indicated on PDCCH. Non-adaptive retransmission is performed on the same resource and with the same MCS as was used for the last transmission attempt [1].

8.4 DRX operation

LTE supports DRX in the downlink, to save the UE battery power during periods of inactivity. In the DRX mode, the UE only monitors PDCCH during a predefined on-duration interval within one of two possible DRX cycles. The UE may turn off its receiver when it does not expect to receive any transmission in the downlink over PDCCH. The UE can transition to DRX mode in one of the following two ways: (1) implicitly based on the expiration of certain configured timers; or (2) explicitly based on the transmission of a DRX command in the form of a MAC control element.

As shown in Figure 8.14, there are a number of timers associated with the DRX mode. The DRX inactivity timer controls the number of subframes for which a UE continues to monitor the downlink before an absence of activity triggers the UE to enter the DRX mode. Upon entering the DRX mode, the UE monitors the downlink for a number of subframes defined by the on-duration timer in every short DRX cycle or long DRX cycle. The short DRX cycle is optional. If it is configured, the UE will follow the short DRX cycle for a specific number of cycles controlled by the short DRX cycle timer before switching to the long DRX

Petitioners' Exhibit 1021
Nokia of America Corp., et al. v. KT Corporation, et al.
Case No. IPR2025-00036; U.S. Patent No. 11,627,631
Page 376 of 1122

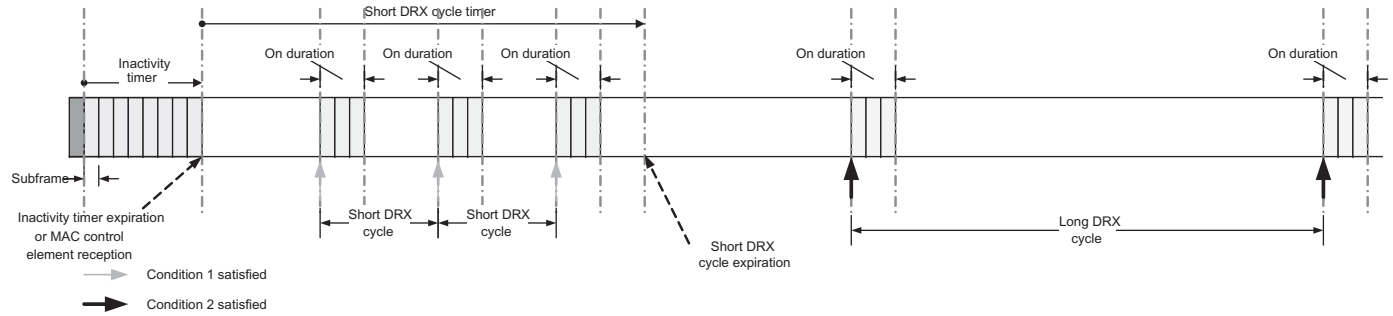


FIGURE 8.14

Illustration of short and long DRX cycles and timers [10].

cycle, if there is no activity. Other timers prevent the UE from entering the DRX mode. These are associated with HARQ downlink retransmissions. If the UE has received data that it was unable to decode and this was not associated with a broadcast HARQ process, then following the expiration of the HARQ RTT timer, which specifies the earliest time at which a UE can expect a retransmission, the DRX retransmission timer is started. The UE must wait for this timer to expire and continue to monitor the downlink before it can enter the DRX mode. Moreover, the UE cannot enter the DRX mode under the following conditions:

- If downlink transmissions are in progress or if the UE has sent a scheduling request.
- If the UE is expecting an uplink grant for HARQ retransmission.
- If the RACH procedure is in progress and the contention resolution timer is running.

In addition to the above timers, the network can order the UE to enter the DRX mode with the DRX command MAC control element. All timers and parameters described in this context are configured by RRC signaling.

A UE may be configured by the RRC sublayer for DRX, which controls the way the UE monitors PDCCH and looks for its C-RNTI, TPC-PUCCH-RNTI, TPC-PUSCH-RNTI, and SPS-C-RNTI (if configured). When the UE is in the RRC_CONNECTED state and if DRX is configured, the UE is allowed to monitor PDCCH intermittently; otherwise, the UE monitors PDCCH continuously. The RRC signaling controls DRX operation by configuring the following timers: *onDurationTimer*; *drx-InactivityTimer*; *drx-RetransmissionTimer* (for each downlink HARQ process except for the broadcast process); *longDRX-Cycle*; *drxStartOffset*; and optionally *drxShortCycleTimer* and *shortDRX-Cycle*. Note that the same activity time applies to all activated serving cells in carrier aggregation scenarios [1].

In Figure 8.14, Conditions 1 and 2 are defined as follows:

Condition 1: $(10\text{SFN} + n_{\text{subframe}})\text{mod}(shortDRX\text{-}Cycle) = (drxStartOffset) \text{mod}(shortDRX\text{-}Cycle)$.

Condition 2: $(10\text{SFN} + n_{\text{subframe}})\text{mod}(longDRX\text{-}Cycle) = drxStartOffset$.

The DRX parameters and timers in the above equations are defined as follows [1]:

- *Active time*: The time interval during which the UE monitors the PDCCH in subframes containing a PDCCH.
- *DRX cycle*: The periodic repetition of the on-duration followed by a potential period of inactivity.
- *drx-InactivityTimer*: The number of consecutive subframes containing a PDCCH, after the subframe in which a PDCCH indicates an initial uplink/downlink user data transmission for the UE.
- *drx-RetransmissionTimer*: The maximum number of consecutive subframes containing a PDCCH immediately after a downlink retransmission is expected by the UE.

Petitioners' Exhibit 1021
Nokia of America Corp., et al. v. KT Corporation, et al.
Case No. IPR2025-00036; U.S. Patent No. 11,627,631
Page 378 of 1122

- *drxShortCycleTimer*: The number of consecutive subframes that the UE is required to follow the *short DRX cycle*.
- *drxStartOffset:* Specifies the subframe where the DRX cycle starts.
- *onDurationTimer*: The number of consecutive subframes containing a PDCCH at the beginning of a DRX cycle. This is the time duration after waking up from DRX that the UE monitors the PDCCH region in the subframe. If the UE successfully decodes a PDCCH, the UE stays awake and starts the inactivity timer.

From the above parameters, the on-duration and inactivity timer have fixed lengths, while the active time has variable length based on scheduling decision and the UE decoding success. Only on-duration and inactivity timer duration are signaled to the UE by the eNB. There is only one DRX configuration applied in the UE at any time and the UE is required to apply an on-duration upon wake-up from the DRX cycle. This is also applicable for the case where the UE has only one real-time service that is being handled through the allocation of predefined resources. This would allow other signaling, mechanisms, such as RRC signaling, to be sent during the remaining portion of the active time. The new transmissions can only occur during the active time, so that when the UE is waiting for one retransmission, it does not have to be awake during the HARQ round-trip time. If the PDCCH has not been successfully decoded during the on-duration, the UE must follow the DRX configuration, i.e., the UE can enter the DRX cycle, if allowed by the DRX configuration. This applies also for the subframes where the UE has been allocated predefined resources.

If the UE successfully decodes a PDCCH for a first transmission, it stays awake and starts the inactivity timer, even if a PDCCH is successfully decoded in the subframes where the UE has also been allocated predefined resources, until a MAC control message informs the UE to reenter the DRX cycle, or until the inactivity timer expires. In both cases, if a short DRX cycle is configured, the UE first follows the short DRX cycle and after a longer period of inactivity the UE follows the long DRX cycle; otherwise, the UE directly enters the long DRX cycle. When the DRX is configured, the network should detect whether the UE remains in the E-UTRAN coverage by requesting the UE to send periodic signals to the network. In the case of carrier aggregation, whenever a UE is configured with only one serving cell, i.e., primary cell, LTE Rel-8/9 DRX scheme applies. In other cases, the same DRX operation applies to all configured and activated serving cells (i.e., identical active time for PDCCH monitoring) [8].

During the DRX procedure, the UE maintains a DRX cycle that is defined as a number of subframes. The UE monitors the PDCCH for a specific number of subframes in a DRX cycle. This time interval is called on-duration and can range from 1 to 200 subframes. The UE may turn off its receiver for rest of the DRX cycle. The UE maintains two DRX cycles, referred to as short DRX cycle and long DRX cycle, which have different durations. The short DRX cycle is optional and targeted for applications, such as voice over IP (VoIP) which typically require transmission of relatively small amounts of data at short but regular intervals. If configured, the UE starts with a short DRX cycle (2−640 subframes) when it enters the DRX mode.

Petitioners' Exhibit 1021
Nokia of America Corp., et al. v. KT Corporation, et al.
Case No. IPR2025-00036; U.S. Patent No. 11,627,631
Page 379 of 1122

When the configurable short DRX timer expires, the UE transitions to the long DRX cycle (10−2560 subframes). The UE can transition to the DRX mode either upon expiration of configured timers or following a DRX command in the form of a MAC control element. Figure 8.15 illustrates different scenarios in DRX operation.

The downlink radio link quality of the primary cell must be monitored by the UE for the purpose of indicating out-of-sync/in-sync status to higher layers. In non-DRX operation mode, the physical layer in the UE in every radio frame assesses the radio link quality over the previous time period against thresholds (Q_{out} and Q_{in}). In DRX operation mode, the physical layer in the UE, at least once every DRX period assesses the radio link quality over the previous time period, against thresholds (Q_{out} and Q_{in}). The threshold Q_{out} is defined as the level at which the downlink radio link cannot be reliably received, corresponding to a 10% block error rate of a hypothetical PDCCH transmission taking into account the

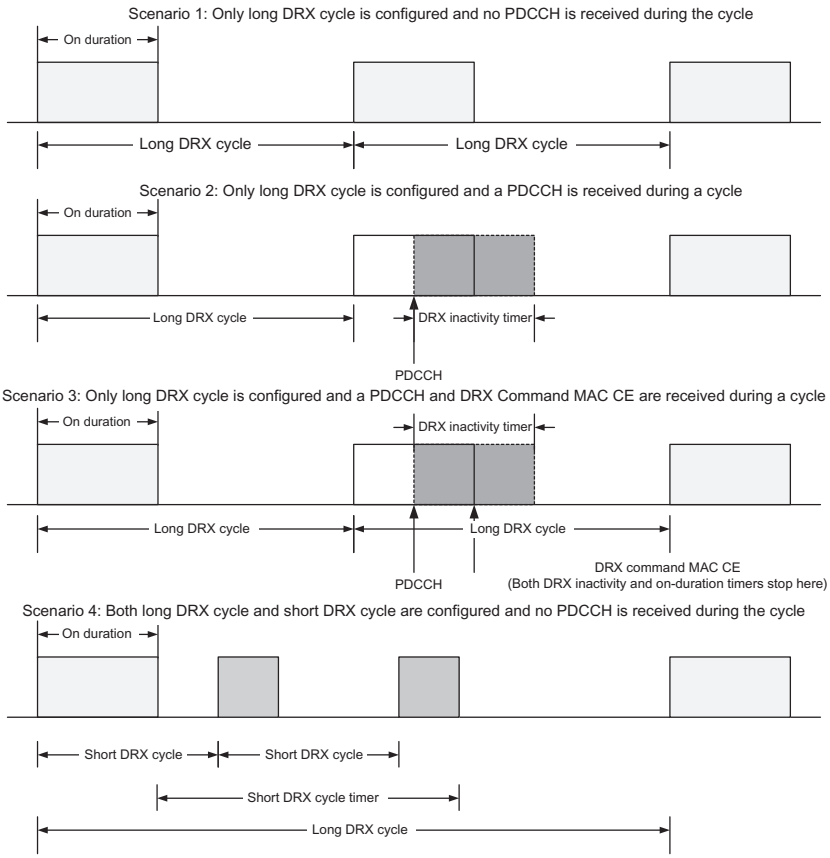


FIGURE 8.15

Illustration of DRX operation [21].

Petitioners' Exhibit 1021
Nokia of America Corp., et al. v. KT Corporation, et al.
Case No. IPR2025-00036; U.S. Patent No. 11,627,631
Page 380 of 1122

physical control format indicator channel (PCFICH) errors with transmission parameters specified in [9]. The threshold Q_{in} is defined as the level at which the downlink radio link quality can be significantly more reliably received than at Q_{out} and corresponds to a 2% block error rate of a hypothetical PDCCH transmission taking into account PCFICH errors with transmission parameters specified in [9].

To investigate the effect of DRX on packet delay, let's assume that the inter-packet arrival times T_{arrival} follow an exponential distribution with a mean of $1/\lambda$ ms, the extra delay T_{d} (in milliseconds), caused by active mode of DRX, can be computed as $T_{\text{d}} = T_{\text{arrival}} \text{mod} T_{\text{DRX-cycle}}$. The probability distribution of the extra delay T_{d} can be expressed as follows [13]:

$$p_{\text{d}}(k) = \frac{1}{T_{\text{DRX-cycle}}} \sum_{i=0}^{T_{\text{DRX-cycle}}-1} \frac{\lambda}{a_i^k(1 - a_i e^{-\lambda})} \tag{8.1}$$

where a_i is the ith order-n root of unity[2] and $p_{\text{d}}(k)$ is the probability that the extra delay is equal to k subframes.

The energy saving of the UE due to use of the DRX mechanism can be expressed as follows [13]:

$$Energy\_Saving\% = 100 \frac{N_{\text{DRX}} E_{\text{DRX}} + N_{\text{Active}} E_{\text{Active}}}{(N_{\text{DRX}} + N_{\text{Active}}) E_{\text{Active}}} \tag{8.2}$$

It is assumed that there are N_{DRX} frames during which the UE is in the DRX mode and N_{Active} frames during which the UE is in the normal operation mode. Furthermore, we assume that the energy consumed per frame is E_{DRX} and E_{Active} during the DRX and active modes, respectively. The ratio of E_{DRX} and E_{Active} is directly related to the number of hardware sub-systems (or modules), that are powered down during the DRX mode [13,14,18].

8.5 MAC control elements

MAC control element are control commands and reports that enable MAC operation. They are transmitted as part of the DL-SCH or UL-SCH and can be piggy-backed to the data payloads. The following CEs have been defined in MAC specification as part of LTE Rel-11:

Downlink

- Timing advance: This CE is used to provide initial and periodic timing adjustment commands to the UE in the uplink.

[2]In mathematics, a root of unity, often called a de Moivre number, is a complex number whose nth power is equal to one. Roots of unity are used in many branches of mathematics, and are especially important in number theory, field theory, and discrete Fourier transform. The notion of root of unity also applies to any algebraic ring with a multiplicative identity element, namely a root of unity is any element of finite multiplicative order. An nth root of unity, where $n = 1, 2, 3, \ldots$ is a positive integer, is a complex number z satisfying the equation $z^n = 1$. An nth root of unity is primitive, if it is not a kth root of unity for some smaller integer k, i.e., $z^k \neq 1 (k = 1, 2, 3, \ldots, n-1)$ [20].

Petitioners' Exhibit 1021
Nokia of America Corp., et al. v. KT Corporation, et al.
Case No. IPR2025-00036; U.S. Patent No. 11,627,631
Page 381 of 1122

- DRX command: This CE initiates DRX mode at the UE and conveys DRX commands to the UE.
- UE contention resolution identity: This CE is used during the RACH procedure to resolve possible contention between multiple UEs that are trying to simultaneously access the network.
- MBMS dynamic scheduling information: This CE is transmitted for each MCH to inform the MBMS-capable UEs of scheduled data transmission on MTCH.
- Activation/deactivation: This CE is used to activate or deactivate secondary cells for the carrier-aggregation-enabled UEs.

Uplink

- Buffer status report (BSR): This CE is used to report the UE's soft buffer status and to enable uplink scheduling.
- Power headroom: This CE is used to report the UE's transmit power relative to maximum permissible value, or whether the UE is currently power limited.
- C-RNTI report: This is used to identify a UE when sending information over CCCH and for the UE to transmit a dedicated C-RNTI during the random access procedure for the purpose of contention resolution.
- Extended power headroom: This CE was specified to support carrier aggregation in LTE Rel-10. In the case of carrier aggregation, the UE reports power headroom of each component carrier independently.

As shown in Figure 8.16, each MAC CE included in the MAC PDU has an associated one-byte subheader in the MAC header with the format R/R/E/LCID, where the LCID indicates the type of MAC CE. The values of LCID for DL-SCH and UL-SCH are listed in Table 8.2.

8.5.1 Uplink timing advance control element

After initial synchronization on RACH, the UE must maintain a reasonably accurate uplink time alignment. This is achieved using the timing advance control element which is sent as part of a MAC PDU on DL-SCH, enabling the eNB to periodically send timing adjustment commands to the UE. The network may also send timing adjustment commands as part of an RAR message. When the

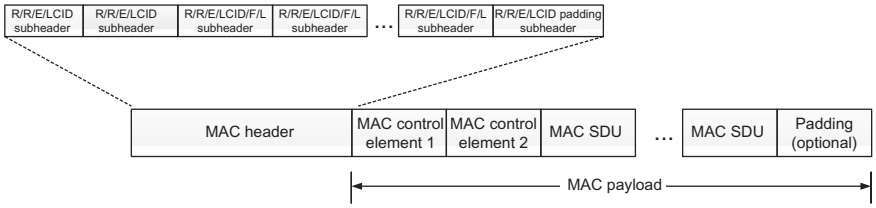


FIGURE 8.16

An example MAC PDU containing MAC header, MAC CEs, MAC SDUs, and padding [1].

Petitioners' Exhibit 1021
Nokia of America Corp., et al. v. KT Corporation, et al.
Case No. IPR2025-00036; U.S. Patent No. 11,627,631
Page 382 of 1122

Table 8.2 Values of the LCID for DL-SCH and UL-SCH [1]

Values of LCID for DL-SCH		Values of LCID for UL-SCH	
Index	**LCID Values**	**Index**	**LCID Values**
00000	CCCH	00000	CCCH
00001–01010	Identity of the logical channel	00001–01010	Identity of the logical channel
01011–11010	Reserved	01011–11000	Reserved
11011	Activation/deactivation	11001	Extended PHR
11100	UE contention resolution identity	11010	PHR
11101	Timing advance command	11011	C-RNTI
11110	DRX command	11100	Truncated BSR
11111	Padding	11101	Short BSR

command is sent as a control element, the timing advance is a 6-bit number that adjusts timing (advances or delays) relative to the current UE radio frame timing. If the command is sent via an RAR message, the timing advance is an 11-bit number that specifies absolute timing relative to the downlink radio frame. The eNB calculates the preferred timing advance based on uplink transmissions from the UE. The eNB also configures the UE's timing alignment timer. If the UE does not receive a timing advance MAC control element before the timing alignment timer expires, it is no longer considered to be uplink-synchronized with the cell.

The UE must apply the timing advance command when it receives it from the eNB. The command received in the nth frame is applied in the $(n + 6)$th frame. The command provides incremental value which adjusts the current timing alignment value. The incremental value may be negative or positive. Positive value advances and negative value delays the uplink transmission timing. If the UE does not receive a timing advance MAC control element before the timing alignment timer expires, it is no longer considered to be synchronized with the cell. When the timer expires, the UE must flush HARQ buffers and reinitialize the HARQ processes, release all PUCCH and sounding reference signal resources. If any uplink transmission is required, the UE must perform contention-based RACH synchronization procedures to obtain timing alignment and an uplink grant before it can transmit in the uplink.

The timing advance command MAC control element in LTE Rel-11 has a fixed size and consists of a single octet as shown in Figure 8.17. The information fields in this control element consist of a timing advance group[3] (TAG) identity (TAG ID), which indicates the TAG identity of the addressed TAG and the timing advance command. The TAG containing the PCell has the TAG identity value of zero. The

[3]A timing advance group is a group of serving cells that is configured by RRC signaling and uses the same timing reference cell and the same timing advance value. Primary timing advance group (pTAG) is the timing advance group containing the PCell. Secondary timing advance group (sTAG) is the timing advance group not containing the PCell [8].

Petitioners' Exhibit 1021
Nokia of America Corp., et al. v. KT Corporation, et al.
Case No. IPR2025-00036; U.S. Patent No. 11,627,631
Page 383 of 1122

length of this field is 2 bits. The timing advance command indicates the index value of timing advance $T_A = (0, 1, 2, \ldots, 63)$ that provides the amount of timing adjustment that the UE has to apply. The length of this field is 6 bits. Note that in the earlier releases of LTE, the leftmost 2 bits were reserved.

8.5.2 BSR control element

The BSR MAC control elements are used to report soft buffer size of either a single logical channel group (LCG) or a set of LCGs. An LCG is a group of logical channels identified by a unique 2-bit LCG ID. The mapping of logical channels to an LCG is set up during RRC configuration. There are up to four LCGs that can be set up per UE. The BSR reports aggregate bits across all logical channels of an LCG. As shown in Figure 8.18, there are two formats for the BSR: short/truncated BSRs indicate a buffer size of one LCG, and long BSR indicates buffer sizes of all four LCGs. The buffer size is encoded in 6 bits and includes all data in a logical channel buffer excluding the RLC/MAC headers. The structure of BSR MAC control elements are shown in Figure 8.18.

The UE generates three different types of BSRs as follows:

1. *Regular BSRs* are reported when data becomes available for a logical channel with higher priority than the logical channels for which data exists in the transmission buffer and has already been reported, when a serving cell changes, requiring the UE to report its buffer sizes to the new cell so that uplink resources can be scheduled, or when the timer *RETX_BSR_TIMER* expires and the UE has data available for transmission. This timer is restarted whenever there is an uplink grant and is used for retransmission of a BSR, if there is no allocation for the previous BSR sent by the UE. The regular BSRs can be short or long, depending on what data is available for transmission, and result in generation of a scheduling request at the physical layer.

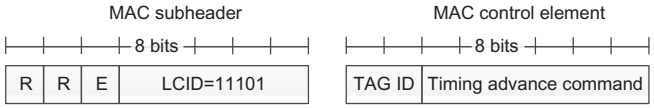


FIGURE 8.17

Uplink timing advance control element [1].

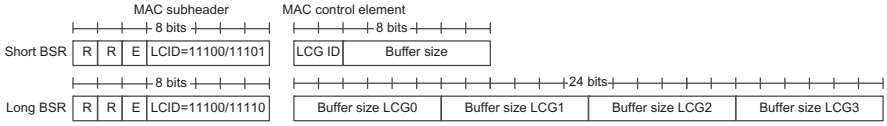


FIGURE 8.18

BSR control elements [1].

Petitioners' Exhibit 1021
Nokia of America Corp., et al. v. KT Corporation, et al.
Case No. IPR2025-00036; U.S. Patent No. 11,627,631
Page 384 of 1122

2. *Padding BSRs* enable the utilization of bits that would otherwise be used for padding. If the number of padding bits to be sent is equal to or greater than BSR MAC CEs, then BSRs can be sent in lieu of padding. Short, long, or truncated types of BSRs can be sent depending on the size of padding. The truncated BSRs are sent when data is available in more than one LCG, but the size of padding precludes sending long BSRs. In that case, the buffer size of the highest priority LCG is reported.
3. *Periodic BSRs* are sent when the configurable timer *PERIODIC_BSR_TIMER* expires. In this case, short or long BSRs can be sent.

8.5.3 Power headroom control element

The UE power headroom report (PHR) control element is used to report the power headroom available in the UE. The PHR is encoded in 6 bits with a reporting range from −23 dB to +40 dB in steps of 1 dB. Positive values indicate the difference between the maximum UE transmit power and current UE transmit power. Negative values indicate the difference between the maximum UE transmit power and the calculated UE transmit power. The UE transmit power is calculated assuming the UE were to transmit according to the current grant with allocated HARQ and RV configuration. The PHR can be configured either for periodic report or when the downlink path loss changes by a specific amount. For periodic reporting, a report is triggered by the expiration of the *PERIODIC_PHR_TIMER*, which can be configured with values between 10 ms and infinity. For threshold reporting, a PHR is triggered when the path loss changes by *DL_PathlossChange* (1, 3, 6, or infinite dB), provided that the configurable timer *PROHIBIT_PHR_TIMER* has

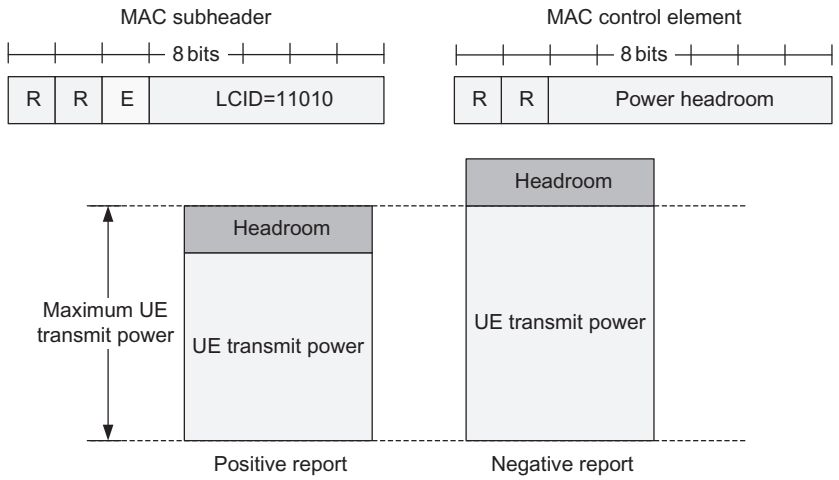


FIGURE 8.19

Power headroom control element [1].

expired. The *PROHIBIT_PHR_TIMER* timer starts when a PHR has been transmitted and can have values between 0 and 1000 ms. The structure of a PHR MAC CE is shown in Figure 8.19, as well as the graphical interpretation of the positive and negative PHRs.

8.5.4 Extended power headroom control element

The extended power headroom MAC control element was specified to support carrier aggregation in LTE Rel-10. In the case of carrier aggregation, the UE reports the power headroom of each component carrier independently. The PHRs provide the serving eNB with information about the difference between the UE maximum power and the estimated transmit power on PUSCH, or the transmit power on PUSCH and PUCCH on the primary carrier. There are two types of PHRs to support simultaneous transmission of PUSCH and PUCCH. Type-1 power headroom is used to report PUSCH transmit power and Type-2 power headroom is used when reporting PUSCH and PUCCH transmit powers. Figure 8.20 shows the order at which the power headroom corresponding to the primary cell and secondary cells are reported in the extended power headroom MAC control element. Note that P_{CMAX_k} in the figure denotes the maximum configured UE transmit power on the kth component carrier. The information fields within the extended power headroom MAC control element are as follows [1]:

- C_i: This bit indicates the presence of a power headroom field for the ith secondary component carrier (secondary cell). The C_i bit is set to one when the power headroom for the ith secondary cell is reported, i.e., the ith active secondary component carrier.
- The reserved bit R is set to zero.
- The information field V indicates whether the reported value of the power headroom is based on a real transmission or a reference. For Type-1 power headroom, $V =$ "0" indicates real transmission on PUSCH and $V = 1$ is indicative of a PUSCH reference format. For Type-2 power headroom, $V =$ "0" indicates real transmission on PUCCH and $V =$ "1" indicates that a PUCCH reference format is used. Furthermore, for both Type-1 and Type-2 power headroom, $V =$ "0" indicates the presence of an octet containing the associated P_{CMAX_k} field, and $V =$ "1" indicates that the octet containing the associated P_{CMAX_k} field is omitted.
- Power Headroom: This 6-bit field indicates the power headroom value.
- P: This field indicates whether the UE applies power backoff due to power management. The UE sets P to one if the corresponding P_{CMAX_k} field might have had a different value if no power backoff due to power management had been applied.
- P_{CMAX_k}: This field indicates the maximum configured UE transmit power on the kth component carrier that is used for calculation of the preceding power headroom value.

Petitioners' Exhibit 1021
Nokia of America Corp., et al. v. KT Corporation, et al.
Case No. IPR2025-00036; U.S. Patent No. 11,627,631
Page 386 of 1122

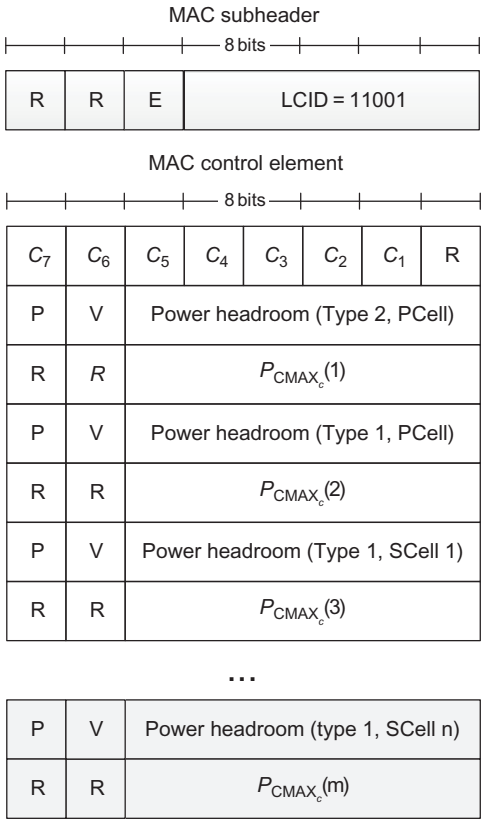


FIGURE 8.20

Extended power headroom control element [1].

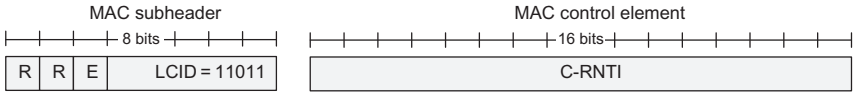


FIGURE 8.21

C-RNTI control element [1].

8.5.5 C-RNTI control element

The C-RNTI MAC control element is used to identify a UE when sending information over CCCH, and for the UE to transmit a dedicated C-RNTI during the random access procedure for the purpose of contention resolution. This CE has a fixed 16-bit size and consists of a single field, as shown in Figure 8.21.

Petitioners' Exhibit 1021
Nokia of America Corp., et al. v. KT Corporation, et al.
Case No. IPR2025-00036; U.S. Patent No. 11,627,631
Page 387 of 1122

8.5.6 Activation/deactivation control element

LTE Rel-10 specified an activation/deactivation mechanism for secondary cells, i.e., activation/deactivation does not apply to the primary cell, in order to enable reasonable UE battery consumption when carrier aggregation is configured for a UE. When a secondary cell is deactivated, the UE does not need to receive PDCCH or PDSCH on that secondary component carrier and cannot transmit in the corresponding uplink of that cell. However, the UE is required to perform channel quality indicator (CQI) measurements on the deactivated secondary cell. When a secondary cell is activated, the UE is required to monitor PDCCH in order to receive PDSCH and to perform CQI measurements on that cell.

If the UE is configured with one or more secondary cells, the network may activate and deactivate the configured secondary cells. The primary cell is always activated. The network activates and deactivates the secondary cells by sending the activation/deactivation MAC control element. Furthermore, the UE maintains an *sCellDeactivationTimer* per configured secondary cell and deactivates the associated secondary cell upon expiration of its timer. The same initial timer value applies to each instance of the *sCellDeactivationTimer* and it is configured by RRC sublayer. The configured secondary cells are initially deactivated upon addition and after a handover.

The activation/deactivation MAC control element is identified by a MAC PDU subheader with a unique LCID, as shown in Figure 8.22. It has a fixed size and consists of a single octet containing a 7-bit carrier activation/deactivation bitmap and one reserved bit which is set to zero. If the *i*th secondary cell is configured, then the C_i bit in this MAC control element indicates activation of the *i*th secondary cell when set to one.

8.5.7 MCH scheduling information control element

The structure of MCH scheduling information MAC control element is illustrated in Figure 8.23. This CE is transmitted for each MCH to inform the MBMS-capable UEs of scheduled data transmission on MTCH and has a variable size. For each MTCH the information fields include a 5-bit LCID which indicates the LCID of the MTCH and an 11-bit stop MTCH indicating the ordinal number of the subframe within the MCH scheduling period, counting only the subframes allocated to the MCH, where the corresponding MTCH stops, with the value of zero corresponding to the first subframe. The special stop MTCH value 2047 indicates that the corresponding MTCH is not scheduled. The range of values between 2043−2046 is reserved.

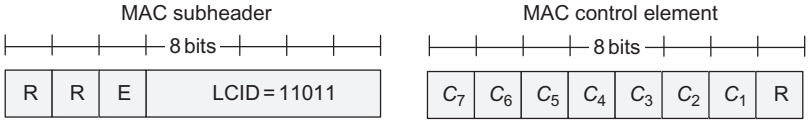


FIGURE 8.22

Activation/deactivation control element [1].

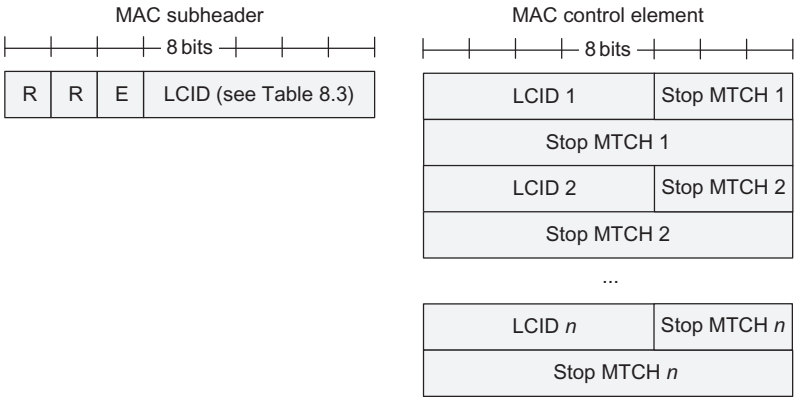


FIGURE 8.23

MCH scheduling information control element [1].

Table 8.3 Values of LCID for MBMS scheduling control element [1]

Index	LCID Values
00000	MCCH (assigned to MTCH, if there is no MCCH on MCH)
00001–11100	MTCH
11101	Reserved
11110	MCH scheduling information
11111	Padding

The MCH may be transmitted in subframes that are configured by an upper layer for MCCH or MTCH transmission. The transmission of an MCH occurs in a set of subframes defined by a *PMCH-Config* parameter. An MCH scheduling information MAC control element is included in the first subframe allocated to the MCH within the MCH scheduling period to indicate the position of each MTCH and unused subframes on the MCH. The UE assumes that the first scheduled MTCH starts immediately after the MCCH or the MCH scheduling information MAC control element, if the MCCH is not present, and the other scheduled MTCH(s) start immediately after the previous MTCH, at the earliest in the subframe where the previous MTCH stops [1] (Table 8.3).

8.5.8 UE contention resolution identity control element

The UE contention resolution identity MAC control element is used during the RACH procedure to resolve possible contention among multiple UEs that are trying to simultaneously access the network. This control element has a fixed 48-bit size and consists of a single field, as shown in Figure 8.24, containing the uplink CCCH SDU.

Petitioners' Exhibit 1021
Nokia of America Corp., et al. v. KT Corporation, et al.
Case No. IPR2025-00036; U.S. Patent No. 11,627,631
Page 389 of 1122

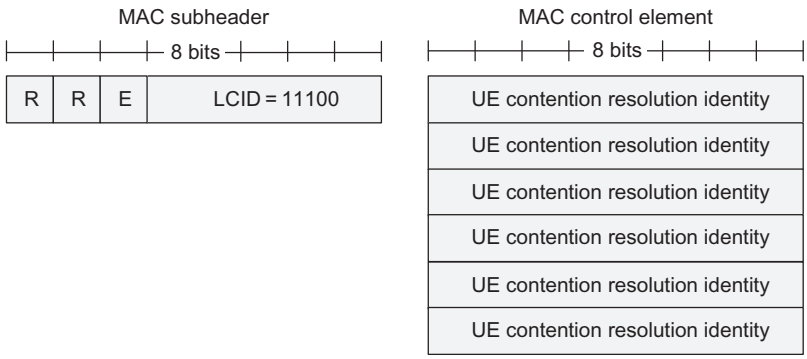


FIGURE 8.24

UE contention resolution identity control element [1].

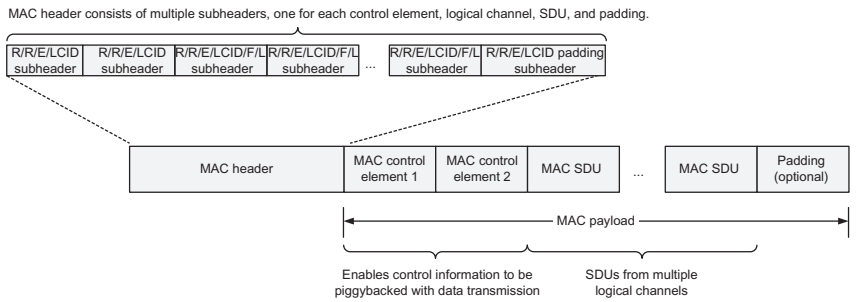


FIGURE 8.25

MAC PDU formation [1].

8.6 MAC PDU packet formats

A MAC PDU consists of a MAC header, zero or more MAC SDUs, zero or more MAC control elements, and optional padding. The MAC header and MAC SDUs may have variable sizes. As shown in Figure 8.25, a MAC PDU header consists of one or more MAC PDU subheaders where each subheader corresponds to a MAC SDU, a MAC control element, or padding. A MAC PDU subheader consists of the six header fields R/R/E/LCID/F/Length except for the last subheader in the MAC PDU and for fixed-size MAC control elements. The last subheader in the MAC PDU and subheaders for fixed-size MAC control elements as well as the subheader for padding consist of the four header fields R/R/E/LCID. Note that a MAC PDU is a bit string that is byte-aligned.

The structure of the MAC PDU used on UL-SCH and DL-SCH is shown in Figure 8.25. Each MAC PDU corresponds to one transport block and consists of a header, control elements, logical channel SDUs (corresponding to RLC PDUs), and

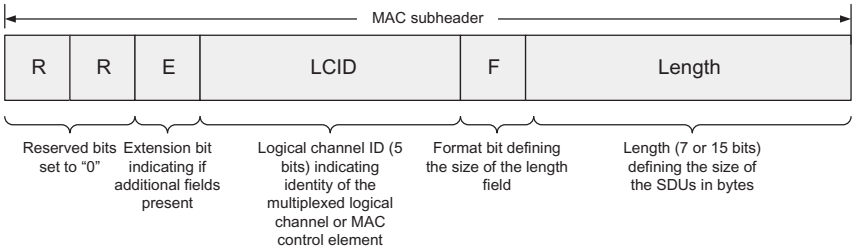


FIGURE 8.26

Structure of a MAC header [1].

optional padding. MAC control elements are used to piggyback control information, such as buffer status or power headroom reports. The MAC header consists of several subheaders. There is one subheader for each MAC control element and each MAC SDU in the PDU. In addition, there can be a subheader to specify padding. For the control element, the subheader identifies the specific control element being sent. For the MAC SDUs, the logical channel number and the size of the SDU are specified. All subheaders are grouped at the start of the MAC PDU in the MAC header. These are followed by the control elements, which are then followed by the MAC SDUs. Any padding occurs at the end of the PDU unless only one or two bytes of padding are required. Then one or two bytes of fixed-size padding subheaders can be included before the subheader corresponding to the first MAC SDU.

The subheader formats for MAC PDUs are shown in Figure 8.26. There are two formats: [R/R/E/LCID] which is used for fixed-length MAC SDUs and MAC control elements; and [R/R/E/LCID/F/Length] that is used for variable length MAC SDUs. The size of the first format is one byte. The size of the second format is either two or three bytes. In each case, the two R bits are reserved bits and are set to "0." The E bit is used to indicate if there are more subheader fields in the MAC header. A value of "1" denotes that another subheader would follow. A value of "0" indicates that a control element or MAC SDU starts at the next byte. The LCID field indicates either the logical channel number associated with the MAC SDU or, in the case of a control element, the specific type of MAC control element. The length field can be either 7 or 15 bits long and specifies the length of the MAC SDU in bytes. The size of the Length field is determined by the F field, which is "0" for 7 bits (128 bytes or less), or "1" for 15 bits.

8.7 MAC scheduling services

The MAC scheduler is responsible for scheduling the transfer of user data and control signaling via transport blocks in downlink and uplink subframes over the LTE air-interface. The MAC scheduler assigns the downlink and uplink physical layer resources used by the eNB and UEs within the cell. The scheduling decisions are based on information from various sources within the eNB radio

Petitioners' Exhibit 1021
Nokia of America Corp., et al. v. KT Corporation, et al.
Case No. IPR2025-00036; U.S. Patent No. 11,627,631
Page 391 of 1122

protocol stack and the UE. In the downlink, the MAC scheduler allocates resources which are used by the eNB MAC sublayer to send transport blocks to specific UEs via DL-SCH. These downlink transport blocks contain:

- Upper-layer data: All upper-layer data, whether this is user data or signaling messages, are fed into the MAC sublayer through logical channels. Whenever one of these logical channels has any data to send over the LTE air-interface, a buffer status indication is provided to the MAC scheduler.
- MAC sublayer data: This can either take the form of a HARQ retransmission or a MAC control element.

In the above cases, the MAC sublayer will provide an indication to the scheduler that it has data ready to send over the LTE air-interface. In the uplink, the MAC scheduler allocates resources to specific UEs which enable them to construct and send transport blocks to the eNB via UL-SCH. Each UE must request the uplink resources (except when semi-persistent scheduling is used) needed to send a transport block. This can be done in a number of ways. When a UE does not have an active connection to a cell, it performs the random access procedure to attach (or reattach) to the cell. When the UE has uplink control resources on the PUCCH physical channel, it sends a scheduling request indication to request uplink resources. When the UE already has resources to send data in the uplink on the UL-SCH, it may indicate to the scheduler that it has more data to send, and therefore requires more uplink resources. The UE does this by sending a BSR MAC control element. Based on HARQ feedback at the eNB, the scheduler might need to allocate uplink resources for HARQ retransmissions by the UE [12].

The output of the scheduling algorithm is a scheduling assignment per uplink and downlink subframe, which is signaled to UEs on the PDCCH. The downlink assignment information will be used by the eNB MAC sublayer to generate the transport blocks which are passed to the eNB physical layer and subsequently sent over the air. The uplink assignment information indicates which UEs have been allocated uplink resources within the subframe. It is also used by the eNB MAC sublayer to identify uplink transmissions in the corresponding uplink subframe. Before any user data can be transferred over the air, the scheduler needs to be configured with a cell-specific configuration, a UE-specific configuration, and finally a bearer-specific configuration for each active UE bearer. Reconfiguration of each UE and/or bearer is also possible. In order to make full use of the information available within the MAC scheduler, certain event-triggered or periodic feedback information is provided to higher layers. Based on this information, the higher layers are able to reconfigure the operation of the cell to provide a more efficient use of the air-interface. For monitoring purposes, the MAC scheduler may also output detailed information about subframe utilization. This may include but is not limited to the following: subframe map showing utilized physical resource blocks (PRBs); a percentage of utilized versus unutilized PRBs; and the number of logical channels/MAC control elements which have not been scheduled.

Petitioners' Exhibit 1021
Nokia of America Corp., et al. v. KT Corporation, et al.
Case No. IPR2025-00036; U.S. Patent No. 11,627,631
Page 392 of 1122

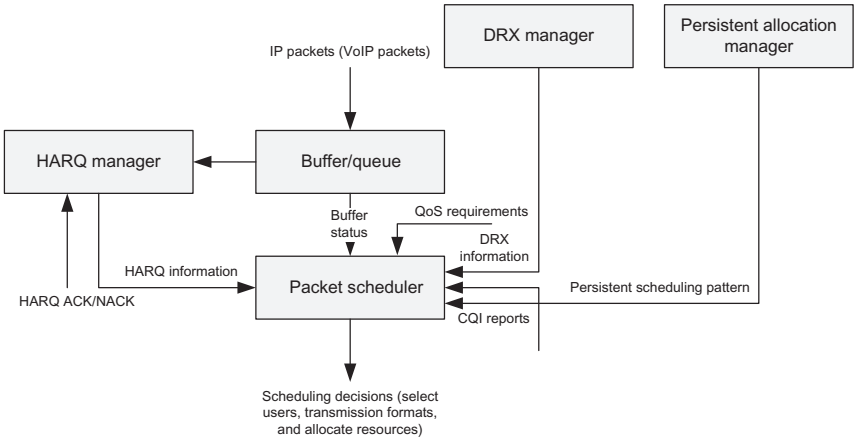


FIGURE 8.27

Main entities involved in packet scheduling in the eNB [15–17].

The scheduler in the eNB distributes the available radio resources in one cell among the UEs, and among the radio bearers of each UE. The details of the scheduling algorithm are left to the eNB implementation, but the signaling to support the scheduling is standardized. In principle, the eNB allocates downlink or uplink radio resources to each UE based on the downlink data buffered in the eNB and the BSRs received from the UE. In this process, the eNB considers the QoS requirements of each configured radio bearer and selects the size of the MAC PDU. The typical mode of scheduling is dynamic scheduling by means of downlink assignment messages for the allocation of downlink transmission resources and uplink grant messages for the allocation of uplink transmission resources; these are valid for specific subframes [12].

Figure 8.27 illustrates the interaction between the main entities involved in eNB scheduling services. These entities include packet scheduler, persistent allocation manager, HARQ manager, and DRX manager. Each newly arrived VoIP packet in the eNB buffer is associated with a discard timer. The discard timer specifies the maximum time a packet is allowed to be buffered in the eNB before it should be dropped. The HARQ manager deals with the new transmissions and pending retransmissions. The DRX manager is responsible for informing the packet scheduler when a specific UE is awake and can receive the L1/L2 control signaling, and thus can be scheduled dynamically. Besides informing each UE of the persistent resource allocation pattern by RRC signaling, the persistent allocation manager also forwards the persistent allocation patterns to the packet scheduler. The packet scheduler is the central controlling entity and makes scheduling decisions based on the buffer status, HARQ information, DRX information, QoS requirements, and persistent resource allocation patterns [13].

These messages also indicate whether the scheduled data is a fresh transmission of a new transport block or a retransmission, using a single-bit NDI. If the

Petitioners' Exhibit 1021
Nokia of America Corp., et al. v. KT Corporation, et al.
Case No. IPR2025-00036; U.S. Patent No. 11,627,631
Page 393 of 1122

value of the NDI is changed relative to its previous value for the same HARQ process, the transmission is the start of a new transport block. These messages are transmitted on PDCCH using a C-RNTI to identify the addressee (UE). This type of scheduling is efficient for service types, such as transport control protocol (TCP) or the signaling radio bearers (SRBs), in which the traffic is bursty and dynamic. The dynamic uplink transmission resource grants are valid for specific single subframes for initial transmissions, although they may also imply a resource allocation in later subframes for HARQ retransmissions [12].

8.7.1 Dynamic and semi-persistent scheduling

The UE may be dynamically scheduled on a per subframe basis, with the control information signaled on the PDCCH. In this case, the UE will be addressed using the C-RNTI. However, the UE may also receive a semi-persistent grant or allocation where the UE is addressed using the SPS-C-RNTI. In this case, the scheduling control information is signaled once via the PDCCH. The UE can then transmit/receive periodically following a pattern defined by the downlink semi-persistent scheduling interval parameter using the same configuration until modified or released. When a dynamic allocation or grant is received that corresponds to a subframe where an semi-persistent scheduling scheduled transmission would occur, the dynamic grant takes precedence. Additionally, any retransmissions would be scheduled dynamically via the PDCCH.

VoIP is characterized by small packet size and very stringent delay and jitter requirements, and a large number of simultaneous users. In LTE, the scheduling of the data traffic is based on the shared-channel transmission and the channel-dependent resource allocation. The eNB allocates radio resources in units of resource blocks to UEs, and sends the scheduling information to each UE on PDCCH. Such dynamic channel-dependent scheduling can exploit the selectivity in both the time and frequency domain, and significantly improve the system throughput. However, applying dynamic scheduling directly for VoIP packets is not desirable. This is mainly due to the small packet size and the constant inter-arrival time of VoIP packets, which results in large control overhead as control information should be transmitted per TTI. Many UEs may be scheduled simultaneously, so the limited resources available on the PDCCH for control signaling become a bottleneck for the VoIP capacity.

The semi-persistent scheduling is a feature that significantly reduces control channel overhead for applications that require persistent radio resource allocations, such as VoIP. In LTE, both downlink and uplink radio resources are fully scheduled since downlink and uplink traffic channels are shared channels. This means that the PDCCH must provide access grant information to indicate which users should decode PDSCH in each subframe, and which users are allowed to transmit on PUSCH in each subframe. Without semi-persistent scheduling, every downlink or uplink resource block allocation must be granted via an access grant

Petitioners' Exhibit 1021
Nokia of America Corp., et al. v. KT Corporation, et al.
Case No. IPR2025-00036; U.S. Patent No. 11,627,631
Page 394 of 1122

message on the PDCCH. This is sufficient for most bursty best effort types of applications, which generally have large packet sizes and thus typically only a few users must be scheduled in each subframe. However, for applications that require persistent allocations of small packets, such as VoIP, the access grant control channel overhead can be greatly reduced with semi-persistent scheduling.

Semi-persistent scheduling introduces a persistent resource allocation that a user should expect on the downlink or can transmit on the uplink. There are many different ways in which semi-persistent scheduling can set up persistent allocations. Note that speech codecs typically generate a speech packet every 20 ms. In LTE, HARQ RTT is 8 ms, which means retransmissions of resource blocks that have failed to be decoded can occur every 8 ms. Once speech packets stop arriving (i.e., silence period), these radio resources can be reassigned to other users. When the user begins talking again, a new semi-persistent scheduling set of radio resources would be assigned for the duration of the new talk spurt. Note that dynamic scheduling of best effort data can occur on top of semi-persistent scheduling, but the semi-persistent scheduling allocations would take precedence over any scheduling conflicts.

In wireless networks, persistent scheduling takes advantage of the traffic characteristics of the application (e.g., VoIP) to increase the number of users running that application in the system. The periodic nature of the packet arrivals from a VoIP source allows the needed resource to be allocated persistently for the period of an active talk spurt. Consequently, base stations can send the allocation information once at the beginning of a talk spurt and avoid sending different allocation information for each subsequent packet. Significant amounts of radio resources that would otherwise be occupied by unnecessary overhead can be used to accommodate VoIP packets from other users. Because VoIP packets are usually small in size, the savings from reduced overhead can significantly increase the overall system capacity. The capacity gain from persistent scheduling, however, can be compromised significantly due to dynamic link adaptation, which is a very common technique in wireless systems to adapt to dynamic variation in wireless channel condition. The underlying concept of persistent and dynamic scheduling is illustrated in Figure 8.28.

When semi-persistent scheduling is enabled by the RRC sublayer, the following information is provided: semi-persistent scheduling C-RNTI; uplink semi-persistent

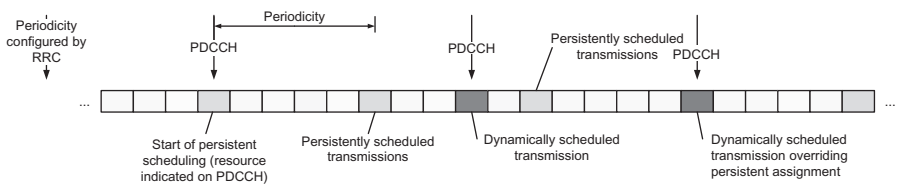


FIGURE 8.28

Illustration of an example of semi-persistent and dynamic scheduling [10].

Petitioners' Exhibit 1021
Nokia of America Corp., et al. v. KT Corporation, et al.
Case No. IPR2025-00036; U.S. Patent No. 11,627,631
Page 395 of 1122

scheduling interval; the number of empty transmissions before implicit release; downlink semi-persistent scheduling interval; and the number of configured HARQ processes for semi-persistent scheduling. When semi-persistent scheduling for uplink or downlink is disabled by the RRC sublayer, the corresponding configured grant or configured assignment is discarded. Semi-persistent scheduling is supported on the PCell only, and is not supported for relay node communication with the E-UTRAN in combination with a relay node subframe configuration.

After a semi-persistent downlink assignment is configured for a UE, the UE's downlink assignments occur every Nth subframe in a subframe whose number n_{subframe} satisfies the following equation $(10\text{SFN} + n_{\text{subframe}}) = [(10\text{SFN}_{\text{start-time}} + n_{\text{subframe}_{\text{start-time}}}) + NT_{\text{semiPersistSchedIntervalDL}}]\text{mod}10240$, where $\text{SFN}_{\text{start-time}}$ and $n_{\text{subframe}_{\text{start-time}}}$ are the SFN and subframe numbers at which the configured downlink assignment was initiated/reinitiated. Following configuration of a semi-persistent scheduled uplink grant for the UE, the UE will sequentially have uplink grants every Nth subframe for which $(10\text{SFN} + n_{\text{subframe}}) = [(10\text{SFN}_{\text{start-time}} + n_{\text{subframe}_{\text{start-time}}}) + NT_{\text{semiPersistSchedIntervalUL}} + \textit{Subframe} - \textit{Offset}(N \bmod 2)]\text{mod}10240$, where $\text{SFN}_{\text{start-time}}$ and $n_{\text{subframe}_{\text{start-time}}}$ are the SFN and subframe number at which the configured uplink grants were initialized/reinitialized. The UE is required to release the configured uplink grant immediately after a certain number of consecutive new MAC PDUs, each containing zero MAC SDUs, have been provided by the multiplexing and assembly entity on the semi-persistent scheduled resource. The retransmissions for semi-persistent scheduling can continue after releasing the configured uplink grant [1].

8.7.2 Proportional fair scheduling algorithm

Proportional fair is a commonly-used scheduling algorithm, which is based on maintaining a balance between two competing interests: maximizing the overall system throughput while at the same time providing all users with a minimum level of service. This is done by assigning each data flow a data rate or a scheduling priority (depending on the implementation) that is inversely proportional to its anticipated resource consumption. The proportional fair (PF) scheduling algorithm calculates a metric for all active users in a given scheduling interval. The user with the highest metric is allocated the resource available in the given interval, while the metrics for all users are updated before the next scheduling interval, and the process repeats. To adapt this simple algorithm to orthogonal frequency division multiple access systems, the definition of scheduling interval and scheduling resource are extended to encompass a two-dimensional OFDMA frame structure. For OFDMA systems, the scheduling interval is typically a radio frame and multiple users may be allocated in the same radio frame. Therefore, in the simplest extension to OFDMA systems, two modifications are made to the PF scheduling algorithm: (1) frames are equally partitioned into regular, fixed scheduling resources that are scheduled sequentially until all available resources are

Petitioners' Exhibit 1021
Nokia of America Corp., et al. v. KT Corporation, et al.
Case No. IPR2025-00036; U.S. Patent No. 11,627,631
Page 396 of 1122

assigned; (2) the metric is updated after scheduling each partition. Note that the number of resources eventually allocated to a user depends on the metric update process and does not preclude a single user from obtaining multiple or all the resources in a frame. For system simulations with the assumption of a fixed overhead allowing up to $N_{\text{Partitions}}$ resource partitions, each partition assignment should be considered as a separate packet transmission. The number of partitions $N_{\text{Partitions}}$, the time constant of the filter used in the metric computation, and the number of active users are simulation parameters. At any scheduling instant t, the scheduling metric $M_i(t)$ for subscriber i used by the PF scheduler is given by the following expression:

$$M_i(t) = \frac{R_{\text{instantaneous}_i}(t)}{[R_{\text{average}_i}(t)]^{\alpha}} \tag{8.3}$$

where $R_{\text{instantaneous}_i}(t)$ is the data rate that can be supported at scheduling instant t for the ith user. $R_{\text{instantaneous}_i}(t)$ is a function of the CQI feedback, and consequently a function of the MCS that can meet the packet error rate requirement. Parameter $R_{\text{average}_i}(t)$ denotes the throughput function smoothed by a low-pass filter at the scheduling instant t for user i. The parameter α is a fairness exponent factor with a default value of one. For a scheduled subscriber $R_{\text{average}_i}(t)$ is computed as follows:

$$R_{\text{average}_i}(t) = \frac{1}{N_{\text{PF}}} R_{\text{instantaneous}_i}(t) + \left(1 - \frac{1}{N_{\text{PF}}}\right) R_{\text{average}_i}(t-1) \tag{8.4}$$

For an unscheduled subscriber, the throughput function is given by:

$$R_{\text{average}_i}(t) = \left(1 - \frac{1}{N_{\text{PF}}}\right) R_{\text{average}_i}(t-1) \tag{8.5}$$

The latency scale of the PF scheduler N_{PF} is given by:

$$N_{\text{PF}} = \frac{T_{\text{PF}} N_{\text{Partitions}}}{T_{\text{Frame}}} \tag{8.6}$$

where T_{PF} represents the latency time scale in units of seconds and T_{Frame} is the frame duration of the system. In some implementations, the scheduler may give priority to HARQ retransmissions.

8.8 RNTI mapping

The users in LTE radio access networks are assigned temporary identifiers for identification while protecting their privacy and confidentiality. Depending on the state of the UE, different types of temporary identifiers are used. Table 8.4 summarizes the RNTIs and their usage in a LTE radio access network. Each RNTI is a 16-bit

Petitioners' Exhibit 1021
Nokia of America Corp., et al. v. KT Corporation, et al.
Case No. IPR2025-00036; U.S. Patent No. 11,627,631
Page 397 of 1122

string that is assigned to a UE depending on the state of the UE in the LTE radio access network. For example, the RA-RNTI is used on PDCCH when RAR messages are transmitted. It unambiguously identifies which time-frequency resource was utilized by the UE to transmit the random access preamble. The DCI formats 1A and 1C with CRCs scrambled with RA-RNTI allocate DL-SCH resources to RAR messages. There is a one-to-one mapping between the RA-RNTI and the time-frequency resource used by the UE when transmitting the random access preamble. The one-to-one association allows the eNB to address RAR messages to a specific UE. The Msg3 acronym in Table 8.4 denotes the *RRC Connection Request* message transmitted on UL-SCH containing a C-RNTI MAC control element or CCCH SDU, submitted from the upper layer and associated with the UE contention resolution identity, as part of a random access procedure [10–12].

The P-RNTI is used during the paging procedure, where the UE searches for DCI formats 1A and 1C whose CRC bits are scrambled with P-RNTI. These DCI

Table 8.4 Various RNTIs and Their Usage in LTE [1]

RNTI	Usage	Transport Channel	Logical Channel
Paging RNTI (P-RNTI)	Paging and system information change notification	PCH	PCCH
SI-RNTI	Broadcast of SI	DL-SCH	BCCH
MBMS RNTI (M-RNTI)	MCCH information change notification	N/A	N/A
RA-RNTI	Random Access Response	DL-SCH	N/A
Temporary C-RNTI	Contention resolution (when no valid C-RNTI is available)	DL-SCH	CCCH
Temporary C-RNTI	Msg3 transmission (RRC connection request)	UL-SCH	CCCH, DCCH, DTCH
Cell RNTI (C-RNTI)	Dynamically scheduled unicast transmission	DL-SCH, UL-SCH	DCCH, DTCH
C-RNTI	Triggering of PDCCH ordered random access	N/A	N/A
SPS C-RNTI	Semi-persistently scheduled unicast transmission (activation, reactivation, and retransmission)	DL-SCH, UL-SCH	DCCH, DTCH
SPS C-RNTI	Semi-persistently scheduled unicast transmission (deactivation)	N/A	N/A
TPC-PUCCH-RNTI	Physical layer uplink power control	N/A	N/A
TPC-PUSCH-RNTI	Physical layer uplink power control	N/A	N/A

Petitioners' Exhibit 1021
Nokia of America Corp., et al. v. KT Corporation, et al.
Case No. IPR2025-00036; U.S. Patent No. 11,627,631
Page 398 of 1122

formats allocate DL-SCH resources to the PCCH and PCH, i.e., the UE proceeds to decode a paging message following detection of a DCI format whose CRC bits are scrambled with P-RNTI. The paging message may include paging information as well as system information change notification, earthquake and tsunami warning system notification, and commercial mobile alert system.

The SI-RNTI is used during the transmission of SIBs on DL-SCH. The UE searches for DCI formats 1A and 1C whose CRC bits are scrambled with SI-RNTI. DCI formats 1A and 1C allocate DL-SCH resources to BCCH. Upon detection of these DCI formats, the UE proceeds to decode the system information message.

The M-RNTI is used during transmission of an MCCH change notification. The UE searches for a DCI format 1C whose CRC is scrambled with M-RNTI. This DCI format includes a bit string of 8 bits, where each bit corresponds to one of the MBSFN areas listed in SIB13. A change in MCCH is signaled by setting the corresponding bit to one.

The temporary C-RNTI is allocated to the UE within the RAR message. The temporary C-RNTI is used for contention resolution when a C-RNTI has not yet been assigned and specifically in the transmission of the RRC connection request on CCCH during initial access. After transmitting Msg3 in the uplink, the UE searches for DCI formats 1A or 1C whose CRC bits are scrambled with the UE's temporary C-RNTI. The successful detection of the temporary C-RNTI is considered success of the contention resolution and assignment of a C-RNTI to the UE. The temporary C-RNTI is also used for scrambling of PUSCH during initial Msg3 transmission on CCCH.

The C-RNTI is assigned to the UE following successful completion of the random access procedure. The C-RNTI is reassigned during the handover procedure by specifying a new value within the *RRC Connection Reconfiguration* message. The C-RNTI is used to identify the UE in all downlink and uplink control and data transmissions when the UE is in the RRC_CONNECTED state. The UE uses the same C-RNTI in all serving cells when supporting carrier aggregation.

The SPS-C-RNTI is allocated to a UE using an *RRC Connection Setup* or an *RRC Connection Reconfiguration* message, when the resources are going to be allocated for more than a single subframe. The transmit power control (TPC) PUSCH/PUCCH RNTI is used for power control of PUSCH/PUCCH. The CRC bits of DCI formats 3 and 3A are scrambled with TPC-PUSCH-RNTI/TPC-PUCCH-RNTI to convey the power control commands to the UE. TPC-PUSCH-RNTI/TPC-PUCCH-RNTI can be allocated using either the *RRC Connection Setup* or *RRC Connection Reconfiguration* messages [10]. The mapping of different types of RNTI to logical channels is depicted in Figure 8.29.

8.9 Random access procedure

The UE must be synchronized in the uplink before it can send signaling or data. For the uplink, the UEs within a cell's coverage area are physically distributed at different distances from the eNB location. As a result, each UE will experience a

Petitioners' Exhibit 1021
Nokia of America Corp., et al. v. KT Corporation, et al.
Case No. IPR2025-00036; U.S. Patent No. 11,627,631
Page 399 of 1122

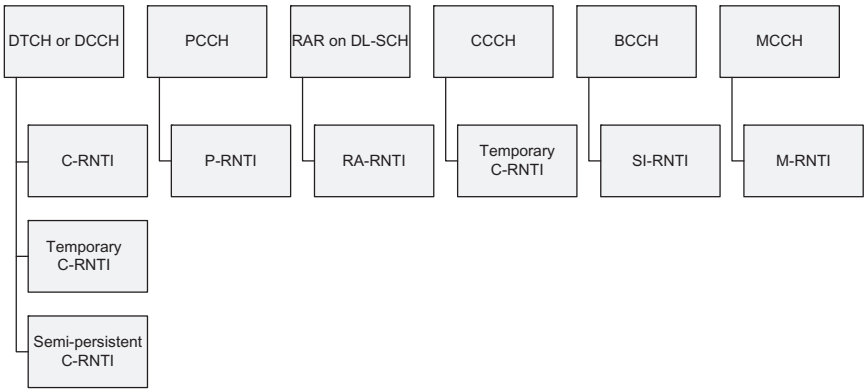


FIGURE 8.29

RNTI mapping to control or traffic logical channels.

different propagation delay when accessing the network. Without synchronization, subframes transmitted from different UEs would likely overlap and interfere with each other. To overcome this problem, the UE performs uplink synchronization procedures on RACH during initial access to the network. In LTE, random access is used for several purposes including initial access when establishing a radio link, i.e., transitioning from RRC_IDLE to RRC_CONNECTED state, reestablishing the radio link after a radio link failure, performing handover when uplink synchronization, needs to be established with the target cell, establishing uplink synchronization if uplink or downlink data arrives when the terminal is in the RRC_CONNECTED state and the uplink is not synchronized, positioning during RRC_CONNECTED state which requires a random access procedure, e.g., when timing advance is needed for UE positioning, and scheduling request if no dedicated scheduling-request resources have been configured on PUCCH.

The process is initiated by sending RACH preambles using physical random access channel (PRACH). The procedure may be contention-based or contention-free. In the contention-based procedure, the UE selects a preamble from a set containing two groups of preamble sequences. If two UEs select the same preamble in the same RACH resource, a collision can result that must be resolved before either UE can access the system. The contention-based RACH is generally used during initial access or if the UE has lost uplink synchronization. In contention-free synchronization, the UE uses a dedicated preamble and it is likely to be already connected to the network and must resynchronize following a handover to a new cell.

Figure 8.30 shows the RACH process at a high level. During the first step the UE transmits a preamble randomly selected from 64 possible preamble sequences divided into two groups. The group from which the UE selects the preamble depends on the size of the message that it would like to transmit and on the

Petitioners' Exhibit 1021
Nokia of America Corp., et al. v. KT Corporation, et al.
Case No. IPR2025-00036; U.S. Patent No. 11,627,631
Page 400 of 1122

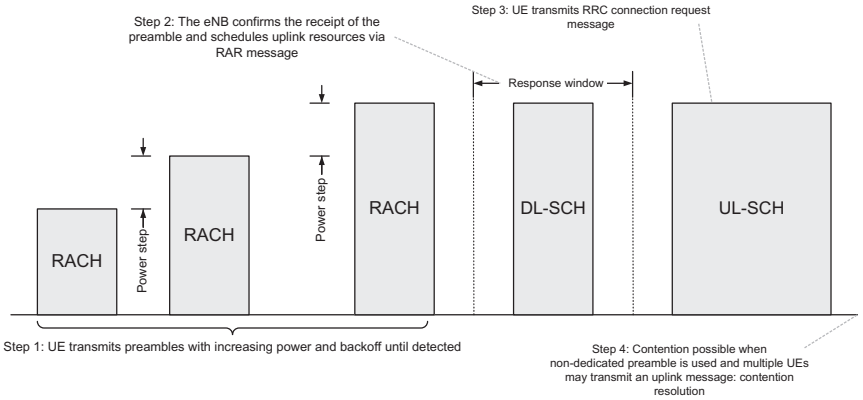


FIGURE 8.30

Illustration of a contention-based random access procedure [21].

calculated path loss to the eNB. Once the preamble is transmitted, the UE monitors the downlink beginning three subframes after the end of the preamble for a duration controlled by a configurable window. If no downlink response is detected, then the preamble is retransmitted with a power that is increased by a configurable parameter. This process continues until the defined maximum number of preamble transmissions is reached. If the preamble is successfully detected by the eNB, then the downlink RAR message is sent by the eNB allocating resources for the UE to transmit its message or enforcing a backoff. In the final step, contention resolution must be performed for a contention-based access attempt. Therefore, as soon as the random access preamble is transmitted and regardless of the possible occurrence of a measurement gap, the UE is required to monitor PDCCH on the primary cell for RAR(s) identified by RA-RNTI during the RAR window (in time) which starts at the subframe that contains the end of the preamble transmission plus three subframes and has the length *ra-ResponseWindowSize* subframes (Figure 8.30) [1].

The UE sets its initial power level to the following value *PREAMBLE_INITIAL_RECEIVED_TARGET_POWER* + *DELTA_PREAMBLE* where *DELTA_PREAMBLE* depends on the type of preamble format. The UE selects the first available RACH resource for the transmission. If there is no response within three subframes + *ra_Response_Window* (defined in number of subframes), the UE assumes the previous transmission was unsuccessful. It selects another RACH preamble, performs the backoff procedure, and transmits again. The power level is increased by *POWER_RAMP_STEP*. This process can be repeated until the *PREAMBLE_TRANSMISSION_COUNTER* limit is reached. In that case, an access failure is declared to the upper layers.

In LTE Rel-10 and when carrier aggregation is supported, the random access procedure is initiated by a PDCCH order or by the MAC sublayer. The random access procedure on a secondary cell is only initiated by a PDCCH order

Petitioners' Exhibit 1021
Nokia of America Corp., et al. v. KT Corporation, et al.
Case No. IPR2025-00036; U.S. Patent No. 11,627,631
Page 401 of 1122

(i.e., non-contention-based random access procedure). If the UE receives a PDCCH order masked with the UE's C-RNTI, and for a specific serving cell, the UE initiates a random access procedure on that serving cell. For random access on the primary cell, a PDCCH order or RRC message optionally indicates the *ra-PreambleIndex* and the *ra-PRACH-MaskIndex* parameters; whereas for random access on a secondary cell, a PDCCH order indicates the *ra-PreambleIndex* (with a value different from 000000) and the *ra-PRACH-MaskIndex* parameters. For the primary TAG, preamble transmission on PRACH and reception of a PDCCH order are only supported for the primary cell [1]. In LTE Rel-11, the random access procedure is also performed on a secondary cell to establish timing alignment for the corresponding secondary TAG. Furthermore, a non-contention-based random access procedure can be performed for obtaining timing advance alignment for a secondary TAG [8].

8.9.1 Contention-based RACH procedure

The UE selects a preamble from the set of preambles. Two groups of sequences are available for a contention-based RACH procedure defined as Group A and Group B. The size of the Group A preamble set is defined by the *sizeofRA-PreamblesGroupA* parameter. The remaining preambles, up to *numberofRA-Preambles*-1, belong to Group B. Group B preambles are utilized if the required message size exceeds *MESSAGE_SIZE_GROUP_A* and the path loss is less than $P_{\max} - PREAMBLE\_INITIAL\_RECEIVED\_TARGET\_POWER - DELTA\_PREAMBLE\_MSG3 - messagePowerOffsetGroupB$ where $P_{\max}$ is the maximum UE transmit power. This enables the eNB to estimate the size of the message that the UE wants to transmit. If the eNB detects a preamble, it sends a RAR message in the DL-SCH. The MAC PDU containing the RAR message is addressed using the RA-RNTI which is calculated as $RA-RNTI = 1 + t\_id + 10f\_id$ where $0 \le t\_id < 10$ is the index of the first subframe of RACH resource within a frame, and $0 \le f\_id < 6$ is the specified RACH resource within that subframe. This forms a one-to-one mapping between the selected RACH resource and the RA-RNTI. The RAR message contains an identifier to enable identification of the preamble sent by the UE, the absolute timing advance, a temporary C-RNTI, and an uplink grant. If the preamble identifier matches the preamble sent by the UE, the UE applies the timing advance and starts the contention resolution procedure (see Figure 8.31).

During contention resolution, the UE transmits an uplink message on CCCH that includes a terminal identifier. If this matches the identifier used in the response from the eNB, then the UE has successfully completed the contention resolution; otherwise, the UE must restart the random access procedure. Upon successful contention resolution, the temporary C-RNTI assigned as part of the RAR message will become the C-RNTI.

Petitioners' Exhibit 1021
Nokia of America Corp., et al. v. KT Corporation, et al.
Case No. IPR2025-00036; U.S. Patent No. 11,627,631
Page 402 of 1122

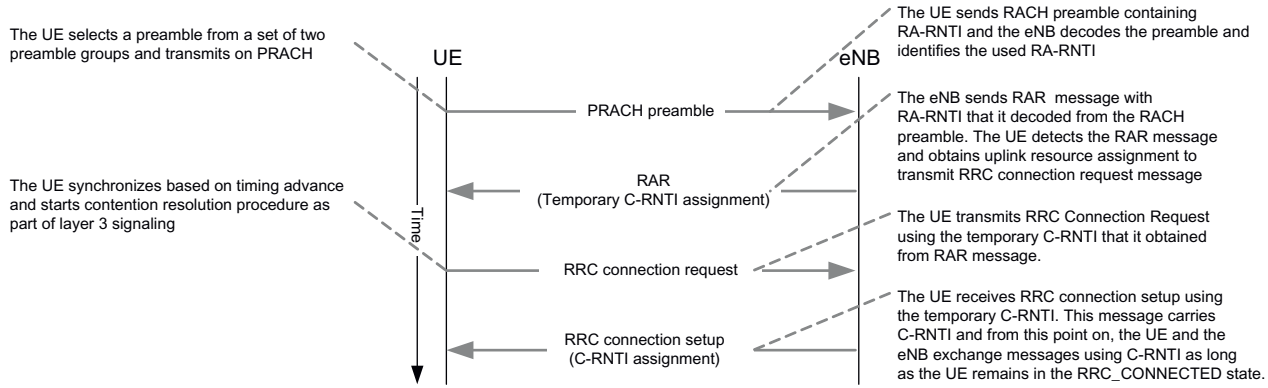


FIGURE 8.31

Breakdown of the contention-based random access procedure [21].

Petitioners' Exhibit 1021
Nokia of America Corp., et al. v. KT Corporation, et al.
Case No. IPR2025-00036; U.S. Patent No. 11,627,631
Page 403 of 1122

8.9.2 Contention-free RACH procedure

During handovers, the UE must synchronize to the target cell using RACH procedures. However, contention-based random access may result in an unacceptable delay. Therefore, a contention-free procedure is defined. In contention-free RACH, the RRC sublayer defines which RACH preamble sequence and which PRACH resources to utilize. The preamble is dedicated to the UE and is different from those used for Groups A and B in the contention-based process, thus avoiding any possible collision. The PRACH resource to be used for the dedicated transmission is indicated as PRACH Mask, which specifies the subframe number in which the UE can transmit the preamble.

Once the UE transmits the dedicated preamble in the first available RACH resource after receiving the command, it waits for a response in the form of an RAR message from the eNB. The same timing and window specification is enforced in this procedure as those associated with the contention-based procedure. Once the RAR message is received on PDCCH, the UE checks whether the random access preamble identifier (RAPID) contained in the message matches the preamble that was sent and, if so, it applies the timing advance and synchronizes with the eNB.

As mentioned earlier, the MAC PDU that carries the RAR message on PDCCH contains a number of RARs, since multiple UEs may transmit on the uplink RACH resource at the same time. As shown in Figure 8.32, the MAC PDU starts with the MAC header, which contains a number of subheaders. For each RAR message, there is a subheader that identifies the RACH Preamble Identifier that was used for the transmission in uplink. The corresponding RAR payload contains the detailed information on the timing advance, uplink grant, and temporary C-RNTI. The MAC header may also include a backoff indicator (BI) subheader which indexes a backoff ranging from 0 to 960 ms. It is applicable to all the UEs that use a specific RACH resource.

The MAC subheader for the RAR message is 8 bits and can have one of the two formats shown in Figure 8.33. Both RAR formats begin with an E field, which is a single bit that indicates if another subheader is present after the current subheader, and a T field, which is a single bit that defines if this is a subheader that assigns uplink resources or informs all UEs that utilize the RACH resource to

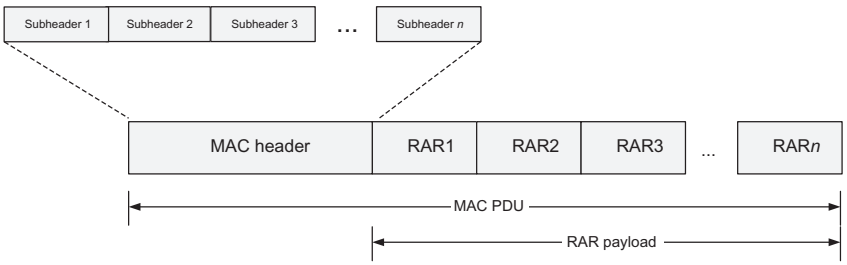


FIGURE 8.32

RAR message structure [1].

backoff. If resources are assigned in a RAR payload, then T is set to "1" and the following field is the 5-bit RAPID value. In this case, there will be an RAR payload to specify the specific grant. If the eNB is enforcing a backoff for all UEs utilizing the RACH resource, then T is set to "0" and the following field consists of two single-bit R (reserved) fields followed by a 4-bit BI that indexes a table of 13 possible backoff periods ranging from 0 to 960 ms.

As shown in Figure 8.34, the RAR payload consists of 48 bits described as follows:

- R: A single reserved bit set to "0."
- TA: The 11-bit timing advance specifies the absolute timing advance that should be applied to the uplink transmissions in units of $16T_s$ (sampling time).
- Uplink grant: 20 bits that specify attributes of the uplink grant. This includes hopping flag (1 bit), defines if frequency hopping is used in the uplink, Fixed-size resource block assignment (10 bits), defines the uplink resource blocks, Truncated MCS (4 bits), TPC command for scheduled PUSCH (3 bits), uplink delay (1 bit), controls which uplink subframe is used for the initial transmission, and CQI request (1 bit), specifies if a CQI report is sent in PUSCH transmission for non-contention-based RACH.
- Temporary C-RNTI: Temporary identifier utilized by the UE until contention resolution is complete.

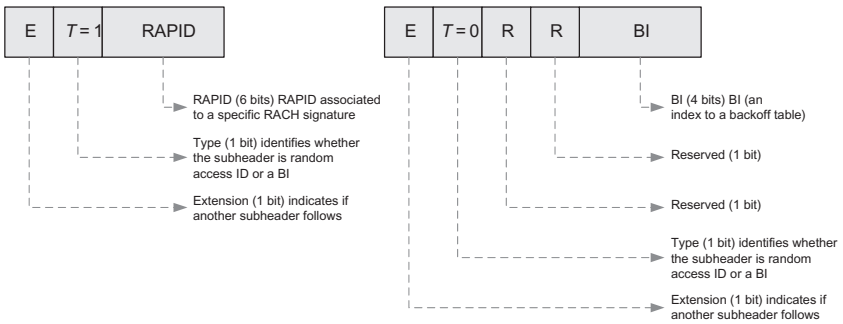


FIGURE 8.33

Structure of RAR subheaders [1].

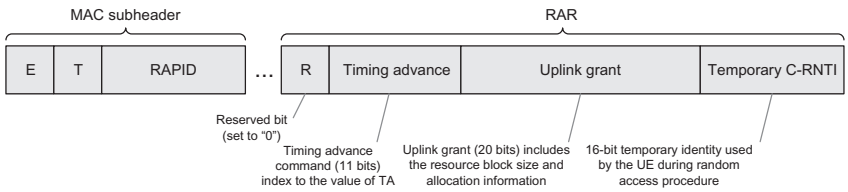


FIGURE 8.34

Structure of RAR payload [1].

Petitioners' Exhibit 1021
Nokia of America Corp., et al. v. KT Corporation, et al.
Case No. IPR2025-00036; U.S. Patent No. 11,627,631
Page 405 of 1122

References

3GPP Specifications

[1] 3GPP TS 36.321, Evolved Universal Terrestrial Radio Access (E-UTRA); Medium Access Control (MAC) Protocol Specification (Release 11), December 2012.

[2] 3GPP TS 36.322, Evolved Universal Terrestrial Radio Access (E-UTRA); Radio Link Control (RLC) Protocol Specification (Release 11), December 2012.

[3] 3GPP TS 36.323, Evolved Universal Terrestrial Radio Access (E-UTRA); Packet Data Convergence Protocol (PDCP) Specification (Release 11), December 2012.

[4] 3GPP TS 36.331, Evolved Universal Terrestrial Radio Access (E-UTRA); Radio Resource Control (RRC) Protocol Specification (Release 11), December 2012.

[5] 3GPP TS 36.211, Evolved Universal Terrestrial Radio Access (E-UTRA), Physical Channels and Modulation (Release 11), December 2012.

[6] 3GPP TS 36.212, Evolved Universal Terrestrial Radio Access (E-UTRA) Multiplexing and Channel Coding (Release 11), December 2012.

[7] 3GPP TS 36.213, Evolved Universal Terrestrial Radio Access (E-UTRA); Physical Layer Procedures (Release 11), December 2012.

[8] 3GPP TS 36.300, Evolved Universal Terrestrial Radio Access (E-UTRA) and Evolved Universal Terrestrial Radio Access Network (E-UTRAN) Overall Description, Stage 2 (Release 11), December 2012.

[9] 3GPP TS 36.133, Evolved Universal Terrestrial Radio Access (E-UTRA); Requirements for Support of Radio Resource Management (Release 11), December 2012.

Books

[10] C. Johnson, Long Term Evolution in 10, second ed., Create Space Independent Publishing Platform, July 2012.

[11] S. Sesia, I. Toufik, M. Baker, LTE, the UMTS Long Term Evolution: From Theory to Practice, second ed., John Wiley & Sons, August 2011.

[12] E. Dahlman, S. Parkvall, J. Skold, 4G: LTE/LTE-Advanced for Mobile Broadband, Academic Press, May 2011.

Articles

[13] Y. Fan, P. Lundén, M. Kuusela, M. Valkama, Efficient semi-persistent scheduling for VoIP on E-UTRA downlink, in: Proceedings of the IEEE VTC-2008, Calgary, Canada, September 2008.

[14] Y. Fan, M. Kuusela, P. Lundén, M. Valkama, Downlink VoIP support for Evolved UTRA, in: Proceedings of the IEEE WCNC-2008, Las Vegas, NV, April 2008.

[15] A. Pokhariyal, T.E. Kolding, Performance of downlink frequency domain packet scheduling for the UTRAN long term evolution, in: Proceedings of the IEEE PIMRC-2006, Helsinki, Finland, September 2006.

[16] K.I. Pedersen, et al., Frequency domain scheduling for OFDMA with limited and noisy channel feedback, in: Proceedings of the IEEE VTC-2007, Baltimore, MD, September 2007.

[17] Y. Sun, et al., Multi-user scheduling for OFDMA downlink with limited feedback for Evolved UTRA, in: Proceedings of the IEEE VTC-2006, Montreal, Canada, September 2006.

Petitioners' Exhibit 1021
Nokia of America Corp., et al. v. KT Corporation, et al.
Case No. IPR2025-00036; U.S. Patent No. 11,627,631
Page 406 of 1122

[18] C.S. Bontu, E. Illidge, DRX mechanism for power saving in LTE, IEEE Commun. Mag. (June 2009).
[19] C. Zhong, et al., A new DRX scheme for LTE-advanced carrier aggregation systems with multiple services, IEEE Vehicular Technology Conference, 2011.
[20] Root of unity, from Wikipedia. <http://en.wikipedia.org/wiki/Root_of_unity>.
[21] LTE system description. <http://www.sharetechnote.com>.

Petitioners' Exhibit 1021
Nokia of America Corp., et al. v. KT Corporation, et al.
Case No. IPR2025-00036; U.S. Patent No. 11,627,631
Page 407 of 1122

CHAPTER

Downlink Physical Layer Functions

9

CHAPTER CONTENTS

9.1 Overview of downlink physical layer processing 402
9.2 Characteristics of wireless channels 404
9.3 LTE/LTE-Advanced operating frequencies and band classes 411
9.4 Principles of OFDM 419
9.4.1 Peak to average power ratio (PAPR) of OFDM signals 426
9.4.2 Effect of non-linearity on OFDM signals 428
9.4.3 Effect of carrier frequency offset on OFDM signals 430
9.4.4 Effect of oscillator phase noise on OFDM signals 434
9.5 Multiple access schemes 437
9.6 Duplex modes 440
9.7 Frame structure 445
9.7.1 Frame structure type 1 446
9.7.2 Frame structure type 2 447
9.7.3 MBSFN subframe structure 452
9.8 Resource structure, allocation, mapping 453
9.8.1 Physical and virtual resource blocks 454
9.8.2 Resource allocation 460
9.8.2.1 Resource allocation type 0 462
9.8.2.2 Resource allocation type 1 463
9.8.2.3 Resource allocation type 2 465
9.8.2.4 PRB bundling 467
9.8.2.5 Resource element group 467
9.9 Time and frequency synchronization 471
9.9.1 Primary synchronization signals 473
9.9.2 Secondary synchronization signals 474
9.10 Downlink reference signals and channel estimation 478
9.10.1 Reference signal design criteria 480
9.10.2 Pilot-Based channel estimation 486
9.10.3 Cell-Specific reference signals 491
9.10.3.1 Received signal strength indicator measurement 496
9.10.3.2 Reference signal received power measurement 496
9.10.3.3 Reference signal received quality measurement 496
9.10.4 UE-Specific reference signals associated with PDSCH 497

© 2014 Elsevier Inc. All rights reserved.

Petitioners' Exhibit 1021
Nokia of America Corp., et al. v. KT Corporation, et al.
Case No. IPR2025-00036; U.S. Patent No. 11,627,631
Page 408 of 1122

9.10.5 CSI reference signals 502
9.10.6 Enhanced PDCCH demodulation reference signals 512
9.10.7 Positioning reference signals 514
9.10.8 MBSFN reference signals 516
9.10.9 Reference signal overhead calculation 518
9.11 Channel coding and modulation 519
9.11.1 Principles of convolutional coding 521
9.11.2 Principles of turbo coding 527
9.11.3 Baseband digital modulation schemes 533
9.11.4 Channel coding, multiplexing, and interleaving 537
9.12 Downlink physical channel processing 546
9.12.1 Physical control format indicator channel 553
9.12.2 Physical broadcast channel 556
9.12.3 Physical hybrid ARQ indicator channel 560
9.12.4 Physical downlink control channel 568
9.12.4.1 PDCCH physical layer processing 568
9.12.4.2 DCI formats 574
9.12.4.3 Common and UE-specific search spaces and blind decoding 576
9.12.5 Enhanced PDCCH 597
9.12.6 Physical downlink shared channel 604
9.13 Principles of multi-antenna transmission 608
9.13.1 Capacity of MIMO channels 610
9.13.2 Instantaneous capacity, ergodic capacity, and outage capacity of MIMO systems 617
9.13.3 Spatial multiplexing and diversity 620
9.13.4 MIMO receivers 624
9.13.4.1 Maximum likelihood receiver 624
9.13.4.2 Successive interference cancelation receiver 624
9.13.4.3 Zero-forcing receiver 625
9.13.4.4 Minimum mean square error receiver 626
9.13.4.5 Maximal ratio combining receiver 627
9.13.4.6 MMSE-interference rejection combining receiver 628
9.13.4.7 Sphere decoding 630
9.13.4.8 CSI feedback 632
9.13.5 Precoding and beamforming 636
9.13.6 Single-user and Multi-user MIMO 642
9.13.7 Collaborative MIMO and collaborative spatial multiplexing 652
9.13.8 Non-linear precoding and dirty-paper coding 654
9.14 LTE/LTE-Advanced downlink multi-antenna transmission schemes 661
9.14.1 Transmit diversity 666
9.14.2 Spatial multiplexing 668
9.14.3 Cyclic delay diversity (CDD) 672
9.14.4 Beamforming and MU-MIMO 674

Petitioners' Exhibit 1021
Nokia of America Corp., et al. v. KT Corporation, et al.
Case No. IPR2025-00036; U.S. Patent No. 11,627,631
Page 409 of 1122

9.15 PDSCH transmission modes 679
9.16 OFDM signal generation 686
9.17 Timing advance 686
9.18 Power control and link adaptation 690
9.18.1 Basic concepts 691
9.18.2 Downlink power allocation 698
9.18.3 PUSCH power control 700
9.18.4 PUCCH power control 703
9.18.5 SRS power control 704
9.18.6 PRACH power control 705
9.18.7 Power headroom 706
9.18.8 Link adaptation 707
References 712

This chapter describes the physical layer protocols and functional processing in LTE/LTE-Advanced downlink direction. As shown in Figure 9.1, the physical layer is the lowest protocol layer in baseband signal processing that interfaces with the physical media through which the signal is transmitted and received. The physical layer receives MAC PDUs (transport blocks) and processes them through channel coding, interleaving, baseband modulation, layer mapping for multi-antenna operation, eigen-precoding, resource element, and antenna mapping functions. The choice of appropriate modulation and coding scheme, and multi-antenna transmission mode, are critical to achieve the desired reliability/robustness and system/webuser throughput in mobile wireless data communications. Typical mobile radio channels tend to be dispersive and time-variant and exhibit severe Doppler effects, multipath delay variation, intra-cell and inter-cell interference, and fading.

A good and robust design of the physical layer ensures that the system can normally operate and overcome the above deleterious effects, and can provide the maximum throughput and lowest latency under various operating conditions. The chapters on physical layer in this book are dedicated to systematic design of physical layer protocols and functional blocks of fourth generation cellular systems, the theoretical background on physical layer procedures, and performance evaluation of physical layer components. The theoretical background is provided to make the book self-contained, and to ensure that the reader understands the underlying theory governing the operation of various functional blocks and procedures. Additional references are provided for further study. While the focus is mainly on the techniques that were incorporated in the design of LTE/LTE-Advanced physical layer, the author has attempted to take a more generic and systematic a IMT-Advanced and beyond cellular systems, so that the reader can understand and apply the learning to the design and implementation of any OFDM-based physical layer irrespective of the radio access technology. Physical layer processes both control- and user-plane signals; however,

Petitioners' Exhibit 1021
Nokia of America Corp., et al. v. KT Corporation, et al.
Case No. IPR2025-00036; U.S. Patent No. 11,627,631
Page 410 of 1122

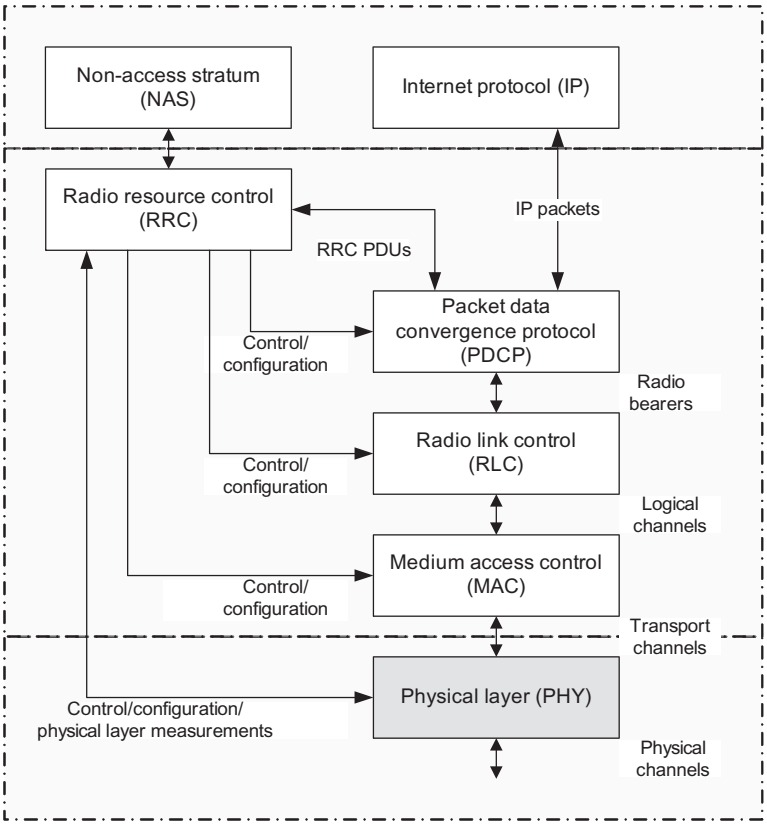


FIGURE 9.1

Physical Layer in LTE Protocol Stack

due to different design requirements and reliability and performance criteria, the procedures tend to be different. We will underline these differences and will describe the methods for selecting the best transmission format for each physical channel.

9.1 Overview of downlink physical layer processing

This section provides an overview of physical layer processing in LTE/LTE-Advanced downlink. The processing steps and the associated control signaling are depicted in Figure 9.2. The main criteria in the design of the LTE/LTE-Advanced physical layer were to increase the application throughput and capacity, reduce access latency, support higher user mobility, minimize intra-cell and inter-cell interference, improve reliability of control and data channel coverage especially

Petitioners' Exhibit 1021
Nokia of America Corp., et al. v. KT Corporation, et al.
Case No. IPR2025-00036; U.S. Patent No. 11,627,631
Page 411 of 1122

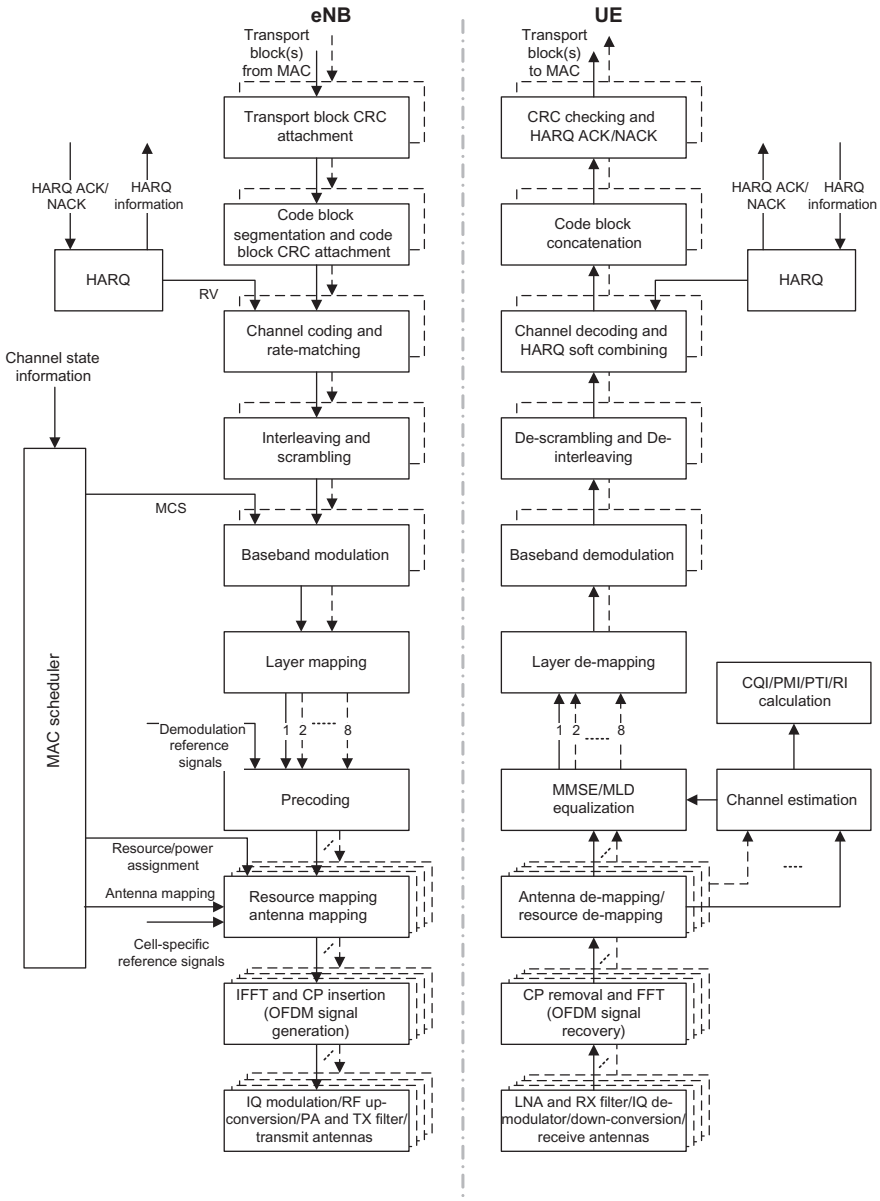


FIGURE 9.2

Downlink physical layer processing in LTE-Advanced [3,156].

Petitioners' Exhibit 1021
Nokia of America Corp., et al. v. KT Corporation, et al.
Case No. IPR2025-00036; U.S. Patent No. 11,627,631
Page 412 of 1122

at the cell-edge, and reduce the complexity and signaling overhead. The overall performance evaluations provided in Chapter 11 suggest that the desired goals have been successfully achieved. In the next sections of this chapter, we describe in detail the functional blocks and protocols of the downlink physical layer and their interactions based on the order that the information is processed as shown in Figure 9.2. It must be noted that although the overall procedure shown in Figure 9.2 is similar for LTE Rel-8/9 and LTE-Advanced Rel-10/11, the number of transmission layers, transmission modes, and multi-antenna processing are different. These differences will be identified in description of each function in the upcoming sections.

9.2 Characteristics of wireless channels

In a wireless communication system, a signal can travel from the transmitter to the receiver over multiple paths. This phenomenon is referred to as multipath propagation where signal attenuation varies on different paths. This effect, also known as multipath fading, can cause stochastic fluctuations in the received signal's magnitude, phase, and angle of arrival. The propagation over different paths is caused by scattering, reflection, diffraction, and refraction of the radio waves by stationary and moving objects, as well as the medium. It is obvious that different propagation mechanisms result in different channel and path loss models. As a result of wave propagation over multipath fading channels, the radio signal is attenuated due to mean path loss, as well as macroscopic and microscopic fading.

In an ideal free-space propagation model, the attenuation of RF signal energy between the transmitter and receiver follows the inverse-square law. The received power expressed in terms of transmitted power is attenuated proportional to the inverse of $L_s(d)$, which is called free space loss. When the receiving antenna is isotropic, the received signal power can be expressed as follows [19,48,49]:

$$P_{RX} = P_{TX} G_{TX} G_{RX} \left(\frac{\lambda}{4\pi d}\right)^2 = \frac{P_{TX} G_{TX} G_{RX}}{L_s(d)} \tag{9.1}$$

where P_{TX} and P_{RX} denote the transmitted and the received signal power, G_{TX} and G_{RX} denote the transmitting and receiving antenna gains, d is the distance between the transmitter and the receiver, and λ is the wavelength of the RF signal.

Macroscopic fading is caused by shadowing effects of buildings and natural obstructions, and is modeled by the local mean of a fast fading signal. The mean path loss $\overline{L}_p(d)$ as a function of distance d between the transmitter and receiver is proportional to the nth power of d relative to the reference distance d_0. In logarithmic scale, it can be expressed as follows:

$$\overline{L}_p(d) = L_s(d_0) + 10n \log(d/d_0) \quad \text{(dB)} \tag{9.2}$$

Petitioners' Exhibit 1021
Nokia of America Corp., et al. v. KT Corporation, et al.
Case No. IPR2025-00036; U.S. Patent No. 11,627,631
Page 413 of 1122

The reference distance d_0 corresponds to a point located in the far-field of the antenna typically 1 km for large cells, 100 m for micro-cells, and 1 m for indoor channels. In Eq. (9.2), $\overline{L}_p(d)$ is the mean path loss, which is typically $10n$ dB per decade attenuation for $d \gg d_0$. The value of n depends on the frequency, antenna heights, and propagation environment, and is equal to 2 in free space. Studies show that the path loss $L_p(d)$ is a random variable with log-normal distribution about the mean path loss $\overline{L}_p(d)$. Let $X \sim \mathbb{N}(0, \sigma^2)$ denote a zero-mean Gaussian random variable with standard deviation σ when measured in decibels, then:

$$L_p(d) = L_s(d_0) + 10n \log(d/d_0) + X \quad \text{(dB)} \tag{9.3}$$

The value of X is often derived empirically based on measurements. A typical value for σ is 8 dB. The parameters that statistically describe path loss due to large-scale fading (macroscopic fading) for an arbitrary location with a specific transmitting–receiving antenna separation include the reference distance d_0, the path loss exponent n, and the standard deviation σ of X [19,48,49].

Microscopic fading refers to the rapid fluctuations of the received signal in time and frequency, and is caused by scattering objects between the transmitting and receiving antennas. When the received RF signal is a superposition of independent scattered components plus a line-of-sight (LoS) component, the envelope of the received signal $r(t)$ has a Rician probability distribution function (PDF), and is referred to as Rician fading. As the magnitude of the LoS component approaches zero, the Rician PDF approaches a Rayleigh PDF. Thus:

$$f(r) = \frac{r(K+1)}{\sigma^2} \exp\left[-K - \frac{(K+1)r^2}{2\sigma^2}\right] I_0\left(\frac{2r}{\sigma}\sqrt{K(K+1)/2}\right) \quad r \geq 0 \tag{9.4}$$

where K and $I_0(r)$ denote the Rician factor and zero-order modified Bessel function of the first kind. In the absence of LoS path ($K = 0$), the Rician PDF reduces to Rayleigh distribution.

Time-varying fading due to scattering objects or transmitter/receiver motion results in Doppler spread. The time spreading effect of small-scale or microscopic fading is manifested in the time-domain as multipath delay spread, and in the frequency-domain as channel coherence bandwidth. Similarly, the time variation of the channel is characterized in the time-domain as channel coherence time, and in the frequency-domain as Doppler spread. In a fading channel, the relationship between maximum excess delay time τ_m and symbol time τ_s can be viewed in terms of two different degradation effects, i.e., frequency-selective fading and frequency non-selective or flat fading. A channel is said to exhibit frequency-selective fading if $\tau_m > \tau_s$. This condition occurs whenever the received multipath components of a symbol extend beyond the symbol's time duration. Such multipath dispersion of the signal results in inter-symbol interference (ISI) distortion. In the case of frequency-selective fading, mitigating the distortion is possible because many of the multipath components are separable by the receiver. A channel is said to

Petitioners' Exhibit 1021
Nokia of America Corp., et al. v. KT Corporation, et al.
Case No. IPR2025-00036; U.S. Patent No. 11,627,631
Page 414 of 1122

exhibit frequency non-selective or flat fading if $\tau_m < \tau_s$. In this case, all received multipath components of a symbol arrive within the symbol time duration; therefore, the components are not resolvable. In this case, there is no channel-induced ISI distortion, since the signal time spreading does not result in significant overlap among adjacent received symbols. There is still performance degradation, because the irresolvable phasor components can add up destructively to yield a substantial reduction in signal-to-noise ratio (SNR). Also, signals that are classified as exhibiting flat fading can sometimes experience frequency-selective distortion.

Figure 9.3 illustrates a multipath-intensity profile $\Lambda(\tau)$ versus delay τ where the term delay refers to the excess delay. It represents the signal's propagation delay that exceeds the delay of the first signal arriving at the receiver. For a typical wireless communication channel, the received signal usually consists of several discrete multipath components. The received signals are composed of a

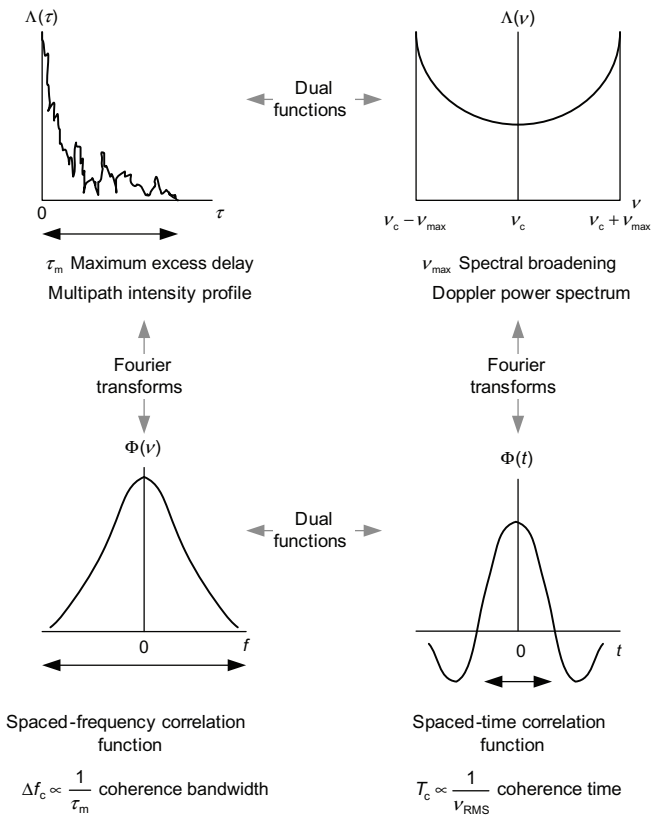


FIGURE 9.3

Illustration of the duality principle in time- and frequency-domains [19,48,49].

Petitioners' Exhibit 1021
Nokia of America Corp., et al. v. KT Corporation, et al.
Case No. IPR2025-00036; U.S. Patent No. 11,627,631
Page 415 of 1122

continuum of multipath components in some channels such as the tropospheric channel. In order to perform measurements of the multipath intensity profile, a wideband signal, i.e., a unit impulse or Dirac delta function, is used. For a single transmitted impulse, the time τ_m between the first and last received component is defined as the maximum excess delay during which the multipath signal power typically falls to some level 10−20 dB below that of the strongest component. Note that for an ideal system with zero excess delay, the function $\Lambda(\tau)$ would consist of an ideal impulse with weight equal to the total average received signal power. In the literature, the Fourier transform of $\Lambda(\tau)$ is referred to as the spaced-frequency correlation function $\Phi(\upsilon)$ [19]. The spaced-frequency correlation function $\Phi(\upsilon)$ is the channel's response to a pair of sinusoidal signals separated in frequency by υ. The coherence bandwidth Δf_c is a measure of the frequency range over which spectral components have a strong likelihood of amplitude correlation. In other words, a signal's spectral components over this range are affected by the channel in a similar manner. Note that Δf_c and τ_m are inversely proportional ($\Delta f_c \propto 1/\tau_m$). The maximum excess delay τ_m is not the best indicator of how any given wireless system will perform over a communication channel, because different channels with the same value of τ_m can exhibit different variations of signal intensity over the delay span. A useful measure of delay spread is most often characterized in terms of the root mean square (RMS) delay spread τ_{RMS} where [20]:

$$\tau_{RMS} = \sqrt{\frac{\int_0^{\tau_m} (\tau - \overline{\tau})^2 \Lambda(\tau) d\tau}{\int_0^{\tau_m} \Lambda(\tau) d\tau}} \tag{9.5}$$

in which the average multipath delay is calculated as follows:

$$\overline{\tau} = \frac{\int_0^{\tau_m} \tau \Lambda(\tau) d\tau}{\int_0^{\tau_m} \Lambda(\tau) d\tau} \tag{9.6}$$

An exact relationship between coherence bandwidth and delay spread does not exist and must be derived from signal analysis of actual signal dispersion measurements in specific channels. If coherence bandwidth is defined as the frequency interval over which the channel's complex-valued frequency transfer function has a correlation of at least 0.9, the coherence bandwidth is approximately $\Delta f_c \approx 1/(50\tau_{RMS})$. A common approximation of Δf_c corresponding to a frequency range over which the channel transfer function has a correlation of at least 0.5 is $\Delta f_c \approx 1/(5\tau_{RMS})$.

A channel is said to exhibit frequency-selective effects if $\Delta f_c < 1/\tau_s$, where the inverse symbol rate is approximately equal to the signal bandwidth W. In

Petitioners' Exhibit 1021
Nokia of America Corp., et al. v. KT Corporation, et al.
Case No. IPR2025-00036; U.S. Patent No. 11,627,631
Page 416 of 1122

practice, W may differ from $1/\tau_s$ due to filtering or data modulation. Frequency-selective fading effects arise whenever a signal's spectral components are not affected equally by the channel. This occurs whenever $\Delta f_c < W$. Frequency non-selective or flat fading degradation occurs whenever $\Delta f_c > W$. Hence, all of the signal's spectral components will be affected by the channel in a similar manner. Flat-fading does not introduce channel-induced ISI distortion, but performance degradation can still be expected due to loss in SNR whenever the signal experiences fading. In order to avoid channel-induced ISI distortion, the channel is required to exhibit flat-fading by ensuring that $\Delta f_c > W$. Therefore, the channel coherence bandwidth Δf_c sets an upper limit on the transmission rate that can be used without incorporating an equalizer in the receiver.

Figure 9.3 shows function $\Phi(t)$ which is known as the spaced-time correlation function, which is the autocorrelation function of the channel's response to a sinusoid. This function specifies the extent to which there is correlation between the channel's response to a sinusoid sent at time t_1 and the response to a similar sinusoid sent at time t_2, where $\Delta t = t_2 - t_1$. The coherence time is a measure of the expected time duration over which the channel's response is essentially invariant. To estimate $\Phi(t)$, a sinusoidal signal is transmitted through the channel and the autocorrelation function of the channel output is calculated. The function $\Phi(t)$ and the parameter T_c provide information about the speed of fading-channel variation. Note that for an ideal time-invariant channel, the channel's response would be highly correlated for all values of Δt and $\Phi(t)$ would be a constant function. If one ideally assumes uniformly distributed scattering around a mobile station with linearly polarized antennas, then the Doppler power spectrum (i.e., the inverse Fourier transform of spaced-time correlation function $\Lambda(\nu)$) has a U-shaped distribution, as shown in Figure 9.3. In a time-varying fading channel, the channel response to a pure sinusoidal tone spreads over a finite frequency range $\nu_c - \nu_{max} < \nu < \nu_c + \nu_{max}$, where ν_c and ν_{max} denote the frequency of the sinusoidal tone and the maximum Doppler spread, respectively. The RMS bandwidth of $\Lambda(\nu)$ is referred to as Doppler spread and is denoted by ν_{RMS} that can be calculated as follows:

$$\nu_{RMS} = \sqrt{\frac{\int_{\nu_c-\nu_{max}}^{\nu_c+\nu_{max}} (\nu-\overline{\nu})^2 \Lambda(\nu) d\nu}{\int_{\nu_c-\nu_{max}}^{\nu_c+\nu_{max}} \Lambda(\nu) d\nu}} \tag{9.7}$$

where:

$$\overline{\nu} = \frac{\int_{\nu_c-\nu_{max}}^{\nu_c+\nu_{max}} \nu \Lambda(\nu) d\nu}{\int_{\nu_c-\nu_{max}}^{\nu_c+\nu_{max}} \Lambda(\nu) d\nu} \tag{9.8}$$

Petitioners' Exhibit 1021
Nokia of America Corp., et al. v. KT Corporation, et al.
Case No. IPR2025-00036; U.S. Patent No. 11,627,631
Page 417 of 1122

The coherence time is typically defined as the time lag for which the signal autocorrelation coefficient reduces to 0.7. The coherence time is inversely proportional to Doppler spread $T_c \approx 1/\nu_{RMS}$. A common approximation for the value of coherence time as a function of Doppler spread is $T_c = 0.423/\nu_{RMS}$. It can be observed that the functions on the right-hand side of Figure 9.3 are dual of the functions on the left-hand side (duality principle).

The angle of spread refers to the spread in angle of arrival (AoA) of the multipath components at the receiver antenna array. At the transmitter, on the other hand, the angle of spread refers to the spread in the angle of departure (AoD) of the multipath components that leave the transmit antennas. If the angle spectrum function $\Theta(\theta)$ denotes the average power as a function of AoA, then the RMS angle spread can be calculated as follows:

$$\theta_{RMS} = \sqrt{\frac{\int_{-\pi}^{+\pi} (\theta - \overline{\theta})^2 \Theta(\theta) d\theta}{\int_{-\pi}^{+\pi} \Theta(\theta) d\theta}} \tag{9.9}$$

where:

$$\overline{\theta} = \frac{\int_{-\pi}^{+\pi} \theta \Theta(\theta) d\theta}{\int_{-\pi}^{+\pi} \Theta(\theta) d\theta} \tag{9.10}$$

The angle of spread causes space-selective fading, which manifests itself as variation of signal amplitude according to the location of antennas. The space-selective fading is characterized by the coherence distance D_c which is the spatial separation for which the autocorrelation coefficient of the spatial fading reduces to 0.7. The coherence distance is inversely proportional to the angle of spread $D_c \propto 1/\theta_{RMS}$.

In Figure 9.3, a duality between multipath intensity function $\Lambda(\tau)$ and Doppler power spectrum $\Lambda(\nu)$ is identified. It means that the two functions exhibit similar behavior across the time-domain and frequency-domain. As the $\Lambda(\tau)$ function identifies expected power of the received signal as a function of delay, $\Lambda(\nu)$ identifies expected power of the received signal as a function of frequency. Similarly, the spaced-frequency correlation function $\Phi(f)$ and spaced-time correlation function $\Phi(t)$ are dual functions. It implies that $\Phi(f)$ represents channel correlation in frequency-domain and $\Phi(t)$ corresponds to channel correlation function in time-domain in a similar manner.

Having reviewed some underlying concepts and characteristics of the wireless channels, let us now focus on some practical aspects of communication (data transmission) over wireless channels, and in particular the use of the above properties in the formation of a channel vector/matrix. As mentioned earlier, a wireless channel exhibits time, frequency, and space-selective variations known as fading. This fading arises due to Doppler, delay, and angle spreads in the scattering environment. The

Petitioners' Exhibit 1021
Nokia of America Corp., et al. v. KT Corporation, et al.
Case No. IPR2025-00036; U.S. Patent No. 11,627,631
Page 418 of 1122

channel spreading can be observed by sending a single impulse in frequency or continuous-wave signal in time or angle (point source) through the channel and receiving a signal spread along the spectral, temporal, or spatial dimension, respectively. A frequency-flat solution, however, can be applied to a frequency-selective channel by decomposing the transmission band into multiple narrow, frequency-flat sub-bands. Specifically, we can apply the solution per sub-carrier in systems employing OFDM. In a rich scattering environment, a frequency-flat MIMO wireless channel can be modeled as a complex Gaussian random process, represented as a time-varying matrix. The channel at each time instance is a Gaussian random variable, specified by the mean and its covariance. A non-zero channel mean signifies the presence of a direct LoS, or a cluster of strong paths, and the channel envelop has the Rician statistics, while zero mean corresponds to the Rayleigh statistics. The channel covariance, on the other hand, encompasses the correlation among the antennas at the transmitter and the receiver. Assuming the channel is stationary, the channel temporal variation can be captured by the channel auto-covariance, measuring the correlation between two channel instances separated by a delay. At zero delay, the channel auto-covariance coincides with the channel covariance [129].

Considering the channel state information at the transmitter (CSIT) at the transmit time in the form of a channel estimate and the estimation error covariance derived from a channel measurement at an initial time and the channel statistics, the main source of irreducible error in channel estimation is the random time variation of the channel between the initial measurement and its use by the transmitter. Therefore, we assume that the initial channel measurement is error free. The error in the channel estimate depends only on the time delay and the channel time selectivity, or the Doppler spread.

Let $\mathbf{H}$ denote the $N_{\mathrm{RX}} \times N_{\mathrm{TX}}$ channel matrix in a system with N_{TX} transmit and N_{RX} receive antennas. The channel has statistical mean $\overline{\mathbf{H}} = \mathscr{E}[\mathbf{H}]$ and covariance $\mathbf{R}_{\mathbf{H}} = \mathscr{E}[\mathbf{h}\mathbf{h}^H] - \overline{\mathbf{h}}\,\overline{\mathbf{h}}^H$, where the lower-case letter denotes the vectorized version of the upper-case matrix. Let us further assume that we have an initial, accurate channel measurement $\mathbf{H}(0)$. The channel auto-covariance $\mathbf{R}(\tau)$ at time delay τ then indicates the correlation between the initial measurement $\mathbf{H}(0)$ and the current channel $\mathbf{H}(\tau)$, defined as $\mathbf{R}(\tau) = \mathscr{E}[\mathbf{h}(\tau)\mathbf{h}^H(0)] - \overline{\mathbf{h}}(\tau)\overline{\mathbf{h}}^H(0)$. Intuitively, when this correlation is strong (i.e., $\mathbf{R}(\tau)$ is large when measured in a suitable norm) then $\mathbf{H}(0)$ is useful for estimating $\mathbf{H}(\tau)$. The strongest correlation is when the delay is zero (i.e., if $\tau \to 0$, then $\mathbf{R}(\tau) \to \mathbf{R}(0)$). In a scalar system, $\mathbf{R}(\tau)$ and $\mathbf{R}(0)$ reduce to scalars $r(\tau)$ and $r(0)$, respectively, and they are related through $r(\tau) = \rho(\tau)r(0)$, where $|\rho(\tau)| \leq 1$ is the temporal correlation coefficient [129].

An important assumption about channel temporal homogeneity is that the temporal correlation-coefficient $\rho(\tau)$ between any pair of transmit-antenna and receive-antenna is identical. This assumption is based on the premise that the channel temporal statistics can be expected to be the same for all antenna pairs. It is now possible to separate the temporal correlation from the spatial correlation in the channel auto-covariance as $\mathbf{R}(\tau) = \rho(\tau)\mathbf{R}(0)$. The temporal correlation $\rho(\tau)$ is a function of the time delay τ and the channel Doppler spread. As an example, in

Petitioners' Exhibit 1021
Nokia of America Corp., et al. v. KT Corporation, et al.
Case No. IPR2025-00036; U.S. Patent No. 11,627,631
Page 419 of 1122

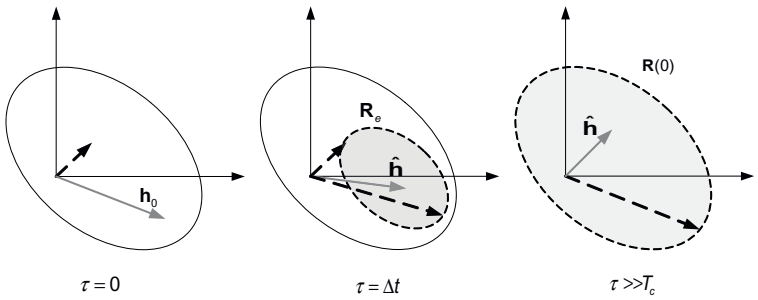


FIGURE 9.4

Illustration of a dynamic CSIT model [129].

Jake's model [21], $\rho(\tau) = J_0(2\pi\tau\nu)$, where ν is the channel Doppler spread and $J_0(\cdot)$ is the zero-order Bessel function of the first kind [35–37].

It can be shown that an estimate of the channel at time τ together with the estimation error covariance using minimum mean-squared error (MMSE) criterion results in the following $\hat{\mathbf{H}}(\tau) = \rho\mathbf{H}(0) - (1-\rho)\overline{\mathbf{H}}$ and $\mathbf{R}_e(\tau) = (1-\rho^2)\mathbf{R}(0)$. The two quantities $\hat{\mathbf{H}}(\tau)$ and $\mathbf{R}_e(\tau)$ function effectively as a new channel mean and a new channel covariance; thus they are referred to as the effective mean and the effective covariance, respectively, and constitute the CSIT. This CSIT ranges from perfect channel knowledge when $\rho = 1$, to pure stochastic when $\rho = 0$. Since the CSIT depends on the value of ρ which captures the channel time variation, it is called dynamic CSIT. The correlation factor ρ functions as a measure of CSIT quality. When $\rho = 1$, the channel estimate coincides with $\mathbf{H}(0)$ and is error free. As ρ approaches to zero, the effect of the initial channel measurement diminishes and the estimate asymptotically approaches the channel mean $\overline{\mathbf{H}}$. In parallel, the estimation error covariance $\mathbf{R}_e$ is zero when $\rho = 1$, and approaches zero as the correlation factor approaches zero. Figure 9.4 illustrates the CSIT variation as a function of the time delay τ. Several special cases of dynamic CSIT are of interest as follows: (1) perfect CSIT, in which the effective covariance is zero and the effective mean is the instantaneous channel matrix; (2) mean CSIT, in which the effective mean is non-zero and arbitrary, but the effective covariance is the identity matrix, corresponding to uncorrelated antennas; (3) covariance CSIT, in which the effective covariance matrix is non-identity and arbitrary, but the effective mean is zero, corresponding to Rayleigh fading. The general case in which both the mean and covariance matrices are arbitrary is referred to as statistical CSIT [129].

9.3 LTE/LTE-Advanced operating frequencies and band classes

The LTE/LTE-Advanced were designed to operate in the frequency bands defined in Table 9.1. The requirements were defined for 1.4, 3, 5, 10, 15, and 20 MHz

Petitioners' Exhibit 1021
Nokia of America Corp., et al. v. KT Corporation, et al.
Case No. IPR2025-00036; U.S. Patent No. 11,627,631
Page 420 of 1122

Table 9.1 E-UTRA Operating Frequencies, Band Classes, and Supported Bandwidths [1,2]

E-UTRA Operating Band (Band Class)	Uplink Operating Band eNB Receive/UE Transmit (MHz) $f_{UL\text{-}low} - f_{UL\text{-}high}$	$N_{Offset\text{-}DL}$	N_{DL}	Downlink Operating Band eNB Transmit/UE Receive (MHz) $f_{DL\text{-}low} - f_{DL\text{-}high}$	$N_{Offset\text{-}UL}$	N_{UL}	Duplex Scheme	Supported Bandwidths (MHz)
1	1920–1980	0	0–599	2110–2170	18000	18000–18599	FDD	5, 10, 15, 20
2	1850–1910	600	600–1199	1930–1990	18600	18600–19199	FDD	1.4, 3, 5, 10, 15, 20
3	1710–1785	1200	1200–1949	1805–1880	19200	19200–19949	FDD	1.4, 3, 5, 10, 15, 20
4	1710–1755	1950	1950–2399	2110–2155	19950	19950–20399	FDD	1.4, 3, 5, 10, 15, 20
5	824–849	2400	2400–2649	869–894	20400	20400–20649	FDD	1.4, 3, 5, 10
6	830–840	2650	2650–2749	875–885	20650	20650–20749	FDD	5, 10
7	2500–2570	2750	2750–3449	2620–2690	20750	20750–21449	FDD	5, 10
8	880–915	3450	3450–3799	925–960	21450	21450–21799	FDD	1.4, 3, 5, 10
9	1749.9–1784.9	3800	3800–4149	1844.9–1879.9	21800	21800–22149	FDD	5, 10, 15, 20
10	1710–1770	4150	4150–4749	2110–2170	22150	22150–22749	FDD	5, 10, 15, 20
11	1427.9–1447.9	4750	4750–4949	1475.9–1495.9	22750	22750–22949	FDD	5, 10
12	699–716	5010	5010–5179	729–746	23010	23010–23179	FDD	1.4, 3, 5, 10
13	777–787	5180	5180–5279	746–756	23180	23180–23279	FDD	5, 10
14	788–798	5280	5280–5379	758–768	23280	23280–23379	FDD	5, 10
15	Reserved			Reserved			FDD	–
16	Reserved			Reserved			FDD	–
17	704–716	5730	5730–5849	734–746	23730	23730–23849	FDD	5, 10
18	815–830	5850	5850–5999	860–875	23850	23850–23999	FDD	5, 10, 15
19	830–845	6000	6000–6149	875–890	24000	24000–24149	FDD	5, 10, 15
20	832–862	6150	6150–6449	791–821	24150	24150–24449	FDD	5, 10, 15, 20

Petitioners' Exhibit 1021
Nokia of America Corp., et al. v. KT Corporation, et al.
Case No. IPR2025-00036; U.S. Patent No. 11,627,631
Page 421 of 1122

21	1447.9–1462.9	6450	6450–6599	1495.9–1510.9	24450	24450–24599	FDD	5, 10, 15
22	3410–3490	6600	6600–7399	3510–3590	24600	24600–25399	FDD	5, 10, 15, 20
23	2000–2020	7500	7500–7699	2180–2200	25500	25500–25699	FDD	1.4, 3, 5, 10
24	1626.5–1660.5	7700	7700–8039	1525–1559	25700	25700–26039	FDD	5, 10
25	1850–1915	8040	8040–8689	1930–1995	26040	26040–26689	FDD	1.4, 3, 5, 10, 15, 20
. . .				Not Specified				
33	1900–1920	36000	36000–36199	1900–1920	36000	36000–36199	TDD	5, 10, 15, 20
34	2010–2025	36200	36200–36349	2010–2025	36200	36200–36349	TDD	5, 10, 15
35	1850–1910	36350	36350–36949	1850–1910	36350	36350–36949	TDD	1.4, 3, 5, 10, 15, 20
36	1930–1990	36950	36950–37549	1930–1990	36950	36950–37549	TDD	1.4, 3, 5, 10, 15, 20
37	1910–1930	37550	37550–37749	1910–1930	37550	37550–37749	TDD	5, 10, 15, 20
38	2570–2620	37750	37750–38249	2570–2620	37750	37750–38249	TDD	5, 10, 15, 20
39	1880–1920	38250	38250–38649	1880–1920	38250	38250–38649	TDD	5, 10, 15, 20
40	2300–2400	38650	38650–39649	2300–2400	38650	38650–39649	TDD	5, 10, 15, 20
41	2496–2690	39650	39650 –41589	2496–2690	39650	39650 –41589	TDD	5, 10, 15, 20
42	3400–3600	41590	41590–43589	3400–3600	41590	41590–43589	TDD	5, 10, 15, 20
43	3600–3800	43590	43590–45589	3600–3800	43590	43590–45589	TDD	5, 10, 15, 20

bandwidth with a specific configuration in terms of the number of physical resource blocks (PRBs). Using carrier aggregation, a number of contiguous and/or non-contiguous frequency bands can be aggregated to create a virtually larger bandwidth. The channel raster is 100 kHz, which means the center frequency must be a multiple of 100 kHz [1]. To support transmission in paired and unpaired spectra, two duplexing schemes are supported, i.e., frequency division duplex (FDD), allowing both full and half-duplex terminal operation, as well as time division duplex (TDD). Table 9.2 gives the band classes where the LTE/LTE-Advanced systems can be deployed.

Figure 9.5 illustrates the relation between the channel bandwidth (BW_{Channel}) and the transmission bandwidth, i.e., the number of permissible PRBs (N_{RB}). The channel edges are defined as the lowest and highest frequencies of the carrier separated by the channel bandwidth; thus $f_C \pm (1/2)BW_{\text{Channel}}$. In the case of carrier aggregation, the aggregated channel bandwidth $BW_{\text{Channel-CA}}$ is defined as $BW_{\text{Channel-CA}} = f_{\text{edge-high}} - f_{\text{edge-low}}$. The lower band edge $f_{\text{edge-low}}$ and the upper band edge $f_{\text{edge-high}}$ of the aggregated channel bandwidth are used as the reference points in frequency for transmitter and receiver requirements, and are subsequently defined as follows: $f_{\text{edge-low}} = f_{\text{C-low}} - f_{\text{offset-low}}$ and $f_{\text{edge-high}} = f_{\text{C-high}} + f_{\text{offset-high}}$. The lower and upper frequency offsets depend on the transmission bandwidth configurations of the lowest and highest assigned edge component carrier, and are defined as $f_{\text{offset-low}} = 0.18N_{\text{RB-low}}/2 + BW_{\text{Guard-band}}$ and $f_{\text{offset-high}} = 0.18N_{\text{RB-high}}/2 + BW_{\text{Guard-band}}$, where $N_{\text{RB-low}}$ and $N_{\text{RB-high}}$ denote the transmission bandwidth configurations for the lowest and highest assigned component carrier, respectively, and $BW_{\text{Guard-band}}$ denotes the nominal guard band. Note that the 0.18 multiplier in the equations is the bandwidth of a PRB in MHz. The aggregated transmission bandwidth is defined as the number of the aggregated resource blocks within the entire assigned aggregated channel bandwidth, and is defined per carrier aggregation band class.

The frequency separation between carriers depends on the deployment scenario and the size of the frequency block available to the network operator, as well as the channel bandwidth. The nominal channel spacing between two adjacent E-UTRA carriers is defined as $\Delta f_{\text{spacing}} = (BW_{\text{Channel(1)}} + BW_{\text{Channel(2)}})/2$, where $BW_{\text{Channel(1)}}$ and $BW_{\text{Channel(2)}}$ parameters are the channel bandwidths of the two respective E-UTRA carriers. The channel spacing can be adjusted to optimize performance in a particular deployment scenario. For intra-band contiguous carrier aggregation bandwidth, the nominal channel spacing between two adjacent E-UTRA component carriers is specified as follows:

$$\Delta f_{\text{spacing-CA}} = 0.3 \left\lfloor \frac{BW_{\text{Channel(1)}} + BW_{\text{Channel(2)}} - 0.1\left|BW_{\text{Channel(1)}} - BW_{\text{Channel(2)}}\right|}{0.6} \right\rfloor \text{(MHz)} \tag{9.11}$$

The channel spacing for intra-band contiguous carrier aggregation can be adjusted to any integer multiple of 300 kHz (less than the nominal channel spacing)

Petitioners' Exhibit 1021
Nokia of America Corp., et al. v. KT Corporation, et al.
Case No. IPR2025-00036; U.S. Patent No. 11,627,631
Page 423 of 1122

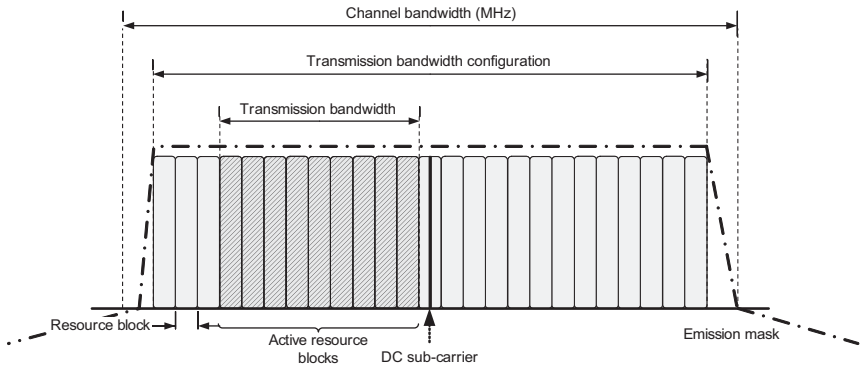


FIGURE 9.5

Relationship between channel bandwidth and transmission bandwidth in E-UTRA [1].

to optimize performance in a particular deployment scenario. The E-UTRA channel raster (including the carrier aggregation scenarios) is 100 kHz for all bands, which means that the carrier center frequency must be an integer multiple of 100 kHz.

The carrier frequency in the downlink/uplink directions is designated by the E-UTRA absolute radio frequency channel number (EARFCN) in the range of 0−65,535. The relation between EARFCN and the downlink carrier frequency (in MHz) is given by $f_{DL} = f_{DL-low} + 0.1(N_{DL} - N_{Offset-DL})$, where f_{DL-low}, N_{DL}, and $N_{Offset-DL}$ parameters are given in Table 9.1. Similarly, the relationship between EARFCN and the uplink carrier frequency (in MHz) for the uplink is defined as $f_{UL} = f_{UL-low} + 0.1(N_{UL} - N_{Offset-UL})$, where f_{UL-low}, N_{UL}, and $N_{Offset-UL}$ parameters are provided in Table 9.1. Note that N_{DL} and N_{UL} in the latter equations are the downlink and uplink EARFCN, respectively.

The channel numbers that designate carrier frequencies which are extremely close to the operating band edges are not used. This implies that the first 7, 15, 25, 50, 75, and 100 channel numbers at the lower operating band edge and the last 6, 14, 24, 49, 74, and 99 channel numbers at the upper operating band edge are not utilized for channel bandwidths of 1.4, 3, 5, 10, 15, and 20 MHz, respectively.

The fragmentation of the suitable and permissible frequency bands for deployment of LTE systems across the globe and the disparity of the operators' network deployments and legacy systems have made significant challenges against worldwide proliferation and accessibility of 4G networks (see Figure 9.6). Figure 9.6 depicts the distribution of the useable frequency bands for commercial LTE/LTE-Advanced deployments across the globe as of August 2012 [161]. In general, typical user equipment has to support multiple communication RF bands and standards (e.g., LTE/LTE-Advanced, UMTS, and 1xEV-DO) in order to allow operation across different regions and operator networks. Enabling the mobile terminals to cover all desired RF

Petitioners' Exhibit 1021
Nokia of America Corp., et al. v. KT Corporation, et al.
Case No. IPR2025-00036; U.S. Patent No. 11,627,631
Page 424 of 1122

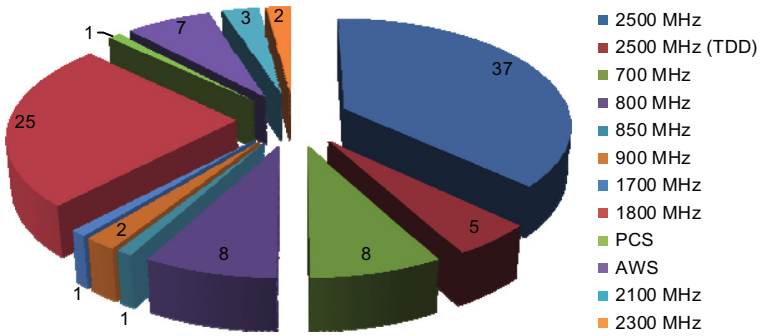


FIGURE 9.6

Distribution of frequency bands for E-UTRA commercial deployments across the world [161].

bands does not only result in an increased chip area due to more complex RF integrated circuit implementation, but also a larger phone form factor to accommodate external filters (see Figure 9.7 as an example of triple-band LTE transceiver). In the case of FDD systems, common handhelds use bulk acoustic wave duplex filters[1] to separate the receive signal from the transmit signal with a nominal frequency separation. These filters are not tunable, and thus require one duplexer per frequency constellation. The selectivity provided by the duplexer must reach a certain level such that third order inter-modulation frequency components are suppressed. These signals are generated by the transmit signal leaking into the receiver and an external interferer in a certain frequency band, thus degrading sensitivity of the entire receiver. Therefore, it is necessary to use either very expensive duplexers that could provide the desired selectivity, or to place an external (i.e., external to RFIC) low-noise amplifier followed by an additional surface acoustic wave filter[2] which is a more common solution. In general, it is not trivial to design extremely broadband RF filters, power or low-noise amplifiers, mixers, etc., to cover a number of contiguous and/or non-contiguous RF bands with optimal performance across the entire operating bands. Figure 9.8 shows the measured and simulated performance of a triple-fed

[1]Bulk acoustic wave filters are electro-mechanical devices typically operating in the frequency range of 2−16 GHz which can be implemented by ladder or lattice filters. Two main variants of bulk acoustic wave filter are thin film bulk acoustic resonator, or FBAR, and solid mounted bulk acoustic resonators [167].

[2]Surface acoustic wave filters are electro-mechanical devices commonly used in RF systems. The electrical signal is converted to a mechanical wave in a device constructed of a piezoelectric crystal or ceramic. This wave is delayed as it propagates across the device, before being converted back to an electrical signal by further electrodes. The delayed outputs are recombined to produce a direct analog implementation of a finite impulse response filter. This hybrid filtering technique has found applications in analog sampled filters. The surface acoustic wave filters are limited to frequencies up to 3 GHz [167].

Petitioners' Exhibit 1021
Nokia of America Corp., et al. v. KT Corporation, et al.
Case No. IPR2025-00036; U.S. Patent No. 11,627,631
Page 425 of 1122

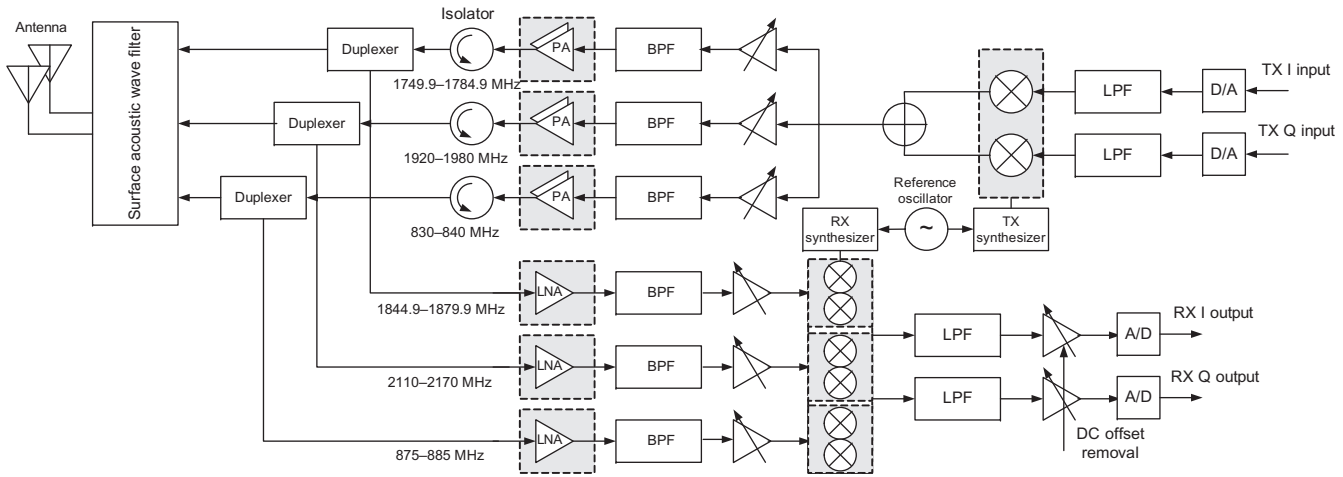


FIGURE 9.7

Example of a Triple-band LTE Transceiver [170].

Petitioners' Exhibit 1021
Nokia of America Corp., et al. v. KT Corporation, et al.
Case No. IPR2025-00036; U.S. Patent No. 11,627,631
Page 426 of 1122

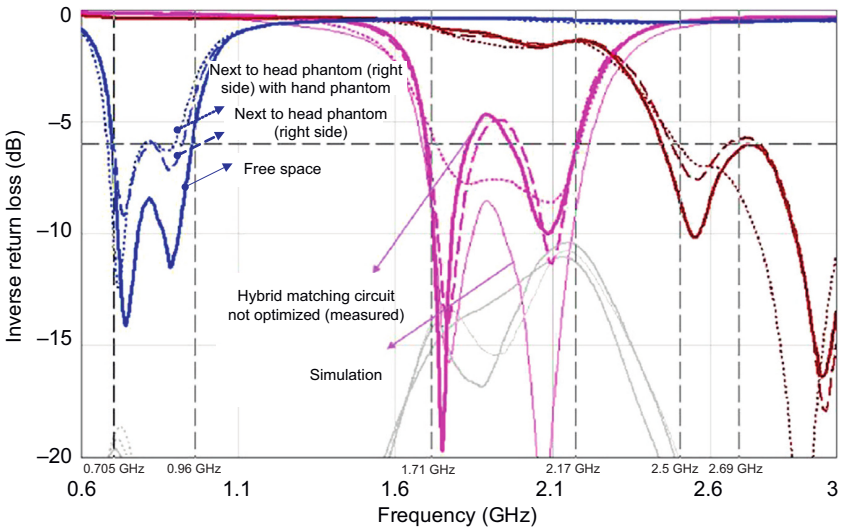


FIGURE 9.8

Simulated and measured inverse return loss of an example triple-fed antenna at 0.8, 1.9, 2.6 GHz [170].

antenna in terms of input return loss[3] (i.e., an indication of the quality of input impedance matching) under three different practical scenarios and in different frequency bands. It can be seen that satisfactory impedance matching is only achieved in a certain frequency region and not across the entire frequency bands, especially if the antennas are covered by hand or head phantoms. This example underlines the practical challenge of designing extremely wideband RF systems to fit into very small user-equipment's form factor in order to enable multi-band multi-mode LTE operation [170].

[3]Return loss is the loss of signal power resulting from the reflection caused at a discontinuity in a transmission media. This discontinuity can be a mismatch with the terminating load or with a device inserted in the line. It is usually expressed as the ratio of the incident power P_i and the reflected power P_r, i.e., RL (dB) = 10 log(P_i/P_r) in dB. The return loss is related to both the standing wave ratio (SWR) and reflection coefficient (Γ). Increasing the value of return loss corresponds to lower SWR. Return loss is a measure of how well the input/output impedances of devices or transmission lines are matched. A match is good, if the return loss value is high. A high return loss is desirable and results in a lower insertion loss. The ratio of the amplitude of the reflected wave V_r to the amplitude of the incident wave V_i is known as the reflection coefficient Γ, which is defined as $\Gamma = V_r/V_i$. When the source and load impedances are known values, the reflection coefficient is given by $\Gamma = (Z_L - Z_0)/(Z_L + Z_0)$ where Z_0 is the impedance of the transmission line toward the source and Z_L is the impedance toward the load. The return loss is the negative of the magnitude of the reflection coefficient in dB. Since power is proportional to the square of the voltage, the return loss is given by RL(dB) = $-$ 20 log(|Γ|) [169].

Petitioners' Exhibit 1021
Nokia of America Corp., et al. v. KT Corporation, et al.
Case No. IPR2025-00036; U.S. Patent No. 11,627,631
Page 427 of 1122

The performance of mobile device antennas is an important factor in the design and implementation of the device (in terms of practical form factor) as well as the ultimate communication quality that a user may expect from that device. This requires adopting an antenna design that yields high performance under realistic conditions in order to ensure satisfaction of LTE/LTE-Advanced system requirements. This challenge will be further intensified in the case of multi-band antenna array design which is required to fit into the small form factor of a mobile device and to provide satisfactory performance (near-field/far-field radiation patterns, gain, return loss, parasitic/spurious effects, etc.) over a large bandwidth.

9.4 Principles of OFDM

The orthogonal frequency division multiplexing (OFDM) is a form of multi-carrier modulation technique that was first introduced over 50 years ago. In a conventional serial data transmission system, the information bearing symbols are transmitted sequentially, with the frequency spectrum of each symbol occupying the entire available bandwidth. Figure 9.9 illustrates an unfiltered quadrature amplitude modulation (QAM) signal spectrum. It is in the form of $\sin(\pi f T_u)/\pi f T_u$ with zero crossing points at integer multiples of $1/T_\mathrm{u}$, where T_u is the QAM symbol period. The concept of OFDM is to transmit the data bits in parallel QAM modulated sub-carriers using frequency division multiplexing. The carrier spacing is carefully selected so that each sub-carrier is located on other sub-carriers' zero-crossing points in the frequency-domain. Although there are spectral overlaps among sub-carriers, they do not interfere with each other if they are sampled at the sub-carrier frequencies. In other words, they maintain spectral orthogonality. As shown in Figure 9.9, the OFDM signal in the frequency-domain is generated through aggregation of N_FFT parallel QAM-modulated sub-carriers, where adjacent sub-carriers, are separated by sub-carrier spacing $1/T_\mathrm{u}$. An example of OFDM signal spectrum as seen on a vector signal analyzer is shown in Figure 9.10.

Since an OFDM signal consists of many parallel QAM sub-carriers, the mathematical expression of the signal in the time-domain can be expressed as follows:

$$s(t) = \mathrm{Re}\left\{ e^{j\omega_c t} \sum_{k=-(N_\mathrm{FFT}-1)/2}^{(N_\mathrm{FFT}-1)/2} \alpha_k \, e^{j2\pi k(t-t_\mathrm{g})/T_\mathrm{u}} \right\} \quad mT_\mathrm{u} \le t \le (m+1)T_\mathrm{u} \qquad (9.12)$$

where $s(t)$ denotes the OFDM signal in the time-domain, α_k is the complex-valued data that is QAM-modulated and transmitted over sub-carrier k, N_FFT is the number of sub-carriers in the frequency-domain, ω_c is the RF carrier frequency, and T_g is the guard interval or the cyclic prefix (CP) length. For a large number of sub-carriers, direct generation and demodulation of the OFDM signal would require arrays of coherent sinusoidal generators which can become excessively complex and expensive. However, one can notice that the OFDM signal is actually the real part of the inverse discrete Fourier transform (IDFT) of the original complex-valued data

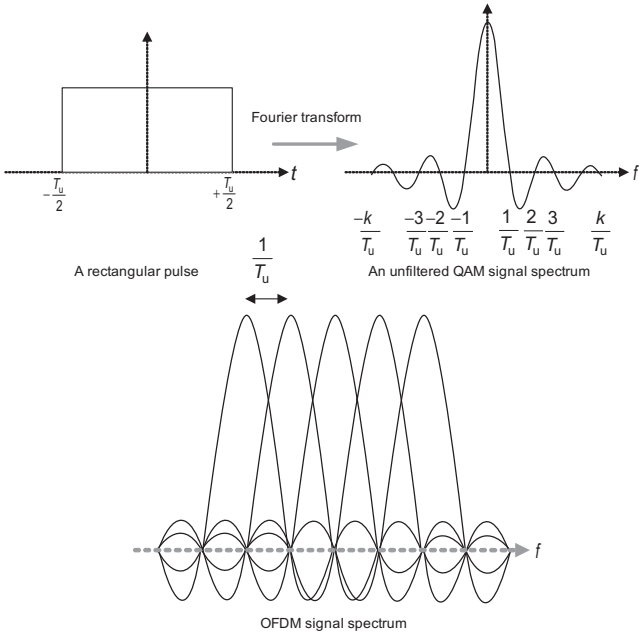


FIGURE 9.9

Illustration of OFDM concept [52].

symbols $\{\alpha_k\}|_{k=-(N_{\text{FFT}}-1)/2,\ldots,(N_{FFT}-1)/2}$. It can be seen that there are $N < N_{\text{FFT}}$ sub-carriers, each carrying the corresponding data α_k. The inverse of the sub-carrier spacing $\Delta f = 1/T_{\text{u}}$ is defined as the OFDM useful symbol duration T_{u}, which is N_{FFT} times longer than that of the original input data symbol duration.

Since IDFT is used in the OFDM modulator, the original data is defined in the frequency-domain, while the OFDM signal $s(t)$ is defined in the time-domain. The IDFT can be implemented via a computationally efficient fast Fourier transform (FFT) algorithm. The orthogonality of sub-carriers in OFDM can be maintained and individual sub-carriers can be completely separated and demodulated by an FFT at the receiver when there is no ISI introduced by the communication channel. In practice, linear distortions such as multipath delay cause ISI between OFDM symbols, resulting in loss of orthogonality and an effect that is similar to co-channel interference. However, when delay spread is small, i.e., within a fraction of the OFDM useful symbol length, the impact of ISI is insignificant, although it depends on the order of modulation implemented by the sub-carriers (see Figure 9.11). A simple solution to mitigate multipath delay is to increase the OFDM effective symbol duration such that it is much larger than the delay spread; however, when the delay spread is large, it requires a large number of sub-carriers and a large FFT size. Meanwhile, the system might become sensitive to Doppler shift and carrier frequency offset (CFO). An alternative approach to mitigate

Petitioners' Exhibit 1021
Nokia of America Corp., et al. v. KT Corporation, et al.
Case No. IPR2025-00036; U.S. Patent No. 11,627,631
Page 429 of 1122

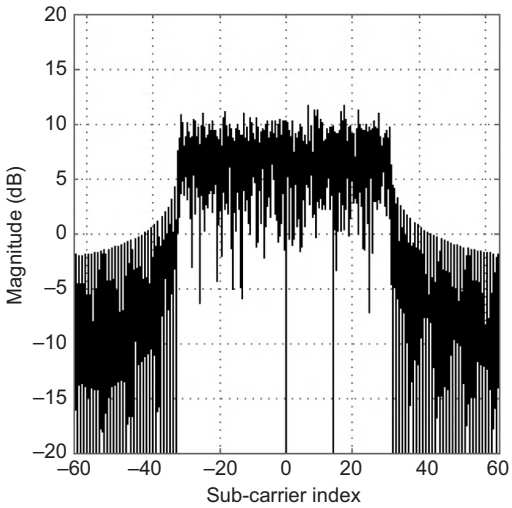


FIGURE 9.10

A snapshot of OFDM signal in the frequency-domain [158].

multipath distortion is to generate a cyclically extended guard interval, where each OFDM symbol is prefixed with a periodic extension of the signal itself, as shown in Figure 9.12 where the tail of the symbol is copied to the beginning of the symbol. The OFDM symbol duration is then defined as $T_s = T_u + T_g$, where T_g is the guard interval or cyclic prefix. When the guard interval is longer than the channel impulse response or the multipath delay, the ISI can be effectively eliminated. The ratio of the guard interval to useful OFDM symbol duration depends on the deployment scenario and the frequency band. Since the insertion of the guard intervals will reduce data throughput, T_g is usually selected less than $T_u/4$. The cyclic prefix should absorb most of the signal energy dispersed by the multipath channel. The entire ISI energy is contained within the cyclic prefix if its length is greater than that of the channel RMS delay spread ($T_g > \tau_{RMS}$). In general, it is sufficient to have most of the delay spread energy absorbed by the guard interval, considering the inherent robustness of large OFDM symbols to time dispersion.

The mapping of the modulated data symbol into multiple sub-carriers also allows an increase in the symbol duration. The symbol duration obtained through an OFDM scheme is much larger than that of a single carrier modulation technique with a similar transmission bandwidth. In general, when the channel delay spread exceeds the guard time, the energy contained in the ISI will be much smaller with respect to the useful OFDM symbol energy, as long as the symbol duration is much larger than the channel delay spread, i.e., $T_s \gg \tau_{RMS}$. Although large OFDM symbol duration is desirable to mitigate the ISI effects caused by time dispersion, large OFDM symbol duration can further reduce the ability to alleviate the effects of fast fading, particularly if the symbol period is large compared to the channel coherence

Petitioners' Exhibit 1021
Nokia of America Corp., et al. v. KT Corporation, et al.
Case No. IPR2025-00036; U.S. Patent No. 11,627,631
Page 430 of 1122

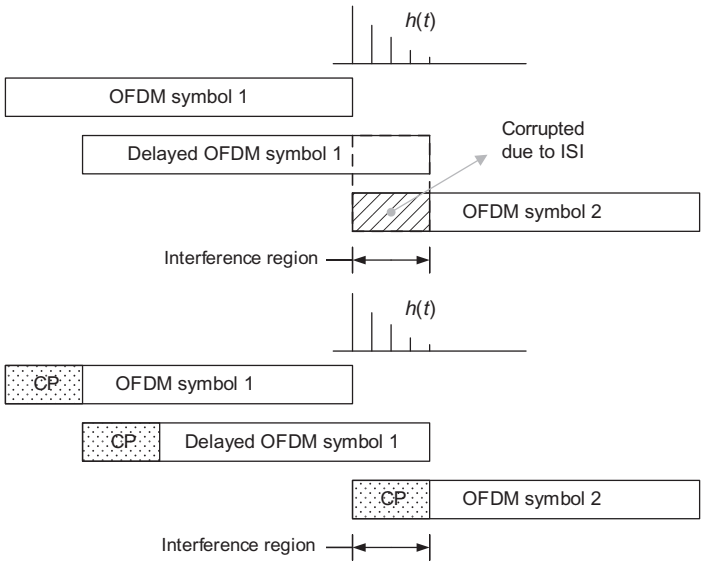


FIGURE 9.11

Illustration of the effect of guard interval for eliminating ISI ($h(t)$ is the hypothetical channel impulse response).

time, then the channel can no longer be considered as time-invariant over the OFDM symbol duration; therefore, this will introduce the inter-sub-carrier orthogonality loss. This can affect the performance in fast fading conditions. Hence, the symbol duration should be kept smaller than the minimum channel coherence time. Since the channel coherence time is inversely proportional to the maximum Doppler spread, the symbol duration T_s must, in general, be chosen such that $T_s \ll 1/\nu_{RMS}$. The large number of OFDM sub-carriers makes the bandwidth of the individual sub-carriers small relative to the overall signal bandwidth. With an adequate number of sub-carriers, the inter-carrier spacing is much smaller than the channel coherence bandwidth. Since the channel coherence bandwidth is inversely proportional to the channel delay spread τ_{RMS}, the sub-carrier separation is generally designed such that $\Delta f \ll 1/\tau_{RMS}$. In this case, the fading on each sub-carrier is flat and can be modeled as a complex-valued constant channel gain. The individual reception of the QAM symbols transmitted on each sub-carrier is therefore simplified to the case of a flat-fading channel. This enables a straightforward introduction of advanced MIMO schemes. Furthermore, in order to mitigate Doppler spread effects, the inter-carrier spacing should be much larger than the RMS Doppler spread $\Delta f \gg \nu_{RMS}$. Since the OFDM sampling frequency is typically larger than the actual signal bandwidth, only a subset of sub-carriers are used to carry QAM symbols. The remaining sub-carriers are left inactive prior to the IFFT, and are referred to as guard sub-carriers. The split between the active and the inactive

Petitioners' Exhibit 1021
Nokia of America Corp., et al. v. KT Corporation, et al.
Case No. IPR2025-00036; U.S. Patent No. 11,627,631
Page 431 of 1122

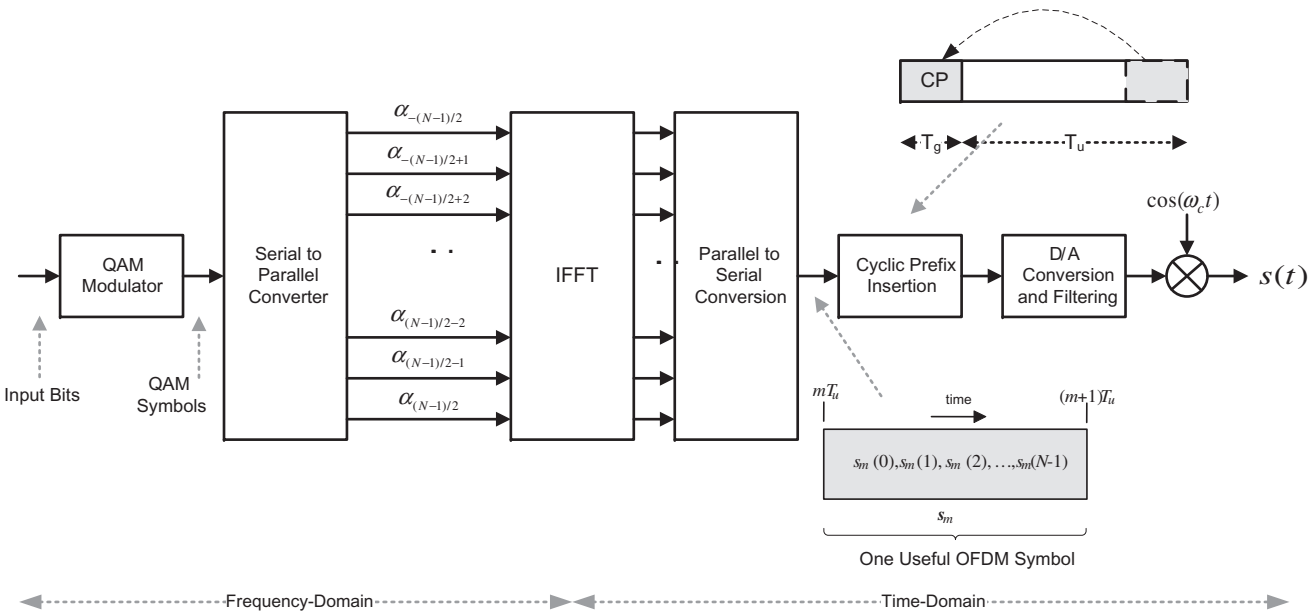


FIGURE 9.12

OFDM signal generation.

Petitioners' Exhibit 1021
Nokia of America Corp., et al. v. KT Corporation, et al.
Case No. IPR2025-00036; U.S. Patent No. 11,627,631
Page 432 of 1122

sub-carriers is determined based on the spectral sharing and regulatory constraints, such as the bandwidth allocation and the spectral mask.

An OFDM transmitter diagram is shown in Figure 9.12. The incoming bit stream is first QAM modulated to form the complex-valued QAM symbols. The QAM symbols are converted from serial to parallel with $N < N_{\text{FFT}}$ complex-valued numbers per block, where N_{FFT} is the size of FFT/IFFT operation. Each block is processed by an IFFT and the output of the IFFT forms an OFDM symbol, which is converted back to serial data for transmission. A guard interval or cyclic prefix is inserted between symbols to eliminate ISI effects caused by multipath distortion. The discrete symbols are filtered and converted to analog for RF up-conversion.

The reverse process is performed at the receiver. A one-tap equalizer is usually used for each sub-carrier to correct channel distortion. The tap coefficients are calculated based on channel information. As shown in Figures 9.9 and 9.10, one can understand that the OFDM signal spectrum is approximately rectangular. Since the OFDM modulator is an IFFT processor, its role is to convert data from the frequency-domain to the time-domain, and then transmit them in the time-domain over the channel. If a spectrum analyzer, which converts the input from the time-domain to the frequency-domain, is used to monitor an OFDM signal, what will be displayed is the original data.

When there is multipath distortion, a conventional single carrier wideband transmission system suffers from frequency selective fading. A complex adaptive equalizer must be used to equalize the in-band fading. The number of taps required for the equalizer is proportional to the symbol rate and the multipath delay. For an OFDM system, if the guard interval is larger than the multipath delay, the ISI can be eliminated and orthogonality can be maintained among sub-carriers. Since each OFDM sub-carrier occupies a very narrow spectrum, in the order of a few kHz, even under severe multipath distortion, they are only subject to flat fading. In other words, the OFDM converts a wideband frequency-selective fading channel to a series of narrowband frequency non-selective fading sub-channels by using the parallel multi-carrier transmission scheme (Figure 9.13). Since OFDM data sub-carriers are statistically independent and identically distributed, based on the central limit theorem, when the number of sub-carriers N_{FFT} is large, the OFDM signal distribution tends to be Gaussian.

In an OFDM system, the SNR is a measure of channel quality and is a key factor of link-level error assessment. There are different methods for calculation of SNR in single-antenna and multi-antenna transmission systems. For single-input/single-output systems, the SNR can be viewed as the received SNR, i.e., the received SNR before the detector. The post-processing SNR is often used for MIMO links, and represents the SNR after combining in the receiver and measures the likelihood that a coded message is decoded successfully. In link-level simulations, the SNR γ is typically calculated using the following method. Let vector $\mathbf{x} = (x_1, x_2, \ldots, x_{N_{\text{TX}}})^H \in \mathbb{C}^{N_{\text{TX}} \times 1}$ denote the transmit signal, where $x_k \in \mathbb{C} \forall k = 1, 2, \ldots, N_{\text{TX}}$ is the complex-valued transmitted symbols from the kth transmit antenna. Note that N_{TX} is the number of transmit antennas. It can be shown that the total transmit signal power can be obtained as $\sigma_{\mathbf{x}}^2 = \text{trace}(\mathbf{R}_{\mathbf{x}})$,

Petitioners' Exhibit 1021
Nokia of America Corp., et al. v. KT Corporation, et al.
Case No. IPR2025-00036; U.S. Patent No. 11,627,631
Page 433 of 1122

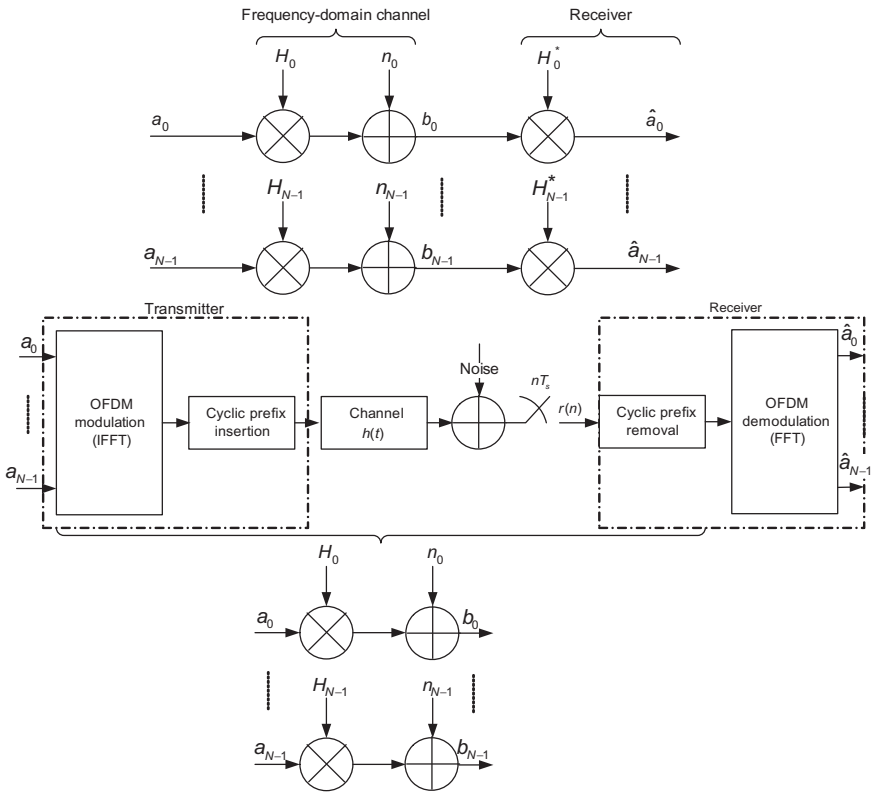


FIGURE 9.13

Single-tap equalization of the OFDM signal [14].

where $\mathbf{R_x}$ denotes the autocorrelation matrix of the transmitted signal. The transmit power from the kth antenna is given as $\sigma_{x_k}^2 = \mathscr{E}\{|x_k|^2\} = 1/N_{\text{TX}}$ (uniformly distributed power). If $\mathbf{H}$ represents the channel matrix with $||\mathbf{H}||_F^2 = N_{\text{TX}}N_{\text{RX}}$[4] in which N_{TX} and N_{RX} denote the number of transmit and receive antennas, respectively, the received signal vector $\mathbf{y}$ can be calculated as $\mathbf{y = Hx + v}$ where the complex-valued Gaussian-distributed noise vector $\mathbf{v} \sim \mathbb{Z}(\mathbf{0}, \sigma_{\mathbf{v}}^2\mathbf{I})$ denotes the noise vector with respect

[4]The p-norm of matrix $\mathbf{H}$ is defined as $\|\mathbf{H}\|_p = \left(\sum_{i=0}^{M-1}\sum_{j=0}^{N-1}|h_{ij}|^p\right)^{1/p}$. In the special case when $p = 2$, the norm is called the Frobenius norm and for $p = \infty$ is called the maximum norm. The Frobenius norm or Hilbert–Schmidt norm of matrix $\mathbf{H}$ are similar, although the latter term is often reserved for the operators on a Hilbert space. In general, this norm can be defined in the following forms: $\|\mathbf{H}\|_p = \sqrt{\sum_{i=0}^{M-1}\sum_{j=0}^{N-1}|h_{ij}|^2} = \sqrt{\text{trace}(\mathbf{H}^H\mathbf{H})} = \sqrt{\sum_{i=0}^{\min(M,N)-1}\zeta_i^2}$ where $\mathbf{H}^H$ denotes the conjugate transpose of matrix $\mathbf{H}$ and ζ_i are the singular values of matrix $\mathbf{H}$. The Frobenius norm is further similar to the Euclidean norm on $\mathbb{R}^N$ and is obtained from an inner product on the space of all matrices. The Frobenius norm is sub-multiplicative and is very useful for numerical linear algebra [31,32,34].

Petitioners' Exhibit 1021
Nokia of America Corp., et al. v. KT Corporation, et al.
Case No. IPR2025-00036; U.S. Patent No. 11,627,631
Page 434 of 1122

to the size of the FFT N_{FFT} and the number of used sub-carriers before the detector N_{Used}. We define the complex-valued Gaussian-distributed noise vector $\mathbf{n} \sim \mathbb{Z}(\mathbf{0}, \sigma_{\mathbf{n}}^2\mathbf{I})$ to be the noise after the FFT operation. The receive SNR before the detector is given as $\gamma_{\text{pre-FFT}} = \frac{||\mathbf{Hx}||_F^2}{N_{\text{RX}}\sigma_{\mathbf{v}}^2} = \sigma_{\mathbf{v}}^{-2}$ whereas the SNR after the FFT operation is given as $\gamma_{\text{post-FFT}} = \frac{||\mathbf{Hx}||_F^2}{N_{\text{RX}}\sigma_{\mathbf{n}}^2} = \sigma_{\mathbf{n}}^{-2}$. It can be seen that the ratio of pre-FFT and post-FFT SNRs $\frac{\gamma_{\text{pre-FFT}}}{\gamma_{\text{post-FFT}}} = \frac{\sigma_{\mathbf{v}}^2}{\sigma_{\mathbf{n}}^2} = \frac{N_{\text{FFT}}}{N_{\text{Used}}}; N_{\text{Used}} \leq N_{\text{FFT}}$ is always positive, implying that the FFT operation suppresses the noise and enhances the SNR [142].

9.4.1 Peak-to-average power ratio of OFDM signals

The peak-to-average power ratio (PAPR) for a single-carrier modulation signal depends on its constellation and the pulse shaping filter roll-off factor. For a Gaussian distributed OFDM signal, the cumulative distribution function (CDF)[5] of PAPR for 99.0%, 99.9%, and 99.99% are approximately 8.3, 10.3, and 11.8 dB, respectively. Since the OFDM signal has a high PAPR, it could be clipped in the transmitter power amplifier (PA), because of its limited dynamic range or non-linearity. Higher output back-off is required to prevent performance degradation and inter-modulation products leaking into adjacent channels. Therefore, RF PAs should be operated in a very large linear region. Otherwise, the signal peaks leak into the non-linear region of the PA causing signal distortion. This signal distortion introduces inter-modulation among the sub-carriers and out-of-band emission. Thus, the PAs should be operated with large power back-offs. On the other hand, this leads to very inefficient amplification and expensive transmitters. Thus, it is highly desirable to reduce the PAPR. In addition to inefficient operation of the PA, a high PAPR requires a larger dynamic range for the receiver analog-to-digital (A/D) converter. To reduce the PAPR, several techniques have been proposed and used such as clipping,[6] channel coding, temporal windowing, tone reservation,[7] and tone injection. However,

[5]The CDF of the real-valued random variable X is defined as $x \rightarrow F_X(x) = P(X \leq x), \forall x \in \mathbb{R}$, where the right-hand side represents the probability that random variable X takes on a real value less than or equal to x. The CDF of X can be defined in terms of the probability density function $f(x)$ as $F(x) = \int_{-\infty}^{x} f(x)\text{d}x$. The complementary CDF (CCDF), on the other hand, is defined as $P(X > x) = 1 - F_X(x)$ [30].

[6]Since the OFDM signal has a high PAPR, it may be clipped in the transmitter power amplifier, because of its limited dynamic range or non-linearity. Higher output back-off is required to prevent BER degradation and intermodulation products spilling into adjacent channels. However, clipping of an OFDM signal has a similar effect to impulse interference, against which an OFDM system is inherently robust. Computer simulations show that for a coded OFDM system, clipping of 0.5% of the time results in a BER degradation of 0.2 dB. At 0.1% clipping, the degradation is less than 0.1 dB [52].

[7]In the tone reservation method, the transmitter and the receiver reserve a subset of tones or sub-carriers for generating PAPR reduction signals. Those reserved tones are not used for data transmission [53].

Petitioners' Exhibit 1021
Nokia of America Corp., et al. v. KT Corporation, et al.
Case No. IPR2025-00036; U.S. Patent No. 11,627,631
Page 435 of 1122

most of these methods are unable to achieve simultaneously a large reduction in PAPR with low complexity, low coding overhead, without performance degradation, and without transmitter-receiver symbol handshake. The PAPR ξ of the OFDM signal, defined in Eq. (9.12), is calculated as follows:

$$\xi = \left. \frac{\max |s(t)|^2}{\mathscr{E}\{|s(t)|^2\}} \right|_{mT_u \le t \le (m+1)T_u} \tag{9.13}$$

In the above equation, $\mathscr{E}\{.\}$ denotes the expectation operator, and m is an integer. From the central-limit theorem, for large values of N_{FFT}, the real and imaginary values of $s(t)$ (from Eq. (9.12) and without the $\mathrm{Re}\{\cdot\}$ operator) would have Gaussian distribution. Consequently, the amplitude of the OFDM signal has a Rayleigh distribution with zero mean and a variance of N_{FFT} times the variance of one complex sinusoid. Assuming the samples to be mutually uncorrelated, the CDF for the peak power per OFDM symbol is given by:

$$P(\xi > \gamma) = [1 - (1 - e^{-\gamma})^{N_{FFT}}] \tag{9.14}$$

From the above equation, it can be seen that a large PAPR occurs only infrequently due to relatively large values of N_{FFT} used in practice.

Figure 9.14 shows the CDF of OFDM PAPR for BPSK and QPSK modulation assuming a 40 MHz channel bandwidth and $N_{FFT} = 128$. We further applied a 90° phase rotation to the sub-carriers in the upper 20 MHz of the

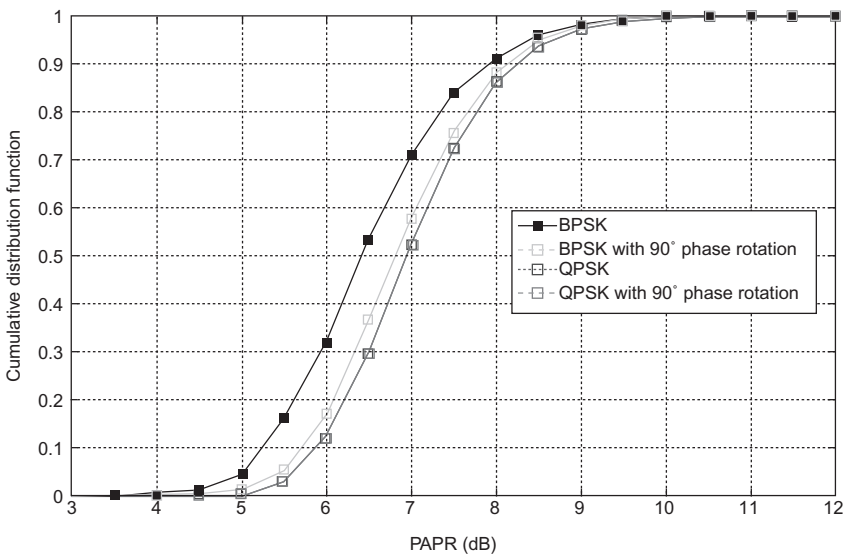


FIGURE 9.14

CDF of OFDM PAPR with BPSK/QPSK modulation and $N_{FFT} = 128$ [159].

Petitioners' Exhibit 1021
Nokia of America Corp., et al. v. KT Corporation, et al.
Case No. IPR2025-00036; U.S. Patent No. 11,627,631
Page 436 of 1122

channel, and investigated the effect on the PAPR reduction [159]. It is shown that large PAPR values are less likely to occur with large FFT sizes, as suggested by Eq. (9.14).

9.4.2 Effect of non-linearity on OFDM signals

Power amplifiers generally have a non-linear amplitude response, where the output power is saturated for large input powers. Most applications require operation in the linear region of the PA response where the output power is a linear function of the input. The larger the linear operation region, or alternatively the higher the saturation point, the more expensive the PA. Therefore, it is imperative to reduce the PAPR of the OFDM signal before processing through the PA. Figures 9.15 and 9.16 illustrate examples of PA AM/AM response and QAM signal constellation fuzziness when the OFDM signal with large PAPR is processed through a PA with a low saturation point (Figure 9.16). In this example, 64QAM modulation, 256-point IFFT with $T_{cp} = (1/4)T_u$, and PA saturation point of 6 dB are assumed.

The modulation accuracy or the permissible signal constellation fuzziness is often measured in terms of an error vector magnitude (EVM) metric. The EVM may be defined as the square root of the ratio of the mean error vector power to

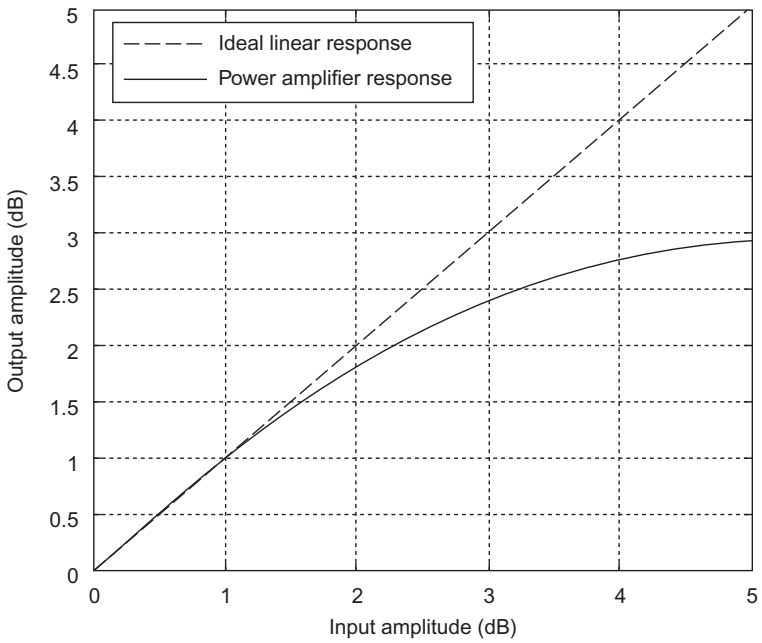


FIGURE 9.15

Example AM/AM response of a power amplifier (saturation point = 6 dB) [141].

Petitioners' Exhibit 1021
Nokia of America Corp., et al. v. KT Corporation, et al.
Case No. IPR2025-00036; U.S. Patent No. 11,627,631
Page 437 of 1122

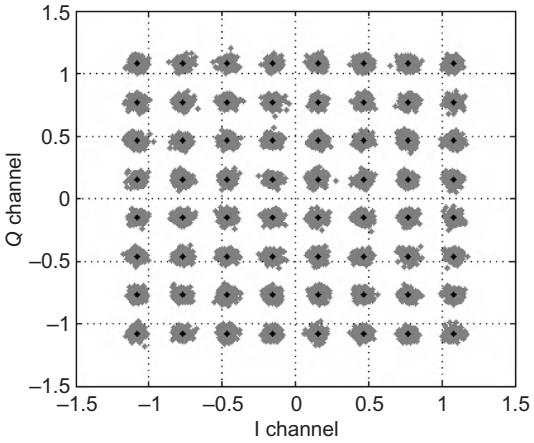


FIGURE 9.16

64QAM signal constellation before and after power amplification [141].

the mean reference signal power expressed as a percentage, i.e., the EVM can be expressed as $\text{EVM} = \sqrt{\mathscr{E}|\mathbf{e}|^2/\mathscr{E}|\mathbf{s}|^2}$ in mathematical form. In other words, the EVM defines the average constellation error with respect to the farthest constellation point (i.e., the distance between the reference signal and measured signal points in the $I-Q$ plane), and is calculated as follows [1]:

$$\text{EVM} = \sqrt{\frac{\sum_{i=0}^{N_{\text{samples}}-1} (\Delta I_i^2 + \Delta Q_i^2)}{N_{\text{samples}} r_{\text{max}}^2}} \tag{9.15}$$

where N_{samples} is the number of symbols used in the measurement period, ΔI_i and ΔQ_i refer to the in-phase (I) and quadrature (Q) components of the ith error vector, and r_{max} denotes the maximum constellation amplitude. The EVM is measured over the continuous portion of a burst occupying at least one-fourth of the transmission frame at maximum power settings. The permissible EVM can be estimated from the transmitter implementation margin, if the error vector is considered noise, which is added to the channel noise. The implementation margin is the excess power needed to maintain the carrier-to-noise ratio (C/N) intact, when going from the ideal to the realistic transmitter. The EVM cannot be measured at the antenna connector, but should be measured by an ideal receiver with a certain carrier recovery loop bandwidth specified as a percentage of the symbol rate. The measured EVM includes the effects of the transmitter filter accuracy, D/A converter, modulator imbalances, untracked phase noise, and PA non-linearity.

Petitioners' Exhibit 1021
Nokia of America Corp., et al. v. KT Corporation, et al.
Case No. IPR2025-00036; U.S. Patent No. 11,627,631
Page 438 of 1122

As mentioned earlier, the EVM is a measure of the difference between the reference waveform and the measured waveform. In practice, before calculating the EVM, the measured waveform is corrected by the sample timing offset and RF frequency offset. Then the IQ origin offset is removed from the measured waveform before calculating the EVM. The measured waveform is further modified by selecting the absolute phase and absolute amplitude of the transmit chain. The EVM value is defined after the front-end IDFT as the square root of the ratio of the mean error vector power to the mean reference signal power expressed as a percentage value.

The basic EVM measurement interval in the time-domain depends on the type of physical channel. The measurement interval is equal to the length of one preamble sequence for the physical random access channel (PRACH), and is equal to the length of one slot for the physical uplink control channel (PUCCH) and physical uplink shared channel (PUSCH) in the time-domain. When the PUSCH or PUCCH transmission slot is shortened due to multiplexing with Sounding Reference Signal (SRS), the EVM measurement interval is accordingly reduced by one symbol. The PUSCH or PUCCH EVM measurement interval is also reduced when the mean power, modulation, or allocation between slots is expected to change. In the case of PUSCH transmission, the measurement interval is reduced by a time interval equal to the sum of 5 μs and the applicable exclusion period adjacent to the point where the power change is expected to occur. The PUSCH exclusion period is applied to the signal obtained after the front-end IDFT. In the case of PUCCH transmission with power change, the PUCCH EVM measurement interval is reduced by one symbol adjacent to the point where the power change is expected to occur [1].

9.4.3 Effect of carrier frequency offset on OFDM signals

As mentioned earlier, an OFDM system transmits information as a series of OFDM symbols. The time-domain samples $x_m(n)$ of the mth OFDM symbol are generated by performing IDFT on the information symbols $X_m(k)|_{k=0,1,\ldots,N_{\text{FFT}}-1}$, as follows [132]:

$$x_m(n) = \frac{1}{N_{\text{FFT}}} \sum_{k=0}^{N_{\text{FFT}}-1} X_m(k) e^{j2\pi k(n-N_{\text{CP}})/N_{\text{FFT}}}; \quad \forall 0 \le n \le N_{\text{FFT}} + N_{\text{CP}} - 1 \qquad (9.16)$$

where N_{FFT} and N_{CP} are the number of data samples and cyclic prefix samples, respectively. The OFDM symbol $x_m(n)$ is transmitted through a channel $h_m(n)$ and is perturbed by a Gaussian noise $z_m(n)$. The channel $h_m(n)$ is assumed to be block stationary, i.e., it is time invariant over each OFDM symbol. With this assumption, the output $y_m(n)$ of the channel can be represented as $y_m(n) = h_m(n)^* x_m(n) + z_m(n)$, where $h_m(n)^* x_m(n) = \sum_{k=-\infty}^{+\infty} h_m(k) x_m(k-n)$ and $z_m(n)$ is a zero-mean additive white Gaussian noise (AWGN) with variance σ_z^2.

Petitioners' Exhibit 1021
Nokia of America Corp., et al. v. KT Corporation, et al.
Case No. IPR2025-00036; U.S. Patent No. 11,627,631
Page 439 of 1122

Since the channel impulse response $h_m(n)$ is assumed to be block stationary, the channel response does not change over each OFDM symbol; however, the channel response $h_m(n)$ may vary across different OFDM symbols, thus it is a function of the OFDM symbol index m.

When the receiver oscillator is not perfectly synchronized to the transmitter oscillator, there can be a CFO $\Delta f_{\text{CFO}} = f_{\text{TX}} - f_{\text{RX}}$ between the transmitter carrier frequency f_{TX} and the receiver carrier frequency f_{RX}. Furthermore, there may be a phase offset θ_0 between the transmitter carrier and the receiver carrier. The mth received symbol $y_m(n)$ can be represented as $y_m(n) = e^{j\{2\pi\Delta f_{\text{CFO}}[n+m(N_{\text{FFT}}+N_{\text{CP}})]T_s+\theta_0\}}[h_m(n)^* x_m(n)] + z_m(n)$, where T_s is the sampling period. The CFO Δf_{CFO} can be represented relative to the sub-carrier bandwidth $(1/N_{\text{FFT}}T_s)$ by defining the relative frequency offset $\delta_{\text{CFO}} = \Delta f_{\text{CFO}} N_{\text{FFT}} T_s$. The CFO attenuates the desired signal and introduces the ICI, thus decreasing the SNR. The SNR of the kth sub-carrier can be expressed as $\text{SNR}_k(\delta_{\text{CFO}}) = (\phi^2_{N_{\text{FFT}}}(\delta_{\text{CFO}})P_h\sigma_x^2/(1-\phi^2_{N_{\text{FFT}}}(\delta_{\text{CFO}}))P_h\sigma_x^2 + \sigma_z^2)$, where $\phi_{N_{\text{FFT}}}(\delta_{\text{CFO}}) = (\sin(\pi\delta_{\text{CFO}})/N_{\text{FFT}}\sin(\pi\delta_{\text{CFO}}/N_{\text{FFT}}))$ in order to demonstrate the dependence of the SNR on the frequency offset [132]. In the latter equation, P_h, σ_x^2, and σ_z^2 denote the total average power of channel impulse response, variance of the signal, and variance of the additive noise, respectively. The sub-carrier index k is dropped since the SNR is the same for all sub-carriers. From this SNR expression, it is clearly seen that the effect of the frequency offset is to decrease the signal power by $\phi^2_{N_{\text{FFT}}}(\delta_{\text{CFO}})$ and to convert the decreased power to interference power. The SNR depends not only on the frequency offset δ_{CFO}, but also on the number of sub-carriers; however, as N_{FFT} increases $\phi^2_{N_{\text{FFT}}}(\delta_{\text{CFO}})$ converges to $\text{sinc}^2(\delta_{\text{CFO}})$. Therefore, the SNR converges to $\text{SNR}(\delta_{\text{CFO}}) = (\text{sinc}^2(\delta_{\text{CFO}})P_h\sigma_x^2/(1-\text{sinc}^2(\delta_{\text{CFO}}))P_h\sigma_x^2 + \sigma_z^2)$ as N_{FFT} becomes increasingly large [132]. The effect of CFO on OFDM signal in the frequency-domain, which appears as inter-carrier interference, for different values of δ_{CFO} is shown in Figure 9.17. Figure 9.18 illustrates the variation of $\text{SNR}(\delta_{\text{CFO}})$ as a function of δ_{CFO} with $\gamma = P_h\sigma_x^2/\sigma_z^2$ as a parameter. In the above equations, the power of inter-carrier interference as a function of relative CFO is defined as $P_{\text{ICI}}(\delta_{\text{CFO}}) = (1-\text{sinc}^2(\delta_{\text{CFO}}))P_h\sigma_x^2$. In practice, the sub-carrier spacing is not the same among different tones due to mismatched oscillators (i.e., frequency offset), Doppler shift, and timing synchronization errors, resulting in inter-carrier interference and loss of orthogonality. It can be seen that the ICI increases with the increase of the OFDM symbol duration (or alternatively decrease of sub-carrier spacing) and the frequency offset. The effects of timing offset are typically less than that of the frequency offset, provided that the cyclic prefix is sufficiently large.

It can be shown that the ICI power can be calculated as a function of the generic Doppler power spectrum $\Lambda(\nu)$ as follows [14]:

$$P_{\text{ICI}} = \int_{-\nu_{\max}}^{\nu_{\max}} \Lambda(\nu)(1-\text{sinc}^2(T_s\nu))\text{d}\nu \tag{9.17}$$

Petitioners' Exhibit 1021
Nokia of America Corp., et al. v. KT Corporation, et al.
Case No. IPR2025-00036; U.S. Patent No. 11,627,631
Page 440 of 1122

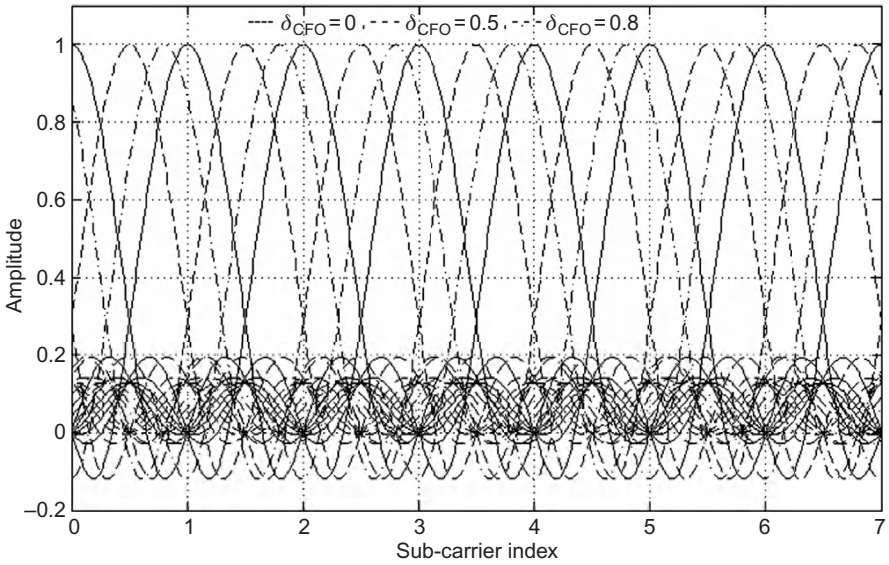


FIGURE 9.17

The effect of carrier frequency offset on OFDM signal for various δ_{CFO} values [159].

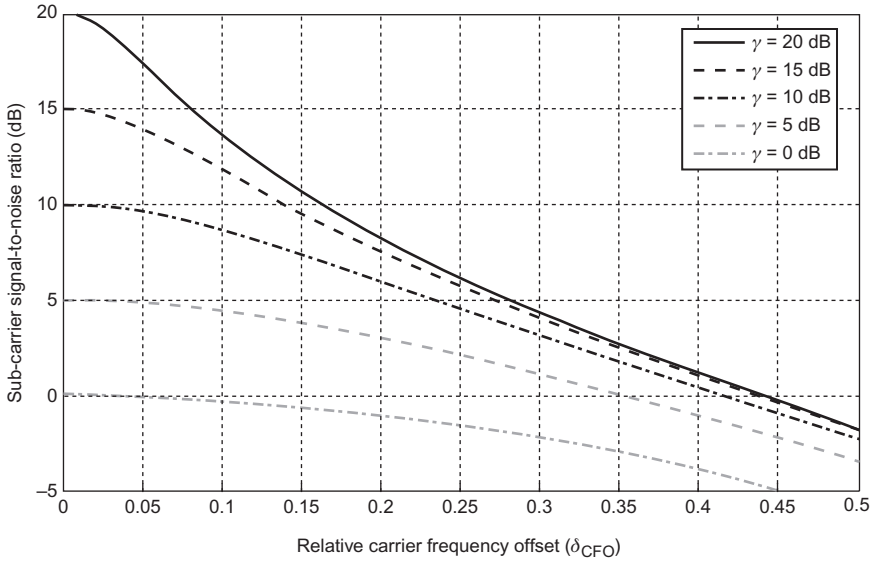


FIGURE 9.18

Variation of the SNR as a function of relative carrier frequency offset δ_{CFO} [159].

Petitioners' Exhibit 1021
Nokia of America Corp., et al. v. KT Corporation, et al.
Case No. IPR2025-00036; U.S. Patent No. 11,627,631
Page 441 of 1122

where $\nu_{\max}$ denotes the maximum Doppler frequency. We further assume that the transmitted signal power is normalized. It can be noted that the ICI generated as a result of CFO is a special case of the above equation when $\Lambda(f) = \delta(f - f_{\text{CFO}})$, in which $\delta(f)$ represents the Dirac delta function. Using the classic Jakes' model of Doppler spread where the spaced-time correlation function is defined as $\Phi(t) = J_0(2\pi\nu t)$ in which $J_0(x)$ denotes the zero-order Bessel function of the first kind [131], the ICI power can be written as follows:

$$P_{\text{ICI}_{\text{Jakes}}} = 1 - 2\int_0^1 (1-f)J_0(2\pi\nu_{\max}T_s f)\mathrm{d}f \tag{9.18}$$

which approximately gives an upper bound on the ICI power due to Doppler spread. Comparison of the power of ICI generated by CFO and Doppler spread suggests that the ICI impairment due to the former is higher than the latter.

The effect of CFO on EVM for an OFDM system with $E_b/N_0 = 30$ dB, $N_{\text{FFT}} = 64$ has also been investigated and is shown in Figure 9.19. It is shown that the EVM increases with increasing values of relative CFO even at such relatively high SNR.

Figure 9.20 shows the bit error rate sensitivity of an OFDM system under AWGN channel to CFO. The increasing values of relative CFO degrade the BER performance of the system.

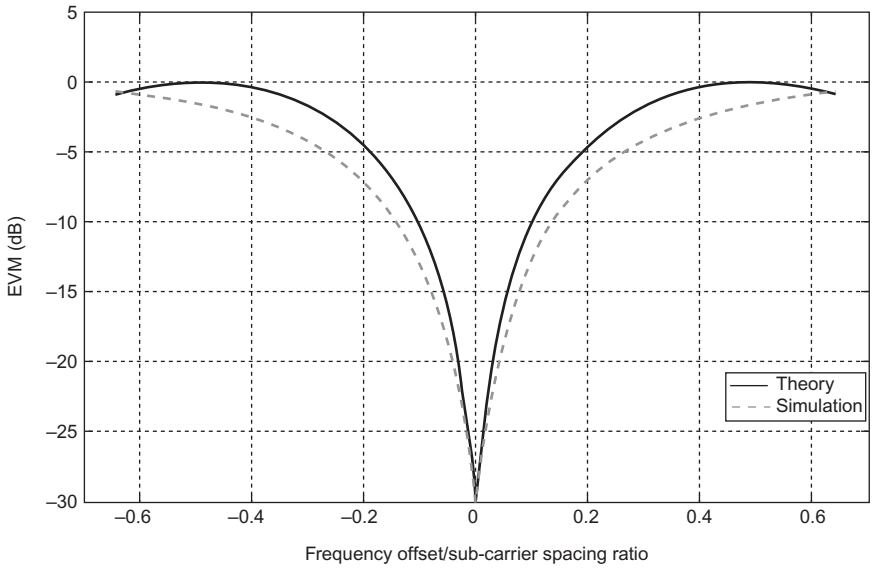


FIGURE 9.19

Error vector magnitude versus frequency offset in OFDM ($E_b/N_0 = 30$ dB, $N_{\text{FFT}} = 64$) [159].

Petitioners' Exhibit 1021
Nokia of America Corp., et al. v. KT Corporation, et al.
Case No. IPR2025-00036; U.S. Patent No. 11,627,631
Page 442 of 1122

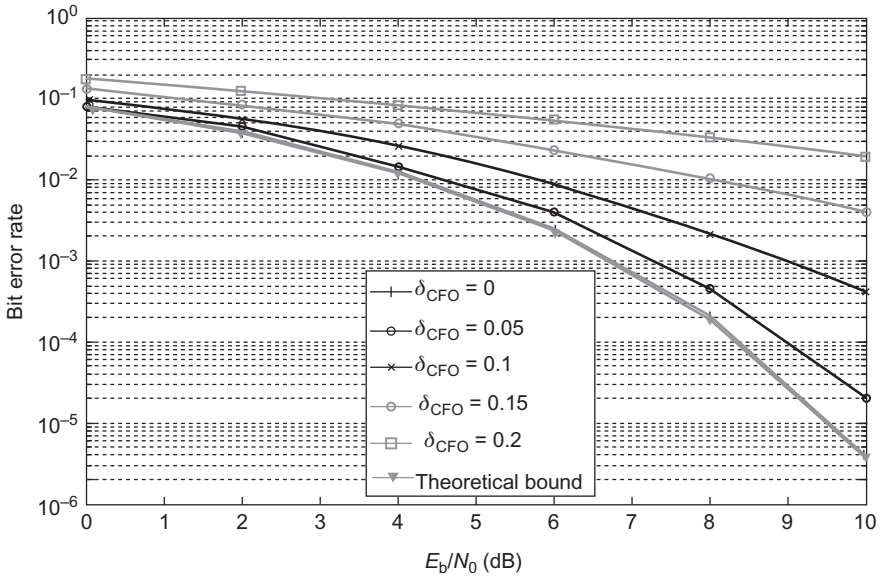


FIGURE 9.20

BER sensitivity to relative CFO δ_{CFO} in an OFDM system in AWGN channel [141].

9.4.4 Effect of oscillator phase noise on OFDM signals

Oscillators are used in typical radio circuits to drive the RF mixers which are utilized for the up-conversion/down-conversion of the band-pass signals. Ideally, the spectrum of the oscillator is expected to have an impulse at the frequency of oscillation with no frequency components elsewhere. However, the spectrum of a practical oscillator's output does exhibit spectrum variation around the oscillation frequency due to phase noise. The impact of local oscillator phase noise on the performance of an OFDM system has been extensively studied in the literature [159]. It has been shown that phase noise may have significant effects on OFDM signals with small sub-carrier spacing (i.e., large OFDM symbol duration in time). Long symbol duration is required for implementing a long guard interval that can mitigate long multipath delay in single frequency operation without excessive reduction of data throughput. The studies suggest that phase noise in OFDM systems can result in two effects: a common sub-carrier phase rotation on all the sub-carriers; and a thermal-noise-like sub-carrier de-orthogonality.

The common phase error, i.e., constellation rotation, on the demodulated sub-carriers is caused by the phase noise spectrum from DC up to the frequency of sub-carrier spacing. This low-pass effect is due to the long integration time of the OFDM symbol duration. This phase error can in principle be corrected by using pilots within the same symbol (in-band pilots). The phase error causes sub-carrier

Petitioners' Exhibit 1021
Nokia of America Corp., et al. v. KT Corporation, et al.
Case No. IPR2025-00036; U.S. Patent No. 11,627,631
Page 443 of 1122

constellation blurring rather than rotation. It results from the phase noise spectrum contained within the system bandwidth. This part of the phase noise is more crucial, since it cannot be easily corrected. The SNR degradation caused by the common phase error can be quantified as $S/N_{\text{phase-rotation}} = 1/(I(\alpha)\beta\,\Delta f)$, where Δf is the sub-carrier spacing, β denotes the upper bound of the phase noise spectral mask, α is the ratio of the equivalent spectrum mask noise bandwidth and sub-carrier spacing, and $I(\alpha) = \int_{-\alpha}^{+\alpha} \text{sinc}(\pi x)\text{d}x$ with $I(0.5) = 0.774$, $I(1) = 0.903$, and $I(\infty) = 0.774$. It can be seen that, when $\alpha > 1$, the common phase error decreases as the sub-carrier spacing decreases [52].

To mathematically model the effect of the phase noise, let us consider the noisy output of an oscillator which contains phase noise $\phi(t)$ as follows $v(t) = A_c \cos(\omega_c t + \phi(t))$. Let us further assume that the stochastic variation of the phase can be modeled as the output of a system with a step function impulse response and input perturbation $n(t)$ as follows: $\phi(t) = \int_{-\infty}^{t} n(\tau)\text{d}\tau$. Based on the above assumption, the single-sided power spectral density of the phase can be written as follows: $S_\phi(f) = S_n(f)/(2\pi f)^2$, in which $S_n(f)$ denotes the noise power spectral density function. As an example, if $S_n(f)$ is modeled as white noise, then $S_\phi(f) \approx f^{-2}$, and if $S_n(f)$ is modeled as flicker noise, then $S_\phi(f) \approx f^{-3}$. Considering that the power spectral density of the phase is difficult to observe, one may alternatively look at the power spectral density of the oscillator's noisy output $v(t)$. It can be shown that the power spectral density of $v(t)$ can be calculated as follows [159]:

$$S_v(f) = \sum_{k=-\infty}^{k=+\infty} \left(\frac{a_k^2 + b_k^2}{2}\right) \frac{\beta k^2 f_c^2}{\beta^2 \pi^2 k^4 f_c^4 + (f - k f_c)^2} \tag{9.19}$$

where $\{a_k\}$ and $\{b_k\}$ denote the Fourier series coefficients of $v(t)$ and β is a constant. Given that we are only interested in evaluating $S_v(f)$ at f_c, the above equation can be simplified as follows:

$$S_v(f) = \left(\frac{a_1^2 + b_1^2}{2}\right) \frac{\beta f_c^2}{\beta^2 \pi^2 f_c^4 + (f - f_c)^2} \tag{9.20}$$

The above function is a Lorentz distribution.[8] We now define function $\Omega(f)$ as the ratio of noise power in the 1 Hz bandwidth at offset f from center frequency to carrier power which is expressed in dBc/Hz. As theoretically expected, having a higher phase noise in the signal does not increase the total power. A signal with higher phase noise will have smaller power near f_c and will have a broader spectrum around the center frequency. Conversely, a signal with lower phase noise

[8]The Cauchy distribution is a continuous probability distribution which is also known as the Lorentz distribution, Cauchy–Lorentz distribution, or Lorentzian function. It describes the distribution of a random variable that is the ratio of two independent standard normal random variables and has the probability density function defined as $f(x; 0, 1) = 1/[\pi(1 + x^2)]$ [30].

Petitioners' Exhibit 1021
Nokia of America Corp., et al. v. KT Corporation, et al.
Case No. IPR2025-00036; U.S. Patent No. 11,627,631
Page 444 of 1122

has a sharper peak at the center frequency with less deviation. Therefore, $\Omega(f)$ can be expressed as follows:

$$\Omega(f) = \frac{1}{\pi}\frac{\gamma}{\gamma^2 + (f - f_c)^2} \quad \gamma = \beta\pi f_c^2 \tag{9.21}$$

It can be shown that $\int_{-\infty}^{+\infty} \Omega(f)\mathrm{d}f = 1$ [159]. Figure 9.21 illustrates the ratio of the noise power to carrier power at $f_c = 500$ Hz for different values of β. It can be seen from the figure, for higher values of β, the spectrum becomes wider with smaller magnitude of the main lobe of the spectrum. Note that a wider main lobe does not increase the total power of the carrier.

In summary, an OFDM system has the following advantages [52]:

- It is sufficiently flexible in meeting various design requirements such as low complexity, bandwidth efficiency and scalability, spectrum shaping, and low sensitivity to various impairments.
- OFDM is well suited to multi-antenna transmission schemes.
- It requires no adaptation to instantaneous channel response for low-order modulations. It is robust to impulse interference and channel variations. Channel estimation is required for high-order QAM modulations.
- As a multi-tone transmission technique, OFDM is less sensitive to shift in sampling time in comparison to serial transmission techniques.

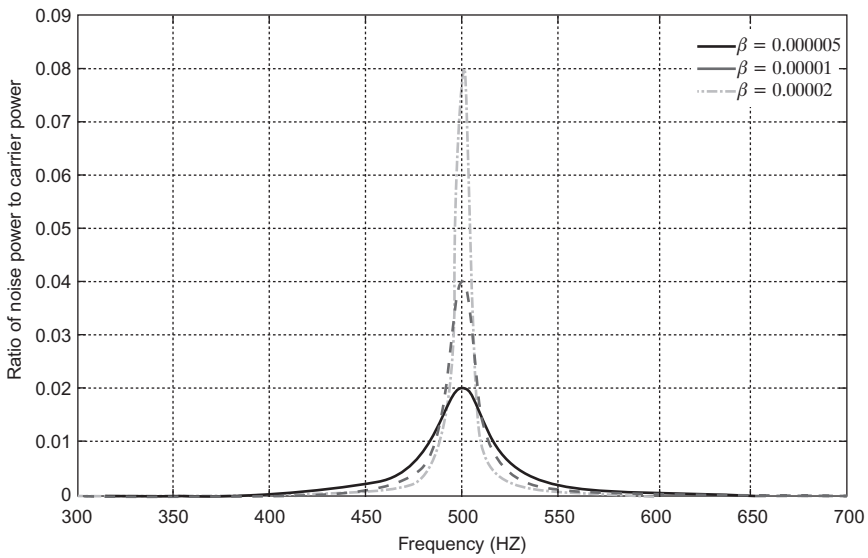


FIGURE 9.21

Plot of the noise power to carrier power $\Omega(f)$ at $f_c = 500$ Hz for different values of β [159].

Petitioners' Exhibit 1021
Nokia of America Corp., et al. v. KT Corporation, et al.
Case No. IPR2025-00036; U.S. Patent No. 11,627,631
Page 445 of 1122

- The bandwidth efficiency of an OFDM system approaches the Nyquist rate as the FFT size increases (this, however, increases system complexity and is subject to an upper limit due to channel variations and CFO).
- For fixed bandwidth efficiency, the complexity (multiplications per symbol) of an FFT-based OFDM system grows logarithmically with the increase of the channel multipath delay spread, in comparison with a linear increase of complexity for equalizers for a single carrier system.
- A properly coded and interleaved OFDM system can exceed the performance of many other practical systems. Higher transmitter output back-off is required in comparison to a single carrier system, because of the high PAPR of an OFDM system.
- As a parallel transmission technique, OFDM is more sensitive to CFO and tone interference than that of a single carrier system.

9.5 Multiple access schemes

Orthogonal frequency division multiple access (OFDMA) is the multi-user variant of the OFDM scheme where multiple access is achieved by assigning subsets of sub-carriers to different users, allowing simultaneous data transmission from several users. In OFDMA, the radio resources are two-dimensional (2D) regions over time (an integer number of OFDM symbols) and frequency (a number of contiguous or non-contiguous sub-carriers). The difference between OFDM and OFDMA is illustrated in Figure 9.22. Similar to OFDM, OFDMA employs multiple closely spaced sub-carriers, but the sub-carriers are divided into groups of sub-carriers where each group is called a resource block. The grouping of sub-carriers into groups of resource blocks is referred to as sub-channelization. The sub-carriers that form a resource block do not need to be physically adjacent. In the downlink, a resource block may be allocated to different users. In the uplink, a user may be assigned to one or more resource blocks.

Sub-channelization defines sub-channels that can be allocated to mobile stations depending on their channel conditions and service requirements. Using sub-channelization, within the same time slot (i.e., an integer number of OFDM symbols), an OFDMA system can allocate more transmit power to user devices with lower SNR, and less power to user devices with higher SNR. Sub-channelization also enables the base station to allocate higher power to sub-channels assigned to indoor mobile terminals, resulting in better indoor coverage.

There are various multiple access schemes that have been used in cellular systems in the past few years which allow the network to share the available radio resources (i.e., time, frequency, code, and space) among a number of users in the cell in the downlink and uplink directions. Figure 9.23 illustrates the concept of resource sharing in various multiple access schemes. As mentioned earlier, OFDMA has been a promising multiple-access scheme that has recently been

Petitioners' Exhibit 1021
Nokia of America Corp., et al. v. KT Corporation, et al.
Case No. IPR2025-00036; U.S. Patent No. 11,627,631
Page 446 of 1122

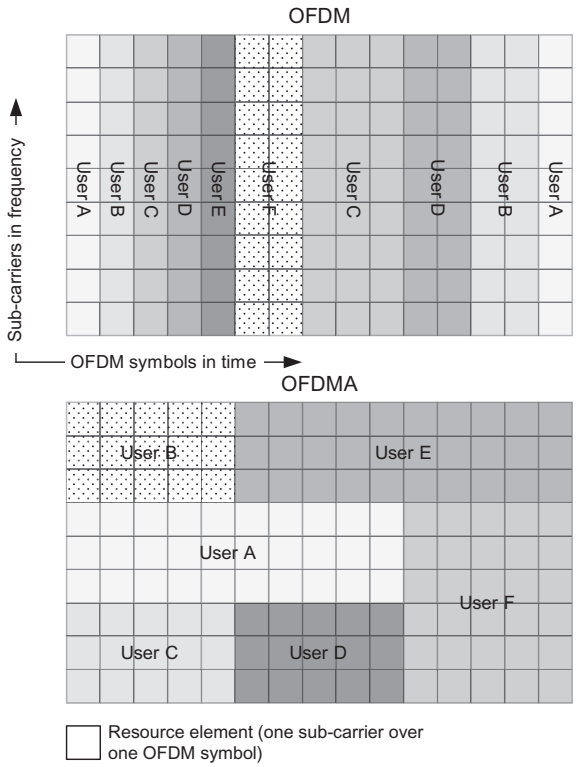


FIGURE 9.22

Illustration of OFDM and OFDMA concepts.

used in mobile broadband radio access technologies. The E-UTRA uses OFDMA and SC-FDMA as the multiple access schemes in the downlink and uplink directions, respectively. The OFDMA/SC-FDMA parameters for the E-UTRA have been chosen to facilitate coexistence with the UTRA on the same platform and sharing the same temporal sampling frequency of 30.72 MHz. The E-UTRA OFDMA/SC-FDMA parameters are given in Table 9.2. The following parameters are compatible with UMTS sampling frequency/chip rate of 3.84 Mcps and frame timing.

The OFDMA/SC-FDMA parameters in E-UTRA satisfy general design criteria for OFDM systems as follows:

$$\begin{aligned} &T_{\mathrm{CP}} \geq \tau_{\mathrm{RMS}} && \text{(to prevent ISI due to delay spread)} \\ &\Delta f \gg \nu_{\max} && \text{(to mitigate ICI due to Doppler spread)} \\ &T_{\mathrm{CP}}\, \Delta f \ll 1 && \text{(for spectral efficiency improvement)} \end{aligned} \tag{9.22}$$

Petitioners' Exhibit 1021
Nokia of America Corp., et al. v. KT Corporation, et al.
Case No. IPR2025-00036; U.S. Patent No. 11,627,631
Page 447 of 1122

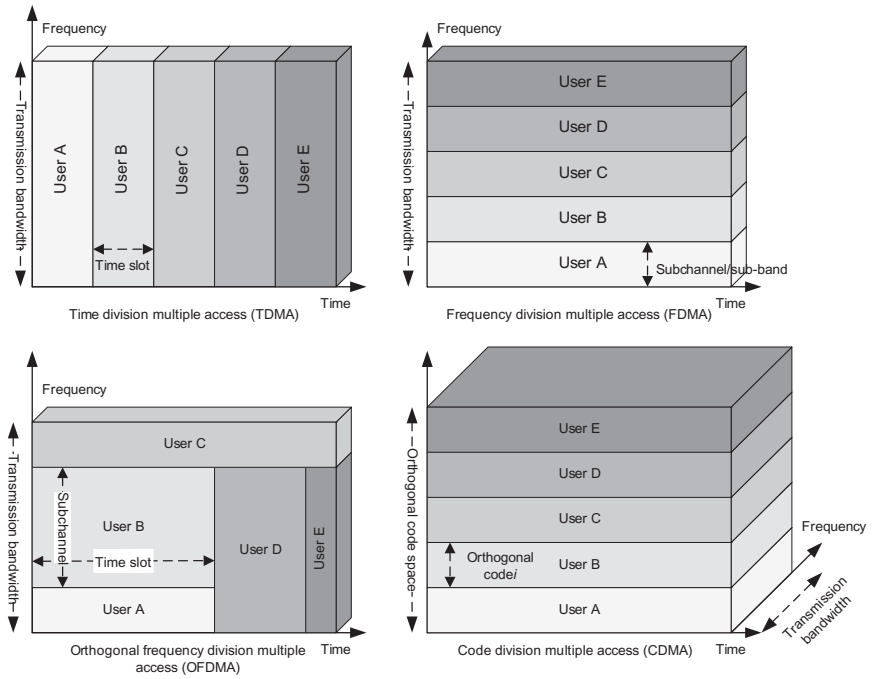


FIGURE 9.23

An illustration of the concept of different multiple access schemes.

In OFDMA, an OFDM symbol is constructed of sub-carriers, the number of which are determined by the FFT size. There are several sub-carrier types: (1) data sub-carriers are used for data transmission; (2) pilot or reference-signal sub-carriers are utilized for channel estimation and coherent detection; and (3) null sub-carriers are not used for pilot/data transmission. The null sub-carriers, including the DC sub-carrier, are used for guard bands. The number of used (or occupied) sub-carriers is always less than the FFT/IFFT size. The guard bands are used to allow spectrum sharing and to reduce the adjacent channel interference and out-of-band emissions. The sampling frequency is selected to be greater than or equal to the channel bandwidth. The number of time samples in a radio frame is always an integer, and to further simplify the design of analog transmit filter the sampling frequency is scaled by a factor greater than one (e.g., the sampling frequency for 20 MHz bandwidth is 30.72 MHz). As given in Table 9.2, the value of the over-sampling factor depends on the channel bandwidth. The E-UTRA supports a large number of channel bandwidths. The channel bandwidths that are integer multiples of 5 MHz are more important. The bandwidths that are not given

Petitioners' Exhibit 1021
Nokia of America Corp., et al. v. KT Corporation, et al.
Case No. IPR2025-00036; U.S. Patent No. 11,627,631
Page 448 of 1122

Table 9.2 E-UTRA OFDMA/SC-FDMA Parameters [3]

Parameter	Value					
Channel bandwidth (MHz)	1.4	3	5	10	15	20
Number of resource blocks $N_{RB}^{DL/UL}$	6	15	25	50	75	100
Number of occupied sub-carriers	72	180	300	600	900	1200
IFFT/FFT size	128	256	512	1024	1536	2048
Sub-carrier spacing Δf (kHz)	15 (7.5)					
Sampling frequency (MHz)	1.92	3.84	7.68	15.36	23.04	30.72
Samples/slot	960	1920	3840	7680	11520	15360
CP size T_{CP} — Normal CP ($\Delta f = 15$ kHz)	5.21 μs (first symbol of the slot) 4.69 μs (other symbols of the slot) $N_s = 7$ symbols/slot $N_{CP}(l) = \begin{cases} 160 & l = 0 \\ 144 & l = 1, 2, \ldots, 6 \end{cases}$					
CP size T_{CP} — Extended CP ($\Delta f = 15$ kHz)	16.67 μs $N_s = 6$ symbols/slot $N_{CP}(l) = 512 \quad l = 0, 1, \ldots, 5$					
CP size T_{CP} — Extended CP ($\Delta f = 7.5$ kHz)	33.33 μs $N_s = 3$ symbols/slot $N_{CP}(l) = 1024 \quad l = 0, 1, 2$					

in Table 9.2 are supported via tone dropping, i.e., dropping the sub-carriers at the edges of the frequency band based on 10 and 20 MHz systems (e.g., for 6 MHz channel bandwidth, the parameter of 10 MHz is used and the edge sub-carriers are dropped to fit the spectrum block).

9.6 Duplex modes

One of the key elements of any radio communication system is the way in which radio communications are maintained in both directions. For cellular systems, it is necessary to enable transmission of data in both directions simultaneously, and this places a number of constraints on the schemes that may be used to control the transmission flow. As a result, the duplex scheme forms a very basic part of the overall specification for a cellular or any radio communication system. The term duplex refers to the bidirectional communications between two devices. When unpaired spectrum, or alternatively the same RF carrier is used for downlink and uplink communications, the transmit/receive functions are time-multiplexed.

When paired spectrum, or alternatively two RF carriers are used for downlink and uplink communications, the transmit/receive functions are frequency-multiplexed. The FDD is a duplex scheme in which uplink and downlink

Petitioners' Exhibit 1021
Nokia of America Corp., et al. v. KT Corporation, et al.
Case No. IPR2025-00036; U.S. Patent No. 11,627,631
Page 449 of 1122

transmissions occur simultaneously using different frequencies. The downlink and uplink frequencies are separated by a sufficiently large frequency offset (see Table 9.1 for various E-UTRA bands). For the FDD scheme to properly operate, it is necessary that the frequency separation, i.e., channel separation between the transmission and reception frequencies, be sufficient to prevent the receiver being excessively affected by the transmitter signal. Receiver blocking is an important issue with FDD schemes, and often highly selective filters may be required. For cellular systems using FDD, filters are required within the base station and also the user terminal to ensure sufficient isolation of the transmitter signal without desensitizing the receiver. While implementation cost is not a significant constraint for the base stations, placing a filter into the user terminals is more of an issue. The use of an FDD system does enable simultaneous transmission and reception of signals. However, two channels are required and this may not always use the available spectrum efficiently. The spectrum used for FDD systems is allocated by the regulatory authorities. Since there is a frequency separation between the uplink and downlink frequencies, it is not normally possible to reallocate spectrum to change the balance between the capacity of the uplink and downlink directions, if there are changing capacity requirements for each direction.

The TDD is a duplex scheme where uplink and downlink transmissions occur at different times, but may share the same frequency. In other words, the downlink and uplink transmissions are multiplexed in time and are not concurrent. While FDD transmissions require a large frequency separation between the transmit and receive frequencies, TDD schemes require a guard time or guard interval between transmission and reception. This must be sufficient to allow the signals traveling from the remote transmitter to arrive before a transmission is started and the receiver is shut down. Although this delay is relatively short, when switching between transmission and reception many times a second, even a small guard time can reduce the efficiency of the system, because a percentage of the time must be used for the guard interval. For small-sized cells, e.g., up to a mile or so, the guard interval is normally small and acceptable. For large cell sizes, it may become an issue.

The guard interval required for TDD will comprise two main elements: (1) a time allowance for the propagation delay for any transmission from a remote transmitter to arrive at the receiver. This will depend upon the distances involved (i.e., cell radius). (2) A time allowance for the transceiver to switch from receive to transmit mode. The switching times can vary considerably depending on the implementation, but can take a few microseconds. As a result, TDD is not normally suitable for use over very large cell sizes as the guard time increases and the spectral efficiency decreases.

It is often found that traffic in both directions is not balanced. Typically there is more data transmitted in the downlink direction of a cellular system. This means that, ideally, the capacity should be greater in the downlink direction. Using a TDD system, it is possible to change the capacity in either direction relatively easily by changing the number of time slots allocated to each direction. Often this is dynamically configurable so it can be altered to meet the demand. A further aspect

Petitioners' Exhibit 1021
Nokia of America Corp., et al. v. KT Corporation, et al.
Case No. IPR2025-00036; U.S. Patent No. 11,627,631
Page 450 of 1122

to be noted with TDD transmission is that of latency. Since the data may not be immediately transmitted, a result of the time multiplexing between transmit and receive circuitry, there may be a small delay between the time that the data is generated until it is actually transmitted in a TDD system. Typically this may be a few milliseconds depending upon the frame timing. Both TDD and FDD have their advantages, and each can be used in different deployment scenarios. Before deciding on a particular type of duplex scheme, it is necessary to analyze the advantages and disadvantages of each duplex mode. Table 9.3 summarizes the relative advantages/disadvantages of TDD and FDD systems.

The E-UTRA supports TDD and FDD schemes with a great extent of commonality in the baseband processing. In order to reduce the implementation complexity and cost of FDD terminals, and further to increase the reuse of baseband functional elements, a half-duplex FDD (H-FDD) operation is supported where the downlink and uplink transmissions are not simultaneous but occur in two different frequencies. As shown in Figure 9.24, classic H-FDD operation does not efficiently utilize the radio resources on the downlink and uplink RF carriers. The complementary grouping and scheduling of users would allow efficient use of downlink and uplink resources in an H-FDD operation. The various duplex schemes are illustrated in Figure 9.24. For H-FDD operation, a guard period (GP) is virtually created by the UE by not receiving the last OFDM symbol(s) of a downlink subframe immediately preceding an uplink subframe in which the UE is active. The length of the GP is the sum of the maximum round-trip propagation delay in the cell, transmit-to-receive, and receive-to-transmit switching delay at the UE.

In E-UTRA, the differences between TDD and FDD schemes are mainly in the physical layer, and therefore are transparent to the higher layers. As a result, there are no significant operational differences between the two modes in the system architecture. At the physical layer, the fundamental design goal was to achieve as much commonality between the two modes as possible. The key design differences between the two stem from the need to support various TDD UL/DL allocations and provide coexistence with other TDD systems. In this regard, several additional features are exclusively developed for E-UTRA TDD. For instance, the FDD and TDD modes differ in the time placement of the downlink synchronization signals. In FDD, the primary and secondary synchronization signals are contiguously placed within one subframe, while in TDD, the two signals are placed in different subframes, separated by two OFDM symbols. However, this separation of the primary and secondary synchronization signals does not affect the performance of synchronization channels relative to FDD systems.

The system-level simulations also show that the sector throughput and cell-edge throughput of E-UTRA TDD and FDD mode are quite similar for best effort traffic when comparing a 10 + 10 MHz FDD system to a 20 MHz TDD system. The spectral efficiency of the TDD mode is slightly degraded due to the

Petitioners' Exhibit 1021
Nokia of America Corp., et al. v. KT Corporation, et al.
Case No. IPR2025-00036; U.S. Patent No. 11,627,631
Page 451 of 1122

Table 9.3 Comparison of TDD and FDD Attributes

Attribute	TDD	FDD
Paired spectrum	Does not require paired spectrum as both transmit and receive occur on the same channel.	Requires paired spectrum with sufficient frequency separation to allow simultaneous transmission and reception.
Hardware cost	Lower cost as no duplexer[a] is needed to isolate the transmitter and receiver.	Duplexer is needed and the implementation cost is higher
Channel reciprocity	Channel propagation is the same in both directions which enables estimation of the downlink channel from the uplink channel.	Channel characteristics are different in both directions due to use of different frequencies.
UL/DL asymmetry	It is possible to dynamically change the UL and DL ratio based on the traffic volume in each direction.	UL/DL bandwidths are determined by frequency allocation designated by the regulatory authorities. It is therefore not possible to dynamically adapt to the traffic volume.
Guard period/ frequency separation	Guard period required to ensure uplink and downlink transmissions do not interfere. Large guard period will limit the capacity. Larger guard period is normally required if distances are increased to accommodate larger propagation delays. Note that a guard band in frequency-domain is required to suppress interference to adjacent bands.	Frequency separation is required to provide sufficient isolation between uplink and downlink. However, large frequency separation does not impact the capacity. Note that a guard band in frequency-domain is required to suppress interference to adjacent bands.
Discontinuous transmission	Discontinuous transmission is required to allow both uplink and downlink transmissions. This can degrade the performance of the RF power amplifier in the transmitter.	Continuous transmission is possible.
Switching point synchronization	Base stations are required to be synchronized with respect to the uplink and downlink transmission times. If neighboring base stations use different uplink and downlink assignments and share the same channel, then interference may occur between cells.	Not applicable.

[a] *A diplexer is a passive device that implements frequency domain multiplexing. Two ports are multiplexed onto a third port. The signals on each input port occupy non-overlapping frequency bands. Consequently, the signals on the input ports can coexist on the output port without interfering with each other. On the other hand, a duplexer is a device that allows bidirectional communication over a single channel. In radar and radio communications systems, the duplexer isolates the receiver from the transmitter while permitting them to share a common antenna. Most radio repeater systems include a duplexer. Duplexers are designed for operation in the frequency band used by the receiver and transmitter, and must be capable of handling the output power of the transmitter. They must provide sufficient isolation between transmitter and receiver to prevent receiver desensitization [34].*

Petitioners' Exhibit 1021
Nokia of America Corp., et al. v. KT Corporation, et al.
Case No. IPR2025-00036; U.S. Patent No. 11,627,631
Page 452 of 1122

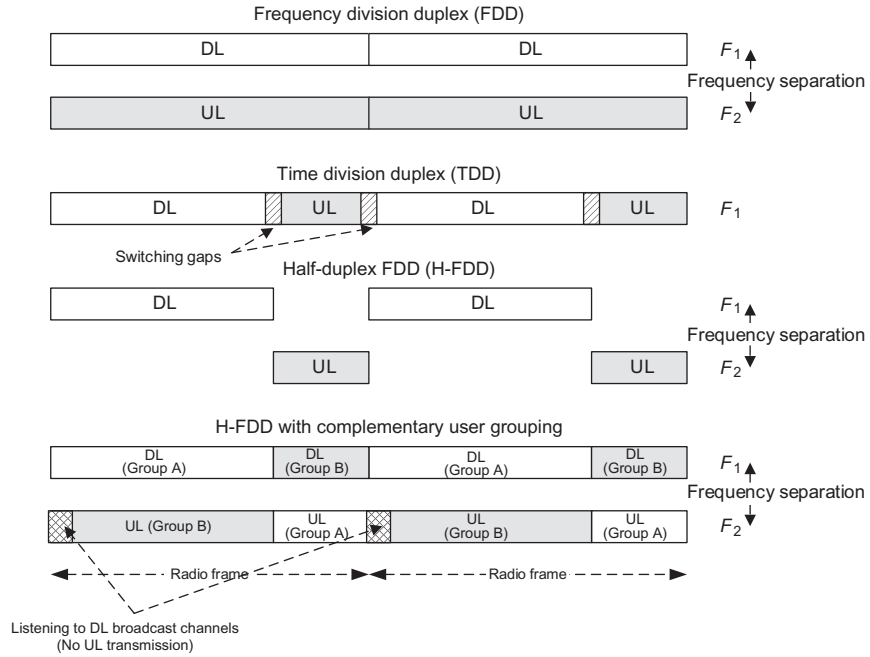


FIGURE 9.24

Illustration of the concept of different duplexing schemes.

additional overhead corresponding to the GP. Another advantage of TDD systems is the flexibility they may offer to network operators in terms of adjusting the DL/UL ratio. This feature allows operators to configure the DL/UL ratio to suit the user traffic in their network.

A common misperception regarding TDD systems is that the uplink coverage of the TDD systems is inferior relative to their FDD counterpart. The link-budget analysis for both systems in the outdoor and indoor environments with compatible system configuration and transmitter and receiver settings shows that the TDD system matches the uplink coverage of the FDD counterpart [10]. In fact, the E-UTRA TDD and FDD modes utilize the same slot/subframe structure and resource block size, thus the same amount of power is transmitted during the same time interval, implying that the coverage will be the same. What has been fueling this misconception is the single-user uplink data rate in an unloaded network at the cell-edge, where an FDD system will show a cell-edge performance that is twice that of the TDD system. It must be noted that the link budget analysis focuses only on the cell-edge single user performance when that user terminal is at the maximum limit of its uplink power, hence it can only be given access to five resource blocks (one resource block every 1 ms for 5 ms, or half of the length of

Petitioners' Exhibit 1021
Nokia of America Corp., et al. v. KT Corporation, et al.
Case No. IPR2025-00036; U.S. Patent No. 11,627,631
Page 453 of 1122

the 10 ms E-UTRA radio frame with DL:UL = 1:1 ratio) to meet the 200 mW maximum power requirement. In comparison, in an FDD system at the cell-edge, one single device will be able to send 200 mW continuously for 10 ms, assuming that the scheduler can give the device access to 10 resource blocks of 1 ms with no waiting time. However, in real-life scenarios, the cells have more than one user and the performance of FDD and TDD systems will be very similar, as the FDD device will not be able to access the full-frame 10 uplink resource blocks similar to an unloaded network. In that case, because the TDD channel is twice as wide as the FDD channel, the user is likely to be given access to as many resource blocks as an FDD system despite the half-uplink time in the frame compared to an FDD frame. For network operators, an E-UTRA TDD will provide the same coverage and very similar sector throughput relative to an E-UTRA FDD system. The TDD with its adaptable DL:UL ratio would allow an optimized and efficient use of the uplink and downlink bandwidths as the operators are able to match the asymmetry of data traffic and to maximize spectrum utilization and efficiency in almost all scenarios [163].

9.7 Frame structure

Downlink and uplink transmissions are structured into radio frames with 10 ms duration. The E-UTRA supports two frame structures, namely, type 1 and type 2 for FDD and TDD duplex schemes, respectively. The radio frames are numbered using a system frame number (SFN). The SFN is defined using a string of 10 bits which provide an integer value from 0 to 1023. Therefore, the SFN repeats once every 10.24 s, i.e., 1024 frames. The eight most significant bits of the SFN are broadcast within the master information block (MIB) of the system information on the broadcast channel (BCH). The remaining bits of SFN are deduced from the four frame cycles used to transmit the MIB (i.e., the first radio frame corresponds to "00" and the fourth radio frame corresponds to "11"). As given in Table 9.2, using the normal cyclic prefix, there are seven OFDM symbols within each slot. In the case of multi-cell aggregation, the same frame structure is used across all serving cells. Transmissions in multiple cells can be aggregated up to four secondary cells (in this context cell refers to RF carriers) in addition to the primary cell.

To provide enhanced multicast and broadcast services, E-UTRA has the capability to transmit multicast and broadcast content over a single frequency network (MBSFN), where a time-synchronized common waveform is transmitted from multiple eNBs, allowing macro-diversity combining of multi-cell transmissions at the UE. The cyclic prefix is utilized to cover the difference in the propagation delays, which makes the MBSFN transmission appear to the UE as a transmission from a single large cell. In LTE, transmission on a dedicated carrier for MBSFN

Petitioners' Exhibit 1021
Nokia of America Corp., et al. v. KT Corporation, et al.
Case No. IPR2025-00036; U.S. Patent No. 11,627,631
Page 454 of 1122

with the possibility to use a longer CP with a sub-carrier bandwidth of 7.5 kHz is supported, as well as transmission of MBSFN on a carrier with both MBMS and unicast transmissions using time division multiplexing [7].

9.7.1 Frame structure type 1

Frame structure type 1 is applicable to both full-duplex FDD and H-FDD schemes. In frame structure type 1, as illustrated in Figure 9.25, each 10 ms radio frame is divided into 10 equally-sized subframes ($T_{\text{frame}} = 307,200T_s = 10T_{\text{subframe}}$). Each subframe consists of two equally sized and consecutive 0.5 ms slots ($T_{\text{slot}} = 15360T_s$). Each slot in turn consists of a number of OFDM symbols which can be either seven (normal cyclic prefix) or six (extended cyclic prefix). As shown in Figure 9.25, the useful symbol time is $T_u = 2048T_s = 66.7\ \mu s$. For a normal cyclic prefix, the first symbol has a cyclic prefix lengths of $T_{CP} = 160T_s = 5.2\ \mu s$. The remaining six OFDM symbols have a cyclic prefix of length $T_{CP} = 144T_s = 4.7\ \mu s$. The reason for different cyclic prefix lengths of the first symbol is to make the overall slot length in terms of time units divisible by 15,360. For the extended mode, the cyclic prefix is $T_{CP} = 512T_s = 16.67\ \mu s$. The length of the cyclic prefix is longer than the delay spread of a few microseconds typically encountered in practice. The normal cyclic prefix is used in urban cells and high data rate applications, while the extended cyclic prefix is used in special cases like multi-cell broadcast and in very large cells (e.g., rural areas, low data rate

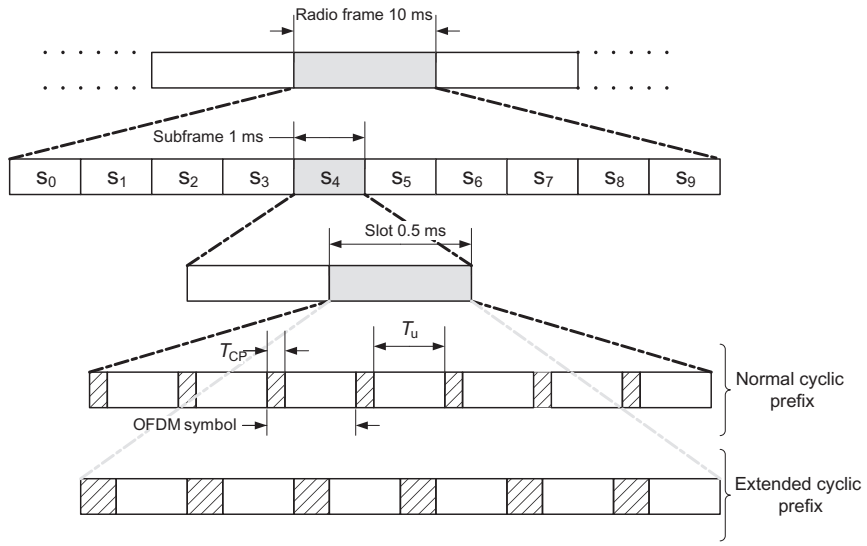


FIGURE 9.25

Frame structure type 1 with different cyclic prefix sizes [3,10].

applications). The cyclic prefix reduces the physical layer capacity by approximately 7.5% in the case of a normal cyclic prefix.

One way to reduce the relative overhead due to cyclic prefix insertion is to reduce the sub-carrier spacing with a corresponding increase in the OFDM symbol duration. However, this will increase the sensitivity of the OFDM transmission to frequency deviations resulting from fast channel variations and large Doppler spread, as well as different types of frequency errors due to RF circuitry. For FDD systems, 10 subframes are separately available for downlink and uplink transmissions in each 10 ms interval. Uplink and downlink transmissions are separated in the frequency-domain. In H-FDD operation, the UE cannot transmit and receive at the same time, while there are no such restrictions in full-duplex FDD.

The transmission time interval (TTI) of the E-UTRA downlink/uplink is 1 ms. The TTI is defined as the duration of the transmission of the physical layer encoded packets over the radio air-interface. In other words, the TTI refers to the length of an independently decodable transmission on the air-link. The data on a transport channel is organized into transport blocks. In each TTI, at most one transport block of variable size is transmitted over the radio air-interface to or from a terminal in the absence of spatial multiplexing. In the case of spatial multiplexing, up to two transport blocks per TTI are transmitted [3].

In the frequency-domain, the number of sub-carriers N_{FFT} ranges from 128 to 2048, depending on the channel bandwidth, with 512 and 1024 for 5 and 10 MHz, respectively, being most commonly used in practice. The sub-carrier spacing is 15 kHz. The sampling rate is chosen as $f_s = 15,000N_{\text{FFT}}$, resulting in a sampling rate that is an integer multiple or sub-multiple of the WCDMA chip rate of 3.84 Mcps. The OFDM parameters have been chosen such that FFT sizes and sampling rates are easily scalable for all operation bandwidths, while at the same time facilitating the implementation of multi-mode terminals with a common reference clock. Not all the sub-carriers are modulated or used. The DC sub-carrier is not used, as well as a number of sub-carriers on either side of the frequency band; thereby, approximately 10% of sub-carriers are used as guard sub-carriers.

9.7.2 Frame structure type 2

Frame structure type 2 is applied to a TDD duplex scheme where the downlink and uplink transmissions are time-multiplexed over the extent of a radio frame (Figure 9.26). Each radio frame of length 10 ms ($T_{\text{frame}} = 307,200T_s$) comprises two half-frames, where each half-frame consists of five subframes of length 1 ms. The supported downlink/uplink ratios (i.e., the ratio of downlink and uplink subframes in a frame) are listed in Table 9.4 and shown in Figure 9.27, where for each subframe in a radio frame, "DL" denotes the subframe reserved for downlink transmissions, "UL" denotes the subframe designated to uplink transmissions, and "S" denotes a special subframe comprising three fields downlink pilot time slot (DwPTS), GP, and uplink pilot time slot (UpPTS). The length of DwPTS and

Petitioners' Exhibit 1021
Nokia of America Corp., et al. v. KT Corporation, et al.
Case No. IPR2025-00036; U.S. Patent No. 11,627,631
Page 456 of 1122

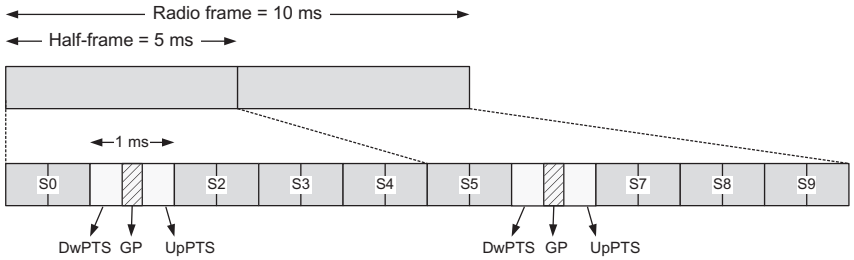


FIGURE 9.26

Frame structure type 2 [3].

Table 9.4 E-UTRA TDD Permissible DL/UL Ratios [3]

E-UTRA TDD Frame Configuration	Switching-Point Periodicity (ms)	Subframe Number									
		0	1	2	3	4	5	6	7	8	9
0	5	DL	S	UL	UL	UL	DL	S	UL	UL	UL
1	5	DL	S	UL	UL	DL	DL	S	UL	UL	DL
2	5	DL	S	UL	DL	DL	DL	S	UL	DL	DL
3	10	DL	S	UL	UL	UL	DL	DL	DL	DL	DL
4	10	DL	S	UL	UL	DL	DL	DL	DL	DL	DL
5	10	DL	S	UL	DL	DL	DL	DL	DL	DL	DL
6	5	DL	S	UL	UL	UL	DL	S	UL	UL	DL

UpPTS are given in Table 9.5, assuming that the total length of DwPTS, GP, and UpPTS is always 1 ms. Each subframe i is defined as two slots $2i$ and $2i + 1$ of length 0.5 ms.

The E-UTRA TDD supports downlink/uplink ratios with both 5 and 10 ms downlink/uplink switching-point periodicity. In the case of 5 ms switching-point periodicity, there are two special subframes within one radio frame. Subframes 0 and 5 and DwPTS are always reserved for downlink transmission due to essential downlink physical channel mapping. The UpPTS interval and the subframe immediately following the special subframe are always reserved for uplink transmission. In case multiple cells are aggregated, and in order to minimize inter-cell interference, the UE may assume the same downlink/uplink ratio across all the cells and that the GPs of the special subframes in different cells have a minimum overlap of $1456T_s$. For the switching from uplink to downlink transmission, no special subframe is provisioned, but the GP includes the sum of switching times from DL to UL and UL to DL. The switching from UL to DL is achieved by provisioning an appropriate timing advance at the UE.

Petitioners' Exhibit 1021
Nokia of America Corp., et al. v. KT Corporation, et al.
Case No. IPR2025-00036; U.S. Patent No. 11,627,631
Page 457 of 1122

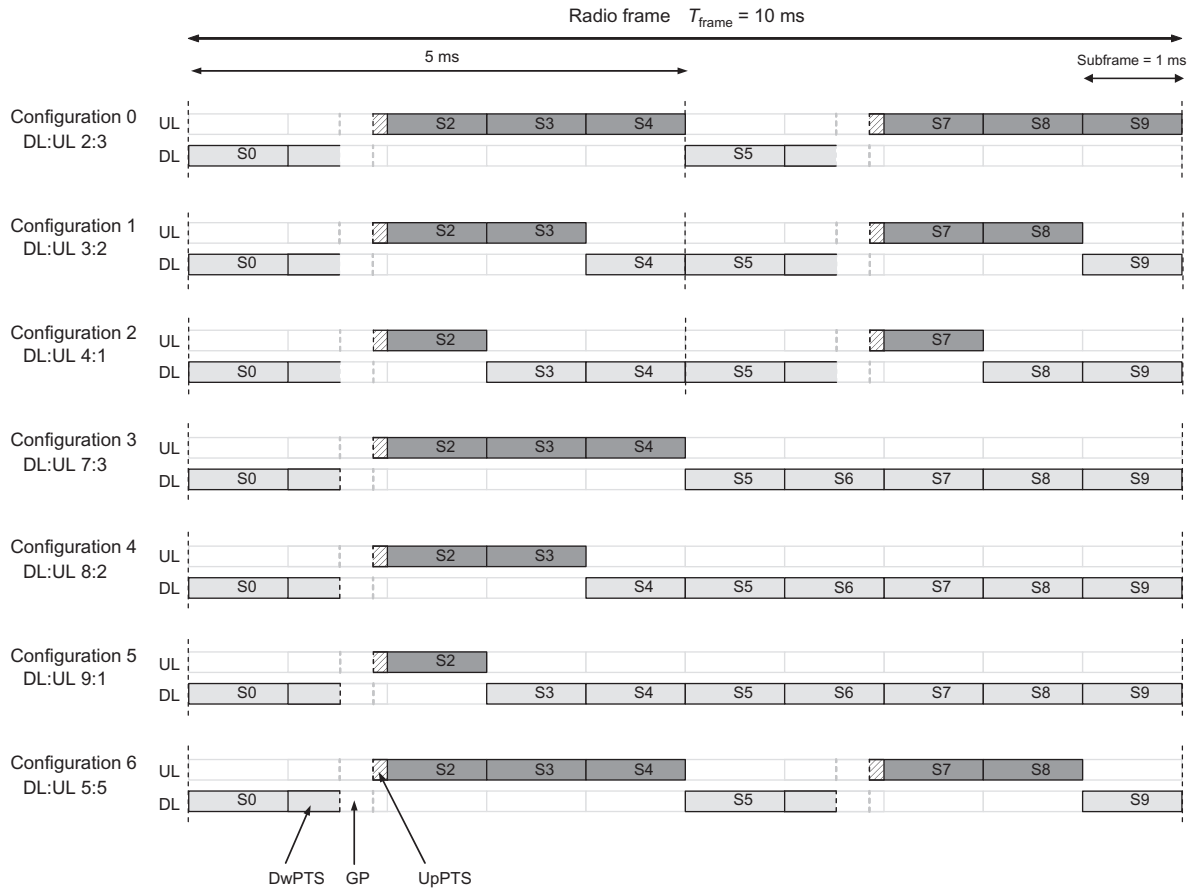


FIGURE 9.27

Illustration of various frame structure type-2 configurations [10].

Petitioners' Exhibit 1021
Nokia of America Corp., et al. v. KT Corporation, et al.
Case No. IPR2025-00036; U.S. Patent No. 11,627,631
Page 458 of 1122

Table 9.5 Various Special Subframe Configurations (DwPTS/GP/UpPTS) [3]

Special Subframe Configuration	Normal Cyclic Prefix in Downlink				Extended Cyclic Prefix in Downlink			
	DwPTS (Duration/ Number of OFDM Symbols)	GP (Number of OFDM Symbols)	UpPTS		DwPTS (Duration/ Number of OFDM Symbols)	GP (Number of OFDM Symbols)	UpPTS	
			Normal Cyclic Prefix in Uplink (Duration/ Number of OFDM Symbols)	Extended Cyclic Prefix in Uplink (Duration/ Number of OFDM Symbols)			Normal Cyclic Prefix in Uplink (Duration/ Number of OFDM Symbols)	Extended Cyclic Prefix in Uplink (Duration/ Number of OFDM Symbols)
0	$6592T_s$ 3	10			$7680T_s$ 3	8		
1	$19760T_s$ 9	4			$20480T_s$ 8	3		
2	$21952T_s$ 10	3	$2192T_s$ 1	$2560T_s$ 1	$23040T_s$ 9	2	$2192T_s$ 1	$2560T_s$ 1
3	$24144T_s$ 11	2			$25600T_s$ 10	1		
4	$26336T_s$ 12	1			$7680T_s$ 3	7		
5	$6592T_s$ 3	9			$20480T_s$ 8	2		
6	$19760T_s$ 9	3			$23040T_s$ 9	1	$4384T_s$ 2	$5120T_s$ 2
7	$21952T_s$ 10	2	$4384T_s$ 2	$5120T_s$ 2	$12800T_s$			
8	$24144T_s$ 11	1			– –	–	– –	– –
9	$13168T_s$ 6	6			– –	–	– –	– –

Petitioners' Exhibit 1021
Nokia of America Corp., et al. v. KT Corporation, et al.
Case No. IPR2025-00036; U.S. Patent No. 11,627,631
Page 459 of 1122

Within a radio frame, an E-UTRA TDD system switches multiple times between downlink and uplink transmissions. In this process, different signal propagation times between eNB and various UEs must be taken into consideration in order to prevent interference with other subframes. The timing advance feature prevents conflicts as a result of switching from uplink to downlink transmission. The UEs are informed by the eNB as to when they must start their uplink transmission. The greater the distance between the eNB and the UE, the earlier the UE starts transmitting. This helps to ensure that all signals reach the eNB with proper timing. When switching from the downlink to the uplink, a GP is inserted between the DwPTS and the UpPTS fields. The duration of the GP depends on the signal propagation round-trip time from the eNB to the UE, as well as on the time the UE requires to switch from receiving to transmitting states. The duration of the GP is configured by the network based on the cell size. Because the overall length of the special subframe remains constant, and the GP length varies based on cell size, the lengths of the DwPTS and UpPTS have to be adjusted. There are ten different special subframe configurations specified for E-UTRA TDD, as given in Table 9.5. The length of the GP determines the maximum supportable cell size. The E-UTRA should support cell sizes of up to 100 km, requiring a GP of approximately 666.7 μs. This is possible by choosing configuration 0 in Table 9.5 for the special subframe.

While the GP separates uplink and downlink transmissions, the other special fields are used for data/control signaling transmission. The DwPTS field carries synchronization and user data, as well as the downlink control channel for transmitting scheduling and control information. The UpPTS field is used for transmitting PRACH and SRS.

An example of coexistence with a legacy TD-SCDMA system [171] is shown in Figure 9.28, which illustrates switching point alignment between the two systems. It must be noted that in order to reduce the number of special subframe patterns in LTE TDD, only few legacy TD-SCDMA frame configurations are supported; therefore, the support is limited to the most common deployment scenarios, e.g., TD-SCDMA DL:UL = 5:2 and DL:UL = 4:3 configurations [163]. Despite the unequal size of the slots in TD-SCDMA and LTE TDD, the use of an

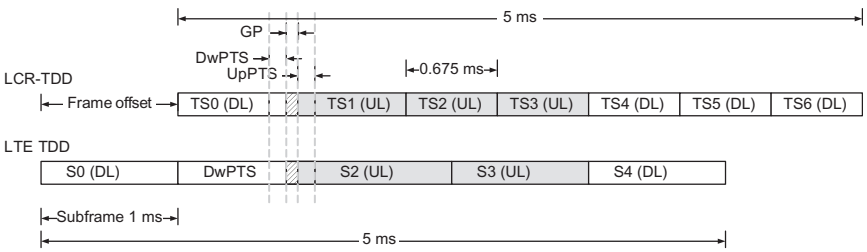


FIGURE 9.28

Example of LTE TDD coexistence with a TD-SCDMA system [163].

Petitioners' Exhibit 1021
Nokia of America Corp., et al. v. KT Corporation, et al.
Case No. IPR2025-00036; U.S. Patent No. 11,627,631
Page 460 of 1122

appropriate frame offset (as shown in Figure 9.28) allows alignment of the special subframes to the possible extent such that uplink and downlink transmissions of the two systems are synchronized [163].

9.7.3 MBSFN subframe structure

In E-UTRA frame structure, each downlink subframe and the DwPTS fields in the case of TDD is divided into a control region, consisting of the first OFDM symbols of the subframe, and a data region, comprising the remaining OFDM symbols of the subframe. A subset of the downlink subframes in a radio frame on a carrier supporting physical downlink shared channel (PDSCH) transmission can be configured as MBSFN subframes by higher layers. Each MBSFN subframe is divided into a non-MBSFN region and an MBSFN region. The non-MBSFN region spans the first one or two OFDM symbols in an MBSFN subframe. The MBSFN region in an MBSFN subframe is defined as the OFDM symbols not used for the non-MBSFN region.

The MBSFN subframes were originally designed to support MBSFN transmissions. However, they have also been found useful in other areas such as E-UTRA relaying functionality or the new carrier types. The MBSFN subframes are viewed as a generic tool, not necessarily related to MBSFN transmissions, which can provide time−frequency resources for enabling non-backward compatible functionalities relative to LTE Rel-8. An MBSFN subframe, as illustrated in Figure 9.29, consists of a control region of length one or two OFDM symbols, which is identical to normal subframes, followed by an MBSFN data region whose content will depend on the usage of the MBSFN subframe. The reason for maintaining the same control region in the MBSFN subframes is in consideration for normal

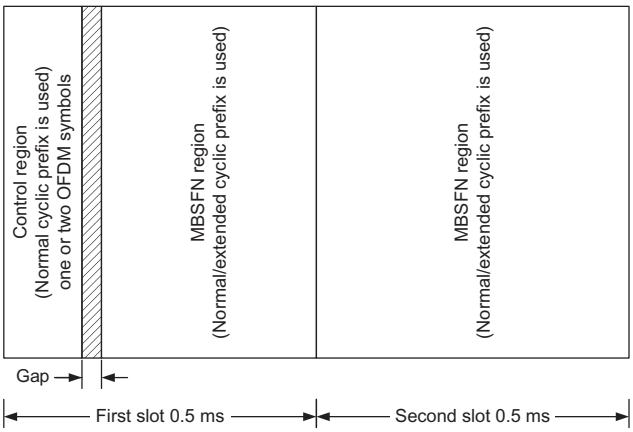


FIGURE 9.29

MBSFN subframe structure [15].

Petitioners' Exhibit 1021
Nokia of America Corp., et al. v. KT Corporation, et al.
Case No. IPR2025-00036; U.S. Patent No. 11,627,631
Page 461 of 1122

operation of LTE Rel-8 UEs, and in order to transmit control signaling necessary for uplink transmissions. All user terminals will be capable of receiving the control region of an MBSFN subframe. This is the main reason for which MBSFN subframes have been found useful for introducing new and non-backward compatible types of signaling and transmission modes in the new releases of LTE, without compromising the backward compatibility with earlier releases. The user terminals that are not capable of receiving transmissions in the MBSFN data region will simply ignore those transmissions.

Information about the set of subframes that are configured as MBSFN subframes in a cell is provided as part of the system information. In principle, an arbitrary pattern of MBSFN subframes can be configured with the pattern repeating after 40 ms. However, since physical signals and other essential information for system operation need to be transmitted in an orderly fashion to the UEs to find and attach to a cell, subframes where such information is mapped cannot be configured as MBSFN subframes. Therefore, subframes 0, 4, 5, and 9 for FDD and subframes 0, 1, 5, and 6 for TDD cannot be configured as MBSFN subframes, leaving the remaining six subframes as candidates for MBSFN subframes.

9.8 Resource structure, allocation, mapping

The minimum time–frequency resource unit used for downlink transmission is a resource element, which is defined as one sub-carrier over one OFDM symbol. For both TDD and FDD duplex schemes, a group of 12 sub-carriers contiguous in frequency over one slot in time form a PRB, i.e., a two-dimensional region corresponding to one slot in the time-domain and 180 kHz (i.e.,12×15 kHz) in the frequency-domain. The transmissions are allocated in units of PRB. More specifically, the data or control signaling in each slot is transmitted via one or several resource elements of $12 \times N_{\mathrm{RB}}^{\mathrm{DL}}$ sub-carriers over $N_{\mathrm{s}}^{\mathrm{DL}}$ OFDM symbols. The value of the parameter $N_{\mathrm{RB}}^{\mathrm{DL}}$ depends on the downlink transmission bandwidth configured for the cell, and is given as $\min(N_{\mathrm{RB}}^{\mathrm{DL}}) \leq N_{\mathrm{RB}}^{\mathrm{DL}} \leq \max(N_{\mathrm{RB}}^{\mathrm{DL}})$, where $\min(N_{\mathrm{RB}}^{\mathrm{DL}}) = 6$ for 1.4 MHz RF channels, and $\max(N_{\mathrm{RB}}^{\mathrm{DL}}) = 110$ for 20 MHz channels. The set of permissible values for $N_{\mathrm{RB}}^{\mathrm{DL}}$ are given in Table 9.2. The number of OFDM symbols in a slot $N_{\mathrm{s}}^{\mathrm{DL}}$ depends on the cyclic prefix length and the sub-carrier spacing configuration as given in Table 9.2.

There are a number of physical channels and physical signals that are mapped to predetermined (or configurable) locations in time and frequency over a radio frame that are used to assist proper operation of the system and the mobile terminals. The downlink physical channels correspond to a set of resource elements carrying data/control signaling information originating from higher protocol layers. The following downlink physical channels are defined in LTE/LTE-Advanced:

- Physical broadcast channel (PBCH): It carries the MIB portion of the system information. It is mapped to six resource blocks which are centered around

Petitioners' Exhibit 1021
Nokia of America Corp., et al. v. KT Corporation, et al.
Case No. IPR2025-00036; U.S. Patent No. 11,627,631
Page 462 of 1122

DC sub-carrier in subframe 0 and utilizes the resource elements which are not reserved for transmission of reference signals or other downlink control signaling. The BCH transport block is mapped to four subframes within a 40 ms interval.

- Physical control format indicator channel (PCFICH): It carries the size of PDCCH and is mapped to the first OFDM symbol in each downlink or special subframe. It contains the information on the number of OFDM symbols used for the downlink control region. The exact location of PCFICH is determined by the cell identity and system bandwidth.
- Physical hybrid-ARQ indicator channel (PHICH): It carries HARQ feedback corresponding to uplink data transmissions.
- Physical downlink control channel (PDCCH): It informs the UE(s) about transport format, resource allocation, HARQ feedback, and uplink grants. It is mapped to the first $L = 1, 2, \text{or } 3$ OFDM symbols in each downlink subframe. The number of the OFDM symbols for PDCCH is obtained via PCFICH. Multiple PDCCHs may be monitored by a UE. It also carries uplink power control commands.
- Physical downlink shared channel (PDSCH): It carriers downlink data transmission for different users as well as upper layer signaling.
- Physical multicast channel (PMCH): It is used to broadcast MBMS services.

In addition to the above physical channels, a set of downlink physical signals corresponding to a predetermined set of resource elements are specified and used by the physical layer which do not carry information originating from higher layers but are extremely important for proper LTE/LTE-Advanced system operation. The downlink physical signals include a variety of reference signals (also known as pilots which allow the UE to estimate the communication channel and coherently detect/decode data and control information that can be either cell-specific or UE-specific) and synchronization signals that provide timing and frequency synchronization, as well as physical identity of the cell to UEs attempting to select/reselect the cell. Figure 9.30 depicts the location of the downlink physical channels and signals in time and frequency within a type 1 frame structure.

9.8.1 Physical and virtual resource blocks

Each resource element is uniquely identified by the index pair (k, l) in a slot where $k = 0, \ldots, 12 \times N_{\text{RB}}^{\text{DL}} - 1$ and $l = 0, \ldots, N_{\text{s}}^{\text{DL}} - 1$ are the indices corresponding to frequency and time dimensions, respectively. Throughout this book, we assume that LTE/LTE-Advanced sub-carrier spacing is 15 kHz and there are 12 sub-carriers in each physical and virtual resource block (VRB) per slot. The structure of resource blocks in the downlink is shown in Figure 9.31. LTE/LTE-Advanced defines two types of resource blocks: physical and VRBs where in the latter, the resource blocks over a slot are permuted across frequency dimension to

Petitioners' Exhibit 1021
Nokia of America Corp., et al. v. KT Corporation, et al.
Case No. IPR2025-00036; U.S. Patent No. 11,627,631
Page 463 of 1122

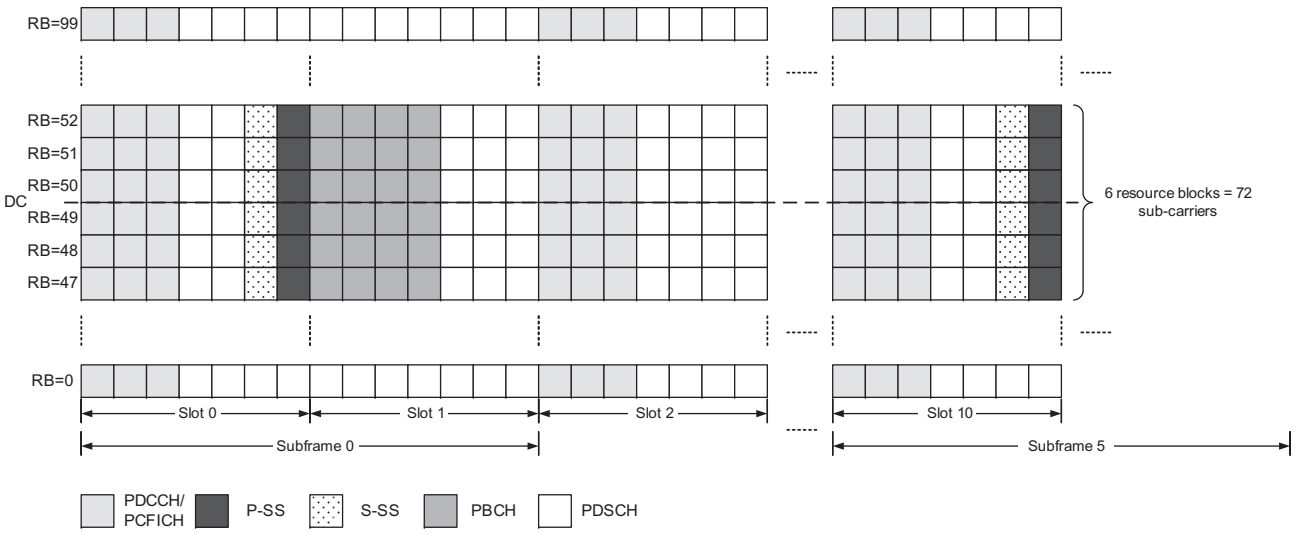


FIGURE 9.30

Physical resource structure and channel mapping (FDD, $N_s^{DL} = 7$, $N_{RB}^{DL} = 100$) [158].

Petitioners' Exhibit 1021
Nokia of America Corp., et al. v. KT Corporation, et al.
Case No. IPR2025-00036; U.S. Patent No. 11,627,631
Page 464 of 1122

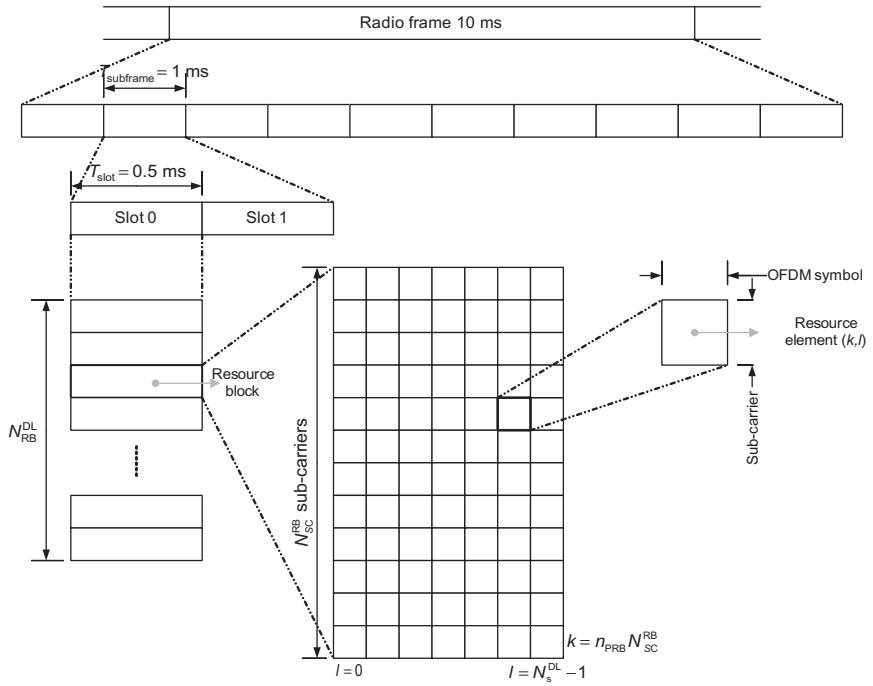


FIGURE 9.31

Resource block structure in time and frequency dimensions [3,162].

take advantage of frequency diversity. Another unit of resource allocation in the downlink is resource block group (RBG), which is a group of resource blocks. Allocating resources in RBG quanta reduces signaling overhead by reducing the number of bits required to uniquely address and identify each RBG relative to individual resource block identification/addressing. The size and number of RBGs depend on the channel bandwidth.

A PRB is defined as N_s^{DL} consecutive OFDM symbols in the time-domain and 12 (or 24 in the case of 7.5 kHz sub-carrier spacing) consecutive sub-carriers in the frequency-domain. A PRB consists of $12 \times N_s^{DL}$ resource elements corresponding to one slot in the time-domain and 180 kHz in the frequency-domain. The PRBs are numbered from 0 to $N_{RB}^{DL} - 1$ in the frequency-domain (see Figure 9.31). The relation between the PRB number n_{PRB} in the frequency-domain and resource elements (k, l) in a slot is given by $n_{PRB} = \lfloor k/12 \rfloor$.

A VRB has the same size as a PRB. There are two types of VRBs: VRBs of localized type and VRBs of distributed type. For each type of VRB, a pair of VRBs over two slots in a subframe is assigned together by a single VRB number n_{VRB}. VRBs of localized type are mapped directly to PRBs such that VRB index

Petitioners' Exhibit 1021
Nokia of America Corp., et al. v. KT Corporation, et al.
Case No. IPR2025-00036; U.S. Patent No. 11,627,631
Page 465 of 1122

n_{VRB} is identical to PRB index n_{PRB}. The VRBs are numbered from 0 to $N_{\text{VRB}}^{\text{DL}} - 1$, where $N_{\text{VRB}}^{\text{DL}} = N_{\text{RB}}^{\text{DL}}$. In the localized allocations, there is a one-to-one mapping between virtual and PRBs, whereas in the distributed case of resource allocation, the VRB numbers are mapped to PRB numbers according to a certain rule and inter-slot hopping is further utilized. In the latter, the first part of a VRB pair is mapped to one PRB and the other part of the VRB pair is mapped to another PRB which is at a predefined gap distance (which causes the inter-slot hopping) in order to achieve frequency diversity gain. This mechanism is especially important for small resource block allocations due to inherently less frequency diversity.

The distributed VRBs are mapped to PRBs such that consecutive VRBs are not mapped to sequential PRBs in the frequency-domain. A single VRB pair may be further split in the frequency-domain. Allocation of distributed resources includes a mapping from logically consecutive VRB pairs to physically non-consecutive PRB pairs to provide frequency diversity among VRB pairs. This is performed by a virtual block-interleaver or permutation scheme which operates on resource block pairs. The allocation of distributed resources further includes splitting of each resource-block pair such that the two resource blocks of the resource-block pair are transmitted with a certain frequency gap which provides additional frequency diversity for a single VRB pair. The latter can be interpreted as the introduction of frequency hopping on a slot basis. We will see later in this section that the associated PDCCH downlink control information (DCI) indicates whether allocated VRBs are of a localized or distributed type in the case of type 2 resource allocations. Thus, it is possible to dynamically switch between distributed and localized allocation, and also mix distributed and localized transmission for different terminals within the same subframe. The exact size of the frequency gap in Figure 9.32 depends on the overall downlink system bandwidth as given in Table 9.6. The gaps have been chosen based on the following criteria: (1) the gap size should be in the order of half of the total bandwidth (in terms of the number of resource blocks) in order to provide sufficient frequency diversity gain; and (2) the gap size should be an integer multiple of P^2, where parameter P is the size of a RBG for resource allocation types 0 and 1. The reason for this constraint is to ensure that distributed transmission as described above and transmissions based on downlink allocation types 0 and 1 can coexist on the same subframe. Due to the constraint that the gap size should be an integer multiple of P^2, the gap size N_{gap} may deviate from precisely half of the system bandwidth when the number of resource blocks is an odd number. In those cases, only a fraction of available resource blocks within the system bandwidth can be used for distributed transmission. An example of distributed resource allocation is shown in Figure 9.32.

The permissible values of gap size N_{gap} are given in Table 9.6. Note that for $6 \le N_{\text{RB}}^{\text{DL}} \le 49$, only one gap value $N_{\text{gap}} = N_{\text{gap}}^{(1)}$ is defined, whereas for $50 \le N_{\text{RB}}^{\text{DL}} \le 110$, two gap values $N_{\text{gap}}^{(1)}$ and $N_{\text{gap}}^{(2)}$ are defined where the choice of the gap value is signaled as part of the downlink scheduling assignment. VRBs of

Petitioners' Exhibit 1021
Nokia of America Corp., et al. v. KT Corporation, et al.
Case No. IPR2025-00036; U.S. Patent No. 11,627,631
Page 466 of 1122

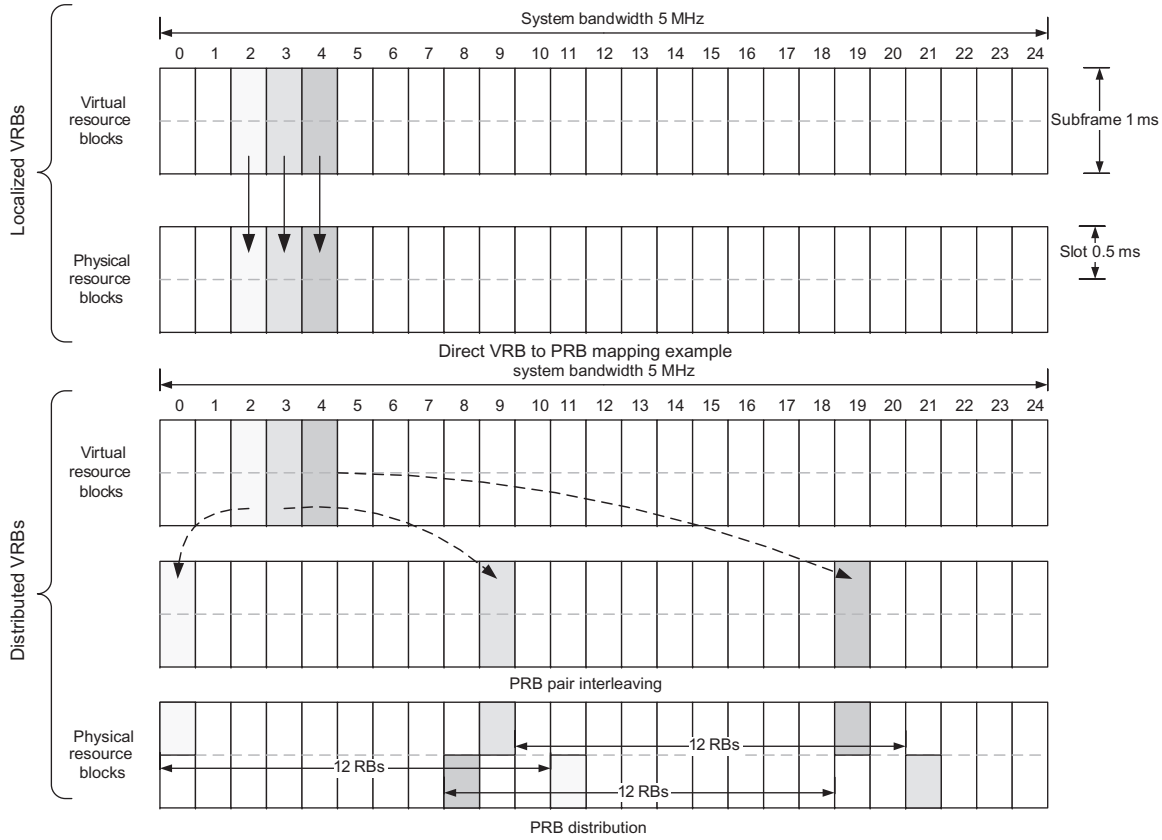


FIGURE 9.32

Illustration of localized and distributed VRB to PRB mapping ($N_{\text{VRB}}^{\text{DL}} = N_{\text{RB}}^{\text{DL}} = 25$) [15].

Petitioners' Exhibit 1021
Nokia of America Corp., et al. v. KT Corporation, et al.
Case No. IPR2025-00036; U.S. Patent No. 11,627,631
Page 467 of 1122

Table 9.6 Distributed VRB Gap Size as a Function of System Bandwidth [3,5]

Total Number of Resource Blocks N_{RB}^{DL}	Gap Size N_{gap}		Resource Block Group Size P
	$N_{gap}^{(1)}$	$N_{gap}^{(2)}$	
6–10	$\lceil N_{RB}^{DL}/2 \rceil$	–	1
11	4	–	2
12–19	8	–	2
20–26	12	–	2
27–44	18	–	3
45–49	27	–	3
50–63	27	9	3
64–79	32	16	4
80–110	48	16	4

distributed type are numbered from 0 to $N_{VRB}^{DL} - 1$, where $N_{VRB}^{DL} = 2\min(N_{gap}, N_{RB}^{DL} - N_{gap}^{(1)})$ or $N_{VRB}^{DL} = 2N_{gap}^{(2)} \left\lfloor N_{RB}^{DL}/2N_{gap}^{(2)} \right\rfloor$ depending on the value of N_{gap}.

Figure 9.33 illustrates the interleaving table for a 10 MHz channel bandwidth when using $N_{gap}^{(1)}$. The VRB indices are written to the table row-by-row and are sequentially read off the table column-by-column. The nulls in the table are ignored and do not generate outputs. When using $N_{gap}^{(1)}$, the VRBs associated with the first half of the output indices from the interleaving table are mapped to the lower set of PRBs starting from the first PRB. The VRBs corresponding to the second half of the output indices from the interleaving table are then mapped to the upper set of PRBs ending at the last PRB. This mapping is applied to the first slot of the subframe. The mapping is cyclically shifted by the gap value $N_{gap}^{(1)}$ for the second slot of the subframe [13]. As shown in Figure 9.34, when using $N_{gap}^{(2)}$ in a 10 MHz bandwidth, two interleaving tables each with six rows are used to define the mapping from VRBs to PRBs. There are some null entries that are inserted in each table [3].

To better understand the difference between the localized and distributed allocations, consider the example shown in Figure 9.35. The frequency response of a multipath fading channel varies with time and frequency due to path loss, shadowing, and user mobility effects. Let us assume that user A and user B are two users with different channel conditions. The base station receives channel quality reports (typically in the form of CINR or SINR measurements) from the mobile stations in the cell. The base station scheduler may adopt either of the following allocation schemes depending on the channel condition reports and other considerations that will be discussed later in this chapter. One allocation strategy is to allocate user A and user B in the sub-channels where the corresponding SINR is

Petitioners' Exhibit 1021
Nokia of America Corp., et al. v. KT Corporation, et al.
Case No. IPR2025-00036; U.S. Patent No. 11,627,631
Page 468 of 1122

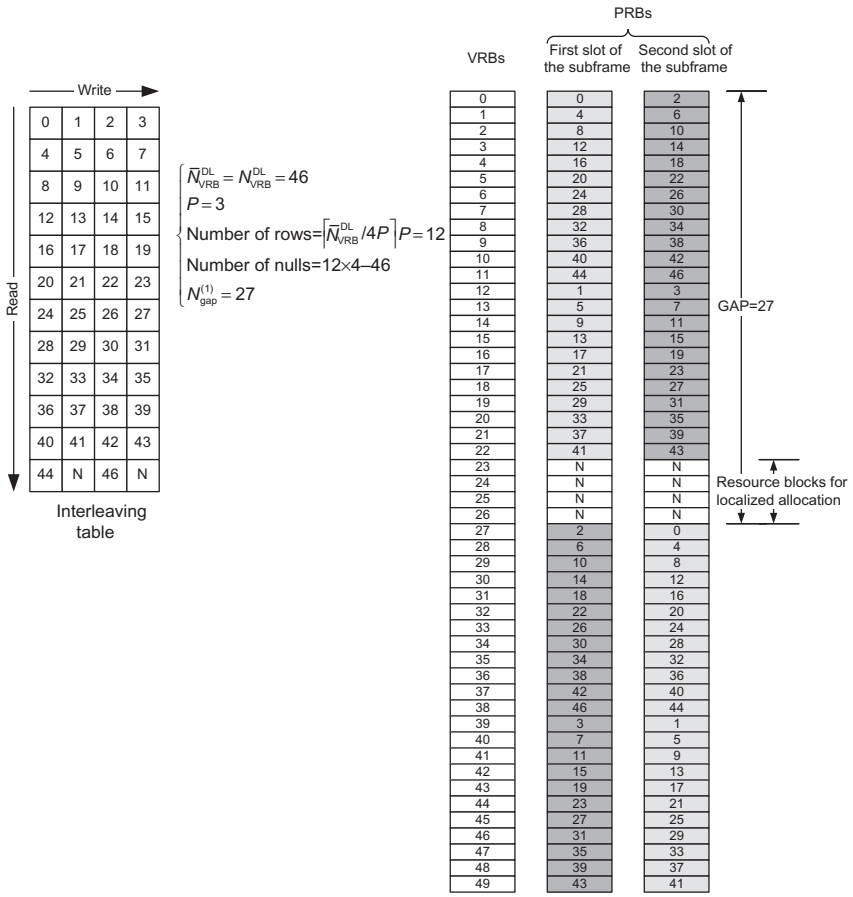


FIGURE 9.33

Illustration of distributed VRB to PRB mapping procedure in 10 MHz using $N_{gap}^{(1)}$ [13].

the best for that user. This is when a frequency-selective scheduling gain can be achieved through allocation of a group of physically adjacent sub-carriers in the sub-channels with relatively strong SINR for that user. Another strategy is to permute the sub-carriers over the entire channel, form a logical group of distributed sub-carriers and assign them to a user. In this case, frequency diversity gain can be achieved through use of distributed resource units for this user.

9.8.2 Resource allocation

One of the main design objectives for signaling of resource allocations, in terms of a set of resource blocks in each subframe, to the active UEs in the cell is to find a

Petitioners' Exhibit 1021
Nokia of America Corp., et al. v. KT Corporation, et al.
Case No. IPR2025-00036; U.S. Patent No. 11,627,631
Page 469 of 1122

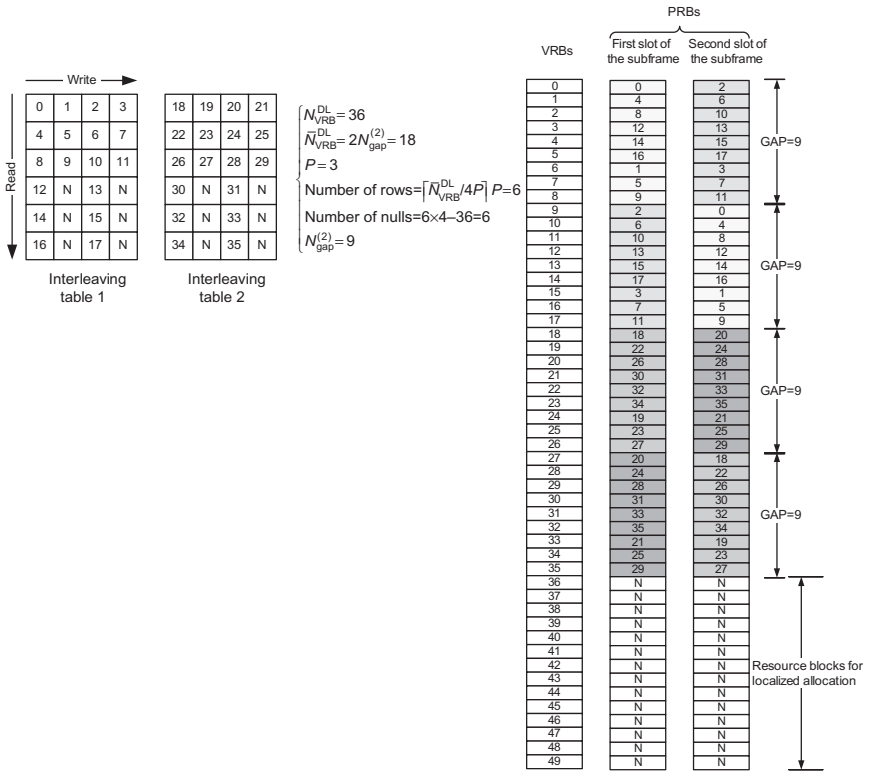


FIGURE 9.34

Illustration of distributed VRB to PRB mapping procedure in 10 MHz using $N_{gap}^{(2)}$ [13].

good trade-off between flexibility and signaling overhead. Indications of localized/distributed resource allocations to different UEs are transmitted via PDCCH. While the exact use of PDCCH depends on the scheduling algorithms implemented in the eNB, it is nevertheless possible to outline some general principles of this operation. The resource allocation field in downlink control information (carried via PDCCH or ePDCCH) is interpreted by the UE depending on the DCI format. A resource allocation field in each DCI includes two parts, a resource allocation header field and information pertaining to the actual resource block assignment. The DCI formats 1, 2, 2A, 2B, 2C and 2D with type 0, and DCI formats 1, 2, 2A, 2B, 2C and 2D with type 1 resource allocation (carried via PDCCH) have the same format and are distinguished from each other via the single bit resource allocation header field which exists depending on the downlink system bandwidth. The PDCCH with DCI format 1A, 1B, 1C, and 1D support type 2 resource allocation, while PDCCH with DCI format 1, 2, 2A, 2B, 2C and 2D support type 0 or type 1

Petitioners' Exhibit 1021
Nokia of America Corp., et al. v. KT Corporation, et al.
Case No. IPR2025-00036; U.S. Patent No. 11,627,631
Page 470 of 1122

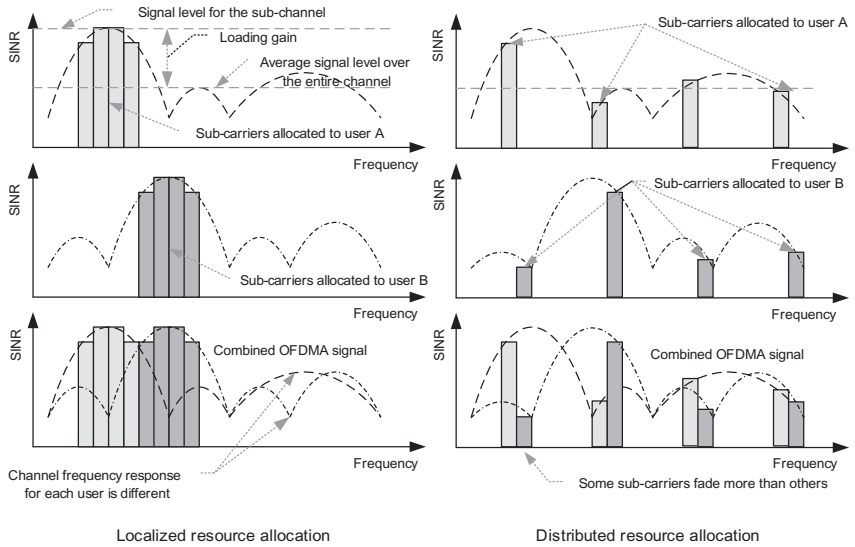


FIGURE 9.35

Comparison of localized and distributed allocation schemes (example) [18].

resource allocation. The DCI formats with a type 2 resource allocation do not have a resource allocation header field [5]. LTE/LTE-Advanced specify three resource allocation schemes in the downlink, where their usage depends on the number resources assigned to the UE, and whether a localized or distributed allocation must be used for the UE considering the channel conditions that the UE is experiencing. In LTE Rel-11, the DCI formats 1, 2, 2A, 2B, 2C and 2D with type 0 and DCI formats 1, 2, 2A, 2B, 2C and 2D with type 1 resource allocation (carried via ePDCCH) have the same format and are distinguished from each other via the single-bit resource allocation header field which exists depending on the downlink system bandwidth. The ePDCCH with DCI format 1A, 1B, and 1D have a type 2 resource allocation.

9.8.2.1 Resource allocation type 0

In resource allocation type 0, the resource block assignment information includes a bitmap indicating the RBGs that are allocated to the scheduled UE where an RBG is a set of consecutive VRBs of localized type. Note that in this case, the granularity of resource assignment is an RBG. The RBG size P is a function of the system bandwidth as given in Table 9.6. The total number of RBGs is given by $N_{\mathrm{RBG}} = \lceil N_{\mathrm{RB}}^{\mathrm{DL}}/P \rceil$. The bitmap is of size N_{RBG} bits and each bit corresponds to a unique RBG in the set. The RBGs are indexed in the order of increasing

Petitioners' Exhibit 1021
Nokia of America Corp., et al. v. KT Corporation, et al.
Case No. IPR2025-00036; U.S. Patent No. 11,627,631
Page 471 of 1122

frequency and non-increasing RBG sizes starting at the lowest frequency (i.e., RBG_0 to $RBG_{N_{RBG}-1}$ are mapped to the most-significant-bit and least-significant-bit of the bitmap, respectively). The RBG is allocated to a UE, if the corresponding bit value in the bitmap is set to "1." Therefore, each bit in the bitmap will select a small contiguous group of resource blocks whose size depends on the bandwidth. The maximum number of resource blocks assigned using type 0 allocation is the entire bandwidth. As an example, consider a total of 50 resource blocks (i.e., 10 MHz system bandwidth), the number of bits in the bitmap is 17. Each bit in the 17-bit bitmap selects a group of three consecutive resource blocks, with the exception of the last group which will only contain two resource blocks, as shown in Figure 9.36.

9.8.2.2 Resource allocation type 1

In resource allocation type 1, a bitmap indicates PRBs inside a selected RBG subset $0 \leq p < P$. The maximum number of resource blocks assignable through type 1 resource allocation is a subset of the entire bandwidth, i.e., a type 1 allocation, even with all bits in the bitmap set to "1" does not span the entire bandwidth. Each bit in the bitmap will select a single resource block from a set of contiguous group of resources whose size and separation depend on the total bandwidth. In resource allocation type 1, the resource block assignment signaling consists of three parts: (1) select a RBG subset; (2) whether to apply an offset when interpreting the bitmap using a shift flag; and (3) the bitmap that indicates to the UE the specific PRBs inside the selected RBG subset.

The size of the bitmap used to address VRBs in a selected RBG subset is given by $N_{RB}^{(1)} = \lceil N_{RB}^{DL}/P \rceil - \lceil \log_2(P) \rceil - 1$. The addressable VRBs within a selected RBG subset start from an offset $n_{shift}(p)$ to the smallest VRB number within the selected RBG subset. The offset is interpreted in terms of the number of VRBs, and is given by $n_{shift}(p) = N_{RB}^{RBG_{subset}}(p) - N_{RB}^{(1)}$ (if the value of the shift bit is non-zero) where the parameter $N_{RB}^{RBG_{subset}}(p)$ denotes the number of VRBs in RBG subset p and is given as follows [5]:

$$N_{RB}^{RBG_{subset}}(p) = \begin{cases} P\left(\left\lfloor \frac{N_{RB}^{DL}-1}{P^2} \right\rfloor + 1\right) & p < \left\lfloor \frac{N_{RB}^{DL}-1}{P} \right\rfloor \bmod P \\ P\left\lfloor \frac{N_{RB}^{DL}-1}{P^2} \right\rfloor + (N_{RB}^{DL}-1) \bmod P + 1 & p = \left\lfloor \frac{N_{RB}^{DL}-1}{P} \right\rfloor \bmod P \\ P\left\lfloor \frac{N_{RB}^{DL}-1}{P^2} \right\rfloor & p > \left\lfloor \frac{N_{RB}^{DL}-1}{P} \right\rfloor \bmod P \end{cases} \tag{9.23}$$

Petitioners' Exhibit 1021
Nokia of America Corp., et al. v. KT Corporation, et al.
Case No. IPR2025-00036; U.S. Patent No. 11,627,631
Page 472 of 1122

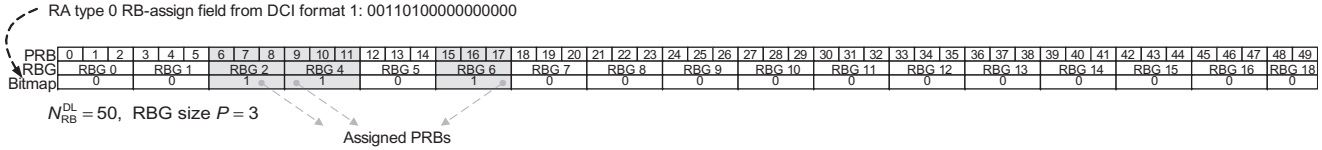


FIGURE 9.36

Example resource allocation type 0 [3,5].

When RBG subset p is addressed, the ith bit ($i = 0, 1, \ldots, N_{\text{RB}}^{(1)} - 1$) in the bitmap field corresponds to VRB number $n_{\text{VRB}}^{\text{RBG}_{\text{subset}}}(p) = \lfloor [i + n_{\text{shift}}(p)]/P \rfloor P^2 + pP + (i + n_{\text{shift}}(p)) \bmod P$. In comparison to resource allocation type 0, the bitmap size for type 1 is always shorter by $\lceil \log_2 P \rceil + 1$ number of bits. As an example, consider a total of 50 resource blocks, the number of bits in the bitmap is 14 (i.e., three bits shorter relative to type 0). Each bit in the 14-bit bitmap will select an individual resource block inside the selected subset, as demonstrated in Figure 9.37.

9.8.2.3 Resource allocation type 2

In resource allocation type 2, the resource block assignment information comprises a set of contiguously allocated localized VRBs or distributed VRBs. When the resource allocation is signaled in PDCCH/ePDCCH with DCI format 1A, 1B, or 1D, a 1-bit flag indicates whether localized VRBs or distributed VRBs are assigned (value "0" indicates localized and value "1" indicates distributed VRB assignment), while distributed VRBs are always assigned in the case of resource allocation signaled with DCI format 1C. A localized VRB assigned to a UE can vary from a single VRB up to a maximum number of VRBs over the system bandwidth. For DCI format 1A, the distributed VRBs allocated to a UE may vary from a single VRB up to $N_{\text{VRB}}^{\text{DL}}$, if the DCI CRC bits are scrambled with P-RNTI, RA-RNTI, or SI-RNTI. With DCI format 1B, 1D, and the CRC scrambled with C-RNTI, or with DCI format 1A and the CRC scrambled with C-RNTI, SPS C-RNTI or temporary C-RNTI, distributed VRB allocations allocated to a UE vary from a single VRB up to $N_{\text{VRB}}^{\text{DL}}$ VRBs, if $6 \le N_{\text{RB}}^{\text{DL}} < 50$, and vary from a single VRB up to 16 if $50 \le N_{\text{RB}}^{\text{DL}} < 110$. Using DCI format 1C, the number of distributed VRB allocations for a UE may range from $N_{\text{RB}}^{\text{step}}$ up to $\lfloor N_{\text{VRB}}^{\text{DL}}/N_{\text{RB}}^{\text{step}} \rfloor N_{\text{RB}}^{\text{step}}$ with an increment of $N_{\text{RB}}^{\text{step}}$, where $N_{\text{RB}}^{\text{step}} = 2$ if $6 \le N_{\text{RB}}^{\text{DL}} < 50$, and $N_{\text{RB}}^{\text{step}} = 4$ if $50 \le N_{\text{RB}}^{\text{DL}} < 110$ [5].

For PDCCH/ePDCCH with DCI format 1A, 1B, or 1D, the type 2 resource allocation field consists of a parameter referred to as resource indication value (RIV) which corresponds to the starting resource block index RB_{start} and the length of the allocation in terms of the number of virtually contiguous resource blocks L_{RB}. The RIV is defined by $\text{RIV} = N_{\text{RB}}^{\text{DL}}(L_{\text{RB}} - 1) + \text{RB}_{\text{start}}$ if $(L_{\text{RB}} - 1) \le \lfloor N_{\text{RB}}^{\text{DL}}/2 \rfloor$; otherwise $\text{RIV} = N_{\text{RB}}^{\text{DL}}(N_{\text{RB}}^{\text{DL}} - L_{\text{RB}} + 1) + (N_{\text{RB}}^{\text{DL}} - 1 - \text{RB}_{\text{start}})$, where $1 \le L_{\text{RB}} < N_{\text{VRB}}^{\text{DL}} - \text{RB}_{\text{start}}$. For DCI format 1C; however, the RIV in type 2 resource allocation field corresponds to starting resource block index $\text{RB}_{\text{start}} = \{0, N_{\text{RB}}^{\text{step}}, 2N_{\text{RB}}^{\text{step}}, \ldots, (\lfloor N_{\text{VRB}}^{\text{DL}}/N_{\text{RB}}^{\text{step}} \rfloor - 1)N_{\text{RB}}^{\text{step}}\}$ and the length in terms of virtually contiguous resource blocks $L_{\text{RB}} = \{N_{\text{RB}}^{\text{step}}, 2N_{\text{RB}}^{\text{step}}, \ldots, \lfloor N_{\text{VRB}}^{\text{DL}}/N_{\text{RB}}^{\text{step}} \rfloor N_{\text{RB}}^{\text{step}}\}$. In other words, in type 2 resource allocation, PRBs are not directly allocated. The type 2 allocation supports both localized and distributed VRB allocation which are distinguished by a flag. The information regarding the starting point of VRB and the length in terms of contiguously allocated VRB can be derived from RIV signaled within the DCI.

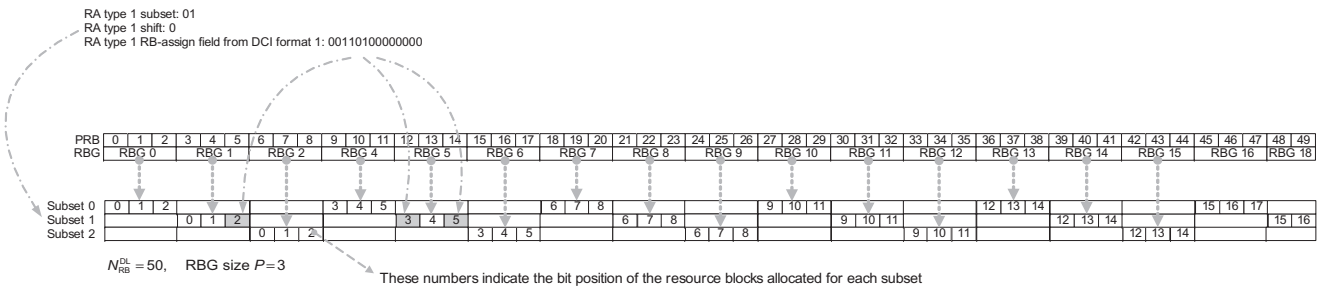


FIGURE 9.37

Example resource allocation type 1 [158].

As an example, consider a total of 50 resource blocks. Let us assume that the eNB is going to assign six localized VRBs starting from resource block 9 in the frequency-domain. Using the above equations for DCI format 1A, the RIV value is calculated as RIV = 259. This RIV is signaled in DCI format 1A, and the UE can unambiguously derive the starting resource block and the number of allocated resource blocks from RIV, as shown in Figure 9.38.

9.8.2.4 PRB bundling

When a UE is configured for operation in transmission mode 9, it may assume that the precoding granularity is multiple resource blocks in the frequency-domain when configured for PMI/RI reporting. In a given serving cell, if a UE is configured in transmission mode 10 and if PMI/RI is reported for all configured CSI processes, then the UE may assume that precoding granularity is multiple resource blocks; otherwise, the precoding granularity is going to be one resource block in the frequency-domain. Fixed bandwidth-dependent precoding resource block groups (PRGs) P' partition the available resource blocks and each PRG consists of a number of consecutive PRBs. If $N_{\mathrm{RB}}^{\mathrm{DL}} \bmod P' > 0$, then the size of one of the PRGs is adjusted to $N_{\mathrm{RB}}^{\mathrm{DL}} - P' \left\lfloor N_{\mathrm{RB}}^{\mathrm{DL}} / P' \right\rfloor$. The PRG size is in descending order starting at the lowest frequency index. The UE may assume that the same precoder is applied to all scheduled PRGs within the bundle. The size of the PRG depends on the system bandwidth, and is given in Table 9.7.

9.8.2.5 Resource element group

Resource element groups (REGs) are the basic unit of resource allocation for PCFICH, PHICH, and PDCCH that are represented by an index pair (k', l'), where k' is the sub-carrier index of the resource element within the REG with the lowest sub-carrier index, and l' is the OFDM symbol index of the REG. In other words, resource-element groups are used for defining the mapping of control channels to resource elements. The mapping of a symbol-quadruplet $\{a(i), a(i+1), a(i+2), a(i+3)\}$ to a resource-element group is defined such that elements $a(i)$ are mapped to resource elements (k, l) of the resource-element group not used for cell-specific reference signals (CRSs) in increasing order of indices k and l, as shown in Figure 9.39.

A REG always contains four consecutive resource elements which are not occupied by a CRS on any antenna port in use. All resource elements within a resource block in the first three OFDM symbols are allocated to REGs. Therefore, the number of resource elements within each REG and the number of REGs within an OFDM symbol are affected by the number of CRSs present on all antenna ports. The number and location of cell-specific reference signals are dependent on the number of antenna ports and the type of cyclic prefix used. Each antenna port has a unique CRS associated with it. Considering the dependency of REG arrangement on CRS configuration, the REG structure for one, two, or four antenna port

Petitioners' Exhibit 1021
Nokia of America Corp., et al. v. KT Corporation, et al.
Case No. IPR2025-00036; U.S. Patent No. 11,627,631
Page 476 of 1122

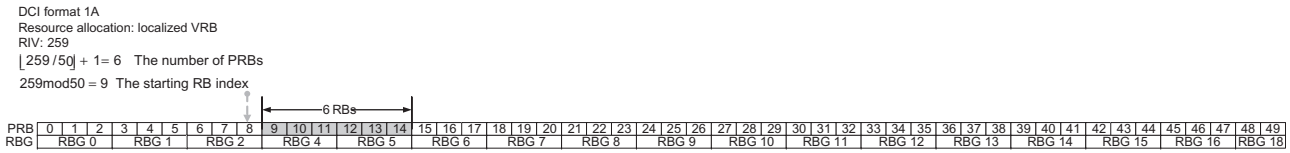


FIGURE 9.38

Example resource allocation type 2 [158].

Petitioners' Exhibit 1021
Nokia of America Corp., et al. v. KT Corporation, et al.
Case No. IPR2025-00036; U.S. Patent No. 11,627,631
Page 477 of 1122

Table 9.7 Precoding Resource Block Group Size [5]

Number of Resource Blocks N_{RB}^{DL}	Precoding Resource Block Group Size P'
≤10	1
11–26	2
27–63	3
64–110	2

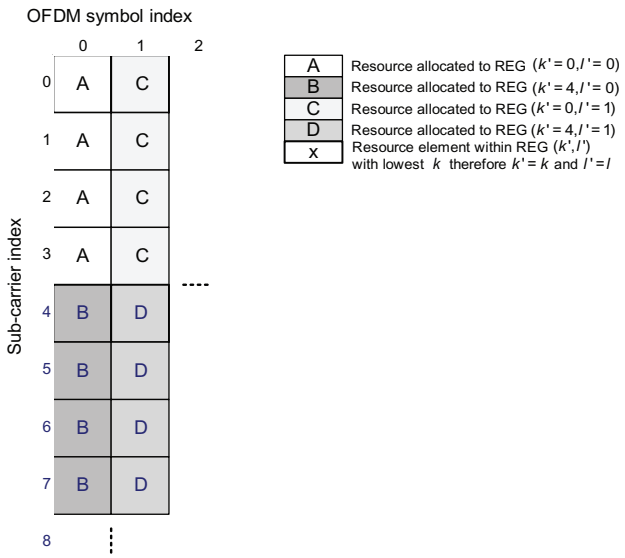


FIGURE 9.39

Resource element group structure [3,160].

configuration is different. However, the REG arrangement for each resource block within a subframe and for each antenna port is identical.

When antenna port 0 or antenna ports 0 and 1 are used, it is assumed that the CRSs are present on both antenna ports 0 and 1. This leads to an REG arrangement for each resource block on the first slot of each subframe, as shown in Figure 9.40. The CRSs are present within the first OFDM symbol. Since four resource elements not including CRSs are required to form a REG, the 12 resource elements over the first symbol in a resource block are divided into two REGs, each containing six resource elements (including two CRSs). On the

Petitioners' Exhibit 1021
Nokia of America Corp., et al. v. KT Corporation, et al.
Case No. IPR2025-00036; U.S. Patent No. 11,627,631
Page 478 of 1122

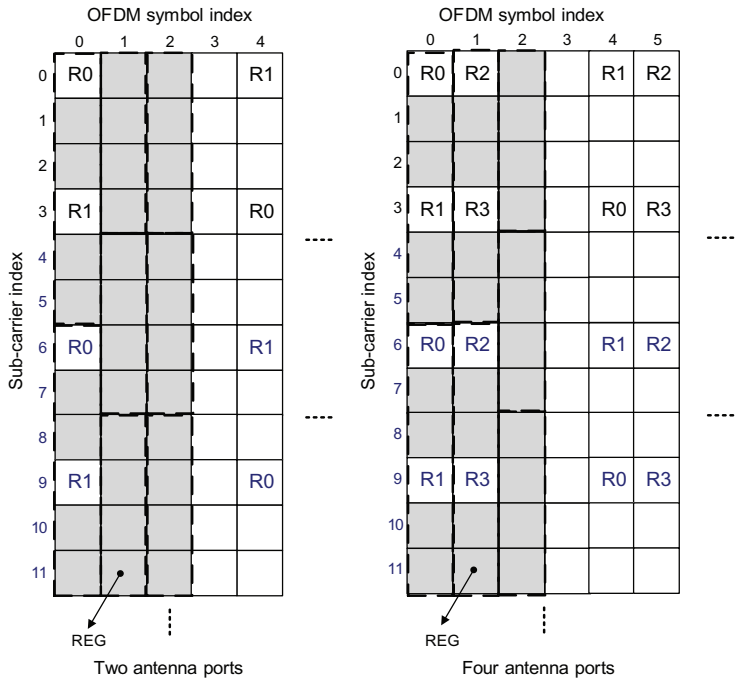


FIGURE 9.40

Resource element group structure with two and four antenna ports [3,160].

second and third OFDM symbols, no CRS is present; therefore; the 12 resource elements over each OFDM symbol are divided into three REGs, each containing four resource elements.

The REG organization in each resource block for four antenna port configuration is illustrated in Figure 9.40. The REG allocation within the first and second OFDM symbols is the same as one or two antenna port configuration. Four CRSs are present on the second OFDM symbol; therefore, eight resource elements are available for the mapping of control information. The 12 reference elements are divided into two REGs, each containing six resource elements. The third OFDM symbol contains no reference signals, so three REGs are available. An extended cyclic prefix subframe contains 12 OFDM symbols as opposed to 14 for the normal cyclic prefix. Since the number of CRSs in a normal or extended cyclic prefix subframe is the same, the limited number of OFDM symbols in an extended cyclic prefix subframe requires the OFDM symbol spacing of the CRSs to be reduced compared to a normal cyclic prefix. This reduction in spacing causes CRSs to be present within the fourth OFDM symbol of an extended cyclic prefix subframe, whereas in a normal cyclic prefix subframe no

Petitioners' Exhibit 1021
Nokia of America Corp., et al. v. KT Corporation, et al.
Case No. IPR2025-00036; U.S. Patent No. 11,627,631
Page 479 of 1122

CRSs are present on the fourth OFDM symbol of the subframe. The number of cell-specific reference symbols within the first three OFDM symbols is identical for normal or extended cyclic prefix, thus the REG configurations are identical.

9.9 Time and frequency synchronization

Synchronization signals are transmitted in every radio frame. The synchronization signals are used for time and frequency synchronization during initialization. As part of the system acquisition process, the UE synchronizes to the OFDM symbol, slot, subframe, half-frame, and radio frame (in that order) using a synchronization signal. Two synchronization signals are defined for system acquisition in E-UTRA: (1) a primary synchronization signal is used to obtain slot, subframe, and half-frame boundary. It also provides cell identity within the cell identity group. (2) A secondary synchronization signal is used to obtain the radio frame boundary. It also enables the UE to determine the cell identity group, which may range from 0 to 167. The synchronization signals are transmitted in the 0th and 5th subframes of every radio frame. In the frequency-domain, the synchronization signals occupy the center 1.08 MHz (equivalent to six resource blocks) of the radio channel (Figure 9.41).

Figure 9.41 shows the location of the primary and secondary synchronization signals in a radio frame. In the time-domain, primary and secondary synchronization signals are transmitted in the 0th and 10th slot (1st slot within 0th and 5th subframe) of every radio frame. Within these slots, the primary and secondary synchronization signals are transmitted in the last two symbols. The primary synchronization signal is transmitted in the last symbol of the 0th and 10th slot. The secondary synchronization signal is transmitted in one before the last symbol of the 0th and 10th slot. The PBCH is mapped to the first four symbols in slot 1 of the frame (just after the primary and secondary synchronization signals). In the frequency-domain, the center 1.08 MHz of the radio channel is reserved for primary and secondary synchronization signals. This is equivalent to six resource blocks or 72 sub-carriers. However, the primary and secondary synchronization signals only require 62 sub-carriers around the DC sub-carrier. The remaining sub-carriers (10 sub-carriers) in these resource blocks are not used for transmission. They provide a guard band between primary and secondary synchronization signal transmissions and other data transmissions.

There are 504 unique physical layer cell identities. The physical layer cell identities are grouped into 168 unique physical layer cell-identity groups, each group contains three unique identities. The grouping is done such that each physical layer cell identity is part of one and only one physical layer cell-identity group. A physical layer cell identity $N_{\mathrm{ID}}^{\mathrm{cell}} = 3N_{\mathrm{ID}}^{(1)} + N_{\mathrm{ID}}^{(2)}$ is thus uniquely defined by a number $N_{\mathrm{ID}}^{(1)}$ in the range of 0−167, representing the physical layer cell-identity group, and a number $N_{\mathrm{ID}}^{(2)}$ in the range of 0−2, denoting the physical layer identity within the physical layer cell-identity group.

Petitioners' Exhibit 1021
Nokia of America Corp., et al. v. KT Corporation, et al.
Case No. IPR2025-00036; U.S. Patent No. 11,627,631
Page 480 of 1122

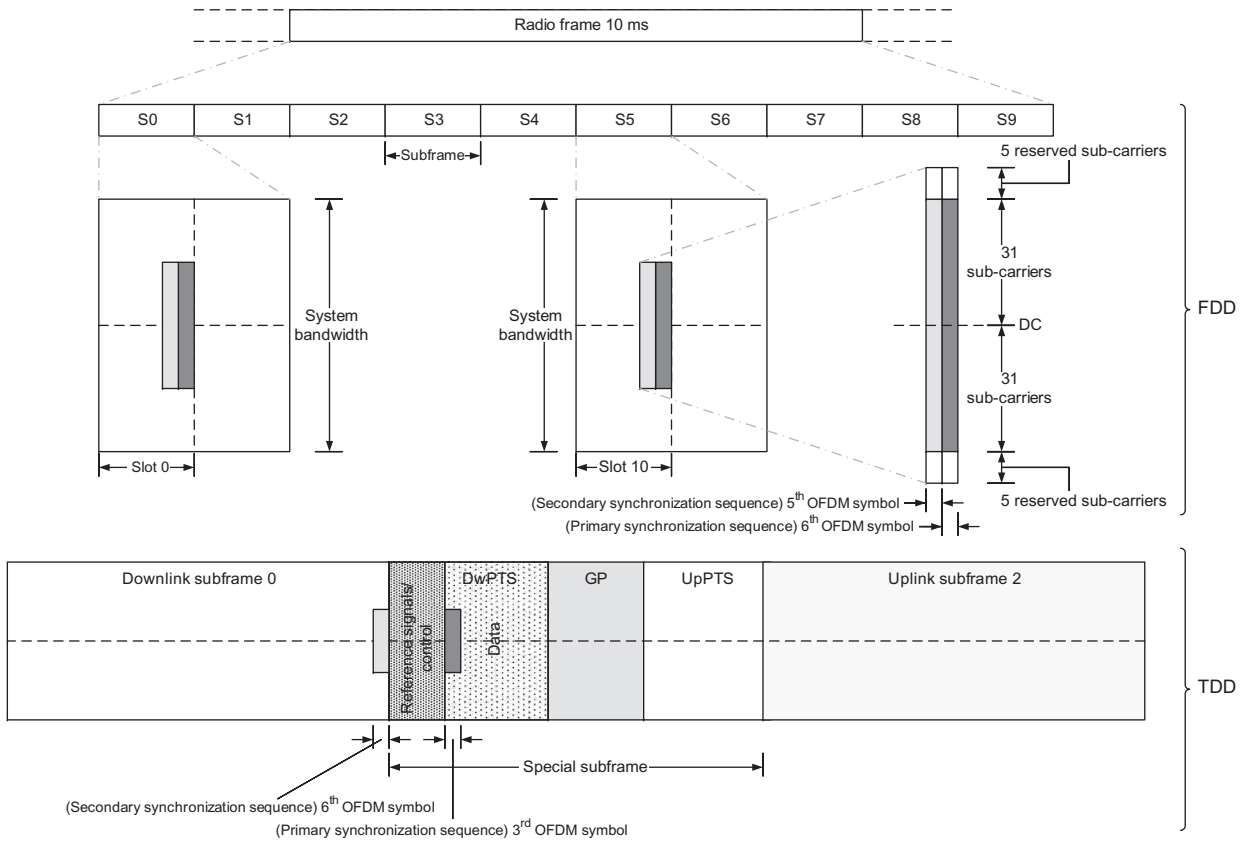


FIGURE 9.41

Location and structure of primary and secondary synchronization signals [3,174].

9.9.1 Primary synchronization signals

The primary synchronization signal is generated from a frequency-domain Zadoff–Chu sequence[9] according to the following equation [3]:

$$d_{\mathrm{u}}(n) = \begin{cases} \mathrm{e}^{-j\frac{\pi un(n+1)}{63}} & n = 0, 1, \ldots, 30 \\ \mathrm{e}^{-j\frac{\pi u(n+1)(n+2)}{63}} & n = 31, 32, \ldots, 61 \end{cases} \tag{9.24}$$

where the Zadoff–Chu root sequence index $u = 25, 29, 34$ if $N_{\mathrm{ID}}^{(2)} = 0, 1, 2$, respectively. The mapping to resource elements depends on the frame structure. The sequence $d(n)$ is mapped to the resource elements according to $a_{\mathrm{kl}} = d(n), n = 0, \ldots, 61$ and $k = n - 31 + 6N_{\mathrm{RB}}^{\mathrm{DL}}$. As shown in Figure 9.41, for frame structure type 1, the primary synchronization signal is mapped to the last OFDM symbol in slots 0 and 10. For frame structure type 2, the primary synchronization signal is mapped to the third OFDM symbol in subframes 1 and 6. The

[9] A Zadoff–Chu sequence is a complex-valued sequence with constant amplitude property whose cyclically shifted versions exhibit low cross-correlation. Thus, under certain conditions, the cyclically shifted versions of each sequence remain orthogonal to one another. A Zadoff–Chu sequence that has not been shifted is referred to as a root sequence. The uth root Zadoff–Chu sequence of prime length N is defined as follows [172]:

$$x_u(n) \triangleq \begin{cases} \mathrm{e}^{-\mathrm{j}[\pi un(n+1)]/N} & 0 \le n < N-1 \quad (N \text{ is an odd integer}) \\ \mathrm{e}^{-\mathrm{j}\pi un^2/N} & 0 \le n < N-1 \quad (N \text{ is an even integer}) \end{cases}$$

where N is an integer, which denotes the length of the Zadoff–Chu sequence. It is easily verified that $x_u(n)$ is periodic with period N, i.e., $x_u(n) = x_u(n+N), \forall n$. In other words, the sequence index u is prime relative to N. For a fixed value of u, the Zadoff–Chu sequence has an ideal periodic autocorrelation property (i.e., the periodic autocorrelation is zero for all time shifts other than zero). For different values of index u, the Zadoff–Chu sequences are not orthogonal, but rather exhibit low cross-correlation. If the sequence length N is selected as a prime number, there are different sequences with periodic cross-correlation of $1/\sqrt{N}$ between any two sequences regardless of time shift. The Zadoff–Chu sequences are a subset of constant amplitude zero autocorrelation (CAZAC) sequences. The properties of Zadoff–Chu sequences can be summarized as follows [172]:

- They are periodic with period N, if N is a prime number, i.e., $x_u(n+N) = x_u(n)$.
- Given N is a prime number, the DFT of a Zadoff–Chu sequence is another Zadoff–Chu sequence conjugated and time-scaled multiplied by a constant factor, i.e., $X_u[k] = x_u^*(vk)X_u[0]$ where v is the multiplicative inverse of u modulo N. It can be shown that $x_u^*(vk) = x_v^*(k)\mathrm{e}^{\mathrm{j}\pi(1-v)k/N}$.
- The autocorrelation of a prime-length Zadoff–Chu sequence with a cyclically shifted version of itself also yields zero autocorrelation sequence, i.e., it is non-zero only at one instant which corresponds to the cyclic shift zero.
- The cross-correlation between two prime-length Zadoff–Chu sequences, i.e., different u, is constant and equal to $1/\sqrt{N}$.
- The Zadoff–Chu sequences have low PAPR.

Petitioners' Exhibit 1021
Nokia of America Corp., et al. v. KT Corporation, et al.
Case No. IPR2025-00036; U.S. Patent No. 11,627,631
Page 482 of 1122

resource elements a_{kl} over OFDM symbols used for transmission of the primary synchronization signal where $k = n - 31 + 6N_{\text{RB}}^{\text{DL}}, n = \{-5, -4, \ldots, -1, 62, 63, \ldots, 66\}$ are reserved as guard sub-carriers.

9.9.2 Secondary synchronization signals

The secondary synchronization signal is generated from interlacing of two length-31 M-sequences[10] $s_0^{(m_0)}(n)$ and $s_1^{(m_1)}(n)$. There are 168 sequences that are generated from cyclic shifts of sequences $s_0^{(m_0)}(n)$ and $s_1^{(m_1)}(n)$. The cyclic shifts are generated based on cell-identity group number, which ranges from 0 to 167. The two sequences are scrambled, with the scrambling sequences $c_0(n)$ and $c_1(n)$ that are obtained based on the primary synchronization signal identity $N_{\text{ID}}^{(2)} \in \{0, 1, 2\}$. The second sequence is further scrambled with additional sequence $z_1^{(m_0)}(n)$. The two sequences are interleaved and mapped to 62 sub-carriers around the DC sub-carrier using BPSK modulation. As shown in Figure 9.42, five sub-carriers on either side are not used, providing a guard band between the primary and secondary synchronization sequences and other data-bearing sub-carriers. The secondary synchronization signals are also used to detect the radio frame boundary. To achieve this, a different variation of the sequence is generated by switching $s_0^{(m_0)}(n)$ and $s_1^{(m_1)}(n)$ in slot 10. The switch produces a different sequence so the UE can distinguish between slot 0 and slot 10.

More specifically, the secondary synchronization signal $d(0), d(1), \ldots, d(61)$ is an interleaved concatenation of two length-31 binary sequences as shown in Figure 9.42. The concatenated sequence is scrambled with a scrambling sequence given by the primary synchronization signal. The combination of two length-31 sequences defining the secondary synchronization signal differs between subframe 0 and subframe 5 according to the following rule:

$$d(2n) = \begin{cases} s_0^{(m_0)}(n)c_0(n) & \text{in subframe 0} \\ s_1^{(m_1)}(n)c_0(n) & \text{in subframe 5} \end{cases} \tag{9.25}$$

[10]Maximum length sequences are pseudo-random binary sequences that are generated using maximal linear feedback shift registers. The *M*-sequences are periodic and reproduce every binary sequence that can be reproduced by the shift registers (i.e., for length-*m* registers, they produce a sequence of length $2^m - 1$). An *M*-sequence is spectrally flat with the exception of a near-zero DC term. Since *M*-sequences are periodic and shift registers cycle through every possible binary value with the exception of the zero vectors, the registers can be initialized to any state with the exception of the zero vectors. A binary polynomial over $GF(2)$ can be associated with the linear feedback shift register. The degree of polynomial is equal to the length of the shift register and the coefficients that are either 0 or 1 correspond to the taps of the register [173].

Petitioners' Exhibit 1021
Nokia of America Corp., et al. v. KT Corporation, et al.
Case No. IPR2025-00036; U.S. Patent No. 11,627,631
Page 483 of 1122

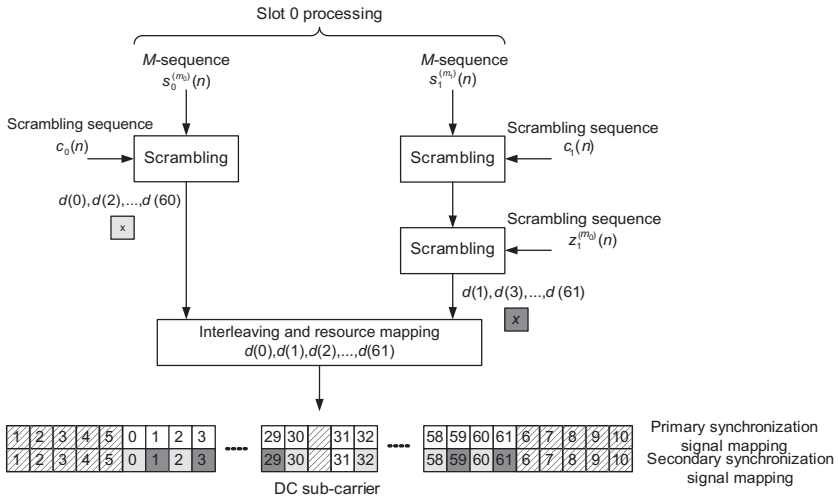


FIGURE 9.42

Secondary synchronization signal generation and mapping.

and:

$$d(2n+1) = \begin{cases} s_1^{(m_1)}(n)c_1(n)z_1^{(m_0)}(n) & \text{in subframe 0} \\ s_0^{(m_0)}(n)c_1(n)z_1^{(m_1)}(n) & \text{in subframe 5} \end{cases} \tag{9.26}$$

where $0 \le n \le 30$ and indices m_0 and m_1 are derived from the physical layer cell-identity group $N_{\text{ID}}^{(1)}$. The two sequences $s_0^{(m_0)}(n)$ and $s_1^{(m_1)}(n)$ are derived from two different cyclic shifts of an M-sequence $\tilde{s}(n)$. The two scrambling sequences $c_0(n)$ and $c_1(n)$ depend on the primary synchronization signal and are characterized by two different cyclic shifts of the M-sequence $\tilde{c}(n)$. The scrambling sequences $z_1^{(m_0)}(n)$ and $z_1^{(m_1)}(n)$ are defined by a cyclic shift of the M-sequence $\tilde{z}(n)$. The mapping of the sequence to resource elements depends on the frame structure. In a subframe for frame structure type 1 and in a half-frame for frame structure type 2, the same antenna port used for transmission of the primary synchronization signal is used for transmission of the secondary synchronization signal. The sequence $d(n)$ is mapped to resource elements according to $a_{\text{kl}} = d(n)$, $\forall n = 0, \ldots, 61$ and $k = n - 31 + 6N_{\text{RB}}^{\text{DL}}$, where $l = N_{\text{s}}^{\text{DL}} - 2$ in slots 0 and 10 for frame structure type 1 and $l = N_{\text{s}}^{\text{DL}} - 1$ in slots 1 and 11 for frame structure type 2 [3].

The primary synchronization signals are detected using non-coherent detection, whereas the secondary synchronization signals can be detected using either coherent or non-coherent detection schemes. Figure 9.43 shows an example algorithm for coherent detection of the secondary synchronization signals. The channel compensation block is used for coherent detection. The received secondary synchronization signals in the frequency-domain can be expressed as

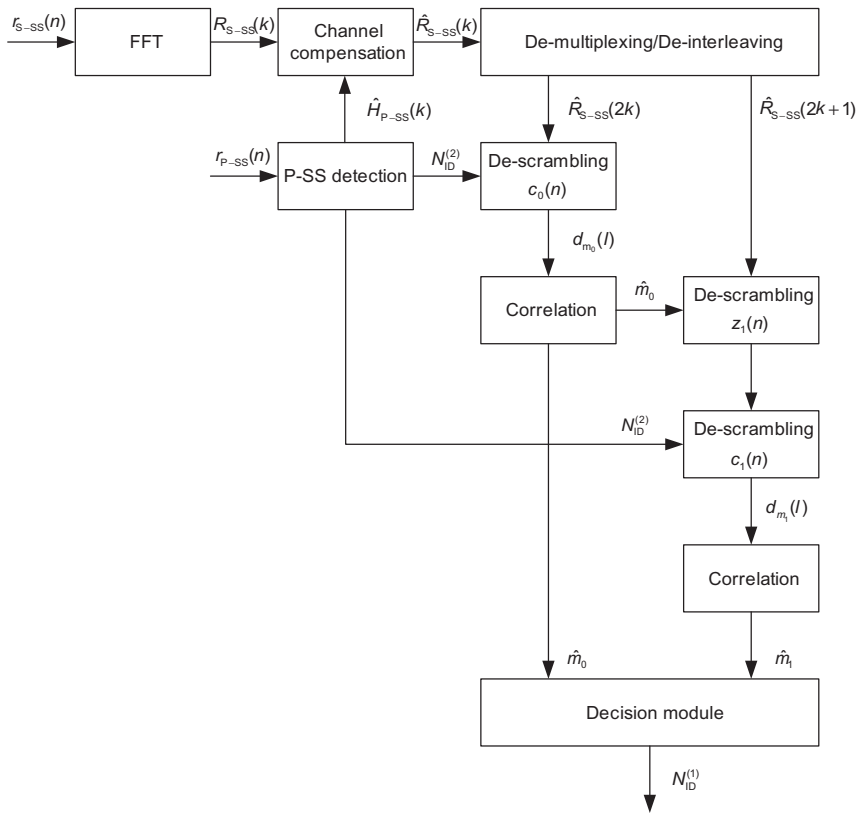


FIGURE 9.43

Example algorithm for coherent detection of secondary synchronization signal [174].

$r_{S-SS}(k) = H(k)d_{S-SS}(k) + w(k)$, where $d_{S-SS}(k)$ is the secondary synchronization signal in the frequency-domain, $H(k)$ is channel frequency response during secondary synchronization signal transmission, and $w(k)$ is the additive white Gaussian noise. For coherent detection, the UE estimates the channel frequency response $\hat{H}(k)$ by using the received primary synchronization sequence. From the UE perspective, the secondary synchronization signal detection is performed after the primary synchronization signal detection; thus the channel can be assumed to be known based on the primary synchronization signal sequence. In the frequency-domain, channel compensated secondary synchronization signal is given by $\hat{R}_{S-SS}(k) = \hat{H}(k)R_{S-SS}(k)$. After channel compensation, the de-interleaved and de-scrambled signal can be expressed as $d_{m_0}(l) = \hat{R}_{S-SS}(2k)c_0(k), d_{m_1}(k) = \hat{R}_{S-SS}(2k+1)c_1(k)z_1^{(\hat{m}_0)}(k)$. The output of coherent detection is the cross-correlation

between the de-scrambled signal and the cyclic shift of a secondary synchronization sequence that can be represented as follows:

$$\hat{m}_0 = \arg \max_i \left| \sum_{l=0}^{30} d_{m_0}(l) s_i(l) \right|^2$$
$$\hat{m}_1 = \arg \max_i \left| \sum_{l=0}^{30} d_{m_1}(l) s_i(l) \right|^2 \quad (9.27)$$

where $\hat{m}_0$ and $\hat{m}_1$ are the ith secondary synchronization signal sequence. Once $\hat{m}_0$ and $\hat{m}_1$ are identified, the frame timing and cell identity group $N_{\mathrm{ID}}^{(1)}$ can be detected (Figure 9.44).

The E-UTRA supports normal and extended cyclic prefix types for various deployment scenarios. The timing of the secondary synchronization signals will change depending on the cyclic prefix type, as shown in Figure 9.44. Prior to successful detection of the secondary synchronization signal, the cyclic prefix type is unknown to the UE and it must be blindly detected by examining the secondary synchronization signals at two possible locations in time. A simple algorithm for determining the cyclic prefix type is introduced in this section as an example. Note that E-UTRA specifications do not specify the receiver architecture and detection methods. This algorithm is based on the principle developed by Van de Beek, where the correlation between the cyclic prefix and its repetition part of the data symbol is calculated for two choices of cyclic prefix type [175]. For each cyclic prefix type, the correlation function is normalized by the associated received secondary synchronization signal power, because the range of values over which the summation is calculated varies with the cyclic prefix type. Let $r(n)$ denote the secondary synchronization signal at the receiver in the time-domain, we define [174]:

$$\rho_i = \sum_{n=0}^{L_i-1} r(n+\tau_i) r^*(n+\tau_i+N)$$
$$P_i = \sum_{n=0}^{L_i-1} |r(n+\tau_i+N)|^2 \quad (9.28)$$

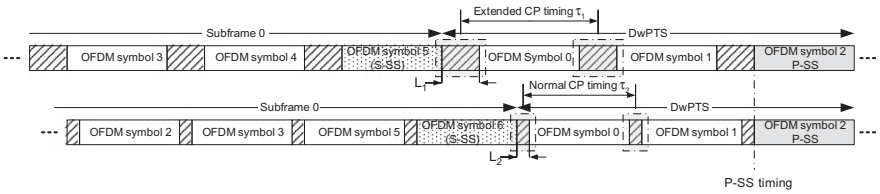


FIGURE 9.44

Illustration of the cyclic prefix detection algorithm [174].

Petitioners' Exhibit 1021
Nokia of America Corp., et al. v. KT Corporation, et al.
Case No. IPR2025-00036; U.S. Patent No. 11,627,631
Page 486 of 1122

where τ_1 and τ_2 represent the normal and extended cyclic prefix timing, respectively, and L_1 and L_2 denote the corresponding cyclic-prefix lengths. The normalized correlation function $U_i = \mathrm{Re}\{\rho_i\}/P_i$ with the larger value indicates the type of cyclic prefix. Therefore, a normal cyclic prefix is considered, if $U_1 > U_2$ and an extended cyclic prefix is assumed, if $U_2 > U_1$. The main advantage of this algorithm is that a correlation value can be accumulated by using an OFDM symbol within one radio frame in order to improve the detection performance at low SNR. In addition, this algorithm can reduce the computational complexity compared to blind detection using secondary synchronization signal detection at the two possible instances in time.

9.10 Downlink reference signals and channel estimation

To facilitate estimation of the multipath communication channel and reliable, coherent detection of data/control signaling, an OFDM system uses reference signals (or pilot symbols). The pilot symbols provide an estimate of the channel frequency response at the pilot locations over the time−frequency grid. It is possible to estimate the channel at other time−frequency locations using interpolation techniques. In E-UTRA, the CRSs are assigned to specific positions within a subframe, depending on the physical cell identity and the specific antenna port from which they are transmitted. The unique positioning of the pilots ensures that they do not interfere with each other and can be used to provide a reliable estimate of the complex-valued channel gains scaling each resource element within the transmitted grid. Using known pilot symbols to estimate the channel matrix, it is possible to equalize the effects of the channel and to reduce noise and interference effects of the received resource blocks. Downlink spatial multiplexing in LTE Rel-10 was enhanced to support up to eight transmission layers, together with an enhanced reference-signal structure. Relying on cell-specific reference signals for higher order spatial multiplexing is less attractive, as the reference signal overhead is not proportional to the instantaneous transmission rank, but rather to the maximum supported transmission rank. LTE Rel-10, therefore, introduced extensive support of UE-specific reference signals for demodulation of up to eight layers. In addition, feedback of channel-state information (CSI) is based on a separate set of reference signals, known as CSI reference signals (CSI-RSs). The CSI-RSs are relatively sparse in frequency but regularly transmitted from all antennas at the base station, while the UE-specific reference signals are denser in frequency but only transmitted when data is transmitted on the corresponding layer. Separating the reference-signal structures supporting demodulation and channel estimation helps to reduce reference-signal overhead, especially for high degrees of spatial multiplexing, and allows for implementation of various beam-forming schemes. In LTE Rel-8, the reference signal is added to the signal after precoding, one CRS per antenna port. From the received CRS, the UE can estimate the channel matrix and determine how the radio channel affected the signal. Using the estimated channel matrix

Petitioners' Exhibit 1021
Nokia of America Corp., et al. v. KT Corporation, et al.
Case No. IPR2025-00036; U.S. Patent No. 11,627,631
Page 487 of 1122

together with the knowledge about the code-book used for precoding, the UE can demodulate the received signal and regenerate the original information. In LTE Rel-10, the demodulation reference signals (DM-RSs) are added to the different data streams before precoding. The knowledge about the reference signal will then provide information about the combined effect of radio channel and precoding, thus prior knowledge about the precoder is not required by the receiver, this case is referred to as non-codebook-based precoding.

The LTE/LTE-Advanced systems make use of reference signals for downlink and uplink channel estimation. The downlink reference signals are used to measure CSI and channel estimation for demodulation. The design of downlink reference signals in LTE Rel-8 primarily relied on a set of cell-specific reference signals that could be used for both purposes. The CRS are wideband reference signals transmitted across the entire downlink system bandwidth in every subframe, and are defined for up to four antenna ports. The presence of cell-specific reference signals in every subframe, while necessary for decoding essential physical channels, results in unreasonably high overhead. To support eight-layer spatial multiplexing in LTE-Advanced, new low duty-cycle wideband reference signals, known as CSI-RSs, were designed for CSI measurements. Furthermore, a new set of UE-specific or DM-RSs were designed to enable channel estimation for demodulation. The LTE Rel-10 DM-RS design efficiently supports high-rank transmissions because it is present only in those PRBs in which higher rank is used [121]. The enhanced PDCCH (ePDCCH) DM-RSs with an identical structure to Rel-10 DM-RSs were added in Rel-11 to support various use cases involving the new FDM-based control channel structure.

LTE/LTE-Advanced defines an antenna port as a logical entity which is distinct from a physical antenna and is associated with a specific set of reference signals such that the channel over which a symbol on the antenna port is conveyed can be distinguished from the channel over which another symbol on the same antenna port is conveyed. There is one resource grid per antenna port. The set of downlink antenna ports supported depends on the reference signal configuration in the cell as given in Table 9.8 [3].

The set of downlink antenna ports supported depends on the reference signal configuration in the cell as follows [3]:

- Cell-specific reference signals support one, two, or four antenna port configurations and are transmitted on antenna ports $p = 0$, $p \in \{0, 1\}$, and $p \in \{0, 1, 2, 3\}$, respectively.
- MBSFN reference signals are exclusively transmitted on antenna port $p = 4$.
- UE-specific or DM-RSs are transmitted on antenna port $p = 5, 7,$ or 8, or one or several of $p \in \{7, 8, 9, 10, 11, 12, 13, 14\}$.
- Positioning reference signals are exclusively transmitted on antenna port $p = 6$.
- CSI reference signals support configuration of one, two, four, or eight antenna ports, and are transmitted on antenna ports $p = 15$, $p = \{15, 16\}$, $p = \{15, 16, 17, 18\}$, and $p = \{15, 16, 17, 18, 19, 20, 21, 22\}$, respectively.

Petitioners' Exhibit 1021
Nokia of America Corp., et al. v. KT Corporation, et al.
Case No. IPR2025-00036; U.S. Patent No. 11,627,631
Page 488 of 1122

Table 9.8 Downlink Antenna Ports and Their Use Cases [3,13]

3GPP Release	Downlink Antenna Port	Associated Reference Signals	Use Cases
8	0–3	Cell-specific reference signals	Single-layer transmission, transmit diversity, SU-MIMO/MU-MIMO
8	4	MBSFN reference signal	Multimedia broadcast and multicast services
8	5	UE-specific reference signal/ demodulation reference signal	Single-layer beamforming
9	6	Positioning reference signal	Location-based services
9	7,8	UE-specific reference signals/demodulation reference signals	Dual-layer beamforming, MU-MIMO
10	9–14	UE-specific reference signals/demodulation reference signals	Multi-layer beamforming, MU-MIMO
10	15–22	CSI reference signals	CSI measurement and reporting
11	107–110	ePDCCH demodulation reference signals	ePDCCH-based transmission and demodulation

- ePDCCH DM-RSs are transmitted on antenna ports $p \in \{107, 108, 109, 110\}$, and are used to support ePDCCH transmission and demodulation.

Based on the above discussion, six types of downlink reference signals are defined as follows, which will be discussed in detail in the next sections:

- Cell-specific reference signals (CRS)
- MBSFN reference signals
- UE-specific or DM-RSs associated with PDSCH
- Positioning reference signals
- CSI-RSs
- DM-RSs associated with ePDCCH

Note that there is one reference signal transmitted per downlink antenna port.

9.10.1 Reference signal design criteria

In this section, we discuss the theoretical criteria for efficient pilot pattern design for OFDM systems. Pilot-based channel estimation is defined as the use of the channel samples estimated at the pilot tones to reconstruct channel samples at the

Petitioners' Exhibit 1021
Nokia of America Corp., et al. v. KT Corporation, et al.
Case No. IPR2025-00036; U.S. Patent No. 11,627,631
Page 489 of 1122

remaining data tones. As a result, the pilot pattern design is essentially a conventional sampling rate selection problem in the two-dimensional signal processing space. In order to avoid aliasing during reconstruction of the channel time–frequency function, the pilot tone selection should follow the two-dimensional sampling theorem. When multiple antennas are used, the receiver must estimate the channel impulse response (or the transfer function) from each of the transmit antennas in order to correctly detect the signal. This is achieved through distributing reference signals (or pilot tones) among the transmit antennas.

Let $\Delta f = 1/T_{\mathrm{u}}$ and $T_{\mathrm{symbol}} = T_{\mathrm{g}} + T_{\mathrm{u}}$ denote the sub-carrier spacing and the OFDM symbol duration (inclusive of the guard interval), respectively. Let us further assume that the pilot sub-carriers are transmitted at integer multiples of sub-carrier spacing and OFDM symbol duration in frequency and time directions, respectively (i.e., $f_{\mathrm{p}} = m/T_{\mathrm{u}}$ and $T_{\mathrm{p}} = nT_{\mathrm{symbol}}$, where m and n are integers). The (m, n) pair represents the pilots' separation in terms of sub-carrier spacing and OFDM symbol duration. From the sampling theorem point of view, the channel's two-dimensional delay-Doppler response $h(\tau, \nu)$ can be fully reconstructed, if the two-dimensional transform function $H(t,f)$ is sampled greater than or equal to the Nyquist rate across time and frequency dimensions. Hence, the time-domain sampling rate must be greater than or equal to the channel's maximum Doppler spread, i.e., $T_{\mathrm{p}} \leq 1/\nu_{\max}$ (the sampling rate in time must be less than the coherence time) and the frequency-domain sampling rate must be greater than or equal to the channel's maximum delay spread, i.e., $f_{\mathrm{p}} \leq 1/\tau_{\max}$ (the sampling rate in frequency must be less than coherence bandwidth). Assuming a wide-sense stationary uncorrelated scattering channel model, and assuming the channel to be constant over one OFDM symbol, the frequency response $H(t,f)$ of the L-path channel is given as [23,140]:

$$H(t,f) = \frac{1}{\sqrt{L}} \sum_{l=1}^{L} \mathrm{e}^{\mathrm{j}(\psi_l + 2\pi\nu_l t - 2\pi f \tau_l)} \tag{9.29}$$

where ψ_l, ν_l, and τ_l denote the phase, Doppler frequency, and delay of the lth path, respectively. All these parameters are independent random variables. In general, the pilot signals are over-sampled in order to ensure a good trade-off between performance and overhead. Therefore, the choice of (m, n) depends on the channel's maximum delay spread and maximum Doppler spread, and must satisfy the following equation according to the two-dimensional sampling theorem [23]:

$$\begin{aligned} n &\leq \frac{1}{2T_{\mathrm{symbol}}\nu_{\max}} \\ m &\leq \frac{T_u}{2\tau_{\max}} \end{aligned} \tag{9.30}$$

It should be noted that the pilot density for a regular pattern can be calculated using Eq. (9.30). From Eq. (9.30), it can be seen that for large values of $\nu_{\max}$

Petitioners' Exhibit 1021
Nokia of America Corp., et al. v. KT Corporation, et al.
Case No. IPR2025-00036; U.S. Patent No. 11,627,631
Page 490 of 1122

(i.e., large Doppler spread, or alternatively small channel coherence time, means that the channel is time-varying), n should be small in order to appropriately track channel time variations. On the other hand, for large values of $\tau_{\max}$ (i.e., large delay spread, or alternatively small coherence bandwidth, means that the channel is frequency selective), m should be small in order to closely follow channel frequency variation. In a regularly spaced pilot pattern, the pilot symbols are evenly spaced in frequency and in time.

Using the default OFDM symbol duration and the sub-carrier spacing given in Table 9.2 (OFDM parameters $T_{\text{symbol}} = 71.36\ \mu s$ and $\Delta f = 1/T_{\text{u}} = 15$ kHz), and assuming that the channel maximum delay spread $\tau_{\max} = 5\ \mu s$ for the radio channels under consideration in LTE/LTE-Advanced evaluation methodology, the most appropriate range for the values of (m, n) can be determined. Since an E-UTRA system is required to support vehicle speeds up to 350 km/h, the maximum Doppler spread is estimated as $\nu_{\max} \approx 810$ Hz at 2.5 GHz carrier frequency. From Eq. (9.30) and the above design parameters, the following pilot spacing constraints are obtained $n \leq 8, m \leq 6$. Figure 9.45 illustrates a regularly spaced

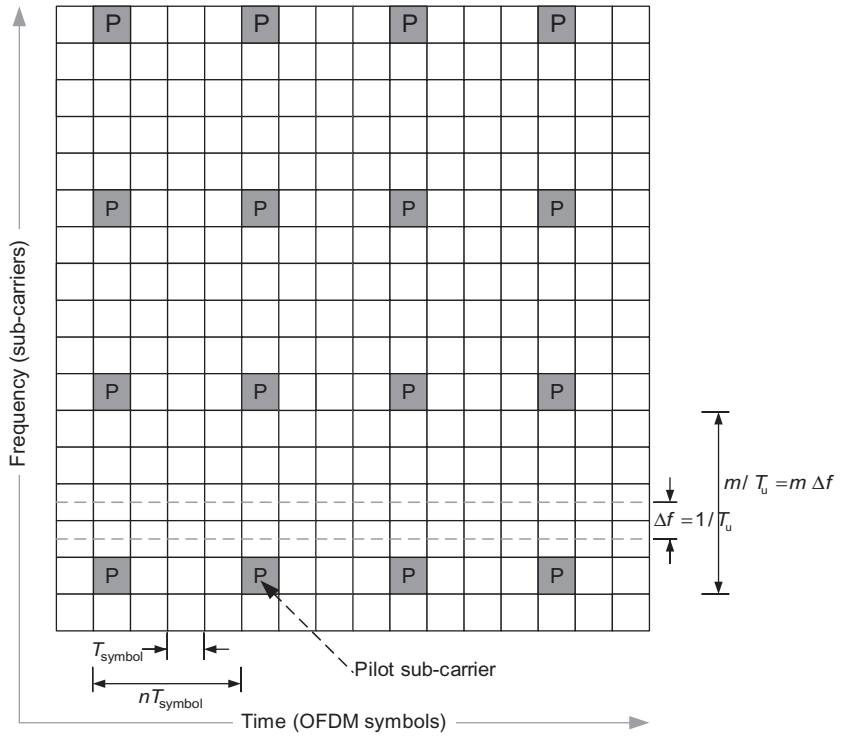


FIGURE 9.45

An example of regular pilot pattern for one spatial layer with $n = 4$ and $m = 5$.

Petitioners' Exhibit 1021
Nokia of America Corp., et al. v. KT Corporation, et al.
Case No. IPR2025-00036; U.S. Patent No. 11,627,631
Page 491 of 1122

two-dimensional pilot pattern for one spatial stream in the time−frequency domain where $n = 4$ and $m = 5$. The above criteria can be generalized to the case of multi-antenna transmission where each transmit antenna is associated with a group of pilot sub-carriers.

In the case of irregular pilot patterns, the pilot symbols can be irregularly placed in time, in frequency, or in both. The irregular patterns can be designed according to a certain criteria, yielding a specific pattern. Other important considerations in the design of pilot structures for support of multi-antenna OFDM systems include the following:

- Identical pilot pattern for each PRB: Pilot spacing in time and frequency must be in proportion with the resource block size. If the location of the pilot tones within a resource block is not maintained the same across all resource blocks within the system bandwidth, or alternatively the pilot sub-carriers have different positions within each resource block, the filtering and interpolation operations during channel estimation become excessively complex.
- Pilot density: Proper pilot overhead must be considered as a trade-off between accurate channel estimation under various mobility conditions and higher throughput.
- Types of pilots: Pilots are typically classified as common (cell-specific) and dedicated (UE-specific). Each UE in the cell can estimate the channel over the entire bandwidth using the common pilots, while dedicated pilots in the UE assigned resource block can be used for channel estimation. In conventional MIMO schemes, the dedicated pilots are typically adaptively precoded. The dedicated pilots can be used in conjunction with common pilots, or in place of common pilots.
- Pilot power boosting: In general, the power of pilot sub-carriers is boosted relative to data sub-carriers in order to enhance the channel estimation with pilot hopping or shifting. To avoid symbol to symbol power fluctuation when using pilot boosting, it is desirable to place the pilot sub-carriers regularly on every symbol, or to employ power adjustment for data sub-carriers over a symbol.
- Per antenna power balance: When using multiple transmit antennas, it is important to maintain balanced power distribution across antennas. For this purpose, if there are two transmit antennas, each OFDM symbol should contain the same number of pilot tones associated with different antenna ports.

As an example and by taking the above additional criteria into consideration, the structure and link-level performance (i.e., bit error rate versus SNR curves) of several hypothetical common pilot patterns for two transmit antennas and two different multi-antenna transmission schemes are shown in Figure 9.46. In this example, the pilot overhead of type A and type B patterns is 11.11% (i.e., 5.5% per antenna port), and the transmit power per antenna is balanced. The type C

Petitioners' Exhibit 1021
Nokia of America Corp., et al. v. KT Corporation, et al.
Case No. IPR2025-00036; U.S. Patent No. 11,627,631
Page 492 of 1122

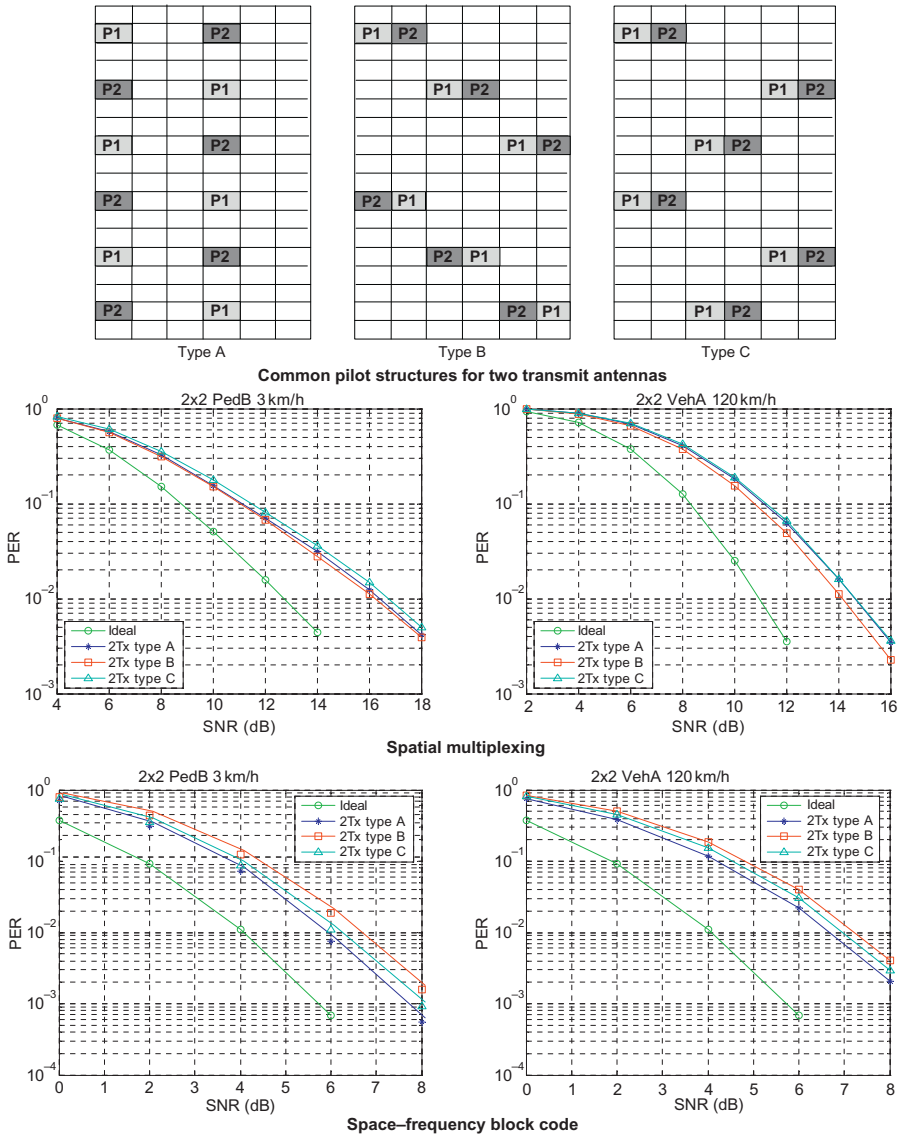


FIGURE 9.46

Channel estimation accuracy of various pilot patterns for two transmit antennas and QPSK-1/2 in different mobility and channel conditions [140].

Petitioners' Exhibit 1021
Nokia of America Corp., et al. v. KT Corporation, et al.
Case No. IPR2025-00036; U.S. Patent No. 11,627,631
Page 493 of 1122

pilot pattern has unbalanced power across antennas and symbols. The pilot tone powers have been boosted by 3 dB relative to data sub-carriers [140].

The accuracy of channel estimation using common pilots affects the performance of downlink/uplink data and control channel decoding. Figure 9.46 shows the link-level performance of spatial multiplexing with the example pilot patterns, where type B provides the best performance under low and high mobility conditions. The ideal channel estimation is used as a reference. Also shown in Figure 9.46 is the link-level performance of space-frequency block codes (SFBCs) with the example pilot patterns. In this case, type A outperforms the other structures. It can be concluded that type A is the best among three example patterns. Note that the example pilot patterns satisfy the sampling theorem constraint of Eq. (9.30). This example underlines the criteria for the design of robust and high performance pilot structures for OFDM-based cellular system operation in a wide range of mobility and channel conditions. The time/frequency characteristics of a number of typical radio channel models, mobility classes, and the associated time−frequency sampling rate requirements are summarized in Table 9.9.

Table 9.9 Characteristics of Typical Radio Channel Models ($T_u = 66.67$ μs and $T_{symbol} = 71.36$ μs)

Channel Model	RMS Delay Spread (ns) ν_{RMS}	Maximum Delay Spread (μs) τ_{max}	Maximum Sampling Rate in Frequency (Number of Sub-carriers) $\frac{T_u}{2\tau_{max}}$
ITU-T Pedestrian A (PedA)	45	0.41	81
ITU-T Pedestrian B (PedB)	750	3.7	9
ITU-T Vehicular A (VehA)	370.4	2.51	13
ITU-T Vehicular B (VehB)	4000	20	1
Typical Urban 6-Ray Model (TU)	1000	5	6
Vehicular Speed Range (km/h)	**Maximum Doppler Spread (Hz) ν_{max}**	**Coherence Time (ms) T_c**	**Maximum Sampling Rate in Time (Number of OFDM Symbols) $\frac{1}{2T_{symbol}\nu_{max}}$**
0−15	~27.78	15.23	252
15−120	~222.22	1.90	31
120−350	~648.15	0.65	10

Petitioners' Exhibit 1021
Nokia of America Corp., et al. v. KT Corporation, et al.
Case No. IPR2025-00036; U.S. Patent No. 11,627,631
Page 494 of 1122

9.10.2 Pilot-based channel estimation

While perfect knowledge of the radio channel can be used to find an upper bound for system performance, such knowledge is not available in practice and the channel needs to be frequently estimated. Channel estimation can be performed in various ways, including the use of frequency and/or time correlation properties of the wireless channel, blind or pilot (reference signal) based channel estimation, and adaptive or non-adaptive channel estimation. Non-parametric methods attempt to estimate the frequency response without relying on a specific channel model. In contrast, the parametric estimation methods assume a certain channel model and determine the parameters of this model. Spaced-time and spaced-frequency correlation functions, discussed earlier, are specific properties of a channel that can be incorporated in the estimation method, improving the quality of estimations. Pilot-based estimation methods are the most commonly used methods in OFDM systems which are applicable in systems where the sender transmits some known signals to the receiver. Blind estimation, on the other hand, relies on some properties of the signal and is rarely used in practical OFDM systems. Adaptive channel estimation methods are typically used for a rapid time-varying channel [69–71].

In this section, we describe a generic pilot-based non-adaptive channel estimation method. In a linear time-invariant AWGN channel, the relationship between the transmitted signal $X_k|_{k=0,1,\ldots,N_{\text{FFT}}-1}$ and received signal Y_k can be expressed as $Y_k = H_k X_k + Z_k$, where Z_k is the frequency-domain noise sampled at the kth sub-carrier frequency, and H_k is the channel transfer-function sampled at the kth sub-carrier frequency. To estimate the channel, pilot symbols are used. Let us assume that every pth sub-carrier contains known pilot symbols $X_{pk}|_{kp=0,p,2p,\ldots,N_p-1}$, where N_p is the total number of pilot sub-carriers across frequency. Using the known pilot symbols X_{pk} and the received symbols Y_{pk} sampled at pilot sub-carriers, the channel transfer function $\hat{H}_k$ sampled at pilot sub-carriers can be written as follows:

$$\hat{H}_{pk} = \frac{Y_{pk}}{X_{pk}} + \frac{Z_{pk}}{X_{pk}} = H_{pk} + W_{pk} \tag{9.31}$$

where W_{pk} is a scaled-noise component at the pkth sub-carrier. Different methods such as one- or two-dimensional linear interpolation can be used to estimate the channel samples at other sub-carrier frequencies.

Channel estimation in OFDM systems is a two-dimensional problem, i.e., the channel transfer function or channel impulse response is a function of time and frequency variables. Due to the computational complexity of two-dimensional estimators, one-dimensional channel estimation methods are more practical. The idea behind one-dimensional estimators is to estimate the channel in one

Petitioners' Exhibit 1021
Nokia of America Corp., et al. v. KT Corporation, et al.
Case No. IPR2025-00036; U.S. Patent No. 11,627,631
Page 495 of 1122

dimension (e.g., frequency), and then estimate the channel in another dimension (e.g., time), thus obtaining a two-dimensional channel estimate. Linear interpolation is a simple method to estimate the channel from channel samples estimated at pilot sub-carriers. This is done by linearly interpolating the channel samples at the two nearest pilot sub-carriers. Although linear interpolation provides some limited noise reduction of the channel estimates at data locations (due to averaging function), it is the simplicity of the solution that is more attractive. It must be noted that averaging window length (i.e., the number of pilots contained in the averaging window) is inversely proportional to the coherence bandwidth of the channel. The one-dimensional linear interpolation method estimates the channel by interpolating the channel transfer function between $\hat{H}_{m,k}$ and $\hat{H}_{m,l}$ (interpolation across frequency), or between $\hat{H}_{m,k}$ and $\hat{H}_{n,k}$ (interpolation across time). The algorithm shown in Figure 9.47 illustrates the procedure for channel estimation across the time−frequency grid based on the known values of the channel at the reference signal locations. Depending on the relative location of the sub-carrier in the time−frequency grid, the channel is estimated via one-dimensional linear interpolation of channel values at neighboring pilots or merely copying or extrapolation of values at the neighboring pilot, if the previous or the next pilot does not exist [160].

The channel transfer function $H_{m,k}$ at time−frequency index (m, k) can be modeled as a linear weighed sum of two-dimensional basis functions evaluated at the kth sub-carrier (frequency index) and at the mth OFDM symbol (time index):

$$H_{m,k} = \sum_{n=0}^{N-1} \alpha_n \phi_n(m, k) \tag{9.32}$$

where $\phi_n(m, k)$ denotes the nth basis function sampled at the mth OFDM symbol and at the kth sub-carrier, α_n is the coefficient of the nth basis function, and N is number of basis functions used in the linear model. By taking a one-dimensional approach, the above two-dimensional problem is reduced to one-dimensional, if one of the time or frequency indices is kept unchanged:

$$H_k = \sum_{n=0}^{N-1} \alpha_n \phi_n(k) \tag{9.33}$$

The channel samples at pilot sub-carriers shown in Eq. (9.33) can be written as:

$$\hat{H}_{pk} = \sum_{n=0}^{N-1} \alpha_n \phi_n(pk) + W_{pk} \tag{9.34}$$

Petitioners' Exhibit 1021
Nokia of America Corp., et al. v. KT Corporation, et al.
Case No. IPR2025-00036; U.S. Patent No. 11,627,631
Page 496 of 1122

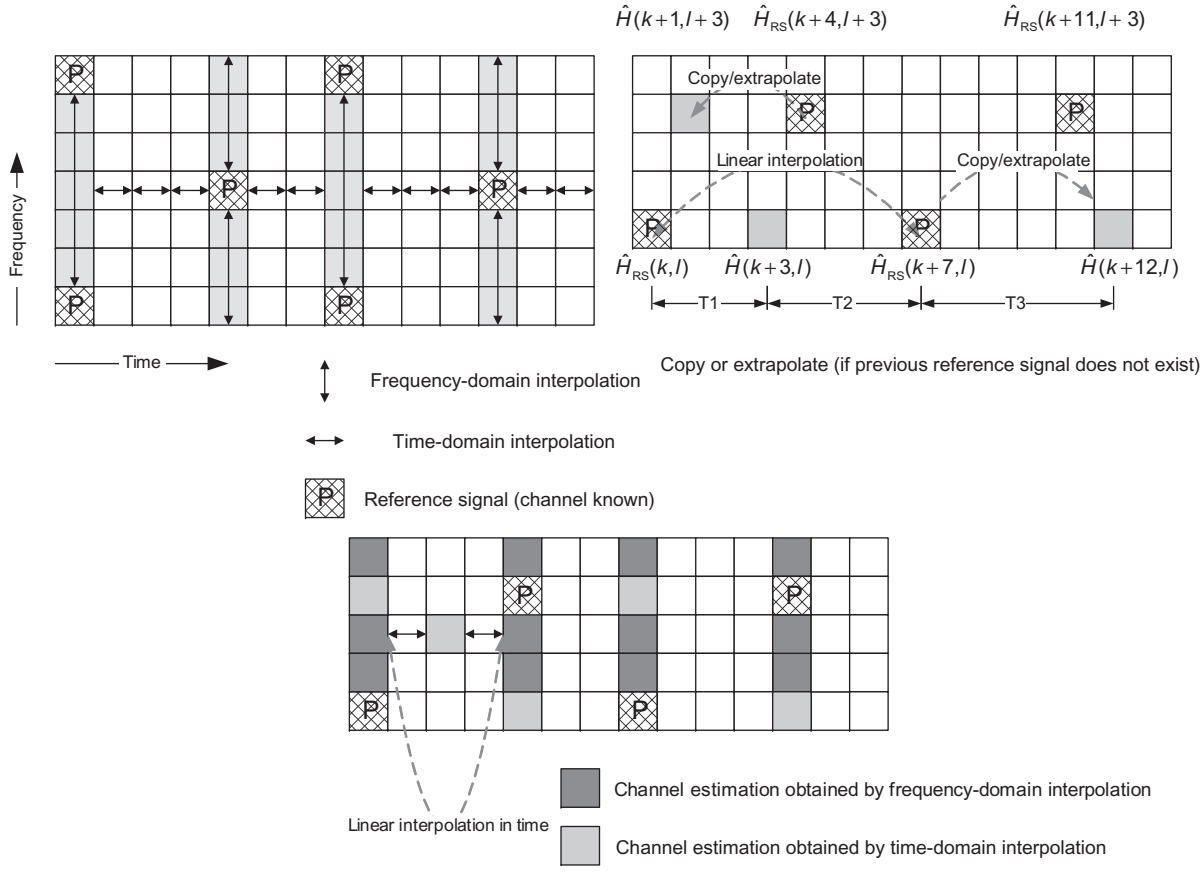


FIGURE 9.47

Two-dimensional channel estimation across frequency and time [176].

Petitioners' Exhibit 1021
Nokia of America Corp., et al. v. KT Corporation, et al.
Case No. IPR2025-00036; U.S. Patent No. 11,627,631
Page 497 of 1122

The above equation can be represented in matrix form as follows:

$$\begin{bmatrix} \hat{H}_0 \\ \hat{H}_p \\ \hat{H}_{2p} \\ \vdots \\ \hat{H}_{N_p-1} \end{bmatrix} = \begin{bmatrix} \phi_0(0) & \phi_1(0) & \phi_2(0) & \dots & \phi_{N-1}(0) \\ \phi_0(p) & \phi_1(p) & \phi_2(p) & \dots & \phi_{N-1}(p) \\ \phi_0(2p) & \phi_1(2p) & \phi_2(2p) & \dots & \phi_{N-1}(2p) \\ \vdots & \vdots & \vdots & \ddots & \vdots \\ \phi_0(N_p-1) & \phi_1(N_p-1) & \phi_2(N_{p-1}) & \dots & \phi_{N-1}(N_{p-1}) \end{bmatrix} \begin{bmatrix} \alpha_0 \\ \alpha_1 \\ \alpha_2 \\ \vdots \\ \alpha_{N-1} \end{bmatrix} + \begin{bmatrix} Z_0 \\ Z_p \\ Z_{2p} \\ \vdots \\ Z_{N_p-1} \end{bmatrix} \tag{9.35}$$

Alternatively, by using matrix notations, the above equation can be rewritten as follows:

$$\hat{\mathbf{H}} = \mathbf{\Phi}\boldsymbol{\alpha} + \mathbf{Z} \tag{9.36}$$

The least square (LS) estimate of the coefficients is calculated by minimizing the squared distance between the actual channel vector $\mathbf{H}$ and the estimated channel vector $\hat{\mathbf{H}}$ as follows:

$$\hat{\boldsymbol{\alpha}}_{\text{LS}} = (\mathbf{\Phi}^{\mathbf{H}}\mathbf{\Phi})^{-1}\mathbf{\Phi}^{\mathbf{H}}\hat{\mathbf{H}} = \mathbf{\Phi}^{-1}\hat{\mathbf{H}} \tag{9.37}$$

where the superscript H denotes conjugate transpose operation, hence:

$$\hat{H}_k = \sum_{n=0}^{N-1} \hat{\alpha}_n \phi_n(k) \tag{9.38}$$

A number of different options exist while selecting the basis functions such as orthogonal polynomials, Fourier series, discrete cosine/sine transform function, etc. There are a number of reasons for using orthogonal polynomials including ease of calculation of $\mathbf{\Phi}^{\mathbf{H}}\mathbf{\Phi}$ since it becomes a diagonal matrix, if matrix $\mathbf{\Phi}$ is orthogonal, resulting in ease of calculation of $\hat{\alpha}_n{}'s$ and the inverse matrix $(\mathbf{\Phi}^{\mathbf{H}}\mathbf{\Phi})^{-1}$ with minimal computational complexity. The degree of orthogonal polynomials can be increased without changes in recursive calculation of $\hat{\alpha}_n{}'s$. When applying the polynomial-based channel estimation, a sliding window is typically used to estimate the channel. This is done to avoid use of high-order polynomials to estimate highly frequency-selective channels. The sliding window approach allows for local approximations to the channel transfer function using a window length larger than the polynomial order, providing a better estimate.

In a special case where the OFDM channel estimation symbols are transmitted periodically and all sub-carriers over an OFDM symbol are used as pilots, the channel estimation algorithm is more simplified. In this case, the receiver uses the estimated channel transfer function to decode the received data within the block until the next pilot symbol arrives. If $Y_k = H_k X_k + Z_k|_{k=0,1,2,\dots,N_{\text{FFT}}-1}$ denotes

Petitioners' Exhibit 1021
Nokia of America Corp., et al. v. KT Corporation, et al.
Case No. IPR2025-00036; U.S. Patent No. 11,627,631
Page 498 of 1122

the received signal at kth sub-carrier (pilot sub-carrier), the LS estimate of the channel transfer function in this case is given as:

$$\hat{\mathbf{H}}_{\mathbf{LS}} = (Y_1/X_1, Y_2/X_2, \ldots, Y_{N_{\text{FFT}}-1}/X_{N_{\text{FFT}}-1})^H = (Y_1, Y_2, \ldots, Y_{N_{\text{FFT}}-1})^H; X_k = 1, \forall k \tag{9.39}$$

The channel transfer function at non-pilot sub-carriers can be estimated using interpolation in time. For convenience, we assume that the pilot sub-carriers have unity magnitude.

An alternative approach to pilot-based channel estimation is the minimum mean squared error (MMSE) method. The MMSE channel estimator exploits the second-order statistics of the channel transfer function to minimize the mean-squared error. Let $\mathbf{R_{HH}} = E(\mathbf{HH}^{\text{H}})$ and σ_Z^2 denote the autocorrelation matrix of the channel vector $\mathbf{H}$ and the additive white Gaussian noise variance, respectively. The MMSE estimate of the channel transfer function is given as:

$$\hat{\mathbf{H}}_{\text{MMSE}} = \mathbf{R_{HH}}[\mathbf{R_{HH}} + \sigma_Z^2(\mathbf{XX^H})^{-1}]^{-1}\hat{\mathbf{H}}_{\mathbf{LS}} = \mathbf{R_{HH}}[\mathbf{R_{HH}} + \sigma_Z^2\mathbf{I}]^{-1}\hat{\mathbf{H}}_{\mathbf{LS}}; \quad \mathbf{XX^H} = \mathbf{I} \tag{9.40}$$

The MMSE estimator performs much better than LS estimators, especially under the low SNR conditions. A major drawback of the MMSE estimator is its high computational complexity, particularly if matrix inversion is necessary every time the input data changes. Figure 9.48 shows an example where the

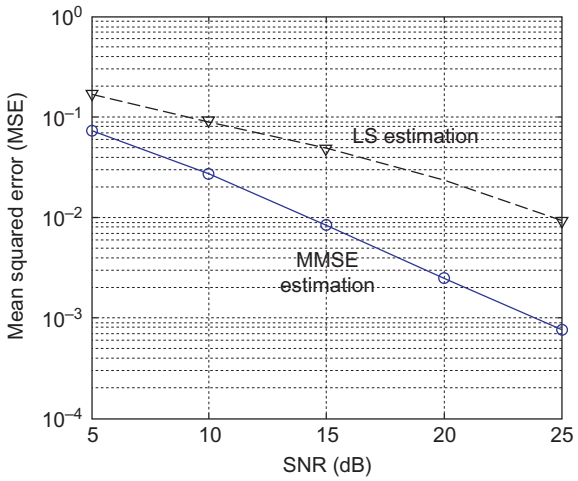


FIGURE 9.48

Example comparison of the LS and MMSE channel estimation algorithms [141].

Petitioners' Exhibit 1021
Nokia of America Corp., et al. v. KT Corporation, et al.
Case No. IPR2025-00036; U.S. Patent No. 11,627,631
Page 499 of 1122

performance of the LS and MMSE channel estimation algorithms has been compared. In this example $N_{\text{FFT}} = 64$ and the channel is modeled as a two-tap delay line filter. The superiority of MMSE over LS estimation in low SNR conditions can be seen in Figure 9.48.

9.10.3 Cell-specific reference signals

The cell-specific reference signals are used during initial cell selection for channel estimation and coherent detection of downlink physical channels. The measurements pertaining to scheduling and handover functions are based on the received signal strength of the CRS transmitted from antenna port zero (and antenna port one). The CRS sequence is a complex pseudo-random sequence, which is a length-31 Gold sequence.[11] The initialization seed for the second M-sequence used for Gold sequence generation is derived from the OFDM symbol number, slot number, and the physical cell identity. The seed is reinitialized at the beginning of each OFDM symbol within a slot. Pseudo-random sequences which are cell-specific are used to differentiate the reference signals transmitted from different cells. There is also a frequency shift that is applied to mapping of the CRS to resource elements to prevent the CRS from adjacent cells overlapping over the time−frequency grid. The generated sequence is transmitted in every slot and is spread throughout the channel bandwidth. The frequency of CRS transmission per slot and actual mapping to resource elements depend on the antenna configuration (Figure 9.49). The CRS symbols between antennas from the same cell are time-division multiplexed; the resource elements used for CRS symbols on one antenna are reserved and are not used on other antenna ports.

The CRSs are transmitted in all downlink subframes in a cell supporting PDSCH transmission. The CRSs are transmitted on one or several of antenna ports 0−3, and are only defined for sub-carrier spacing of 15 kHz. The reference-signal sequence $r_l^{n_s}(m)$ is defined as $r_l^{n_s}(m) = (1/\sqrt{2})(1 - 2c(2m)) + \mathrm{j}(1/\sqrt{2})(1 - 2c(2m+1))$, $\forall m = 0, 1, \ldots, 2N_{\text{RB}}^{\text{DL}} - 1$, where index n_s denotes the slot number within a radio frame, $l = 0, 1, \ldots, 6$ (or 5 in case of an extended cyclic prefix) represents the OFDM symbol number within slot n_s, and $c(i)$ is a pseudo-random sequence, which is initialized with $c_{\text{init}} = 2^{10}[7(n_s + 1) + l + 1](2N_{\text{ID}}^{\text{cell}} + 1) + 2N_{\text{ID}}^{\text{cell}} + N_{\text{CP}}$ at the start

[11] A Gold sequence is a type of binary sequence that is often used in telecommunication and satellite navigation. Gold sequences have bounded small cross-correlations within a set. A set of Gold sequences consists of $2^n - 1$ sequences each with a period of $2^n - 1$. A set of Gold sequences can be generated by taking two maximum-length sequences of the same length $2^n - 1$ such that their absolute cross-correlation is less than or equal to $2^{(n+2)/2}$, where n is the size of the linear feedback shift register used to generate the maximum length sequence [130]. The set of $2^n - 1$ (logical) exclusive OR of the two sequences in their various phases is a set of Gold codes. The highest absolute cross-correlation in this set of codes is $2^{(n+2)/2} + 1$ for even n, and $2^{(n+1)/2} + 1$ for odd n. The exclusive OR of two Gold codes from the same set is another Gold code with arbitrary phase [130].

Petitioners' Exhibit 1021
Nokia of America Corp., et al. v. KT Corporation, et al.
Case No. IPR2025-00036; U.S. Patent No. 11,627,631
Page 500 of 1122

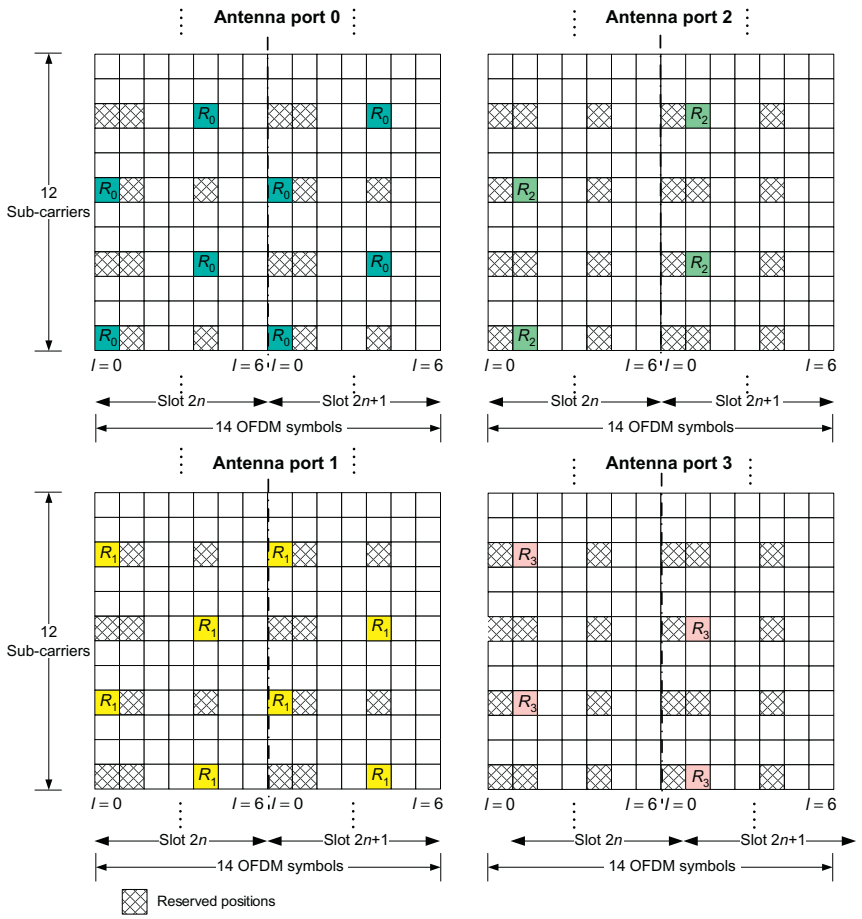


FIGURE 9.49

Mapping of cell-specific reference signals to antenna ports 0, 1, 2, and 3 for four transmit antennas over a resource block using a normal cyclic prefix [3].

of each OFDM symbol.[12] Note that $N_{CP} = 1$ for a normal cyclic prefix and $N_{CP} = 0$ for an extended cyclic prefix. The reference signal sequence $r_l^{n_s}(m)$ is mapped to complex-valued modulation symbols a_{kl}^p that are designated as reference symbols for

[12]Pseudo-random sequences are defined by a length-31 Gold sequence. The output sequence $c(n), \forall n = 0, 1, \ldots, M-1$ of length M is defined by $c(n) = (x_1(n + N_C) + x_2(n + N_C))\text{mod } 2$ in which $x_1(n + 31) = (x_1(n + 3) + x_1(n))\text{mod}2, x_2(n + 31) = (x_2(n + 3) + x_2(n + 2) + x_2(n + 1) + x_2(n))\text{mod } 2$, and $N_C = 1600$. The first m-sequence is initialized with $x_1(0) = 1, x_1(n) = 0, n = 1, 2, \ldots, 30$. The second M-sequence is initialized by $c_{\text{init}} = \sum_{i=0}^{30} x_2(i)2^i$ with the value depending on the application of the sequence [3].

Petitioners' Exhibit 1021
Nokia of America Corp., et al. v. KT Corporation, et al.
Case No. IPR2025-00036; U.S. Patent No. 11,627,631
Page 501 of 1122

antenna port p in slot n_s as $a_{kl}^{p} = r_{l}^{n_s}(m')$, where the parameters are given as follows [3]:

$$k = 6m + (v + v_{\text{shift}}) \bmod 6; \quad l = \begin{cases} 0, N_{s}^{\text{DL}} - 3 & \text{if } p \in \{0,1\} \\ 1 & \text{if } p \in \{2,3\} \end{cases}$$

$$m = 0, 1, \ldots, 2N_{\text{RB}}^{\text{DL}} - 1; \qquad m' = m + \max(N_{\text{RB}}^{\text{DL}}) - N_{\text{RB}}^{\text{DL}} \tag{9.41}$$

The variables v and v_{shift} define the position in the frequency-domain for different reference signals, where v is given by the following expression [3]:

$$v = \begin{cases} 0 & \text{if } p = 0 \text{ and } l = 0 \\ 3 & \text{if } p = 0 \text{ and } l \neq 0 \\ 3 & \text{if } p = 1 \text{ and } l = 0 \\ 0 & \text{if } p = 1 \text{ and } l \neq 0 \\ 3(n_s \bmod 2) & \text{if } p = 2 \\ 3 + 3(n_s \bmod 2) & \text{if } p = 3 \end{cases} \tag{9.42}$$

A cell-specific frequency shift is given by $v_{\text{shift}} = N_{\text{ID}}^{\text{cell}} \bmod 6$ (Figure 9.50). As shown in Figure 9.50, the resource element allocation for CRSs cycles once every six physical cell identity values, i.e., cell identity values that are integer multiples of 6 has the same resource element allocation as cell identity 0. This corresponds to one cycle for every two physical layer cell-identity groups. The resource elements

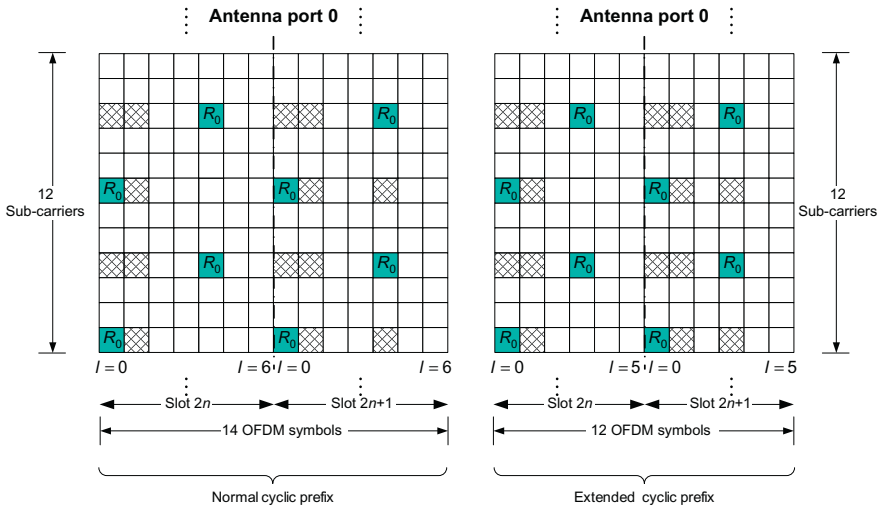


FIGURE 9.50

Cell-specific reference signal mapping for normal and extended cyclic prefix subframes [3].

(k, l) used for transmission of CRSs on an any of the antenna ports in a slot are not used for any transmission on another antenna port in the same slot and are set to zero. In an MBSFN subframe, CRSs are only transmitted in the non-MBSFN region of the MBSFN subframe. Figure 9.49 shows the CRS mapping to the resource grid. The procedure for generation of the CRSs is illustrated in Figure 9.51.

Given a different number of available OFDM symbols in a subframe with an extended cyclic prefix, the mapping of the CRSs is different than that for subframes with a normal cyclic prefix. Figure 9.50 illustrates and compares the CRS mapping in subframes with a normal and extended cyclic prefix associated with antenna port 0 and 4 transmit antennas. While the number of resource elements mapped with reference signals is the same, the CRS overhead in subframes with an extended cyclic prefix is higher due to a lower number of total sub-carriers in a resource block.

As shown in Figure 9.51, the CRSs are based on length-31 Gold pseudo-random sequences. The length-31 Gold pseudo-random sequence is generated with the seed c_{init}, based on the slot number, symbol number, cell identity, and cyclic prefix type. While the sequence itself is 230 bits long, the number of bits from the sequence selected for transmission is based on the largest channel bandwidth, which is currently 20 MHz. Therefore, $4\max(N_{\text{RB}}^{\text{DL}})$ bits are selected from

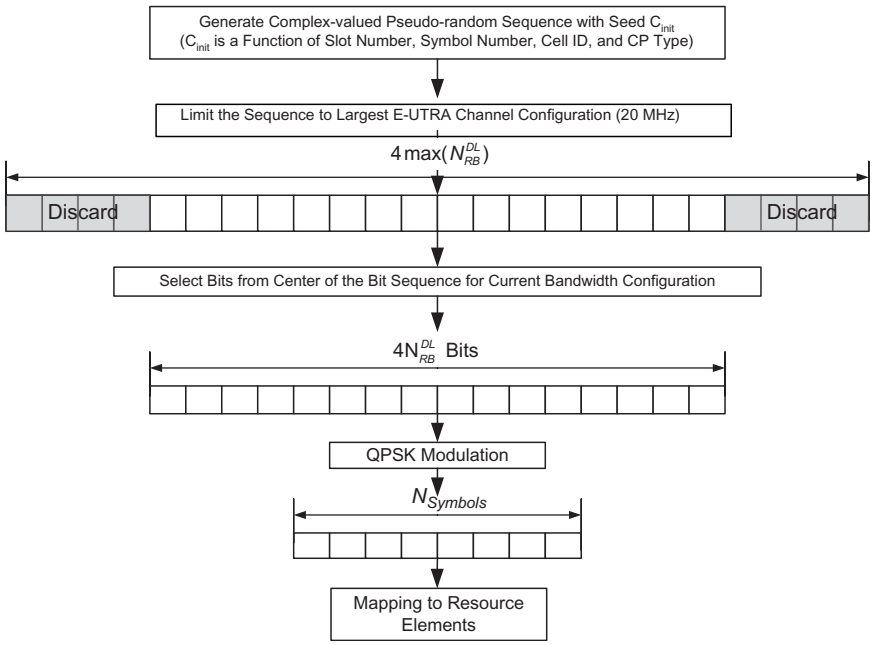


FIGURE 9.51

Generation of cell-specific reference signals.

Petitioners' Exhibit 1021
Nokia of America Corp., et al. v. KT Corporation, et al.
Case No. IPR2025-00036; U.S. Patent No. 11,627,631
Page 503 of 1122

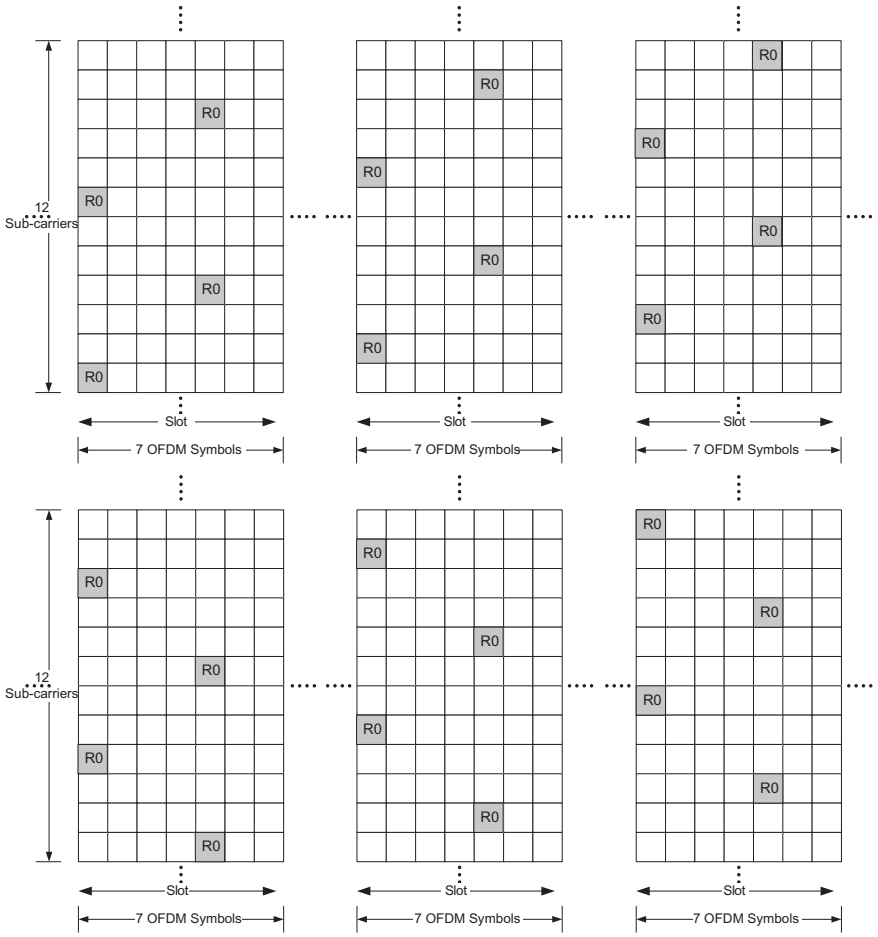


FIGURE 9.52

Dependency of cell-specific reference signals location on physical cell identifier [13].

the sequence where $\max(N_{\mathrm{RB}}^{\mathrm{DL}})$ is the maximum number of resource blocks in 20 MHz. From $4\max(N_{\mathrm{RB}}^{\mathrm{DL}})$, $4N_{\mathrm{RB}}^{\mathrm{DL}}$ bits are selected, where $N_{\mathrm{RB}}^{\mathrm{DL}}$ is the number of resource blocks corresponding to the system bandwidth. The bits are selected from the center of the truncated sequence for the maximum channel configuration. This ensures that the same reference symbols are present around PBCH regardless of channel bandwidth. The PBCH uses the six resource blocks (72 subcarriers) at the center of the channel. The UE can use these symbols for channel estimation for PBCH detection without knowing the overall channel bandwidth. The channel bandwidth in terms of resource blocks is determined from the

Petitioners' Exhibit 1021
Nokia of America Corp., et al. v. KT Corporation, et al.
Case No. IPR2025-00036; U.S. Patent No. 11,627,631
Page 504 of 1122

PBCH. After PBCH is decoded, the UE determines the length of the reference signal used for the current channel configuration.

9.10.3.1 Received signal strength indicator measurement

Received signal strength indicator (RSSI) is the total power that UE observes across the entire system bandwidth. This includes the main signal and co-channel non-serving cell signal, adjacent channel interference, and the thermal noise within the specified frequency band. This is the power of the received signal prior to demodulation, thus the UE can measure this power without any synchronization and demodulation [6].

9.10.3.2 Reference signal received power measurement

Reference signal received power (RSRP) is defined as the linear average over the power contributions of the resource elements that carry cell-specific reference signals within the considered measurement bandwidth. For the purpose of RSRP calculation, the R_0 cell-specific reference signals are used; however, if the UE can reliably detect R_1 cell-specific reference signals, then it may use R_1 in addition to R_0 in order to calculate RSRP. The reference point for the RSRP measurement is the antenna connector of the UE. If the UE uses a receive diversity scheme, the reported RSRP value must not be lower than individual RSRP measured at any of the diversity branches. There are requirements for both absolute and relative RSRP. The absolute requirements range from ± 6 to ± 11 dB, depending on the noise level and environmental conditions. Measuring the difference in RSRP between two cells on the same frequency (intra-frequency measurement) is a more accurate operation for which the requirements vary from ± 2 to ± 3 dB. The requirements widen again to ± 6 dB when the cells are on different frequencies (inter-frequency measurement) [6].

9.10.3.3 Reference signal received quality measurement

Reference signal received quality (RSRQ) is defined as the ratio $\text{RSRQ} = N_{\text{RB}}\,\text{RSRP}/\text{RSSI}_{E\text{-UTRA}}$ (dB), where N_{RB} is the number of resource blocks over which the measurement is conducted. Note that the value of RSRQ in decibels is always negative, since the denominator is larger than the numerator. The measurements in the numerator and denominator are conducted over the same set of resource blocks. The E-UTRA carrier RSSI comprises the linear average of the total received power observed only in OFDM symbols containing the cell-specific reference symbols for antenna port zero over N_{RB} resource blocks in the measurement bandwidth by the UE from all sources, including co-channel serving and non-serving cells, adjacent channel interference, and thermal noise. If higher-layer signaling indicates certain subframes for performing RSRQ measurements, then RSSI is measured over all OFDM symbols in the designated subframes. The reference point for the RSRQ is the antenna connector of the UE. If the UE uses a receive diversity scheme, the reported RSRP value must not be lower than individual RSRQ measured at any of the diversity branches.

Petitioners' Exhibit 1021
Nokia of America Corp., et al. v. KT Corporation, et al.
Case No. IPR2025-00036; U.S. Patent No. 11,627,631
Page 505 of 1122

Table 9.10 RSRQ Mapping [6]

Reported RSRQ Value	Measured Quantity (dB)
RSRQ_00	$RSRQ < -19.5$
RSRQ_01	$-19.5 \leq RSRQ < -19$
RSRQ_02	$-19 \leq RSRQ < -18.5$
...	...
RSRQ_32	$-4 \leq RSRQ < -3.5$
RSRQ_33	$-3.5 \leq RSRQ < -3$
RSRQ_34	$-3 \leq RSRQ$

Measuring RSRQ becomes particularly important near the cell-edge when decisions need to be made regardless of absolute RSRP to perform a handover to the target cell. Reference signal receive quality is used only during connected states. Intra- and inter-frequency absolute RSRQ accuracy varies from ± 2.5 to ± 4 dB, which is similar to the inter-frequency relative RSRQ accuracy of ± 3 to ± 4 dB.

It must be noted that RSRQ measurement provides additional information when RSRP is not sufficient to make a reliable handover or cell reselection decision. The RSRQ is the ratio of the RSRP and the RSSI, which depends on the measurement bandwidth, and thereby the number of resource blocks. The RSSI value includes the total received wideband power from all interference and thermal noise sources. Since RSRQ combines signal strength as well as interference level, its value further assists mobility management in E-UTRA. The UE typically measures RSRP or RSRQ per instructions from the network (via RRC messages) and reports the values back to the eNB. When it reports the RSRQ value, it does not use the real RSRQ value; rather it sends a non-negative value ranging from 0 to 34, and each of these values are mapped to a specific range of real RSRQ values as given in Table 9.10. The reporting range of RSRQ is defined from -19.5 dB to -3 dB with 0.5 dB resolution. As an example, assume that only reference signals are transmitted in a resource block and that data, noise, and interference are not considered. In this case, the RSRQ is equal to -3 dB. If cell-specific reference signals and the sub-carriers carrying data are equally powered, the RSRQ is equal to 1/12 or -10.79 dB.

9.10.4 UE-Specific reference signals associated with PDSCH

It was mentioned that cell-specific reference signals are transmitted on each antenna port. An antenna port is generally used as a generic term for signal transmission under identical channel conditions. The symbols that are transmitted via identical antenna ports are subject to the same channel conditions. In order to determine the characteristics of the channel from an antenna port, a UE must carry out a separate channel estimation for each antenna port. Therefore, separate

Petitioners' Exhibit 1021
Nokia of America Corp., et al. v. KT Corporation, et al.
Case No. IPR2025-00036; U.S. Patent No. 11,627,631
Page 506 of 1122

reference signals that are suitable for estimating the respective channel are defined for each antenna port. There is one resource grid per antenna port. The cell-specific reference signals are used for both coherent detection and mobility-related measurements. Their structure in time and frequency ensures sufficient channel estimation accuracy. An LTE-Advanced eNB is required to support LTE Rel-8 user terminals. Since the structure of PCFICH, PHICH, PDCCH, PBCH, and PDSCH (transmit diversity only) is unchanged in Rel-10, the support of CRS is also required for LTE-Advanced UEs in order to detect these essential physical channels. The UE-specific reference signals are supported for transmission of PDSCH, and are transmitted on antenna ports $p = 5$, $p = 7$, $p = 8$, or $p = 7, 8, \ldots, N_l + 6$, where N_l is the number of spatial layers used for transmission of PDSCH. The UE-specific reference signals or DM-RS can be precoded and support non-codebook-based precoding. The DM-RS pattern for a higher number of layers has been extended from dual-layer format of transmission mode 8 in Rel-9 to eight layers in Rel-10. The CSI-RS is transmitted on each physical or virtual antenna port, and is only used for channel state measurement/reporting purposes. Its channel estimation accuracy can be relatively poorer compared to that of DM-RS. In Rel-8, the CRS is used for both demodulation and measurement purposes. When using precoding in conjunction with CRSs, the precoding information must be sent to the UE, and the CRS power is boosted to support various types of geometry. The Rel-8 E-UTRA downlink MIMO transmission modes are based on CRS. Figure 9.53 shows the CRS-based procedure for precoding where the cell-specific reference signals are inserted after the data is precoded. Therefore, the cell-specific reference signals do not contain information about the

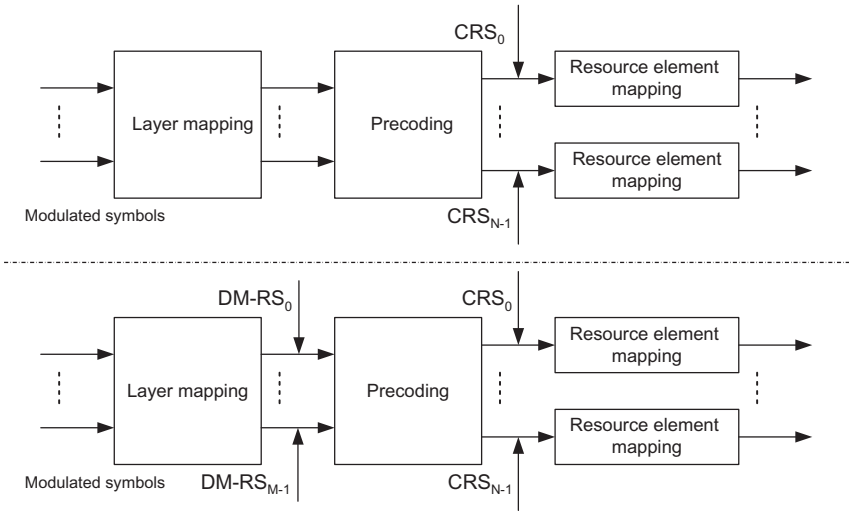


FIGURE 9.53

Comparison of the CRS and DM-RS usage in Rel-8 and Rel-10 of E-UTRA [110].

Petitioners' Exhibit 1021
Nokia of America Corp., et al. v. KT Corporation, et al.
Case No. IPR2025-00036; U.S. Patent No. 11,627,631
Page 507 of 1122

precoding scheme, and codebook information must be separately sent to the UE. In contrast, in LTE-Advanced, downlink MIMO transmission is based on DM-RS and CSI-RS. Figure 9.53 shows the DM-RS-based procedure for precoding where UE-specific reference signals are precoded in the same way as the data. Therefore, no separate precoding information is sent to the UE. Note that in LTE Rel-10, DM-RS is used for demodulation and CSI-RS is used for channel state measurement purposes. Unlike CRS-based precoding, the precoding information is not needed for demodulation.

It was stated earlier that UE-specific reference signals are used for transmission of the downlink shared channel and are transmitted on antenna port(s) $p = 5$, $p = 7$, $p = 8$ or $p = 7, 8, \ldots, N_l + 6$, where N_l is the number of layers (up to eight). It must be noted that the UE-specific reference signals on any antenna port are a valid reference for data demodulation, if the data transmission is associated with the corresponding antenna port. The UE-specific reference signals are exclusively transmitted on the resource blocks to which the corresponding user data is mapped. The UE-specific reference signal is not mapped to resource elements (k, l) that are reserved for transmission of control signaling, physical channels, or physical signals.

For antenna port 5, the UE-specific reference-signal sequence $r_{n_s}(m)$ is defined by $r_{n_s}(m) = (1/\sqrt{2})[1 - 2c(2m)] + \mathrm{j}(1/\sqrt{2})[1 - 2c(2m+1)]$, $\forall m = 0, 1, \ldots, 12N_{\mathrm{RB}} - 1$, where N_{RB} denotes the number of resource blocks allocated to the corresponding data transmission. The pseudo-random sequence $c(i)$ was defined earlier. The pseudo-random sequence generator is initialized with $c_{\mathrm{init}} = \left(\lfloor n_s/2 \rfloor + 1\right)\left(2N_{\mathrm{ID}}^{\mathrm{cell}} + 1\right)2^{16} + n_{\mathrm{RNTI}}$ at the start of each subframe where n_{RNTI} is the 16-bit radio network temporary identifier (RNTI) of the UE. For antenna ports $p \in \{7, 8, \ldots, N_l + 6\}$, the UE-specific reference-signal sequence $r_{n_s}(m)$ is defined by $r_{n_s}(m) = (1/\sqrt{2})[1 - 2c(2m)] + \mathrm{j}(1/\sqrt{2})[1 - 2c(2m+1)]$, where $m = 0, 1, \ldots, 12N_{\mathrm{RB}}^{\mathrm{DL}} - 1$ (for normal cyclic prefix) or $m = 0, 1, \ldots, 16N_{\mathrm{RB}}^{\mathrm{DL}} - 1$ (for extended cyclic prefix). The pseudo-random sequence $c(i)$ is defined similar to the previous section. Prior to LTE Rel-11, the pseudo-random sequence generator was initialized with $c_{\mathrm{init}} = \left(\lfloor n_s/2 \rfloor + 1\right)\left(2N_{\mathrm{ID}}^{\mathrm{cell}} + 1\right)2^{16} + n_{\mathrm{SCID}}$ at the start of each subframe. The value of the scrambling identity n_{SCID} is zero unless specified otherwise. For a data transmission on ports 7 or 8, n_{SCID} is indicated by the DCI format 2B or 2C. In the case of DCI format 2B, $n_{\mathrm{SCID}} = 0$ if the scrambling identity field is zero. It must be noted that CQI estimation at the terminal is always based on cell-specific reference signals. In LTE Rel-11, and as a result of the introduction of the new PDCCH structure based on the UE-specific reference signals, the initialization of the DM-RS sequences associated with antenna ports $p \in \{7, 8, \ldots, N_l + 6\}$ was modified as follows: $c_{\mathrm{init}} = \left(\lfloor n_s/2 \rfloor + 1\right)\left(2N_{\mathrm{ID}}^{(n_{\mathrm{SCID}})} + 1\right)2^{16} + n_{\mathrm{SCID}}$, where $N_{\mathrm{ID}}^{(i)}|_{i=0,1}$ is defined as $N_{\mathrm{ID}}^{(i)} = N_{\mathrm{ID}}^{\mathrm{cell}}$, if no value for $N_{\mathrm{ID}}^{\mathrm{DM\text{-}RS}_i}$ is conveyed by higher layers, or if DCI format 1A is used for the DCI associated with PDSCH transmission; otherwise $N_{\mathrm{ID}}^{(i)} = N_{\mathrm{ID}}^{\mathrm{DM\text{-}RS}_i}$ [3].

Petitioners' Exhibit 1021
Nokia of America Corp., et al. v. KT Corporation, et al.
Case No. IPR2025-00036; U.S. Patent No. 11,627,631
Page 508 of 1122

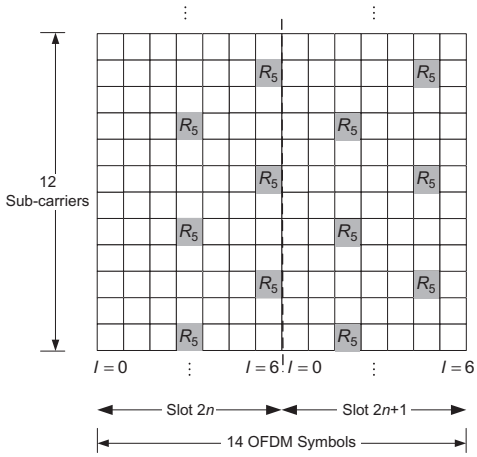


FIGURE 9.54

Mapping of UE-specific reference signals to antenna port 5 [3].

In a PRB with index n_{PRB} allocated for data transmission on antenna port 5, and assuming the normal cyclic prefix, the DM-RS $r_{n_s}(m)$ is mapped to the complex-valued modulation symbols a_{kl}^{p} over slot n_s as $a_{kl}^{5} = r_{n_s}(3l'N_{\text{RB}} + m')$, where $m' = 0, 1, \ldots, 3N_{\text{RB}} - 1$ denotes the number of UE-specific reference signal resource elements within a respective OFDM symbol allocated to user data transmission, $l' = \{0, 1\}$ for even-numbered slots, and $l' = \{2, 3\}$ for odd-numbered slots.

The UE-specific reference signal pattern for up to two layers, or alternatively rank-2 transmission, is identical to that of LTE Rel-9 to maintain backward compatibility. For up to four layers, the DM-RS pattern is obtained by extending LTE Rel-9 UE-specific reference signal pattern using a combination code-division and frequency-division multiplexing, as shown in Figure 9.55. The four precoded layers (antenna ports 7−10) are grouped into two groups of two resource elements that are spread with the same length-2 Walsh−Hadamard[13] orthogonal cover codes (OCCs) as in Rel-9. The UE-specific reference signals in different groups are frequency-multiplexed on adjacent sub-carriers. This pattern has been shown to provide reasonable performance for a variety of channel conditions and UE speeds [121].

[13]In coding theory, the Walsh−Hadamard code is a linear code over a binary alphabet that maps messages of length 2^n. The Walsh−Hadamard code is unique in that each non-zero codeword has a Hamming weight of exactly 2^{n-1}, which implies that the distance of the code is also 2^{n-1} resulting in a $[2^n, n, 2^{n-1}]_2$ code. The Walsh−Hadamard code is locally decodable, which enables recovery of parts of the original message with high probability, while only looking at a small fraction of the received codeword [27,40].

Petitioners' Exhibit 1021
Nokia of America Corp., et al. v. KT Corporation, et al.
Case No. IPR2025-00036; U.S. Patent No. 11,627,631
Page 509 of 1122

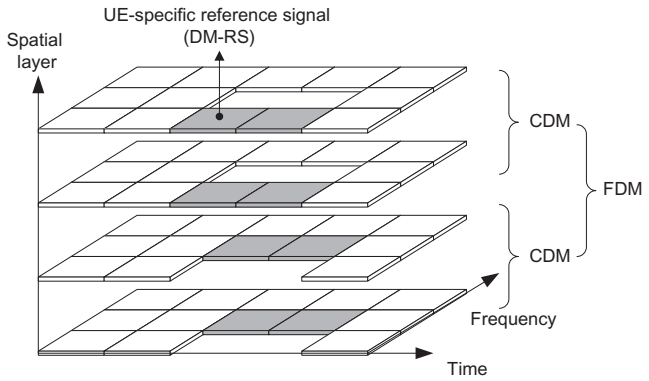


FIGURE 9.55

Code and frequency division multiplexing of the UE-specific reference signals [177].

For rank-8 transmission on antenna ports 7−14, the UE-specific reference signal pattern of Figure 9.55 is further extended using a hybrid CDM/FDM approach with two CDM groups each using a Walsh−Hadamard OCC of length 4, as shown in Figure 9.56. The UE-specific reference signals for each layer are spread across four resource elements, all having the same frequency location but different time locations within the subframe. This approach maintains the balanced power property of the rank-4 UE-specific pilot design and is optimized for pedestrian mobility class, which is the most likely use case for eight-layer transmission. The OCCs of length two are embedded in the OCC of length four to ensure backward compatibility with LTE Rel-9. The mapping of the OCCs to resource elements is shown in Figure 9.56. The mapping for odd and even resource blocks (in the frequency-domain) is different in order to provide orthogonality in both time and frequency dimensions. Such orthogonality improves the performance of channel estimation in high Doppler scenarios, and reduces the inter-carrier interference across the two CDM groups in the presence of frequency offsets. The OCC mapping also enables power balancing across OFDM symbols by peak power randomization [14]. The reference sequence for up to eight layers is the same as in Rel-9, except for antenna ports $AP_p|_{p=9,10,\ldots,14}$ where only one sequence initialization is possible.

In mathematical terms, for antenna ports $AP_p|_{p=7,8,\ldots,N_l+6}$, in a PRB with frequency-domain index n_{PRB} assigned for the corresponding user data transmission, part of the reference sequence $r(m)$ is mapped to complex-valued modulation symbols a_{kl}^{p} in a subframe (assuming normal cyclic prefix) as follows: $a_{kl}^{p} = w_p(l')\, r[3l'\max(N_{\text{RB}}^{\text{DL}}) + 3n_{\text{PRB}} + m']$, where $w_p(i) = \overline{w}_p(i)$ if $(m' + n_{\text{PRB}})\text{mod } 2 = 0$ or $w_p(i) = \overline{w}_p(3-i)$ if $(m' + n_{\text{PRB}})\text{mod } 2 = 1$, where $\overline{w}_p(i)$ is given in Table 9.11. The UE-specific reference signal patterns for different transmission ranks (number of spatial layers) are shown in Figure 9.57.

Petitioners' Exhibit 1021
Nokia of America Corp., et al. v. KT Corporation, et al.
Case No. IPR2025-00036; U.S. Patent No. 11,627,631
Page 510 of 1122

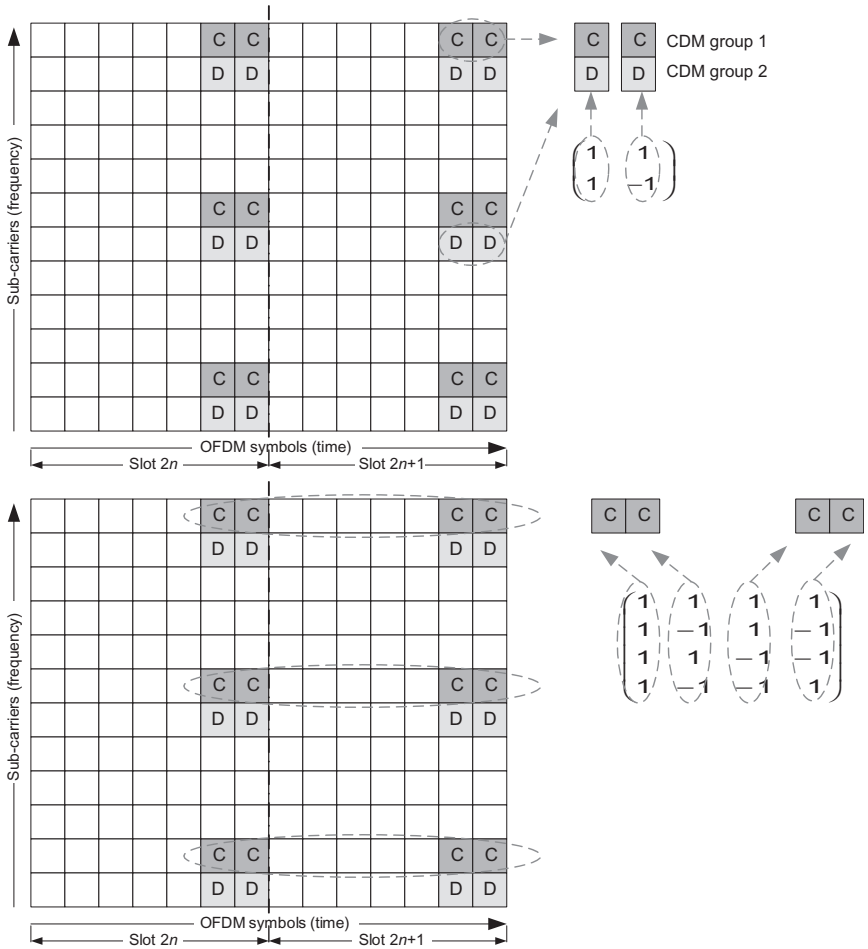


FIGURE 9.56

Length-2 and length-4 OCC mapping and DM-RS structure [121].

9.10.5 CSI reference signals

The new multi-user MIMO techniques that were proposed as part of Rel-10 and beyond require some level of CSI knowledge at the base station so that the system can dynamically adapt to the radio channel conditions experienced by the user terminals in order to optimize the performance. In TDD systems, this information is intuitively obtained from the uplink direction based on the reciprocity of the wireless channel, provided that the channel fading is sufficiently slow and transceivers at the base and mobile stations are calibrated, due to the fact that the

Petitioners' Exhibit 1021
Nokia of America Corp., et al. v. KT Corporation, et al.
Case No. IPR2025-00036; U.S. Patent No. 11,627,631
Page 511 of 1122

Table 9.11 Orthogonal Cover Code of Length 4 [3]

Antenna Port p	$[\overline{w}_p(0)$	$\overline{w}_p(1)$	$\overline{w}_p(2)$	$\overline{w}_p(3)]$
7	[+1	+1	+1	+1]
8	[+1	−1	+1	−1]
9	[+1	+1	+1	+1]
10	[+1	−1	+1	−1]
11	[+1	+1	−1	−1]
12	[−1	−1	+1	+1]
13	[+1	−1	−1	+1]
14	[−1	+1	+1	−1]

same carrier frequency is used for transmission and reception. On the other hand, due to the asymmetry of FDD systems, feedback information over the uplink is required. Full CSI could cause an excessive overhead in some scenarios, thus quantized or statistical CSI are used in practice. In addition, terminal mobility can cause further degradation of the system performance, if the CSI arriving at the eNB is already outdated. Multi-antenna techniques in a multi-user scenario have the role of delivering streams of data in a spatially multiplexed manner to different users in such a way that all the degrees of freedom of a MIMO system are utilized. The idea is to perform intelligent space-division multiple access or multi-user beamforming so that the transmission of the base station is adapted to each user's instantaneous channel conditions in order to achieve the maximum gain in the direction of that user. The base station collects information on the CSI of each UE and subsequently decides on the optimal resource allocation strategy for each user.

Channel state information reference signals were introduced as part of Rel-10 to enable channel state measurement and reporting by UEs for up to eight downlink transmit-antennas to facilitate eNB precoding functions in transmission mode 9. LTE Rel-10 supports transmission of CSI-RS for 1, 2, 4, and 8 transmit antennas. The CSI-RSs also enable the UE to estimate the CSI for multiple neighbor cells in addition to its serving cell, to support multi-cell cooperative transmission schemes. The following principles have been incorporated in the design of the CSI-RS [14]:

- It is desirable to place CSI-RS at locations with uniform spacing in the frequency-domain.
- It is desirable to minimize the number of subframes containing CSI-RS in the time-domain so that a UE can estimate the CSI for different antenna ports and different cells with a minimal wake-up (active state) duty cycle when the UE is in DRX mode to reduce UE power consumption.
- The overall CSI-RS overhead involves a trade-off between accurate CSI estimation for efficient operation and minimizing the impact on legacy UEs

Petitioners' Exhibit 1021
Nokia of America Corp., et al. v. KT Corporation, et al.
Case No. IPR2025-00036; U.S. Patent No. 11,627,631
Page 512 of 1122

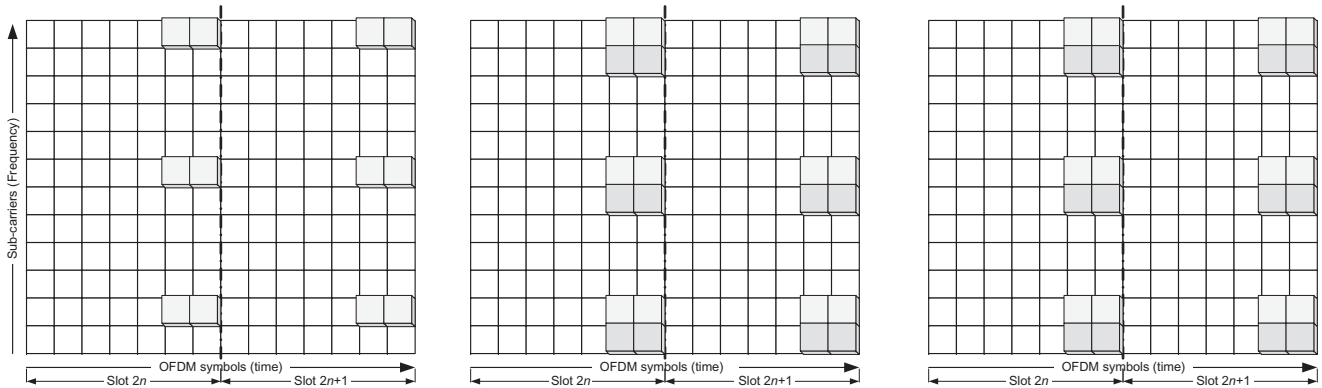


FIGURE 9.57

Mapping of UE-specific reference signals to resource blocks for different numbers of layers [177].

Petitioners' Exhibit 1021
Nokia of America Corp., et al. v. KT Corporation, et al.
Case No. IPR2025-00036; U.S. Patent No. 11,627,631
Page 513 of 1122

which are unaware of the presence of CSI-RS. Furthermore, the data sub-carriers of the legacy UE are punctured by the CSI-RS transmissions. Figure 9.58 shows that a CSI-RS density of one resource element per resource block per antenna port is a reasonable choice, as the throughput degradation compared to ideal CSI estimation is negligible.

- The CSI-RSs of different antenna ports within a cell, and ideally from other cells, should be orthogonally multiplexed to enable accurate CSI estimation.
- To ensure backward compatibility, CSI-RSs should not be mapped to the resource elements used for CRSs and control channels, as well as avoiding resource elements used for the Rel-10 UE-specific reference signals.

A set of CSI-RSs were designed in Rel-10, taking the above design considerations into account. An example CSI-RS pattern for 1, 2, 4, and 8 antenna ports is shown in Figure 9.58. The OCC codes of length 2 are used, so that CSI-RSs on two antenna ports share two resource elements on a given sub-carrier. The pattern shown in Figure 9.58 is applicable to frame structure type 1 and frame structure type 2 [121].

The CSI-RS patterns follow a nested structure, meaning that the resource elements used in the case of two CSI-RS antenna ports are a subset of those used for four and eight antenna ports; this helps to simplify the implementation. The total number of supported CSI-RS patterns is 40, which can be used to give a frequency-reuse factor of 5 between cells with eight antenna ports per cell, or a factor of 20 in the case of two antenna ports. It can be seen that collisions may occur with resource elements used for the DM-RS antenna ports defined in Rel-8 for PDSCH transmission mode 7. Therefore, it may be desirable to avoid scheduling UEs in transmission mode 7 in subframes containing CSI-RS. This pattern is designed to avoid collisions with the Rel-8 UE-specific reference signal antenna port, as this port is more suited to TDD operation where channel reciprocity can be more effectively exploited to support beamforming. However, this pattern only offers frequency-reuse factors between 3 and 12 depending on the number of antenna ports per cell [14].

The CSI-RS configuration is UE-specific. When the CSI-RS is configured, it is only present in certain subframes conforming to a given duty cycle and subframe offset. The duty cycle and offset of the subframes containing CSI-RSs and the CSI-RS pattern used in those subframes are provided to a Rel-10 UE through RRC signaling. The duty cycle and subframe offset are jointly coded, while the CSI-RS pattern is configured independently of these parameters. It should be noted that in subframes containing CSI-RSs, the rate-matching for PDSCH transmissions to Rel-10 UEs is considerate of the resource elements used for CSI-RS and the encoded PDSCH data is only mapped to the neighboring sub-carriers, whereas PDSCH transmissions to the legacy UEs are punctured by CSI-RS transmissions. Therefore, the density and periodicity of the CSI-RSs should be chosen

Petitioners' Exhibit 1021
Nokia of America Corp., et al. v. KT Corporation, et al.
Case No. IPR2025-00036; U.S. Patent No. 11,627,631
Page 514 of 1122

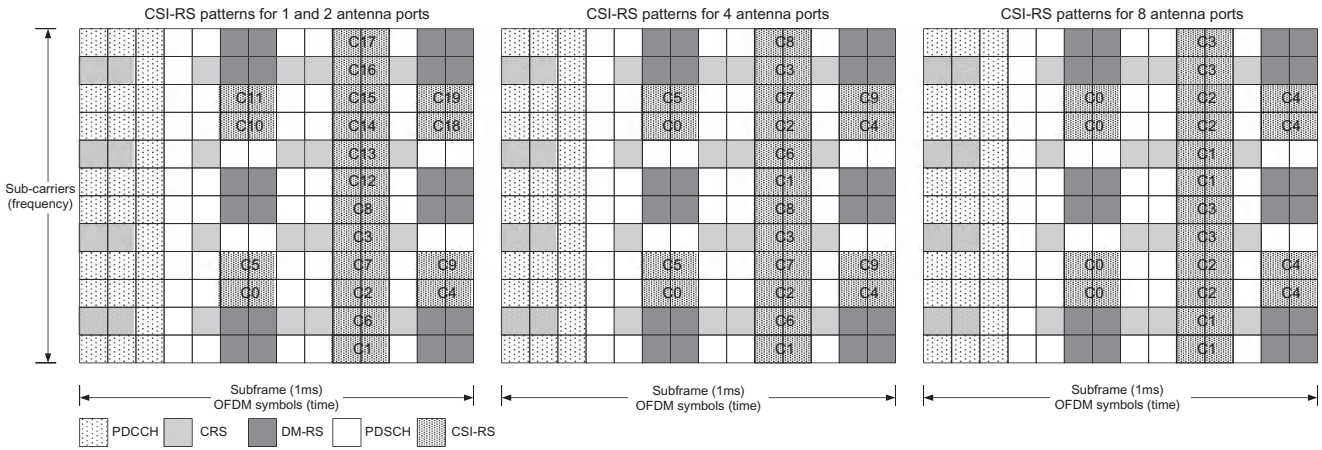


FIGURE 9.58

CSI-RS patterns for 1, 2, 4, and 8 transmit antennas [3,121].

such that the impact of puncturing[14] on the performance of these users is negligible.

In the context of cooperative MIMO, it may be possible to improve the performance of channel estimation, and especially interference estimation, by coordinating CSI-RS transmissions across multiple cells. In Rel-10 it is possible to mute a specific set of sub-carriers in data transmissions from a cell. The locations of these resource elements can be chosen to avoid colliding with CSI-RS transmissions from other cells, thus improving the inter-cell interference measurement quality. The muting pattern is signaled to the UEs using a 16-bit bitmap, where each bit corresponds to a 4-port CSI-RS configuration for frame structure type 1 or type 2. As a result, all the resource elements in the selected 4-port CSI-RS configuration are muted and the UE can assume zero transmission power on those resource elements, unless they are used to transmit CSI-RSs. In subframes in which CSI-RS muting is configured, data transmissions for Rel-10 UEs are rate-matched around the muted resource elements in the same way as for CSI-RSs. Data transmitted to Rel-8/9 UEs is punctured at the muted resource elements [15].

The CSI-RSs are transmitted on one, two, four, or eight antenna ports $AP_p = \{p = 15\}, \{p = 15, 16\}, \{p = 15, \ldots, 18\}, \{p = 15, \ldots, 22\}$ and are only defined for sub-carrier spacing of 15 kHz. The reference signal sequence is defined as $r_l^{n_s}(m) = (1/\sqrt{2})[1 - 2c(2m)] + \mathrm{j}(1/\sqrt{2})[1 - 2c(2m+1)], \quad \forall m = 0, 1, \ldots, \max(N_{\mathrm{RB}}^{\mathrm{DL}}) - 1$, where n_s is the slot number within a radio frame and $l = 0, 1, \ldots, 6$ (or 5 for an extended cyclic prefix) is the OFDM symbol number within the slot. The pseudo-random sequence $c(i)$ was defined in the previous sections. The pseudo-random sequence generator is initialized with $c_{\mathrm{init}} = 2^{10}(7(n_s + 1) + l + 1)(2N_{\mathrm{ID}}^{\mathrm{CSI}} + 1) + 2N_{\mathrm{ID}}^{\mathrm{CSI}} + N_{\mathrm{CP}}$ at the start of each OFDM symbol where $N_{\mathrm{CP}} = 1$ for a normal cyclic prefix and $N_{\mathrm{CP}} = 0$, otherwise. In subframes configured for CSI-RS transmission, the reference signal sequence $r_l^{n_s}(m)$ is mapped to complex-valued modulation symbols $a_{kl}^p = w_\alpha r_l^{n_s}(m')$ which have been designated as reference symbols on AP_p where $m' = m + \lfloor [\max(N_{\mathrm{RB}}^{\mathrm{DL}}) - N_{\mathrm{RB}}^{\mathrm{DL}}]/2 \rfloor; m = 0, 1, \ldots, N_{\mathrm{RB}}^{\mathrm{DL}} - 1$ and $w_\alpha = 1$ for $p \in \{15, 17, 19, 21\}$ and $w_\alpha = (-1)^\alpha$ for $p \in \{16, 18, 20, 22\}$. The virtual CSI identifier in the above equation is equal to the cell identity unless configured by higher layers.

[14] In coding theory, puncturing is the process of removing some of the parity bits after encoding with an error-correction code. This has the same effect as encoding with an error-correction code with a higher rate, or less redundancy. However, with puncturing the same decoder can be used regardless of how many bits have been punctured, thus puncturing considerably increases the flexibility of the system without significantly increasing its complexity. In some cases, a predefined pattern of puncturing is used in an encoder. Then, the inverse operation, known as de-puncturing, is implemented by the decoder. Puncturing is used in UMTS and LTE during the rate-matching process. Puncturing is often used with the soft decoding and Viterbi algorithm [27,40].

Petitioners' Exhibit 1021
Nokia of America Corp., et al. v. KT Corporation, et al.
Case No. IPR2025-00036; U.S. Patent No. 11,627,631
Page 516 of 1122

The following parameters for CSI-RS are configured via higher layer signaling [5]:

- Number of CSI-RS ports
- CSI-RS configuration
- CSI-RS subframe configuration $I_{\text{CSI-RS}}$
- Subframe configuration period $T_{\text{CSI-RS}}$
- Subframe offset $T_{\text{Offset-CSI-RS}}$
- UE assumption on reference PDSCH transmitted power for CSI feedback P_c. The parameter P_c is the assumed ratio of PDSCH energy per resource element (EPRE)[15] to CSI-RS EPRE when UE derives CSI feedback and takes values in the range of [−8 dB to 15 dB] in 1 dB step sizes.

Multiple CSI-RS configurations can be used in a given cell, which include zero or one configuration for which the UE can assume non-zero transmission power, and zero or more configurations for which the UE can assume zero transmission power. The UE assumes that CSI-RSs are not transmitted in the special subframe(s) in the case of frame structure type 2, in subframes where transmission of a CSI-RS would collide with transmission of synchronization signals, PBCH, or system information block type 1 messages, in subframes configured for transmission of paging messages for any UE with the cell-specific paging configuration. The resource elements (k, l) that are used for transmission of CSI-RS on any of the antenna ports $AP_p = \{15\}, \{15, 16\}, \{17, 18\}, \{19, 20\}, \{21, 22\}$ are not used for transmission of PDSCH on any antenna port in the same slot, and are not used for CSI-RS on any antenna port other than those in the above set of antennas in the same slot. The mapping of CSI-RS for 1, 2, 4, and 8 antenna ports are shown in Figure 9.58 [3].

Depending on the number of CSI-RS antenna ports, there are multiple reuse patterns on different locations which share a common base pattern. In the case of 1, 2, 4, and 8 antenna ports, there are 40, 20, 10, and 5 reuse patterns, respectively, allowing different cells to utilize different reuse patterns to avoid inter-cell CSI-RS collision. In addition, the base patterns for different numbers of CSI-RS antenna ports have a nested structure, allowing for simpler CSI-RS transmitter and receiver implementation. Each antenna port's CSI-RS is spread over two adjacent resource elements across time such that two different CSI-RSs are code-

[15]Downlink power control determines the energy per resource element (EPRE). The term resource element energy denotes the energy prior to cyclic prefix insertion. The EPRE is calculated by averaging the energy over all constellation points based on the modulation scheme applied. A UE may assume downlink cell-specific reference signal EPRE is constant across the downlink system bandwidth and constant across all subframes until different cell-specific RS power information is received. The downlink cell-specific reference-signal EPRE can be derived from the downlink reference-signal transmit-power information provided by higher layers. The downlink reference-signal transmit power is defined as the linear average over the power contributions in Watts of all resource elements that carry cell-specific reference signals within the operating system bandwidth [5].

Petitioners' Exhibit 1021
Nokia of America Corp., et al. v. KT Corporation, et al.
Case No. IPR2025-00036; U.S. Patent No. 11,627,631
Page 517 of 1122

division multiplexed over two adjacent resource elements. One of the advantages of code-division-multiplexing in this case, relative to other multiplexing schemes such as FDM, is that CDM can balance transmission power across antenna ports in the frequency-domain. The CSI-RS density is related to the channel estimation accuracy. In general, larger CSI-RS density may provide better CSI measurement accuracy while reducing downlink resource utilization. Therefore, adequate CSI-RS density, where the CSI-RS occupies minimum downlink resources while providing reasonable CSI measurement accuracy, is desirable. Since CSI-RS is only used for downlink CSI measurement, its granularity is coarse due to feedback overhead; the system performance is relatively insensitive to the channel measurement accuracy as compared to that for DM-RS. Therefore, a reduced-overhead CSI-RS transmitted only once every 5, 10, 20, 40, or 80 ms is utilized in the LTE-Advanced. A typical transmission of CSI-RS, which may consist of four antenna ports with periodicity of 10 ms, would only require an overhead equivalent to 0.2% of the entire time and frequency resources. The low overhead is achieved by allocating a single resource-element-pair per CSI-RS antenna port, except when the CSI-RS has only one antenna port, where two resource elements are allocated per resource block pair (Table 9.12). The configuration period $T_{\text{CSI-RS}}$ and the subframe offset $T_{\text{Offset-CSI-RS}}$ for CSI-RSs are given in Table 9.13. The parameter $I_{\text{CSI-RS}}$ can be configured separately for CSI-RSs for which the UE assumes non-zero and zero transmission power. Those subframes containing CSI-RSs must satisfy the following equation $\left(10n_{\text{subframe}} + \lfloor n_s/2 \rfloor - T_{\text{Offset- CSI-RS}}\right) \text{mod} T_{\text{CSI-RS}} = 0$ [5,14].

Although different CSI-RS patterns are likely to be used in neighboring cells to minimize CSI-RS collision, neighbor cells' downlink data signals may still significantly interfere with CSI-RS received at a cell-edge UE in a heavily loaded network in interference-limited scenarios. In addition, accurate CSI measurement for neighbor cells is also required for support of coordinated multipoint transmissions. To mitigate the interference effects and to facilitate CSI measurement of neighbor cells, LTE-Advanced supports data reference element muting, whereby data reference elements colliding with CSI-RS in a neighbor cell are transmitted with zero transmission power (i.e., muted resource elements).

Table 9.12 Relative Overhead of CSI-RS

Number of Antenna Ports	1	2	4	8
Cell-specific reference signal	4.76	9.52	14.28	–
UE-specific reference signal	7.14	7.14	14.28	14.28
CSI reference signal	$1.19/T_{\text{CSI-RS}}$	$1.19/T_{\text{CSI-RS}}$	$2.38/T_{\text{CSI-RS}}$	$4.76/T_{\text{CSI-RS}}$

Note that CSI-RS overhead is a function of CSI-RS periodicity $T_{\text{CSI-RS}}$ in number of subframes.

Petitioners' Exhibit 1021
Nokia of America Corp., et al. v. KT Corporation, et al.
Case No. IPR2025-00036; U.S. Patent No. 11,627,631
Page 518 of 1122

Table 9.13 CSI Reference Signal Subframe Configuration [5]

CSI-RS Subframe Configuration Parameter $I_{CSI\text{-}RS}$	CSI-RS Periodicity $T_{CSI\text{-}RS}$ (Subframes)	CSI-RS Subframe Offset $T_{Offset\text{-}CSI\text{-}RS}$
0–4	5	$I_{CSI\text{-}RS}$
5–14	10	$I_{CSI\text{-}RS} - 5$
15–34	20	$I_{CSI\text{-}RS} - 15$
35–74	40	$I_{CSI\text{-}RS} - 35$
75–154	80	$I_{CSI\text{-}RS} - 75$

For an LTE-Advanced UE, the eNB applies code rate-matching around the muted resource elements so that the LTE-Advanced UE is able to decode the allocated data sub-carriers.

As mentioned earlier, a cell can be configured with one, two, four, or eight antenna-port CSI-RS. The exact CSI-RS structure, including the exact set of resource elements used for CSI-RS in a resource block, depends on the number of antenna ports for which the CSI-RS is configured within the cell and may vary for different cells. There are 40 possible positions within a resource-block pair that the CSI-RS can be mapped, and in a given cell, a subset of the corresponding resource elements is used for CSI-RS transmission. In the case of two antenna-port CSI-RS within a cell, the CSI-RS consists of two adjacent reference symbols per resource-block pair. The CSI-RS pair is separated by applying OCCs to the reference-symbol pair. Thus, there can be 20 different CSI-RS configurations based on the 40 possible reference-symbol positions.

In the case of four or eight antenna-port CSI-RS, the CSI-RS are pairwise frequency multiplexed. Thus, there is a possibility for ten or five different antenna ports for which the CSI-RS is configurations, each supporting four or eight CSI-RS, respectively. In the case of a single antenna-port CSI-RS, the same structure as for two antenna-port CSI-RS is used, although with only one of the OCCs. The overhead of a single antenna-port CSI-RS, in terms of occupied resource elements, is the same as two antenna-port CSI-RSs. In the time-domain, the CSI-RS can be transmitted with different periods, ranging from 5 to 80 ms. With a 5 ms period, the overhead per CSI-RS is roughly 0.12% per CSI-RS (one resource element per CSI-RS per resource-block pair, in every fifth subframe), thus longer periods result in lower overhead. The exact subframe in which CSI-RS is transmitted in a cell can also be configured, allowing for separation of CSI-RS transmissions among cells in the time-domain, in addition to using different sets of resource elements within the same subframe. In subframes in which CSI-RS is transmitted, the CSI-RS is transmitted in every resource block across the frequency. In other words, the CSI-RS transmission covers the entire cell bandwidth and by this means it is considered a wideband reference signal.

Petitioners' Exhibit 1021
Nokia of America Corp., et al. v. KT Corporation, et al.
Case No. IPR2025-00036; U.S. Patent No. 11,627,631
Page 519 of 1122

As mentioned above, when DM-RSs are transmitted within a resource block, the corresponding resource elements on which the reference signals are transmitted are explicitly avoided when mapping PDSCH symbols to the resource block. This restricted resource mapping, which is obviously not understood by legacy UEs, is possible as DM-RSs can be assumed to be transmitted only in resource blocks in which terminals supporting such reference signals are scheduled. In general, a legacy terminal is assumed to be never scheduled in a resource block where DM-RSs are transmitted. The situation is somewhat different for CSI-RS. As CSI-RS is transmitted within all resource blocks in the frequency-domain, it would not be practically possible to assume that legacy terminals are never scheduled in a resource block in which CSI-RS is transmitted. If the PDSCH mapping were modified to explicitly avoid the resource elements in which CSI-RS is transmitted, the mapping would not be recognized by legacy terminals. In order to alleviate this problem, the PDSCH is mapped consistent with LTE Rel-8, i.e., the mapping is not modified to avoid the resource elements on which CSI-RS is transmitted, and CSI-RS is transmitted on top of the corresponding PDSCH symbols. This will obviously impact the PDSCH demodulation performance, as some PDSCH symbols will be interfered by CSI-RS transmission. However, the remaining PDSCH symbols will not be impacted and the PDSCH will still be decodable with some acceptable performance degradation. On the other hand, if a Rel-10 terminal is scheduled in a resource block in which CSI-RS is transmitted, the PDSCH mapping is modified to explicitly avoid the resource elements on which the CSI-RS is transmitted. The remaining resource elements are used for PDSCH transmission within the cell. However, it is also possible to additionally configure one or several subsets of the resource elements as muted CSI-RS.

A muted CSI-RS has the same structure as an unmuted CSI-RS, except that nothing is actually transmitted on the corresponding resource elements. A muted CSI-RS can thus be seen as a normal CSI-RS with zero power. The motivation for inclusion of the muted CSI-RS is to enable creation of transmission holes corresponding to actual CSI-RS transmissions in neighboring cells in order to: (1) make it possible for a terminal to receive CSI-RS of neighboring cells, without being severely interfered by transmissions in its serving cell. The CSI estimation on neighboring cells would be necessary for multi-cell-transmission techniques and (2) to reduce the interference to CSI-RS transmissions in other cells. This is especially applicable to heterogeneous networks where overlapping layers with cells of substantially different transmit power are expected to coexist in the same frequency band. There can be one or multiple sets of muted CSI-RS in a cell. In the case of interference avoidance to neighboring cells, it is typically sufficient to use a single set of muted CSI-RS, as one should typically avoid interference to a single lower-power cell. When muted CSI-RS are used to alleviate intra-cell interference, in order to improve reception of CSI-RS from neighboring cells, multiple sets of muted CSI-RS are needed since neighboring cells may use different CSI-RS configurations.

Petitioners' Exhibit 1021
Nokia of America Corp., et al. v. KT Corporation, et al.
Case No. IPR2025-00036; U.S. Patent No. 11,627,631
Page 520 of 1122

9.10.6 Enhanced PDCCH demodulation reference signals

The LTE Rel-8 PDCCH was designed with the underlying assumption that each eNB with collocated antennas serves each cell in the network and different cells are distinguished through different physical cell identifiers. Furthermore, the UE relies on CRSs to detect and decode PDCCH content. However, the increasing mobile data traffic necessitates the use of dense and heterogeneous networks wherein multiple low-power remote radio heads (RRHs) with geographically displaced antennas share the same cell identity with the overlaying macro eNB. The cell capacity may be dramatically increased due to spatially split gain of RRHs. In such cases, if one common PDCCH region is shared among the macro eNB and all RRHs, the time-division-multiplexed PDCCH suffers from limited capacity when confined to three OFDM symbols. Moreover, since the legacy interleaved PDCCH spans across the entire system bandwidth, frequency-domain inter-cell interference coordination schemes for control channels transmitted by different RRHs cannot be utilized by PDCCH.

A Rel-11 work item initiated the design of a new downlink control channel structure referred to as ePDCCH which relies on DM-RSs for coherent detection and is frequency-division-multiplexed with data region. The use of DM-RSs would allow precoding and beamforming of the downlink physical control channels in the future. Figure 9.59 illustrates the structure of ePDCCH in a subframe and how it can coexist with the legacy PDCCH without affecting the interoperability with the legacy LTE systems [178]. As shown in the figure, the ePDCCH regions are time-division-multiplexed with the legacy PDCCH region, are frequency-division-multiplexed with PDSCH, and avoid other essential physical channels and signals. Since ePDCCH only relies on UE-specific reference signals for demodulation, the use of ePDCCH in MBSFN subframes would eliminate the reliance on CRS for control channel demodulation in the future releases of LTE.

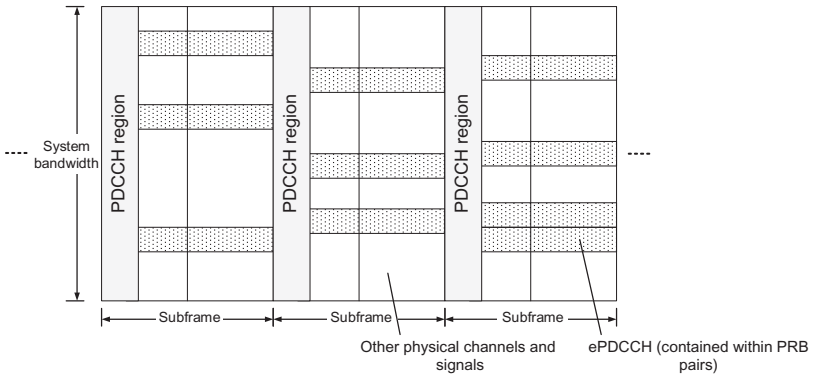


FIGURE 9.59

Enhanced PDCCH structure [149–155].

Petitioners' Exhibit 1021
Nokia of America Corp., et al. v. KT Corporation, et al.
Case No. IPR2025-00036; U.S. Patent No. 11,627,631
Page 521 of 1122

Each ePDCCH may contain multiple enhanced control channel elements (eCCEs), and multiple eCCEs can be aggregated to achieve different coding rates which depend on the channel conditions of the UE to guarantee a block error rate (BLER) of less than 1%. The existing structure of the PDCCH relies on CRS for channel estimation and coherent detection. It is shown that CRS has more overhead and is less effective when using closed-loop precoding techniques, beamforming, and MU-MIMO. The beamforming of the control channels can significantly improve the performance of the cell-edge users. The use of DM-RS or UE-specific reference signals instead of CRS would facilitate the use of beamforming for the control channels. Figure 9.60 illustrates a hypothetical beam-formed ePDCCH and depicts the localized and distributed ePDCCH mapping to the resource elements and antenna ports [149–155].

The ePDCCH DM-RSs are transmitted on antenna ports $p \in \{107, 108, 109, 110\}$ and are used as a reference for ePDCCH coherent demodulation. An ePDCCH DM-RS is not transmitted over resource element (k, l), where k denotes the frequency index and l denotes the OFDM symbol index within a slot, when one of the physical channels or physical signals are transmitted using the same resource element regardless of their antenna port. For the antenna port $p \in \{107, 108, 109, 110\}$, the reference-signal sequence $r(m)$ is defined by the equation $r(m) = (1/\sqrt{2})(1 - 2c(2m)) + j(1/\sqrt{2})(1 - 2c(2m + 1))$, where $m = 0, 1, \ldots,$

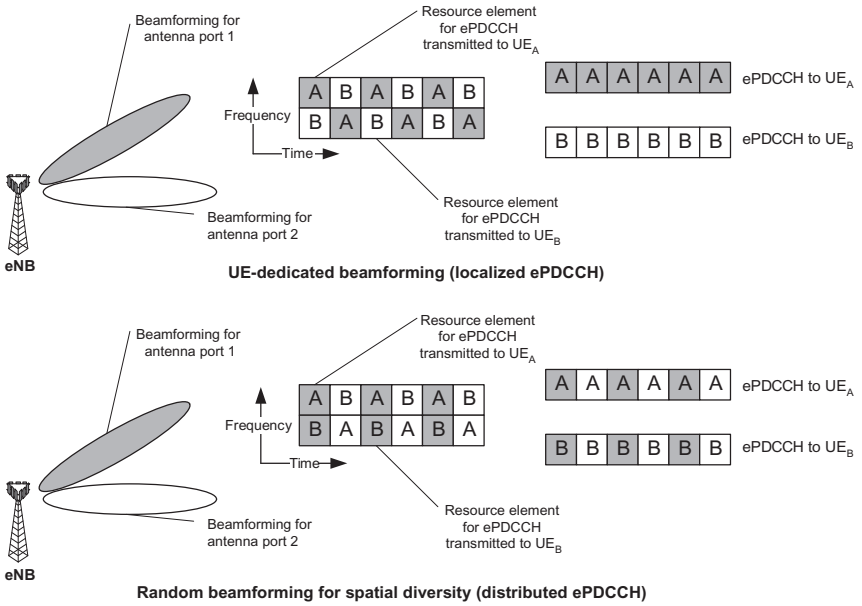


FIGURE 9.60

Possible use of beamforming for transmission of ePDCCH [149–155].

Petitioners' Exhibit 1021
Nokia of America Corp., et al. v. KT Corporation, et al.
Case No. IPR2025-00036; U.S. Patent No. 11,627,631
Page 522 of 1122

$12\max(N_{RB}^{DL}) - 1$ for a normal cyclic prefix, and $m = 0, 1, \ldots, 16\max(N_{RB}^{DL}) - 1$ for an extended cyclic prefix. The pseudo-random sequence $c(i)$ was defined in the previous sections and is initialized with the initial value $c_{init} = \left(\lfloor n_s/2 \rfloor + 1\right)\left(2N_{ID}^{ePDCCH(i)} + 1\right)2^{16} + N_{SCID}^{ePDCCH}$ at the start of each subframe where $N_{SCID}^{ePDCCH} = 2$ and $N_{ID}^{ePDCCH(i)}|_{i=0,1}$ is configured by higher layers, and index i denotes the set of ePDCCH associated with the DM-RS. For the antenna port $p \in \{107, 108, 109, 110\}$ in a PRB n_{PRB} assigned to the associated ePDCCH, the reference signal sequence $r(m)$ is mapped to complex-valued modulation symbols a_{kl}^{p} in a subframe according to the following mapping rule $a_{kl}^{p} = w_p(l')r(3l'\max(N_{RB}^{DL}) + 3n_{PRB} + m')$ for a normal cyclic prefix, where $w_p(i) = \overline{w}_p(i)$, if $(m' + n_{PRB}) \bmod 2 = 0$, and $w_p(i) = \overline{w}_p(3 - i)$ if $(m' + n_{PRB}) \bmod 2 = 1$ and the frequency index is given by $k = 5m' + 12n_{PRB} + k'$. The length-4 orthogonal cover sequence $\overline{w}_p(i)$ is defined in Table 9.14.

For an extended cyclic prefix, ePDCCH DM-RSs are not supported on antenna ports $p = 109$ and $p = 110$. The resource elements (k, l) used for transmission of ePDCCH DM-RSs to a single UE on any antenna ports in the set $S = \{107, 108\}$ or $S = \{109, 110\}$ is not used for transmission of ePDCCH on any other antenna port in the same slot, and further it is not used for DM-RSs to the same UE on any antenna port other than those in set S in the same slot. The mapping of the ePDCCH DM-RSs to resource elements within a UE-allocated resource block is identical to that corresponding to UE-specific reference signals on antenna port numbers 7−10 when replacing the antenna port numbers with 107−110 in Figure 9.57 for a normal cyclic prefix [3].

9.10.7 Positioning reference signals

Positioning is defined as the process of determining the location and/or velocity of a device using radio signals. The positioning reference signals (PRS) were introduced in LTE Rel-9 on antenna port 6, after the cell-specific reference signals were not found suitable for positioning due to the fact that the required probability of detection could not be guaranteed. A neighbor cell with its synchronization signals (primary/secondary synchronization signals) and reference

Table 9.14 The Sequence $\overline{w}_p(i)$ for Normal Cyclic Prefix [3]

Antenna Port p	$[\overline{w}_p(0)$	$\overline{w}_p(1)$	$\overline{w}_p(2)$	$\overline{w}_p(3)]$
107	[+1	+1	+1	+1]
108	[+1	−1	+1	−1]
109	[+1	+1	+1	+1]
110	[+1	−1	+1	−1]

Petitioners' Exhibit 1021
Nokia of America Corp., et al. v. KT Corporation, et al.
Case No. IPR2025-00036; U.S. Patent No. 11,627,631
Page 523 of 1122

signals is seen as detectable, when the SINR is at least −6 dB [121,179]. Simulations during development of Rel-9 have shown that this can be only guaranteed for 70% of all cases for the third best-detected cell, which means the second best neighboring cell by assuming an interference-free environment, which cannot be ensured in a realistic scenario. The PRS design has some similarities with cell-specific reference signals as defined in LTE Rel-8. The PRS is a pseudo-random QPSK sequence that is mapped to resource elements in diagonal patterns with shifts in frequency and time to avoid collision with CRSs, and to avoid overlapping with the control channels.

The PRS is defined by its bandwidth $N_{\mathrm{RB}}^{\mathrm{PRS}}$ in terms of number of resource blocks used for PRS, time offset ($T_{\text{offset-PRS}}$), duration $N_{\text{subframe}}^{\mathrm{PRS}}$ in terms of number of consecutive subframes, and its periodicity T_{PRS}. It must be noted that the PRS bandwidth is always smaller than the actual system bandwidth ($N_{\mathrm{RB}}^{\mathrm{PRS}} < \max(N_{\mathrm{RB}}^{\mathrm{DL}})$). The PRS is always mapped around the carrier center frequency and the unused DC sub-carrier in the downlink. In a subframe where PRS is configured, typically no PDSCH is transmitted. The positioning reference symbols of a certain cell can be configured to correspond to empty resource elements of the neighboring cells, thus enabling detection of the PRSs with satisfactory SIR values when receiving neighbor-cell PRSs [121].

Positioning reference signals are only transmitted in resource blocks over downlink subframes that are configured for PRS transmission. If both normal and MBSFN subframes are configured as positioning subframes within a cell, the OFDM symbols in the MBSFN subframe use the same cyclic prefix type as the first subframe in the frame. However, if MBSFN subframes are only configured to contain PRSs in a cell, the OFDM symbols configured for PRSs in the MBSFN region of these subframes use an extended cyclic prefix type. In a subframe configured for PRS transmission, the starting positions of the OFDM symbols configured for PRS transmission is identical to those in a subframe in which all OFDM symbols have the same cyclic prefix length as the OFDM symbols configured for PRS transmission. Positioning reference signals are transmitted on antenna port 6, and are not mapped to resource elements (k, l) allocated to BCH and primary and secondary synchronization channels regardless of their associated antenna ports. PRSs are only defined for sub-carrier spacing of 15 kHz.

The reference-signal sequence $r_l^{n_s}(m)$ is defined by $r_l^{n_s}(m) = (1/\sqrt{2})[1 - 2c(2m)] + j(1/\sqrt{2})[1 - 2c(2m+1)]$, $\forall m = 0, 1, \ldots, 2\max(N_{\mathrm{RB}}^{\mathrm{DL}}) - 1$, where $n_s = 0, 1, \ldots, 19$ is the slot number within a radio frame, $l = 0, 1, \ldots, 6$ is the OFDM symbol number within the slot. The pseudo-random sequence $c(i)$ is defined similar to the previous sections. The pseudo-random sequence generator in this case is initialized by $c_{\text{init}} = 2^{10}[7(n_s + 1) + l + 1](2N_{\mathrm{ID}}^{\mathrm{cell}} + 1) + 2N_{\mathrm{ID}}^{\mathrm{cell}} + N_{\mathrm{CP}}$ at the start of each OFDM symbol where $N_{\mathrm{CP}} = 1$ for a normal cyclic prefix and $N_{\mathrm{CP}} = 0$ for an extended cyclic prefix. The reference signal sequence $r_l^{n_s}(m)$ is mapped to complex-valued modulation symbols a_{kl}^p designated to the PRS on antenna port $p = 6$ such that $a_{kl}^p = r_l^{n_s}(m')$ where in the case of a normal cyclic prefix

Table 9.15 Positioning Reference Signal Subframe Configuration Parameters [3]

PRS Configuration Index I_{PRS}	PRS Periodicity T_{PRS}(Subframes)	PRS Subframe Offset $T_{offset-PRS}$(Subframes)
0–159	160	I_{PRS}
160–479	320	$I_{PRS} - 160$
480–1119	640	$I_{PRS} - 480$
1120–2399	1280	$I_{PRS} - 1120$
2400–4095		Reserved

$m' = m + \max(N_{RB}^{DL}) - N_{RB}^{PRS}$. The bandwidth for PRSs and N_{RB}^{PRS} is configured by higher layers and the cell-specific frequency shift is given by $\nu_{shift} = N_{ID}^{cell} \bmod 6$.

The cell-specific subframe configuration period T_{PRS} and the cell-specific subframe offset $T_{offset-PRS}$ for transmission of PRSs are given in Table 9.15 (see Figure 9.61). The PRS configuration index I_{PRS} is configured by higher layers. Positioning reference signals are transmitted only in configured downlink subframes and, in the case of TDD duplex scheme, are not transmitted in special subframes. The PRS is transmitted in N_{PRS} consecutive subframes that are configured by higher layers. The PRS location in time is given by $(10n_{subframe} + \lfloor n_s/2 \rfloor - T_{offset-PRS}) \bmod T_{PRS} = 0$. A UE may assume that downlink PRS EPRE is constant across the PRS bandwidth and across all OFDM symbols that contain positioning reference signals in a given PRS occurrence. The structure of the positioning reference signals in the time- and frequency-domain is illustrated in Figure 9.61.

9.10.8 MBSFN reference signals

Support of MBMS in LTE has certain impacts on the physical layer design. It starts with the use of the cyclic prefix, since it is essential for the OFDM system that multipath versions of the signal arrive at the receiver within the cyclic prefix to avoid ISI. As we have multiple, but synchronized transmission from different broadcast/multicast sources, the expected delay spread is much larger than that for unicast operation. Therefore, in order to support multicast and broadcast services, MBSFN uses an extended cyclic prefix while the majority of today's LTE networks are based on a normal cyclic prefix. In the case of the mixed (or time-division-multiplexed) MBSFN and unicast operation, the subframes that are supposed to carry MBMS content are divided into a non-MBSFN and an MBSFN region. The non-MBSFN region can occupy one or two OFDM symbols at the beginning of the subframe. In this region, PCFICH, PDCCH, and PHICH will be mapped to ensure interoperability with user terminals that do not support MBSFN. For proper operation of the network, it is required to schedule terminals to receive or transmit data, page them, or provide feedback on their recent uplink transmission. In this region, CRSs and a normal cyclic prefix will be used. The MBSFN-region will carry PMCH. The extended cyclic prefix and sub-carrier spacing of

Petitioners' Exhibit 1021
Nokia of America Corp., et al. v. KT Corporation, et al.
Case No. IPR2025-00036; U.S. Patent No. 11,627,631
Page 525 of 1122

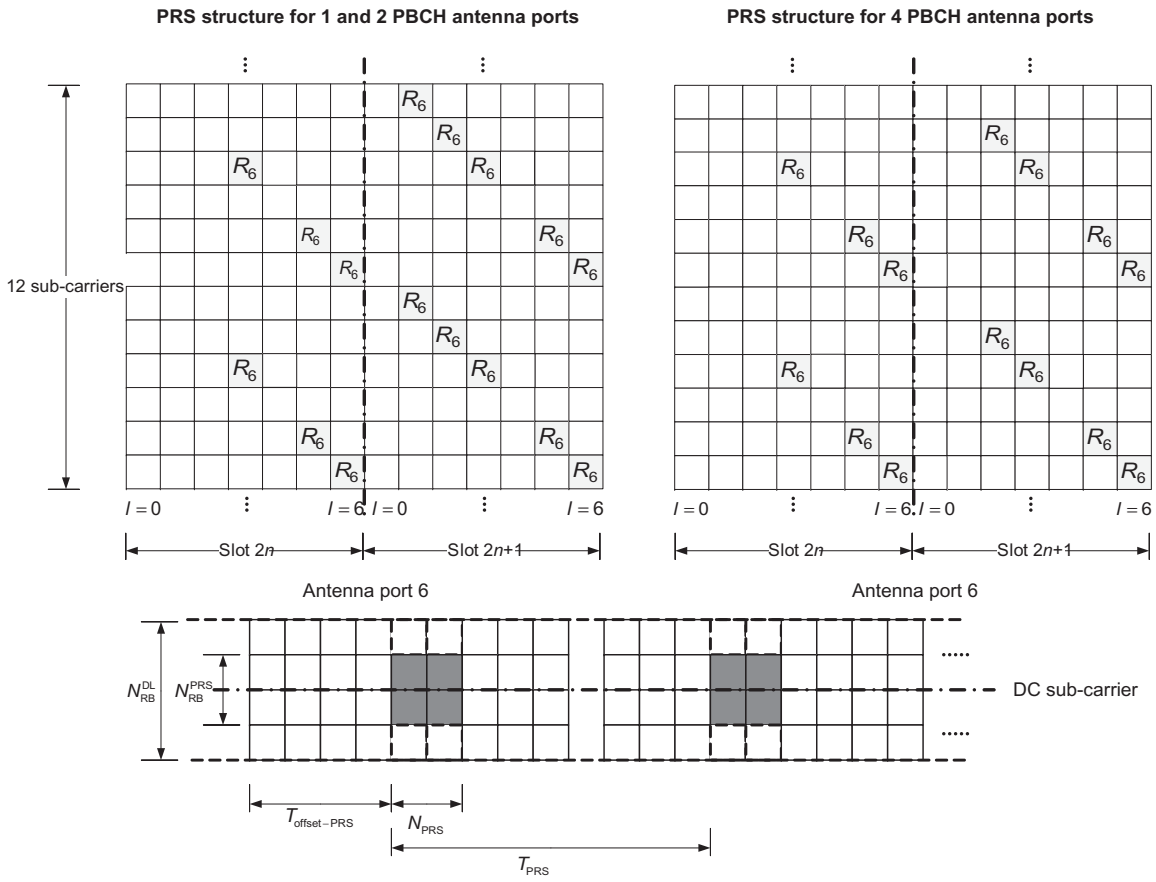


FIGURE 9.61

Structure of PRS in time- and frequency-domain [3,179].

15 kHz (or 7.5 kHz) are used in this region in order to contain the time difference of the cells that belong to an MBSFN area, while transmitting the same content to the terminals. In order to enable coherent demodulation at the terminal, as well as proper channel estimation, the use of CRSs is not sufficient. Thus new reference signals for MBMS transmission have been designed as part of Rel-9. Each cell belonging to the MBSFN area will transmit the same MBSFN reference signal pattern at the exact same time−frequency position. The MBSFN reference signals have a tighter spacing in the frequency-domain due to the frequency-selective nature of the radio channel. In contrast to the CRSs, the initialization sequence for the MBSFN reference signal does not depend on the physical cell identity, rather on the MBSFN identity provided by system information block type 13 [179].

The MBSFN reference signals are transmitted on antenna port 4 in the MBSFN region of MBSFN subframes, only if PMCH is transmitted. These reference signals are only defined for an extended cyclic prefix. The MBSFN reference-signal sequence $r_l^{n_s}(m)$ is obtained as $r_l^{n_s}(m) = (1/\sqrt{2})[1 - 2c(2m)] + j(1/\sqrt{2})\ [1 - 2c(2m+1)],\ \forall m = 0, 1, \ldots, 6\max(N_{\mathrm{RB}}^{\mathrm{DL}}) - 1$, where $n_s = 0, 1, \ldots, 19$ is the slot number within a radio frame, $l = 0, 1, \ldots, 5$ is the OFDM symbol number within the slot, and $c(i)$ is the pseudo-random sequence defined similar to the previous sections, which is initialized by $c_{\mathrm{init}} = 2^9[7(n_s + 1) + l + 1](2N_{\mathrm{ID}}^{\mathrm{MBSFN}} + 1) + N_{\mathrm{ID}}^{\mathrm{MBSFN}}$ at the start of each OFDM symbol. The reference-signal sequence $r_l^{n_s}(m')$ in OFDM symbol l is mapped to complex-valued modulation symbols a_{kl}^p on antenna port $p = 4$ according to $a_{kl}^p = r_l^{n_s}(m')$, where $m' = m + 3(\max(N_{\mathrm{RB}}^{\mathrm{DL}}) - N_{\mathrm{RB}}^{\mathrm{DL}})$. Figure 9.62 illustrates the resource elements used for MBSFN reference signal transmission.

9.10.9 Reference signal overhead calculation

The reference signals regardless of their types add to the overhead and reduce the number of available resource elements in a subframe for user data allocation. The amount of overhead typically increases when multiple transmit antennas and/or an extended cyclic prefix is used. Among various types of reference signals used in LTE/LTE-Advanced, the cell-specific reference signals correspond to the highest amount of overhead, as they are always on and span the entire system bandwidth. The overhead concerning other types of reference signals varies depending on the number of antenna ports, periodicity of the configured reference signals, number of UE-allocated resource blocks, etc. The overhead is calculated as the number of resource elements in each resource block pair that is designated to the reference signals relative to the total number of resource elements in each resource block pair. The total number of resource elements is also a function of the cyclic prefix type. Table 9.16 provides the overhead figures associated with each reference signal type for FDD systems. The overhead of the reference signals in TDD systems is also a function of the downlink/uplink subframe configuration and the number of OFDM symbols in the DwPTS portion of the special subframes [13].

Petitioners' Exhibit 1021
Nokia of America Corp., et al. v. KT Corporation, et al.
Case No. IPR2025-00036; U.S. Patent No. 11,627,631
Page 527 of 1122

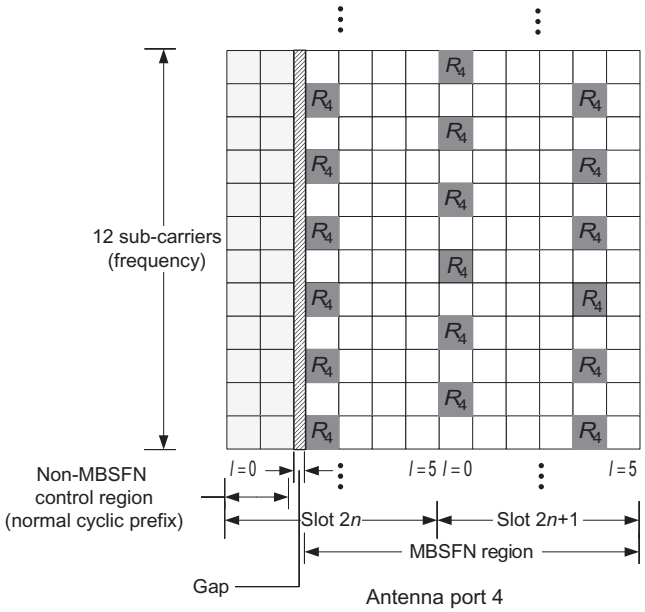


FIGURE 9.62

MBSFN reference signal structure [3,13].

9.11 Channel coding and modulation

Forward error correction (FEC) channel coding schemes are commonly used to improve the efficiency and robustness of wireless digital communication systems. On the transmitter side, an FEC encoder adds redundancy to the input data in the form of parity bits, while at the receiver, the redundancy is utilized by the FEC decoder to correct a number of channel errors. The use of FEC schemes would allow tolerance of more channel errors than otherwise can be tolerated without FEC. The use of FEC schemes enables the wireless communication systems to operate with a lower transmit power, to transmit over longer distances, to tolerate more interference, and to transmit at a higher data rate. A binary FEC encoder receives k bits at a time and produces a codeword of n bits, where $n > k$. While there are 2^n possible sequences of n bits, only 2^k codewords are used. The ratio k/n is the code rate and is denoted by R. Lower code rates corresponding to small values of R can generally correct more channel errors than higher code rates, and therefore are more robust. However, higher code rates are more bandwidth efficient because of lower overhead due to parity or redundancy bits. Thus, the selection of the code rate is a trade-off between energy efficiency and bandwidth efficiency. For every combination of code rate R, code word length n, baseband modulation scheme, channel type, and receiver noise power, there is a theoretical

Table 9.16 Reference Signal Overhead in FDD Mode [13]

Release	Type of Reference Signal	Number of Antenna Ports	Antenna Ports	Number of Reference Signals per Resource Block Pair	Overhead (%) Normal Cyclic Prefix	Overhead (%) Extended Cyclic Prefix
8	Cell-specific reference signals	1	0	8	4.8	5.6
		2	0,1	16	9.5	11.1
		4	0,1,2,3	24	14.3	16.7
	UE-specific (demodulation) reference signals	1	5	12	7.1	8.3
	MBSFN reference signals	1	4	18	–	12.5
9	Positioning reference signals	1	6	16 (14)	9.5	9.7
	UE-specific (demodulation) Reference Signals	2	7,8	12	7.1	8.3
10	UE-specific (demodulation) reference signals	1	7	12	7.1	8.3
		2	7,8	12	7.1	8.3
		4	7–10	24	14.3	16.6
		8	7–14	24	14.3	16.6
	CSI reference signals	1	15	2	$1.19/T_{\text{CSI-RS}}$	$1.39/T_{\text{CSI-RS}}$
		2	15,16	2	$1.19/T_{\text{CSI-RS}}$	$1.39/T_{\text{CSI-RS}}$
		4	15–18	4	$2.38/T_{\text{CSI-RS}}$	$2.78/T_{\text{CSI-RS}}$
		8	15–22	4	$2.38/T_{\text{CSI-RS}}$	$2.78/T_{\text{CSI-RS}}$
11	ePDCCH demodulation reference signals	4	107–110	12(24)	7.1–14.3	8.3–16.6

Petitioners' Exhibit 1021
Nokia of America Corp., et al. v. KT Corporation, et al.
Case No. IPR2025-00036; U.S. Patent No. 11,627,631
Page 529 of 1122

lower limit on the amount of energy that must be used to convey one bit of information. This limit is called the channel capacity of the communication channel [33]. Since the dawn of information theory, engineers and mathematicians have tried to construct codes that achieve performance close to Shannon capacity [27,33,39]. The introduction of convolutional turbo codes (CTCs) in 1993 followed by the invention of block turbo codes (BTCs) in 1994 closed much of the performance gap with the maximum channel capacity. Turbo codes are essentially parallel concatenated convolutional codes (PCCCs) with an internal interleaving mechanism combined with an iterative soft-decision decoding algorithm. In this section, we first review the principles of convolutional and turbo coding, and then we describe the channel coding and modulation schemes that are used in LTE/LTE-Advanced systems.

Before we proceed to the next sections, we need to clarify that detection, decision-making, hypothesis testing, and decoding are synonymous. The word detection refers to the effort to decide whether some phenomenon is present or not on the basis of some observations. For example, a radar system uses the data to detect whether a target is present. The meaning has been extended in the communication field to detect which one, among a set of mutually exclusive alternatives, is correct. Decision-making is the process of deciding between a number of mutually exclusive alternatives. Hypothesis testing is the same, and here the mutually exclusive alternatives are called hypotheses. Decoding is the process of mapping the received signal into one of the possible sets of codewords or transmitted symbols. We use the word hypotheses for the possible choices in what follows, since the word conjures up the appropriate intuitive image [100–108].

9.11.1 Principles of convolutional coding

Convolutional codes have been extensively used in telecommunication systems such as digital video, radio, mobile, and satellite communication in order to achieve reliable data communication [27]. Prior to the invention of the turbo codes, convolutional code was the most efficient coding scheme that provided the closest performance to the Shannon limit. A generic convolutional encoder (k, n, K) is characterized by a shift register with K stages, k input bits, and n output bits. The rate of the convolutional code is defined as $R = k/n$. A convolutional encoder is a discrete linear time-invariant system and can be viewed as a finite-state machine with 2^{K-1} states. Therefore, convolutional codes are linear codes which do not divide the source stream into blocks, but instead read and transmit bits continuously. The transmitted bits are a linear function of the past source bits. Usually the rule for generating the transmitted bits involves feeding the present source bit into a linear-feedback shift-register of length K, and transmitting one or more linear functions of the state of the shift register in each iteration. The resulting transmitted bit stream is the convolution of the source stream with a linear filter (Figure 9.63). The impulse–response function of this filter may have finite or infinite duration depending on the choice of feedback shift-register,

Petitioners' Exhibit 1021
Nokia of America Corp., et al. v. KT Corporation, et al.
Case No. IPR2025-00036; U.S. Patent No. 11,627,631
Page 530 of 1122

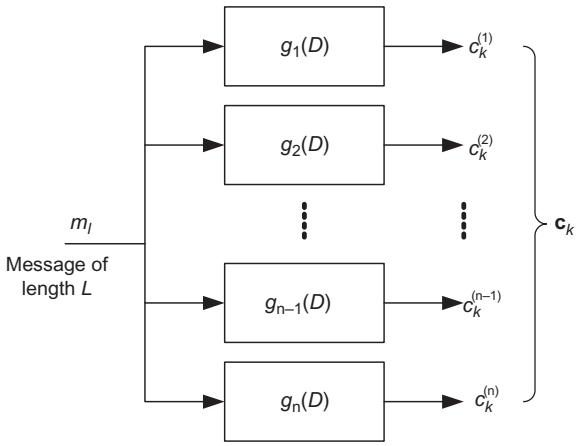


FIGURE 9.63

General form of (1/n) convolutional coder [27,40].

i.e., recursive or non-recursive convolutional codes. As an example, consider the LTE convolutional coder with $k = 1, n = 3, K = 6$, and $R = 1/3$. The linear combinations are defined via $n = 3$ generator sequences where $\mathbf{G} = \{\mathbf{g}_0, \mathbf{g}_1, \ldots, \mathbf{g}_{n-1}\}$ and $\mathbf{g}_i = \{g_{i0}, g_{i1}, \ldots, g_{i(K-1)}\}$. The generator sequences used in Rel-8 of LTE are given by $\mathbf{g}_0 = \{1\ 0\ 1\ 1\ 0\ 1\ 1\}$, $\mathbf{g}_1 = \{1\ 1\ 1\ 1\ 0\ 0\ 1\}$, and $\mathbf{g}_2 = \{1\ 1\ 1\ 0\ 1\ 0\ 1\}$ as shown in Figure 9.63. Puncturing is used to make an arbitrary k/n rate code from a basic rate 1/2 or 1/3 code by deleting some bits in the encoder output. For example, if we want to make a code with rate 2/3, we should take the basic 1/2-encoder output and transmit every second bit from the first branch and every bit from the second branch.

Traditional channel coding techniques achieve coding gain at the expense of bandwidth expansion, where coding gain is defined as the reduction in required E_b/N_0 for a given error probability. In the case of band-limited channels, bandwidth expansion is usually not possible. Trellis-coded modulation schemes use redundant non-binary modulation in conjunction with a finite state encoder. For each symbol interval, the encoder selects one of a set of M-ary waveforms, thereby generating a sequence of coded waveforms. The noisy signals at the receiver are detected and decoded by a soft-decision maximum-likelihood (ML) detector/decoder. Coding gain can be achieved without sacrificing data rate or expanding bandwidth, but at the expense of increasing decoder complexity.

A convolutional encoder, which is an example of trellis coding, is a finite-state machine, i.e., the output is a function of both the current input and the state of the encoder. A convenient way of characterizing such a state-oriented process is through a trellis diagram. Figure 9.64 illustrates a trellis diagram for a

Petitioners' Exhibit 1021
Nokia of America Corp., et al. v. KT Corporation, et al.
Case No. IPR2025-00036; U.S. Patent No. 11,627,631
Page 531 of 1122

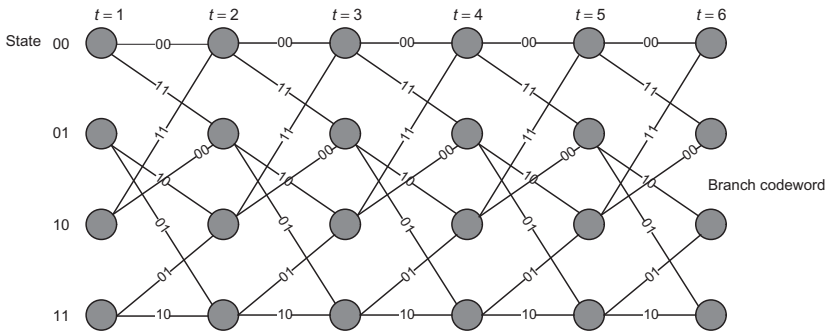


FIGURE 9.64

Four-state Trellis diagram [27,40].

hypothetical four-state convolutional encoder. The number of stages in the encoder shift register is referred to as its constraint length K, and the contents of the rightmost $K-1$ stages define the state of the encoder. Each node of the trellis represents a distinct state at a given time. A branch between any two states represents the transition between those states, and is labeled with the output code sequence associated with that transition. The most important property of the trellis diagram is that every possible sequence of message bits into the encoder corresponds to a unique path through the trellis and a unique sequence of coded bits, and vice versa. The task of the decoder is to estimate the path that the encoded message traverses through the trellis. If all input message sequences are equally likely, a decoder that will achieve the minimum probability of error is one that compares the conditional probabilities $p(\mathbf{z}_j|\mathbf{u}_m)$, where $\mathbf{z}_j$ is the received sequence and $\mathbf{u}_m$ is one of the possible transmitted sequences, and chooses the sequence corresponding to the ML. The decoder chooses $\mathbf{u}_{m'}$ if $p(\mathbf{z}_j|\mathbf{u}_{m'}) = \max_{\forall \mathbf{u}_m} p(\mathbf{z}_j|\mathbf{u}_m)$. Finding the sequence which maximizes $p(\mathbf{z}_j|\mathbf{u}_m)$ is equivalent to finding the sequence $\mathbf{u}_{m'}$ that has the greatest similarity to $\mathbf{z}_j$. Over a hard-decision channel, the similarity is often estimated by the Hamming distance between received and candidate sequences, and over a soft-decision channel it is estimated by the Euclidean distance. Since an ML decoder will choose the trellis path whose corresponding sequence $\mathbf{u}_{m'}$ is at the minimum distance to the received sequence $\mathbf{z}_j$, the ML problem is identical to the problem of finding the shortest distance through the trellis diagram [19]. A comparison of the performance of a rate 1/2 convolutional code with hard- and soft-decision decoding ($K = 7$ and BPSK modulation) over an AWGN channel is shown in Figure 9.66. The advantage of a soft-decision decoding over a hard-decision decoding convolutional coder (approximately $+2$ dB coding gain) can be seen in this example. The performance of the same encoder with hard-decision decoding under Rayleigh multipath fading and AWGN channels for different number paths has been calculated and compared in Figure 9.66.

Petitioners' Exhibit 1021
Nokia of America Corp., et al. v. KT Corporation, et al.
Case No. IPR2025-00036; U.S. Patent No. 11,627,631
Page 532 of 1122

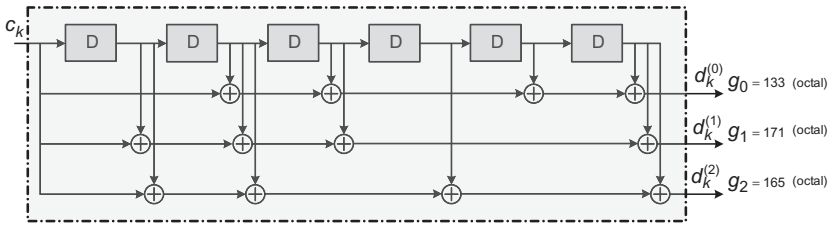


FIGURE 9.65

LTE rate 1/3 tail-biting convolutional encoder [4].

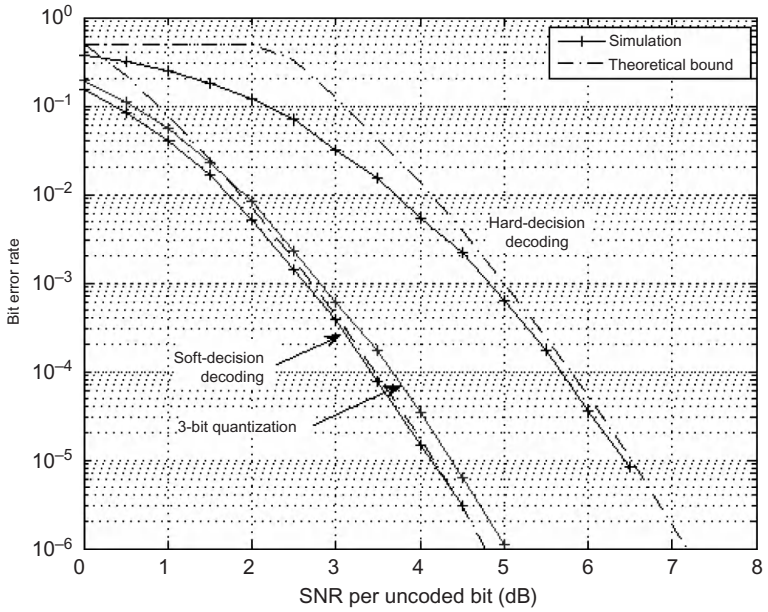


FIGURE 9.66

Performance of rate 1/2 convolutional code ($K = 7$ and BPSK modulation) over AWGN channel [141].

In order to terminate a convolutional code, some bits are appended to the information sequence such that the shift-register's content returns to the initial state. Each of the k input sequences of length L bits is padded with K zeros, and these kL input sequences jointly generate $n(K + L)$ output bits. The effective rate of the terminated convolutional code is now $R_{\text{effective}} = kL/n(K + L) < k/n$, which is less than the nominal rate due to the addition of redundancy. Thus, terminating the trellis of a convolutional code is essential in the code's performance for packet-based communications.

Petitioners' Exhibit 1021
Nokia of America Corp., et al. v. KT Corporation, et al.
Case No. IPR2025-00036; U.S. Patent No. 11,627,631
Page 533 of 1122

Tail-biting convolutional coding is a technique of trellis termination which avoids the rate loss incurred by zero-tail termination at the expense of a more complex decoder. Tail-biting encoding ensures that the starting state of the encoder is the same as its ending state, and that this state value does not necessarily have to be the all-zero state. For a rate $1/n$ feed-forward encoder, this is achieved by initializing the K memory elements of the encoder with the last K information bits of a block of data of length L and ignoring the output. All of the L bits are then input to the encoder and the resulting nL output bits are used as the codeword. In comparison, the zero-tail termination method appends K zeros to a block of data to ensure the feed-forward encoder starts from and ends in the all-zero state for each block. This incurs a rate loss due to the extra tail bits (i.e., non-informational bits) that are transmitted.

The ML tail-biting decoding involves determining the best path in the trellis under the constraint that it starts and ends in the same state. One way to implement this method is to run M parallel Viterbi algorithms, where M is the number of states in the trellis, and select the decoded bits based on the Viterbi algorithm that gives the best metric. However, this makes the decoding M times more complex relative to the zero-tailed encoding.

The structure of the LTE rate 1/3 tail-biting convolutional encoder with constraint length 7 shown in Figure 9.67. The bit sequence input for a given code block to channel coding is denoted by $(c_0, c_1, \ldots, c_{K-1})$, where K is the number of bits to be encoded. The initial value of the shift register (the initial state) of the encoder is set to the values corresponding to the last 6 information bits in the input stream, so that the initial and final states of the shift register are the same. Therefore, if the content of the shift register is denoted by $(s_0, s_1, s_2, s_3, s_4, s_5)$, then the initial value of the shift register is set to $s_i = c_{(K-1-i)}$. The encoder output streams $d_k^{(0)}$, $d_k^{(1)}$, and $d_k^{(2)}$ correspond to the first, second, and third parity streams [4].

The performance of an example rate 1/2 tail-biting convolution coder in an AWGN channel with different modulation orders, coding rates, and data frame sizes using a Viterbi decoder has been evaluated and shown in Figure 9.68 where the wrap depth is a predetermined number of trellis stages used as a parameter in the figure. One way to estimate the required wrap depth for MAP decoding[16] of a

[16]There are a number of possible criteria to use in making decisions, and initially, we assume that the criterion is to maximize the probability of choosing correctly. That is, when the experiment is performed, the resulting sample point maps into a sample value h for H and a sample value y for Y. The decision-maker observes y (but not h) and maps y into a decision $\hat{H}(y)$. The decision is correct if $\hat{H}(y) = h$. In principal, maximizing the probability of choosing correctly is almost trivially simple. Given y, we calculate $p_{H|Y}(h|y)$ for each $h, 0 \le h \le M-1$. This is the probability that h is the correct hypothesis conditional on y. Thus the rule for maximizing the probability of being correct is to choose $\hat{H}(y)$ to be that h for which $p_{H|Y}(h|y)$ is maximized. This is denoted as $\hat{H}(y) = \arg\max_h[p_{H|Y}(h|y)]$. If the maximum is not unique, it makes no difference to the probability of being correct which maximizing h is chosen. To be explicit, we will choose the smallest maximizing h. The conditional probability $p_{H|Y}(h|y)$ is called an *a posteriori* probability, and thus the above decision rule is called the maximum a posteriori probability (MAP) rule [45].

Petitioners' Exhibit 1021
Nokia of America Corp., et al. v. KT Corporation, et al.
Case No. IPR2025-00036; U.S. Patent No. 11,627,631
Page 534 of 1122

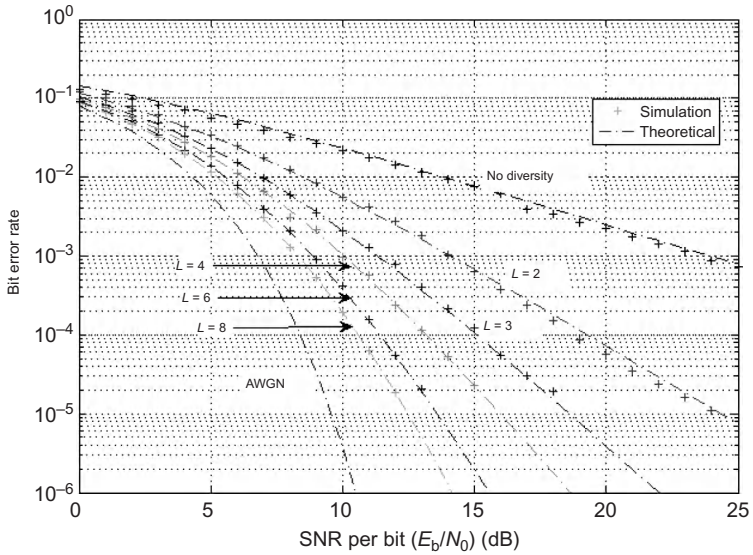


FIGURE 9.67

Performance of rate 1/2 convolutional code (K = 7 and BPSK modulation) in multi-path Rayleigh fading channel [141].

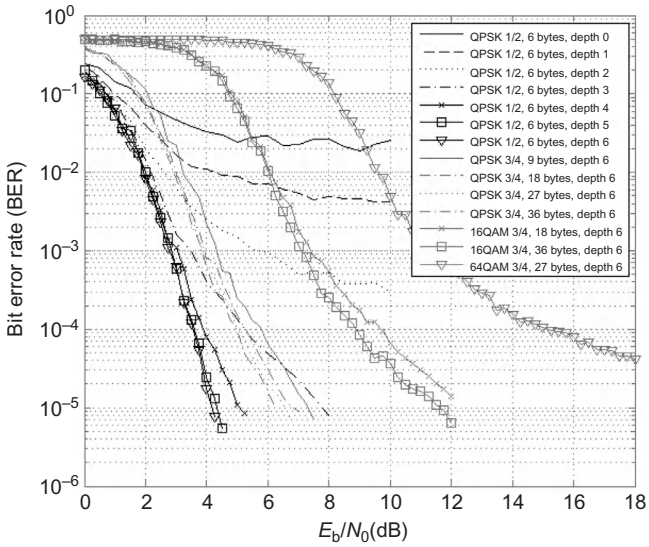


FIGURE 9.68

Performance of an example rate 1/2 tail-biting convolutional coder in an AWGN channel [144].

Petitioners' Exhibit 1021
Nokia of America Corp., et al. v. KT Corporation, et al.
Case No. IPR2025-00036; U.S. Patent No. 11,627,631
Page 535 of 1122

tail-biting convolutional code is to conduct hardware or software experiments, requiring a circular MAP decoder with a variable wrap depth to be implemented in order to measure the decoded bit error rate versus E_b/N_0 for successively increasing wrap depths. The minimum decoder wrap depth that provides the minimum probability of decoded bit error for a specified E_b/N_0 is found when further increases in wrap depth do not decrease the error probability, as shown in Figure 9.68. It can be seen that the link-level BER performance improves when increasing the depth and the performance does not significantly change after a certain limit. The effect of different data frame sizes (6, 9, 18, 27, and 36 bytes) on the BER performance has been investigated and is shown in the figure.

9.11.2 Principles of turbo coding

In information theory, one can ideally approach the Shannon limit as closely as desired using soft-decision decoding of a long block code, or a convolutional code with a large constraint length. In practice, however, decoding of these codes becomes very computationally intensive. Similar to any conventional error correcting codes, the turbo codes work by imposing a structure on the transmitted bit sequence. If the received bit sequence does not match this known structure, the receiver declares an error has occurred. If the number of errors is sufficiently small and the structure is robust, the receiver can detect the erroneous bits and reconstruct the correct bit sequence. A strong error correcting code has two key characteristics: (1) the encoder imposes a structure that maximizes the difference (or the distance) between any two valid bit sequences; and (2) the decoder utilizes all the information available at the receiver's end including the redundancy and previously unsuccessful transmissions. Thus, the decoder can determine which valid bit sequence is most likely the one that has been transmitted. The first significant difference between a turbo code and conventional code is the use of a recursive systematic encoder. A typical convolutional coder uses a non-recursive structure. By feeding one of the outputs back to the input, a recursive encoding structure is obtained. The recursive structure is systematic, i.e., the input bits appear directly as part of the encoded bit stream. Therefore, a systematic structure enables the combination of two codes in order to construct a stronger composite code. The input bit stream only needs to be transmitted once. The computed parity bits from each of the two constituent encoders are transmitted separately. The recursive structure interacts with the interleaver to give the composite code some unique performance characteristics. The optimum decoder for any code is an ML decoder. In the ML decoding, the receiver produces a probability that each received bit is either 0 or 1. The ML decoder then uses these received bit probabilities, along with its knowledge of the structure imposed by the encoder, to compute the probability of every possible transmitted bit sequence. The most probable transmitted bit sequence is then chosen as the decoded bit sequence. The ML decoding is theoretically optimal

Petitioners' Exhibit 1021
Nokia of America Corp., et al. v. KT Corporation, et al.
Case No. IPR2025-00036; U.S. Patent No. 11,627,631
Page 536 of 1122

and can achieve the lowest probability of decoder failure or probability of error. However, there is no efficient way to practically compute these probabilities when the block size is large. This leads to the use of suboptimal, but realizable, decoding methods.

The second unique feature of turbo codes is their decoder, which is based on iterative application of ML decoding. The ML decoding of a convolutional code would be easy, if the constraint length (register size) is short; however, short codes are relatively weak. Combining two such codes produces a much stronger code, but now ML decoding becomes intractable. Each shorter code can be ML decoded if we assume the other code has already been decoded. This leads to an iterative decoding strategy, which is to decode the first code and then use the resulting updated probabilities to decode the second code. Once this is done, the updated results can more accurately decode the first code. This decoding strategy shares the limitations of all iterative solution methods, including the possibility of entrapment in a local minimum. The decoder output is not necessarily the true global ML solution. But the study of the corresponding link-level BER curves suggests that it tends to be a very good solution.

In a convolutional code, the input bit sequence usually has tail bits added. This initializes the encoder state to all zeros at the end of the bit sequence. In a turbo coder, this implies that a valid bit sequence cannot contain a single one. It must either be all zeros, or it must contain two or more ones. Because encoding is a linear process, this implies that any valid input sequence must differ from any other valid input sequence in at least two bits. In this case, if we consider only the first decoder's output, it differs from the correct output in two positions. However, the turbo encoder contains an interleaver. It must be noted that the two constituent encoders are operating on the same set of bits, but in a different order. Therefore, although the error bits are close together for the first decoder, they are widely separated in the second decoder's input. As a result, the second decoder's output differs from the correct output in many bit positions. It will see the incorrect bit sequence as highly implausible. This is the basic principle of operation of the turbo codes, and is the key to the high performance of turbo codes at low SNRs. Erroneous information sequences that look reasonable to one decoder are likely to be rejected by the other decoder. This is also the rationale for the error floor at higher SNRs. Since the interleaver is random, there are a few error patterns that will look plausible to both decoders. As the SNR increases, these weak patterns come to dominate the BER curve.

One of the most interesting characteristics of a turbo code is that it is not just a single code. It is, in fact, a combination of two codes that work together to achieve a synergy that would not be possible by merely using one code by itself. As shown in Figure 9.69, a turbo code is formed from the parallel concatenation of two constituent encoders separated by an interleaver. Each constituent encoder can be any form of FEC coder used for conventional data communications. However, in practice, the constituent encoders are identical convolutional

Petitioners' Exhibit 1021
Nokia of America Corp., et al. v. KT Corporation, et al.
Case No. IPR2025-00036; U.S. Patent No. 11,627,631
Page 537 of 1122

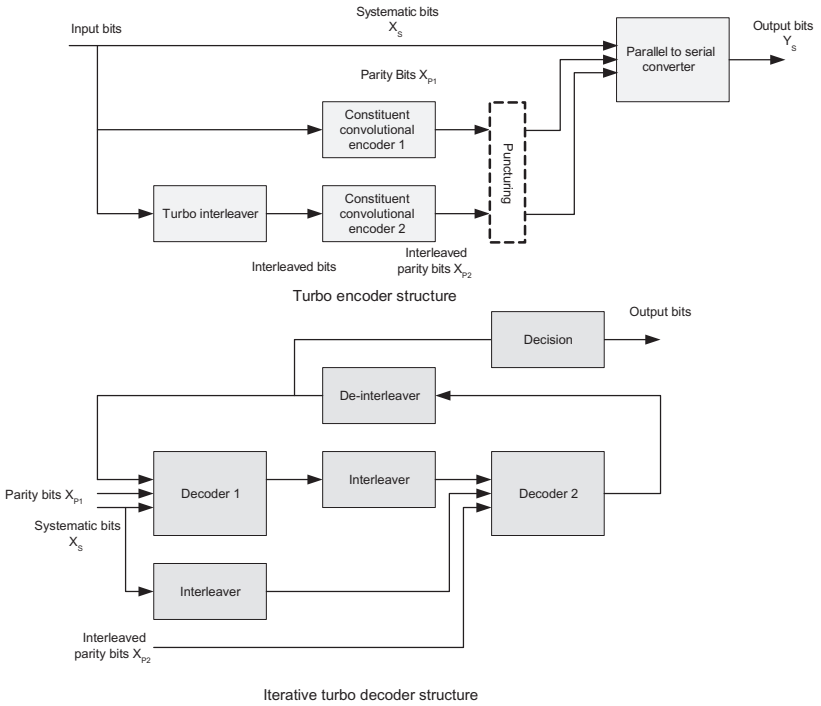


FIGURE 9.69

Generic structure of turbo encoder and iterative decoder [27,40].

encoders. As can be seen in Figure 9.69, the turbo coder consists of two identical constituent encoders. The input data stream and the parity outputs of the two parallel encoders are then serialized into a single turbo codeword. The interleaver is a critical component of the turbo code. It is a simple functional block that rearranges the order of the data bits in a prescribed, but irregular, manner. Although the same set of data bits is present at the output of the interleaver, the order of these bits has been changed. It must be noted that the interleaver used by a turbo coder is quite different than the rectangular interleavers that are commonly used in wireless systems to help mitigate the effect of deep fading. While a rectangular channel interleaver tries to space the data out according to a regular pattern, a turbo interleaver randomizes the ordering of the data in an irregular manner.

The operation of a turbo encoder and decoder can be described as follows. Let the binary input bits $\{0, 1\}$ be represented by bipolar levels $\{+1, -1\}$ and assigned to the variable d, which may take on the values $d = +1$ and $d = -1$. For an AWGN channel, the conditional probability density functions $f(x|d = -1)$

Petitioners' Exhibit 1021
Nokia of America Corp., et al. v. KT Corporation, et al.
Case No. IPR2025-00036; U.S. Patent No. 11,627,631
Page 538 of 1122

and $f(x|d=+1)$ are referred to as likelihood functions. The common hard-decision criterion, known as ML, selects the symbol $d_k=+1$ or $d_k=-1$ depending on the intercept point of received signal value x_k and the above conditional probability density functions using a fixed threshold of λ (decision point); thus, $d_k=+1$ if $x_k>\lambda$, otherwise, $d_k=-1$. Another decision rule, known as a maximum *a posteriori* probability (MAP) criterion takes into account the *a posteriori* probabilities $f(d=+1|x)$ and $f(d=-1|x)$ to construct the hypotheses H_1 and H_2 as follows:

$$f(d=+1|x) \underset{H_2}{\overset{H_1}{\gtrless}} f(d=-1|x) \tag{9.43}$$

That is, one selects hypothesis $H_1(d=+1)$, if the $f(d=+1|x)>f(d=-1|x)$; otherwise, $H_2(d=-1)$ is selected. Using the Bayes' theorem [30], the above *a posteriori* probabilities can be replaced by their equivalent expressions, yielding:

$$f(x|d=+1)p(d=+1) \underset{H_2}{\overset{H_1}{\gtrless}} f(x|d=-1)p(d=-1) \tag{9.44}$$

The likelihood ratio test is constructed as follows:

$$\frac{f(x|d=+1)p(d=+1)}{f(x|d=-1)p(d=-1)} \underset{H_2}{\overset{H_1}{\gtrless}} 1 \tag{9.45}$$

If the input bits are independent and identically distributed random variables, the above equation is simplified as follows:

$$\frac{f(x|d=+1)}{f(x|d=-1)} \underset{H_2}{\overset{H_1}{\gtrless}} 1 \tag{9.46}$$

By taking the logarithm of the above likelihood ratio, a useful metric known as log-likelihood ratio (LLR) is obtained, which is a real-valued number representing the soft-decision output of the detector:

$$L(d|x)=\log\left(\frac{f(x|d=+1)}{f(x|d=-1)}\right)+\log\left(\frac{p(d=+1)}{p(d=-1)}\right)=L(x|d)+L(d) \tag{9.47}$$

where $L(x|d)$ is the LLR of test statistics x obtained through measuring the channel output x under the condition that either $d=+1$ or $d=-1$ may have been transmitted, and $L(d)$ denotes the *a priori* LLR of the data bit d as shown in Figure 9.70. The introduction of a decoder would improve the reliability of the above decision-making process. For a systematic code, it can be shown that the LLR (soft output) expression at the output of the decoder can be written as $L_{\text{output}}(\hat{d})=L_{\text{input}}(\hat{d})+L_{\text{e}}(\hat{d})$, where $L_{\text{input}}(\hat{d})$ is the LLR of a data bit at the output of the detector (or the input to the decoder), and $L_{\text{e}}(\hat{d})$ represents additional

Petitioners' Exhibit 1021
Nokia of America Corp., et al. v. KT Corporation, et al.
Case No. IPR2025-00036; U.S. Patent No. 11,627,631
Page 539 of 1122

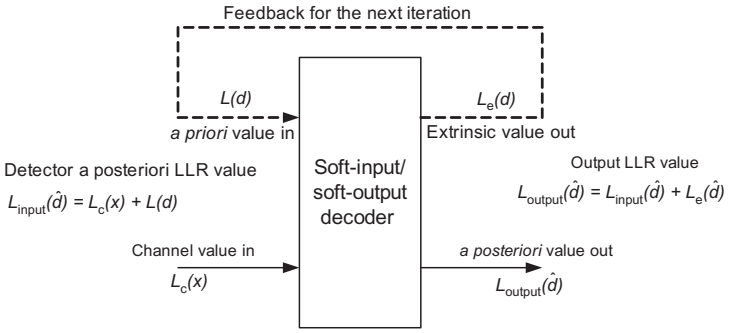


FIGURE 9.70

Illustration of soft-input/soft-output decoder for turbo codes [40,102].

information that is obtained from the decoding process (see Figure 9.70). The output sequence of a systematic decoder consists of values representing data and parity bits. Thus, the decoder output LLR can be decomposed into a data component that is associated with the detector measurement and the extrinsic component that is represented by the decoder contribution due to parity. The soft-decision component $L_{\text{output}}(\hat{d})$ is a real number that provides a hard-decision as well as the reliability of that decision. The sign of the parameter $L_{\text{output}}(\hat{d})$ denotes the hard-decision, i.e., for positive values of $L_{\text{output}}(\hat{d})$, decide $\hat{d} = +1$ and for negative values of $L_{\text{output}}(\hat{d})$, decide $\hat{d} = -1$. The magnitude of $L_{\text{output}}(\hat{d})$ denotes the reliability of the decision [98,102].

Turbo decoding relies on the exchange of probabilistic information between the two soft-input soft-output decoders shown in Figure 9.69. The extrinsic information is the result of the decoder's estimation of bit d, but not taking its own input into account. It is precisely this extrinsic information that is exchanged iteratively between the two soft-decision decoders during the decoding process. Subtracting the decoder's input from its output prevents the decoder from acting as a positive feedback amplifier and introduces stability in the feedback process. Usually, after a given number of iterations, one observes that the two decoders converge to a stable final decision for d. In practice, depending on the nature of the soft-decision decoder, scaling or clipping operations may be applied to the extrinsic information in order to ensure convergence within a small number of iterations. It is shown in the literature that the Max-Log-MAP decoding algorithm can make a good trade-off between performance and complexity, with the added advantage of not requiring any knowledge of the noise level (Figure 9.71). A stop criterion facilitates the convergence of the iterative decoding process and helps reduce the average power consumption of the decoder by reducing the average number of iterations required to decode a block without compromising performance [100–108].

Petitioners' Exhibit 1021
Nokia of America Corp., et al. v. KT Corporation, et al.
Case No. IPR2025-00036; U.S. Patent No. 11,627,631
Page 540 of 1122

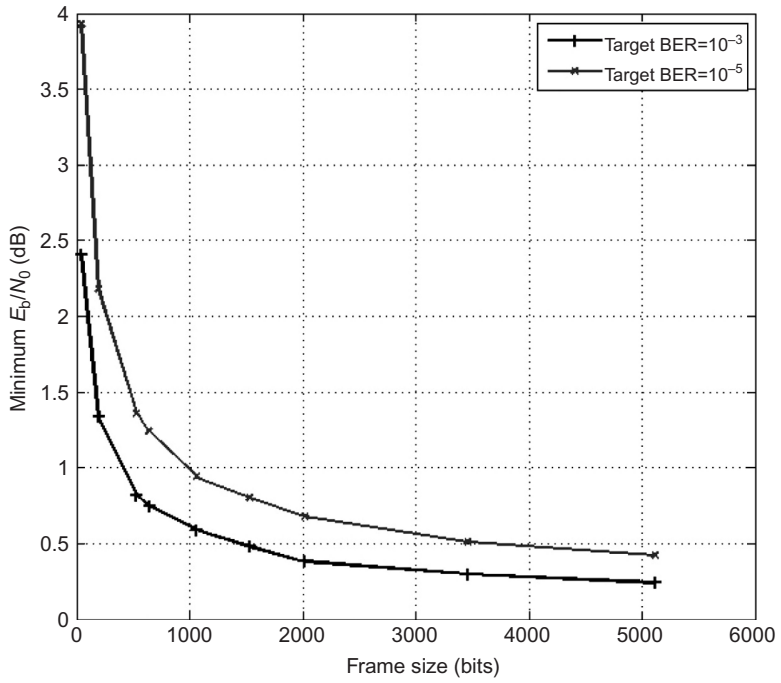


FIGURE 9.71

Minimum $E_b = N_0$ to achieve a target BER using the UMTS/LTE turbo coder ($R = 1/3$) with BPSK modulation over an AWGN channel [144].

For practical applications, it is often necessary to adapt the turbo code parameters to those of the application. The systematic bits are always present at the output of the turbo encoder; however, depending on the desired code rate, the parity bits from the two constituent encoders may be punctured prior to transmission (see Figure 9.69). The puncturing mechanism involves deleting some of the parity bits prior to transmission. As an example, if the minimum code rate of a turbo coder is 1/5, a code rate of 1/3 can be generated by deleting the second parity output of each encoder. Note that the puncturing pattern for each code rate must be known by the decoder for correct interpretation of the received bits [40].

It is shown that for smaller input frame sizes, less iteration is required; however, the performance of the turbo coder is improved by increasing the frame size. This is due to an increase in interleaver gain as the input frame size becomes larger. Figure 9.71 shows the minimum E_b/N_0 required to achieve a BER of 10^{-3} and 10^{-5} for various frame sizes using a UMTS/LTE turbo encoder with a minimum code rate of $R = 1/3$. In general, turbo codes are more suited for applications with large packet sizes and their performance degrades for small packet sizes.

Petitioners' Exhibit 1021
Nokia of America Corp., et al. v. KT Corporation, et al.
Case No. IPR2025-00036; U.S. Patent No. 11,627,631
Page 541 of 1122

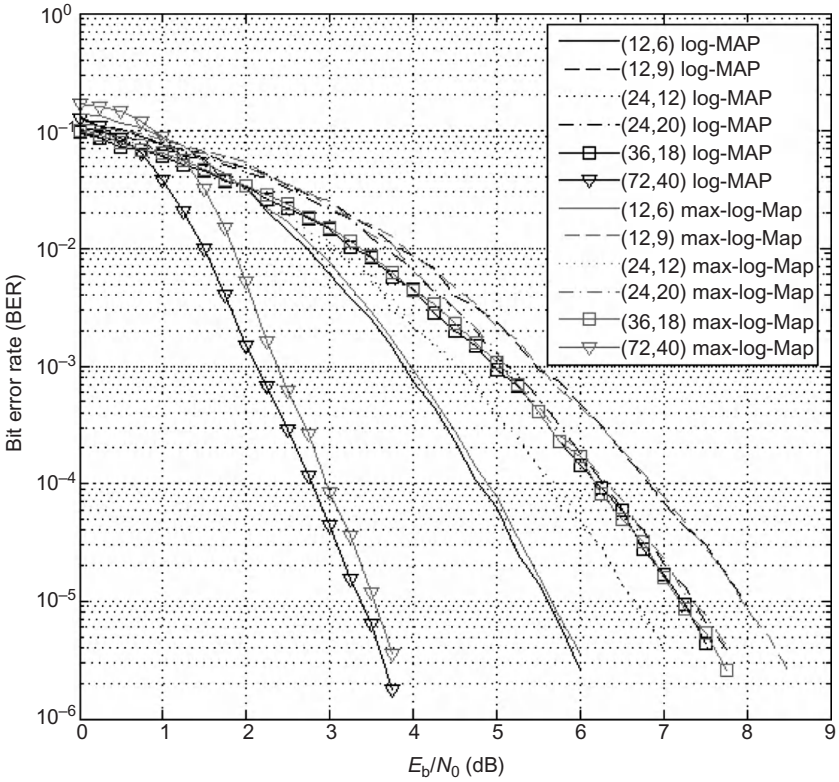


FIGURE 9.72

Comparison of the BER performance of a BTC turbo coder in AWGN channel with different code rates, frame sizes, and detector types [144].

Furthermore, the delay due to turbo interleaver might become prohibitive for delay-sensitive applications. Figure 9.72 shows the BER performance of a BTC turbo coder as a function of E_b/N_0 for various code rates, frame sizes, and detector types. In Figure 9.72, notation (n, k) denotes the number of input k and output n bytes [144].

9.11.3 Baseband digital modulation schemes

Modulation is a process by which a carrier signal is altered according to information in a message signal. For the typical baseband modulation types (PSK, DPSK, FSK, QAM, or PAM), gray-coded constellations are obtained by selecting the gray parameter in the corresponding baseband modulation function. The mapping

Petitioners' Exhibit 1021
Nokia of America Corp., et al. v. KT Corporation, et al.
Case No. IPR2025-00036; U.S. Patent No. 11,627,631
Page 542 of 1122

or assignment of k information bits to $M = 2^k$ possible signal amplitudes may be done in a number of ways. The preferred assignment is the one in which the adjacent signal amplitudes differ by one binary digit since the most likely errors caused by noise involve the erroneous selection of an adjacent amplitude to the transmitted signal amplitude. In that case, only a single bit error occurs in the k-bit sequence. This mapping is referred to as gray coding. The criteria that must be taken into account when choosing a digital modulation method include the following:

- Power efficiency, i.e., the E_b/N_0 ratio for a specific error probability
- Bandwidth efficiency, i.e., the data rate per unit bandwidth
- Performance in multipath fading channels and under non-linear distortion
- Implementation cost and complexity

However, the above requirements cannot be satisfied at the same time, and some trade-off is necessary. In order to explain the latter statement, let us define a few basic terms in this context. A constellation diagram is a graphical representation of the complex envelope of each possible symbol state. The power efficiency is related to the minimum distance between the points in the constellation. The bandwidth efficiency is related to the number of points in the constellation. The gray coding is used to assign groups of bits to each constellation point. In gray coding, adjacent constellation points differ by a single bit.

The two most common digital modulation schemes used in cellular systems are M-ary PSK and M-ary QAM modulation schemes. In M-ary PSK, a group of n bits are transmitted using $M = 2^n$ different phases, whereas M-ary QAM uses a combination of amplitude and phase modulation to convey the information. Study of the literature suggests that the minimum code distance $d_{\min}$ is smaller for M-ary ASK than for M-ary PSK or M-ary QAM for the same average transmitted power, which translates into poorer error performance because the signal envelope is not constant, it results in poor performance under non-linear distortion condition. The minimum distance $d_{\min}$ is smaller for M-ary PSK compared to that for M-ary QAM for the same average transmitted power, resulting in poorer error performance. However, a constant envelope results in good performance under nonlinear distortion. The minimum distance $d_{\min}$ is larger for M-ary QAM relative to that for M-ary ASK or M-ary PSK for the same average transmitted power, which means better error performance. Nonetheless, since the signal envelope is not constant, poor error performance is expected under non-linear distortion. Pulse shaping is then used to reduce the bandwidth requirements of the modulated signal. The Nyquist technique can be used to reduce the bandwidth requirement and to eliminate ISI. The non-Nyquist techniques reduce the bandwidth requirement, but do not eliminate ISI. Note that in all M-ary modulation schemes, a group of n bits is transmitted in each signaling interval $T = T_b \log_2 M$ and the modulated signal bandwidth is inversely proportional to the signaling interval. It can be shown that the probability of error (i.e., error per bit) equations as a function of E_b/N_0 for M-ary

Petitioners' Exhibit 1021
Nokia of America Corp., et al. v. KT Corporation, et al.
Case No. IPR2025-00036; U.S. Patent No. 11,627,631
Page 543 of 1122

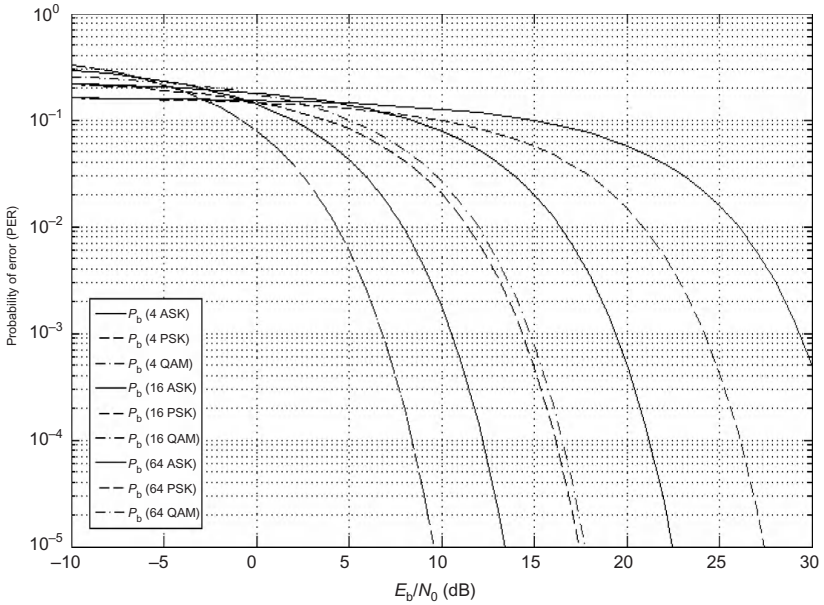


FIGURE 9.73

Probability of error as a function of energy per bit for different digital modulation schemes [159].

ASK, M-ary PSK, and M-ary QAM can be written as follows (see Figure 9.73 for graphical presentation):

$$
\begin{aligned}
p_{\mathrm{b}} &= \frac{1}{\log_2 M}\left(1-\frac{1}{M}\right) Q\left(\sqrt{\frac{3\log_2 M}{M^2-1}\frac{E_{\mathrm{b}}}{N_0}}\right) && M\text{-ary ASK} \\
p_{\mathrm{b}} &= \frac{1}{\log_2 M} Q\left(\sqrt{\log_2 M \frac{E_{\mathrm{b}}}{N_0}\sin^2\left(\frac{\pi}{M}\right)}\right) && M\text{-ary PSK} \\
p_{\mathrm{b}} &= \frac{2}{\log_2 M}\left(1-\frac{1}{\sqrt{M}}\right) Q\left(\sqrt{\frac{3\log_2 M}{2(M-1)}\frac{E_{\mathrm{b}}}{N_0}}\right) && M\text{-ary QAM}
\end{aligned}
\tag{9.48}
$$

In the above equations, E_{b}/N_0 denotes the energy per bit, M is the modulation order, and $Q(\cdot)$ denotes the error function.[17]

[17]In mathematics, the error function is defined as $Q(x) = (2/\sqrt{\pi})\int_0^x \mathrm{e}^{-\tau^2}\,\mathrm{d}\tau$. An alternative definition is sometimes referred to as the complementary error function in the literature is given as $Q(x) = (2/\sqrt{\pi})\int_x^\infty \mathrm{e}^{-\tau^2}\,\mathrm{d}\tau$ [30].

Petitioners' Exhibit 1021
Nokia of America Corp., et al. v. KT Corporation, et al.
Case No. IPR2025-00036; U.S. Patent No. 11,627,631
Page 544 of 1122

The modulation mapping function in the transmission chain takes binary input $b_0 b_1 \ldots b_{N_{\text{modulation order}}-1}$ with $b_i =$ "0" or "1" and produces the complex-valued modulation symbols $x = \gamma(I + \mathrm{j}Q)$ in the output with the value of γ chosen to achieve equal average power. For each modulation, symbol, b_0 denotes the most significant bit. In the case of BPSK modulation, $N_{\text{modulation order}} = 1$; thus a single bit is mapped to the modulation symbol x with $\gamma = 1/\sqrt{2}$. In the case of QPSK modulation, $N_{\text{modulation order}} = 2$ and a pair of bits are mapped to complex-valued modulation symbol x with $\gamma = 1/\sqrt{2}$. In the case of 16QAM modulation, $N_{\text{modulation order}} = 4$ and quadruplets of bits $b_0 b_1 b_2 b_3$ are mapped to the complex-valued modulation symbol x and $\gamma = 1/\sqrt{10}$. In the case of 64QAM modulation, $N_{\text{modulation order}} = 6$ and six information bits $b_0 b_1 b_2 b_3 b_4 b_5$ are mapped to the modulation symbol x with $\gamma = 1/\sqrt{42}$. The constellation format for various modulation schemes is illustrated in Figure 9.74.

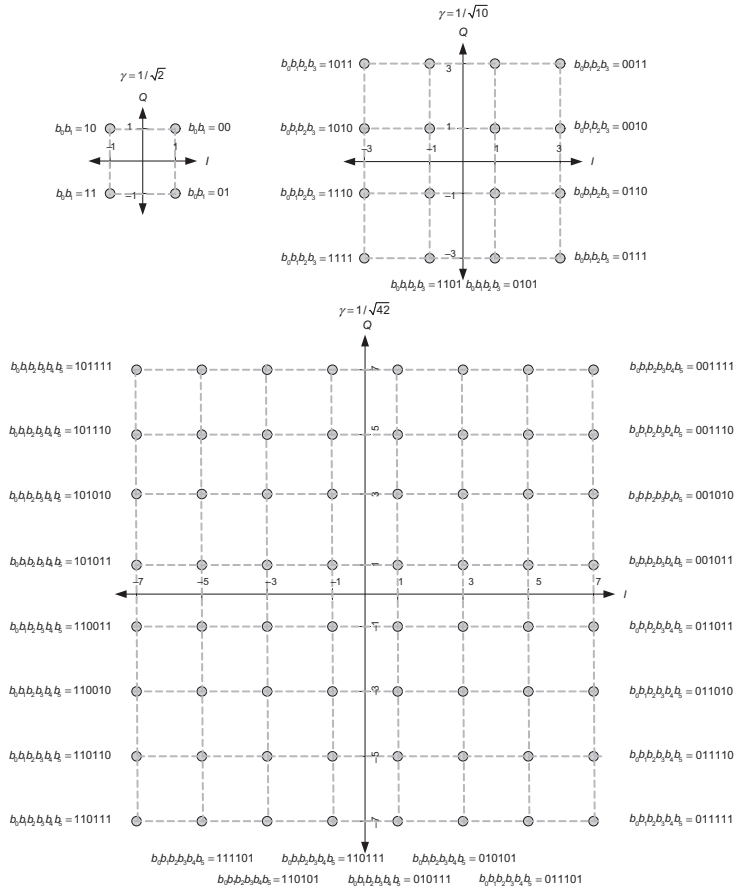


FIGURE 9.74

QPSK, 16QAM, and 64QAM constellations [3].

Figures 9.75 and 9.76 show the performance of the M-ary QAM and M-ary PSK signals in an AWGN channel in terms of probability of error as a function of SNR per bit for different values of modulation order M. It can be seen that for a given target error rate, the required SNR per bit increases with increasing modulation order, i.e., higher modulation orders can only be used in good channel conditions. The latter suggests that in poor channel conditions, more robust modulation schemes must be used.

9.11.4 Channel coding, multiplexing, and interleaving

The baseband modulation schemes supported in the downlink and uplink of LTE are QPSK, 16QAM, and 64QAM. While all three modulation schemes are supported in the downlink in all UE categories, the use of 64QAM in the uplink is only supported in the higher UE categories, and lower UE categories only support QPSK and 16QAM. The channel coding scheme for transport blocks in LTE is turbo coding similar to that of UMTS, with a basic code rate of $R = 1/3$, two eight-state constituent encoders and a contention-free quadratic permutation polynomial (QPP)[18] turbo interleaver [4]. Trellis termination is performed by taking the tail bits from the shift register feedback after all information bits are encoded. The tail bits are padded after the encoding of information bits. Before the turbo coding, transport blocks are segmented into octet-aligned segments with a maximum information block size of 6144 bits. Error detection is performed using 24-bit CRC. Link adaptation (adaptive modulation and coding) with various modulation schemes and channel coding rates is applied to the shared data channel. The same coding and modulation is applied to all groups of resource blocks

[18]In mathematics, a permutation polynomial for a given finite ring is a polynomial that performs a permutation of the elements of the ring, i.e., the mapping Z/nZ is a one-to-one mapping. In the case of finite rings Z/nZ, such polynomials have been studied and applied in the interleaver component of error detection and correction algorithms. For the finite ring Z/nZ, one can construct quadratic permutation polynomials. This is possible, if and only if, n is divisible by p^2 for some prime number p. The construction is simple, but it can produce permutations with desirable properties. As an example, consider $f(x) = 2x^2 + x$ for the ring $Z/4Z$. One can observe that $f(0) = 0$; $f(1) = 3; f(2) = 2; f(3) = 1$, hence the polynomial defines the permutation $\begin{bmatrix} 0 & 1 & 2 & 3 \\ 0 & 3 & 2 & 1 \end{bmatrix}$. Note that a ring is an algebraic structure which generalizes the main properties of the addition and the multiplication of integers, real numbers, complex numbers, and square matrices. It consists of a set together with two binary operations usually called addition and multiplication, which satisfy the following set of axioms: (1) the addition is associative and commutative, it has an identity and each element in the set has an additive inverse, thus the set is an Abelian group (or commutative group) under addition; (2) the multiplication is associative, but is not necessarily commutative, it has an identity and distributes over addition [31,32].
In general, let us assume $n = \alpha_1^{k_1}\alpha_2^{k_2}\ldots\alpha_m^{k_m}$, in which α_i is a prime number. It can be proved that any polynomial $f(x) = \beta_0 + \sum_{0<i\le M}\beta_i x^i$ defines a permutation for the ring Z/nZ if and only if all the polynomials $f_{\alpha_k}(x) = \beta_{0_{\alpha_k}} + \sum_{0<i\le M}\beta_{i_{\alpha_k}} x^i$ define the permutations for all rings $Z/\alpha_m^{k_m}Z$, in which $\beta_{i_{\alpha_k}}$ is the remainder of β_i modulo $\alpha_i^{k_i}$ [31,32].

Petitioners' Exhibit 1021
Nokia of America Corp., et al. v. KT Corporation, et al.
Case No. IPR2025-00036; U.S. Patent No. 11,627,631
Page 546 of 1122

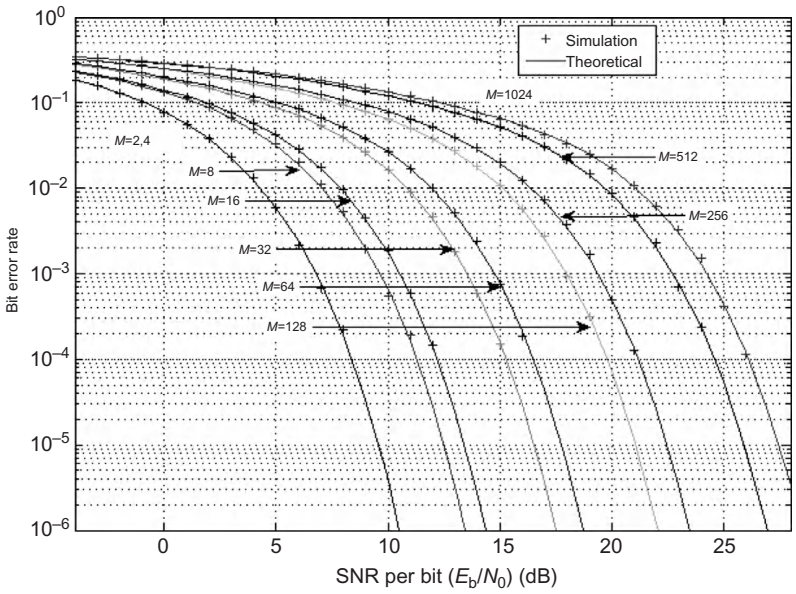


FIGURE 9.75

Performance of *M*-ary QAM in an AWGN channel [141].

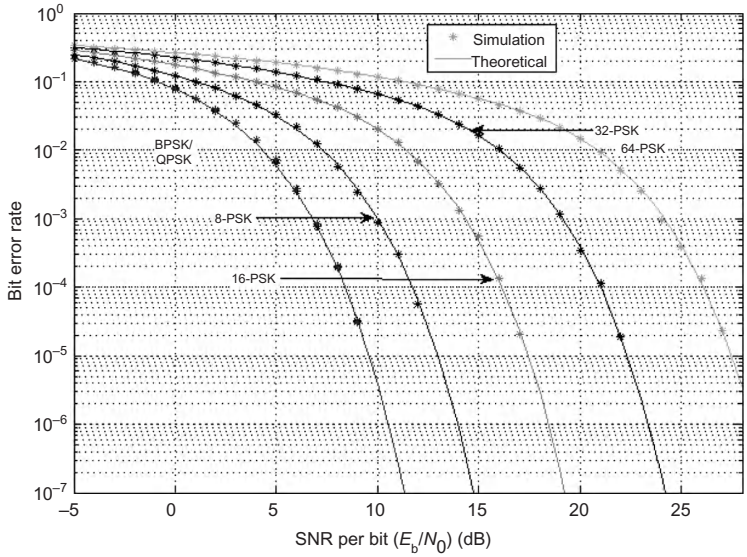


FIGURE 9.76

Performance of coherent *M*-ary PSK over an AWGN channel [141].

Petitioners' Exhibit 1021
Nokia of America Corp., et al. v. KT Corporation, et al.
Case No. IPR2025-00036; U.S. Patent No. 11,627,631
Page 547 of 1122

belonging to the same MAC PDU scheduled for one user within one TTI and within a single stream.

The user data and control information from the MAC sub-layer are encoded prior to transmission of the transport blocks over the radio link. The channel coding in E-UTRA is a combination of error detection, error correction, rate-matching, interleaving and transport channel, or control information mapping to the appropriate physical channels. As shown in Figure 9.77, the channel coding procedure for BCH transport blocks is different from that of the DL-SCH, PCH, and MCH. Depending on the type of the transport channel, a different coding scheme and coding rate is applied as given in Table 9.17. The first stage of the channel coding process is to append 16/24 bit CRC to the input transport block.

In the case of BCH, the information (i.e., MIB) is received by the channel coding unit in the form of one transport block every 40 ms. A 16-bit CRC is calculated over the entire transport block and appended to the input transport block. Let $(a_0, a_1, \ldots, a_{N_A-1})$ denote the bits in a BCH transport block delivered to the physical layer. The parity bits are denoted by $(p_0, p_1, \ldots, p_{N_P-1})$ where $N_P = 16$.

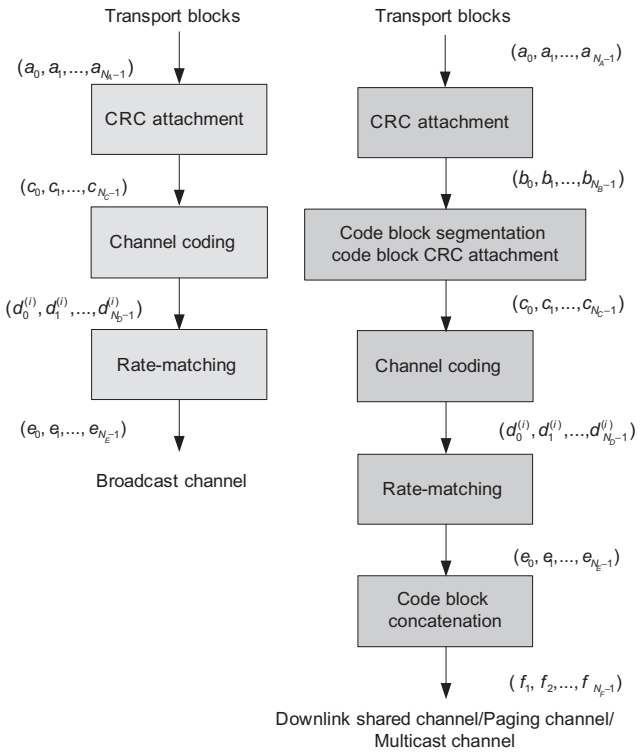


FIGURE 9.77

Channel coding procedure for downlink transport blocks [4].

Petitioners' Exhibit 1021
Nokia of America Corp., et al. v. KT Corporation, et al.
Case No. IPR2025-00036; U.S. Patent No. 11,627,631
Page 548 of 1122

Table 9.17 Channel Coding Scheme for Various Transport Channels/Control Information in E-UTRA [4]

Channel/ Information	Channel/ Information Types	Coding Scheme	Coding Rate	CRC Size (Bits)
Transport channels	Uplink shared channel (UL-SCH)	Turbo coding	1/3	24
	Downlink shared channel (DL-SCH)			24
	Paging channel (PCH)			24
	Multicast channel (MCH)			24
	Broadcast channel (BCH)	Tail-biting convolutional coding	1/3	16
Control Information	Downlink control information (DCI)	Tail-biting convolutional coding	1/3	16
	Control format indicator (CFI)	Block code	1/16	–
	HARQ indicator (HI)	Repetition code	1/3	–
	Uplink control information (UCI)	Block code	Variable	16
		Tail-biting convolutional coding	1/3	

Following the calculation of the CRC bits, they are scrambled according to the eNB multi-antenna configuration with binary sequence $(x_0, x_1, \ldots, x_{15})$ to form the output sequence $(c_0, c_1, \ldots, c_{N_C-1})$, where the first A bits of the latter sequence are formed by the input transport block and the last 16 bits are the masked CRC bits. The masking sequence is given as follows:

$$(x_0, x_1, \ldots, x_{15}) = \begin{cases} (0,0,0,0,0,0,0,0,0,0,0,0,0,0,0,0) & N_{\text{TX}} = 1 \\ (1,1,1,1,1,1,1,1,1,1,1,1,1,1,1,1) & N_{\text{TX}} = 2 \\ (0,1,0,1,0,1,0,1,0,1,0,1,0,1,0,1) & N_{\text{TX}} = 4 \end{cases} \tag{9.49}$$

where N_{TX} denotes the number of antenna ports in the eNB that are used for transmission of the PBCH. The CRC-attached information bits denoted by $(c_0, c_1, \ldots, c_{N_C-1})$ are processed through a tail-biting convolutional coder. The channel-coded bits, denoted by $(d_0^{(i)}, d_1^{(i)}, \ldots, d_{N_D-1}^{(i)})$ where $i = 0, 1, 2$ is the coded stream number to sub-block interleaver and $N_D = N_C$ is the number of bits on the ith coded stream, are fed to the rate-matching block. The use of tail-biting convolutional coding necessitates that the initial value of the shift register of the encoder be set to the values corresponding to the last 6 information bits in the input stream so that the initial and final states of the shift register are the same.

The rate-matching function for channel-coded transport channels is defined per coded block, and consists of interleaving of the three coded streams

Petitioners' Exhibit 1021
Nokia of America Corp., et al. v. KT Corporation, et al.
Case No. IPR2025-00036; U.S. Patent No. 11,627,631
Page 549 of 1122

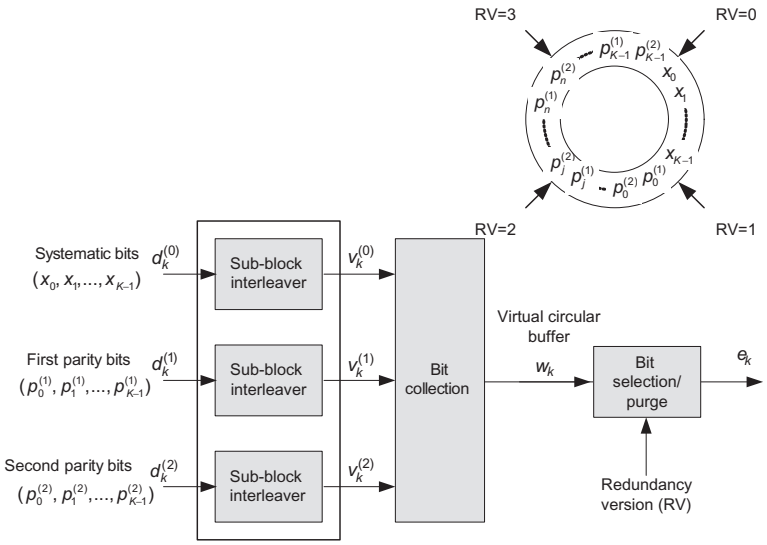


FIGURE 9.78

Rate-matching process of the coded information [4,15].

$d_k^{(0)}$,$d_k^{(1)}$, and $d_k^{(2)}$ followed by the collection of bits and generation of a virtual circular buffer as depicted in Figure 9.78.

The rate-matching block generates an output bit stream with the desired code rate. As the number of bits available for transmission depends on the available resources, the rate-matching algorithm is capable of producing any arbitrary code rate. The three bit streams from the channel coding module are interleaved followed by bit collection to generate a circular buffer. Bits are selected and pruned from the circular buffer to create an output bit stream with the desired code rate, as shown in Figure 9.78. The three sub-block interleavers used in the rate-matching block are identical. Interleaving is a technique to reduce the impact of burst errors on a signal so that consecutive bits of data will not be corrupted. The sub-block interleaver reshapes the coded bit sequence, row-by-row, to form a matrix with $C_{\text{sub-block}} = 32$ columns and $R_{\text{sub-block}}$ rows, where $R_{\text{sub-block}}$ is determined by finding the minimum integer that satisfies the following equation: $R_{\text{sub-block}} C_{\text{sub-block}} \leq N_D$. If $R_{\text{sub-block}} C_{\text{sub-block}} > N_D$, then N_{NULL} null bits are appended to the front of the encoded input sequence such that $R_{\text{sub-block}} C_{\text{sub-block}} = N_D + N_{\text{NULL}}$. For $d_k^{(0)}$ and $d_k^{(1)}$ bit streams, an inter-column permutation is performed on the matrix to reorder the columns as follows: 0, 16, 8, 24, 4, 20, 12, 28, 2, 18, 10, 26, 6, 22, 14, 30, 1, 17, 9, 25, 5, 21, 13, 29, 3, 19, 11, 27, 7, 23, 15, and 31 for turbo-coded transport blocks, and 1, 17, 9, 25, 5, 21, 13, 29, 3, 19, 11, 27, 7, 23, 15, 31, 0, 16, 8, 24, 4, 20, 12, 28, 2, 18, 10, 26, 6, 22, 14, and 30 for transport blocks coded by convolutional coder. For the $d_k^{(0)}$ and $d_k^{(1)}$ bit

Petitioners' Exhibit 1021
Nokia of America Corp., et al. v. KT Corporation, et al.
Case No. IPR2025-00036; U.S. Patent No. 11,627,631
Page 550 of 1122

streams, the output of the block interleaver is the bit sequence readout column-by-column from the inter-column permutated matrix to create a stream $K' = R_{\text{sub-block}} C_{\text{sub-block}}$ bits long. For the $d_k^{(2)}$ bit stream, the elements in the matrix are permutated separately based on the permutation pattern shown above, but modified to create a permutation which is a function of $(R_{\text{sub-block}}, C_{\text{sub-block}}, k, K')$. This creates three interleaved bit-stream mapping $d_k^{(0)} \rightarrow v_k^{(0)}; d_k^{(1)} \rightarrow v_k^{(1)}; d_k^{(2)} \rightarrow v_k^{(2)}$. The bit collection stage creates a virtual circular buffer by combining the three interleaved encoded bit streams. The block interleaver output $v_k^{(1)}$ and $v_k^{(2)}$ are combined by successive interlacing of their values. This combination is then appended to the end of $v_k^{(0)}$ to create the circular buffer w_k as illustrated in Figure 9.79. Interlacing allows equal levels of protection for each parity sequence [4].

Following the bit collection procedure, the bits are selected and trimmed from the virtual circular buffer to create an output sequence length which meets the desired code rate. The HARQ error correction scheme is incorporated into the rate-matching algorithm of LTE/LTE-Advanced. For any desired code rate, the coded bits are sent out serially from the circular buffer from a starting location, given by the HARQ redundancy version (see Figure 9.78), wrapping around to the beginning of the buffer, if the end of the buffer is reached. The null bits are discarded. Different redundancy versions, and hence starting points, allow for the retransmission of selected data. Being able to select different starting points enables the two main methods of recovering data at the receiver in the HARQ process: (1) chase combining where retransmissions contain the same data and parity bits; (2) incremental redundancy where retransmissions contain different information so the receiver gains more knowledge upon each retransmission. The rate-matched code blocks are now concatenated back together. This is done by sequentially concatenating the rate-matched blocks together to create the output of the channel coding process $(f_1, f_2, \ldots, f_{F-1})$, as shown in Figure 9.77.

In the case of DL-SCH, PCH, and MCH transport channels, the CRC calculation and addition to the information block is similar to BCH, except that 24-bit CRC is used and no CRC masking is done since in this case, the multi-antenna configuration is part of DCI. As shown in Figure 9.80, the input bits to the code block segmentation are denoted by $(b_0, b_1, \ldots, b_{N_B-1})$, where $N_B = N_A + 24$. In LTE/LTE-Advanced, a minimum code block size of 40 bits and maximum

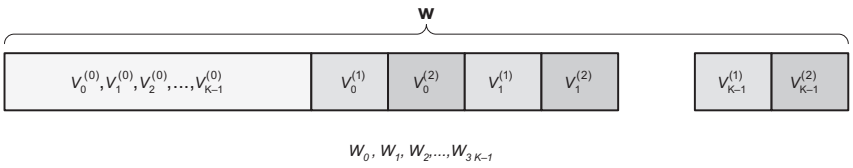


FIGURE 9.79

Structure and content of the virtual circular buffer [160].

Petitioners' Exhibit 1021
Nokia of America Corp., et al. v. KT Corporation, et al.
Case No. IPR2025-00036; U.S. Patent No. 11,627,631
Page 551 of 1122

code block size of 6144 bits are specified so that the block sizes are compatible with the block sizes supported by the turbo interleaver. If the length of the input block N_B is greater than the maximum code block size, the input block is segmented. When the input block is segmented, it is segmented into $N_C = \lceil N_B/6120 \rceil$ code blocks. Each code block is appended with a 24-bit CRC to the end. Padding bits are added to the front of each block so that code block sizes match a set of permissible turbo interleaver block sizes. If no segmentation is necessary, only one code block is generated. If N_B is less than 40 bits, then padding bits (zeros) are added to the beginning of the code block to attain a total of 40 bits. The code blocks then undergo turbo coding.

A PCCC turbo coder with two recursive convolutional encoders and a contention-free QPP interleaver is used as a channel coder in LTE/LTE/Advanced for traffic channels as shown in Figure 9.81.

The outputs of the encoder are three streams $d_k^{(0)}, d_k^{(1)}$, and $d_k^{(2)}$ in order to achieve a code rate of 1/3. As shown in Figure 9.81, the input to the first constituent encoder is the input bit stream to the turbo coding block. The input to the second constituent encoder is the output of the QPP interleaver, which is a permutated version of the input sequence. There are two output sequences from each encoder which are the systematic bits (x_k, x'_k) and parity bits (z_k, z'_k). Only one of the systematic bit sequences x_k is used as the output, as the other one x'_k is simply a permutated version of the former systematic sequence. The transfer function for each constituent encoder is given by $G(D) = [1, g_1(D)/g_0(D)]$. The first

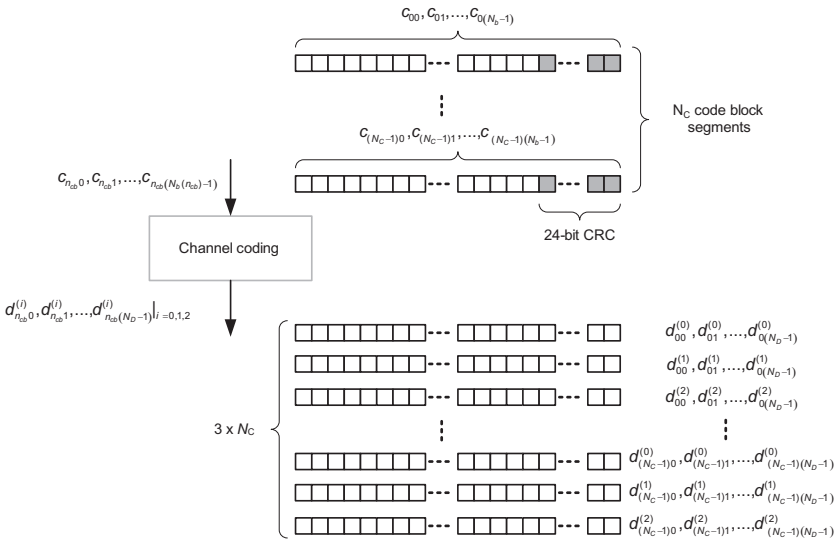


FIGURE 9.80

Code block segmentation and CRC attachment for DL-SCH [4,158,160].

element in the latter equation represents the systematic output transfer function, and the second element denotes the recursive convolutional output transfer function, where $g_0(D) = 1 + D^2 + D^3; g_1(D) = 1 + D + D^3$. The output for each sequence can be calculated using the transfer function.

The encoder is initialized with all zeros. If the code block to be encoded is the zeroth code block and the number of padding bits $N_{\text{Padding}} > 0$, then the encoder input is set to zero for $k = 0, 1, \ldots, N_{\text{Padding}} - 1$, and $d_k^{(0)}, d_k^{(1)}, k = 0, 1, \ldots, N_{\text{Padding}} - 1$ are set to null at the output. In a conventional convolutional coder, the coder is driven to an all zero state upon termination by appending zeros to the end of the input data stream. Since the decoder is aware of the start and end state of the encoder, it can decode the data. Driving a recursive coder to an all zeros state using this method is not possible. To overcome this problem trellis termination is used where, upon termination, the tail bits are fed back to the input of each encoder using a switch (see Figure 9.81). The first three tail bits are used to terminate each encoder.

The role of the interleaver is to spread the information bits such that in the event of an error, the two codes are affected differently allowing data to still be recoverable. As shown in Figure 9.81, the input bits to the turbo code QPP interleaver are denoted by $c_0, c_1, \ldots, c_{N_C-1}$, where N_C is the number of input bits. The output bits from the turbo code QPP interleaver are denoted by $c'_0, c'_1, \ldots, c'_{K-1}$. The output of the interleaver is a permutated version of the input data $c'_i = c_{\Phi(i)}, i = 0, 1, \ldots, K-1$ where $\Phi(i) = (f_1 i + f_2 i^2) \bmod K$. The coefficients f_1

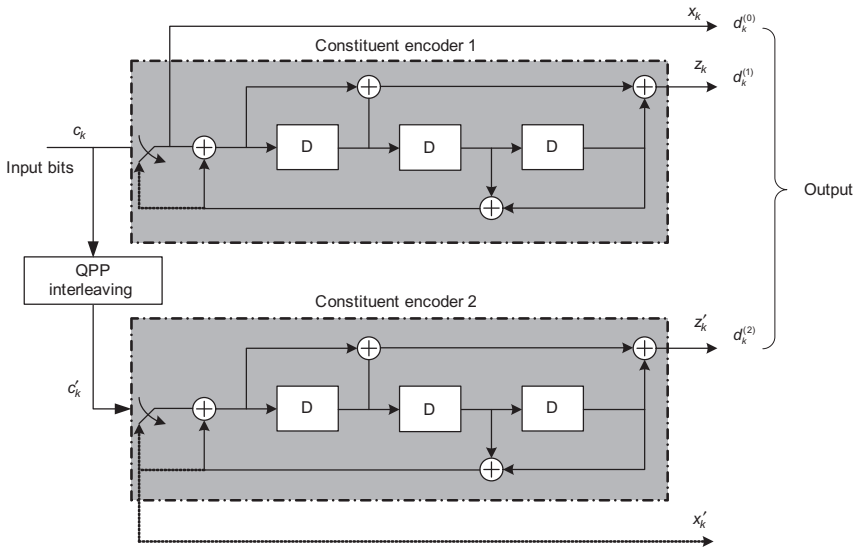


FIGURE 9.81

Structure of an LTE turbo coder [4].

and f_2 are chosen depending on the length of the input data. As an example, if $K = 40$ then $f_1 = 3$, $f_2 = 10$, consequently one can find the permutation pattern as $\Phi(i) = \{0, 13, 6, 19, 12, 25, 18, 31, 24, 37, 30, 3, 36, 9, 2, 15, 8, 21, 14, 27, 20, 33, 26, 39, 32, 5, 38, \ldots\}$. Following processing at the rate-matching block, as explained earlier and shown in Figure 9.82, the rate-matched code blocks are sequentially concatenated to create the output of the channel coding process as $f_k, k = 0, 1, \ldots, N_F - 1$ (Figure 9.83). The sequence of coded bits corresponding to one transport block following code block concatenation is referred to as one codeword. In the case of multiple transport blocks per TTI, the transport block to codeword mapping is performed depending on the DCI Format [3,4].

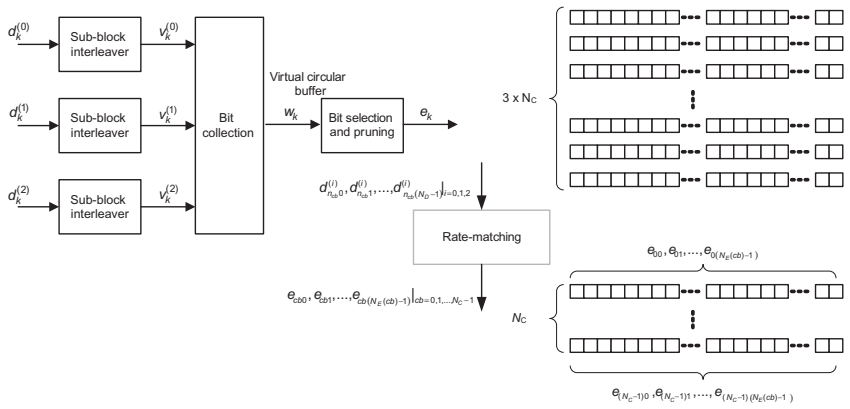


FIGURE 9.82

Illustration of the rate-matching process [158].

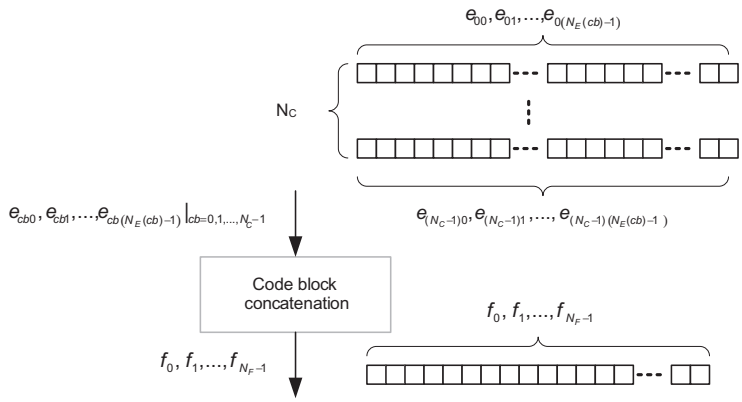


FIGURE 9.83

Illustration of the block concatenation process [158].

Petitioners' Exhibit 1021
Nokia of America Corp., et al. v. KT Corporation, et al.
Case No. IPR2025-00036; U.S. Patent No. 11,627,631
Page 554 of 1122

9.12 Downlink physical channel processing

This section describes the general physical layer processing structure through which physical channels are processed. As shown in Figure 9.84, data arrives at the coding unit in the form of a maximum of two transport blocks in each TTI. The transport blocks are appended with a CRC which is further scrambled with user identity. If the size of the transport blocks is larger than the maximum coding block size permitted by the physical layer, the code blocks are segmented, and a new CRC is calculated and affixed to each code block. Channel coding and rate-matching are later performed, and the code blocks are concatenated to create the codewords that are the input to the physical channel processing units. In order to generate the baseband signal corresponding to a downlink physical channel, the following processing steps are taken in sequence: (1) scrambling of coded bits in each of the codewords to be transmitted on a physical channel; (2) modulation of scrambled bits to generate complex-valued modulation symbols; (3) mapping of the complex-valued modulation symbols to one or several transmission layers; (4) precoding of the complex-valued modulation symbols on each layer for transmission on the antenna ports; (5) mapping of complex-valued modulation symbols for each antenna port to resource elements; and (6) generation of a complex-valued time-domain OFDM signal for each antenna port. Figure 9.84 depicts the entire physical channel processing from the point that one transport block is delivered to the physical layer by the MAC sub-layer to the point where the $I-Q$ components of the baseband signal to be transmitted on each antenna port are generated.

One or two coded transport blocks (or codewords) can be transmitted simultaneously on PDSCH depending on the precoding scheme used. The codewords undergo scrambling, modulation, layer mapping, precoding and resource element mapping procedures as shown in Figure 9.84. In the following, the function of each block in Figure 9.84 will be described. The specific details about physical layer processing pertaining to physical channels will be described in the next sections.

The block of coded bits $(b_0^l, b_1^l, \ldots, b_{(N_c^l-1)}^l)$ corresponding to codeword $l = 0, 1$, where N_c^l is the number of bits in codeword l transmitted on a physical channel in one subframe are scrambled prior to modulation, resulting in a block of scrambled

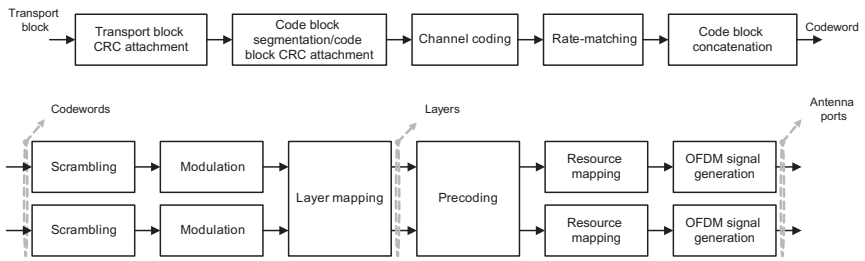


FIGURE 9.84

Overview of downlink physical channel processing in LTE/LTE-Advanced [3,4].

Petitioners' Exhibit 1021
Nokia of America Corp., et al. v. KT Corporation, et al.
Case No. IPR2025-00036; U.S. Patent No. 11,627,631
Page 555 of 1122

bits $(\hat{b}_0^l, \hat{b}_1^l, \ldots, \hat{b}_{(N_c^l-1)}^l)$ in which $\hat{b}_i^l = (b_i^l + c^l(i))\text{mod } 2$. The scrambling sequence $c^l(i)$ was defined in previous sections. The scrambling sequence generator is initialized at the start of each subframe with the value of c_{init} whose definition depends on the transport channel type as follows: $c_{\text{init}} = n_{\text{RNTI}}2^{14} + l2^{13} + \lfloor n_s/2 \rfloor 2^9 + N_{\text{ID}}^{\text{cell}}$ for PDSCH, and $c_{\text{init}} = \lfloor n_s/2 \rfloor 2^9 + N_{\text{ID}}^{\text{MBSFN}}$ for PMCH. In the expression for PDSCH scrambling sequence initialization, n_{RNTI} corresponds to the RNTI associated with the PDSCH transmission to a specific user. The maximum number of codewords that can be transmitted in one downlink subframe is two.

For each codeword, the block of scrambled bits $(\hat{b}_0^l, \hat{b}_1^l, \ldots, \hat{b}_{(N_c^l-1)}^l)$ are modulated using one of the modulation schemes supported in the downlink, i.e., QPSK, 16QAM, 64QAM, resulting in a block of complex-valued modulation symbols $(d_0^l, d_1^l, \ldots, d_{(N_s^l-1)}^l)$. The complex-valued modulation symbols for each of the codewords are mapped to one or several layers. The complex-valued modulation symbols $(d_0^l, d_1^l, \ldots, d_{(N_s^l-1)}^l)$ for each codeword are mapped to the layers $\mathbf{x}_i = (x_i^0, x_i^1, \ldots, x_i^{N_l-1})^{\text{T}}$, $i = 0, 1, \ldots, N_s^l - 1$ where N_l is the number of layers and N_s^l is the number of modulation symbols per layer.

It will be discussed later in this chapter that LTE Rel-8/9 supports multi-antenna schemes in both downlink and uplink directions. In the downlink direction, up to four transmit antennas may be used with the maximum number of codewords of two, irrespective of the number of antennas. Advanced antenna techniques such as spatial multiplexing and beamforming were supported in the downlink to increase peak data rates and capacity. In downlink SU-MIMO, the eNB may transmit one or more layers to the same UE to take advantage of capacity gains associated with using multiple transmit/receive antennas in rich scattering environments. The UE provides the channel quality feedback and the preferred number of layers as well as the precoding matrix index to the eNB. In downlink MU-MIMO, the eNB attempts to increase capacity by transmitting to multiple users using its multiple transmit antennas at the same time and also using the same time-frequency resources. The UEs must feedback channel state information so that the eNB can schedule the UEs with sufficient channel separation together. The transmitted data is precoded to maximize throughput for users and minimize inter-user interference. In uplink direction, only MU-MIMO was supported, i.e., there is only one modulated symbol stream per UE to be received by the eNB; however, multiple UEs may transmit on the same time−frequency resources. Considering the specified UE categories for LTE Rel-8/9, one can expect two transmit antenna in the downlink and one transmit antenna in the uplink to be the baseline configuration for early LTE deployments. LTE-Advanced extended the MIMO capabilities of LTE Rel-8/9 to eight transmit antennas in the downlink and four transmit antennas in the uplink as well as new SU-MIMO and MU-MIMO modes in the downlink and uplink.

When using transmit diversity, the layer mapping is done with only one codeword, and the number of layers N_l is equal to the number of antenna ports used for

Petitioners' Exhibit 1021
Nokia of America Corp., et al. v. KT Corporation, et al.
Case No. IPR2025-00036; U.S. Patent No. 11,627,631
Page 556 of 1122

transmission of the corresponding physical channel. In the case of transmit diversity with two layers, even-indexed modulation symbols are mapped to layer 0 and odd-indexed modulation symbols are mapped to layer 1. In the case of transmit diversity with four layers, the input symbols are mapped to layers sequentially as shown in Figure 9.85. If the total number of input symbols is not divisible by four ($N_s^0 \bmod 4 \neq 0$), then two null symbols are appended to the end of the symbol sequence. This creates a total number of symbols which is an integer multiple of four, as the original number of symbols will always be an integer multiple of two [3,160].

For spatial multiplexing, the mapping of complex-valued modulation symbols to spatial layers depends on the number of codewords and the number of layers, as illustrated in Figures 9.85 and 9.86 for single codeword and dual codeword layer mapping, respectively. In this case, the number of layers N_l is less than or equal to the number of antenna ports used for transmission of the corresponding physical channel. The case of a single codeword mapped to multiple layers is only applicable when the number of CRSs is four, or when the number of UE-specific reference signals is two or larger. If only one layer is used, then $x_i^0 = d_i^0$ for $i = 0, 1, \ldots, N_s^l - 1$. When one codeword is mapped to two layers, even-indexed modulation symbols are mapped to layer 0 and odd-indexed modulation symbols are mapped to layer 1. If two codewords are mapped to two layers, then codeword 0 is mapped to layer 0 and codeword 1 is mapped to layer 1. In the case of three layers, codeword 0 is mapped to layer 0, even symbols within codeword 1 are mapped to layer 1, and odd symbols within codeword 1 are mapped to layer 2. In the case of four layers, two codewords must be used. In this case, the even symbols of codeword 0 are mapped to layer 0, and the odd symbols are mapped to layer 1. The even symbols of codeword 1 are mapped to layer 2, and the odd symbols are mapped to layer 3. The above layer mapping schemes for spatial multiplexing are illustrated in Figures 9.85 and 9.86. Note that LTE Rel-10 supports downlink spatial multiplexing up to eight layers. The mapping of modulation symbols to 5, 6, 7, or 8 layers with two codewords is simply the extension of the above symbol mapping method [3].

The precoding block in Figure 9.84 receives input complex-valued vectors $\mathbf{x}_i = (x_i^0, x_i^1, \ldots, x_i^{N_l - 1})^{\mathrm{T}}$, with $i = 0, 1, \ldots, N_s^l - 1$ and N_s^l denoting the number of modulation symbols per layer, from the layer-mapping block and generates a block of complex-valued vectors $\mathbf{y}_i = (y_i^0, y_i^1, \ldots, y_i^{N_P - 1})^{\mathrm{T}}$ to be mapped to resource elements on each antenna port, where $i = 0, 1, \ldots, N_s^p - 1$, N_s^p denotes the number of symbols per antenna port, N_p is the number of antenna ports used for transmission of the corresponding physical channel, and y_i^p represents the ith symbol for antenna port p. For transmission on a single antenna port, the precoding function is defined as $y_i^p = x_i^0$ where $p \in \{0, 4, 5, 7, 8\}$ is the number of the single-antenna ports used for transmission of the physical channel, $i = 0, 1, \ldots, N_s^p - 1$, and $N_s^p = N_s^l$ [3].

The precoding function for spatial multiplexing using antenna ports associated with CRSs is only used in conjunction with layer mapping and supports two or four antenna ports. The set of antenna ports is given by $p \in \{0, 1\}$ or $p \in \{0, 1, 2, 3\}$.

Petitioners' Exhibit 1021
Nokia of America Corp., et al. v. KT Corporation, et al.
Case No. IPR2025-00036; U.S. Patent No. 11,627,631
Page 557 of 1122

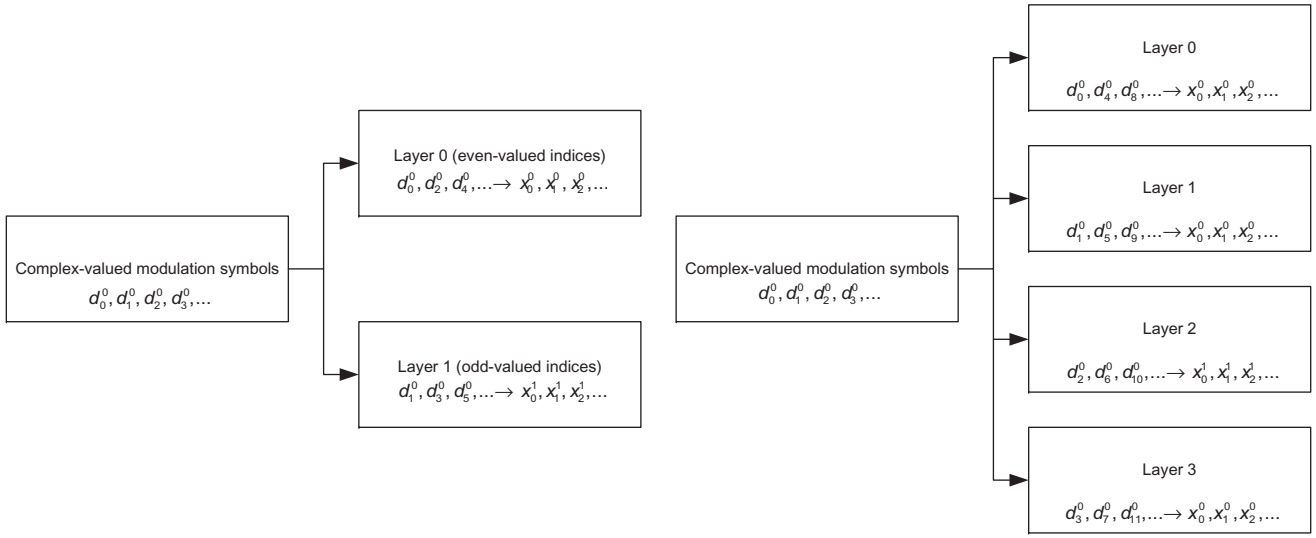


FIGURE 9.85

Layer mapping for 2 and 4 layer transmit diversity (single codeword) [3,160].

Petitioners' Exhibit 1021
Nokia of America Corp., et al. v. KT Corporation, et al.
Case No. IPR2025-00036; U.S. Patent No. 11,627,631
Page 558 of 1122

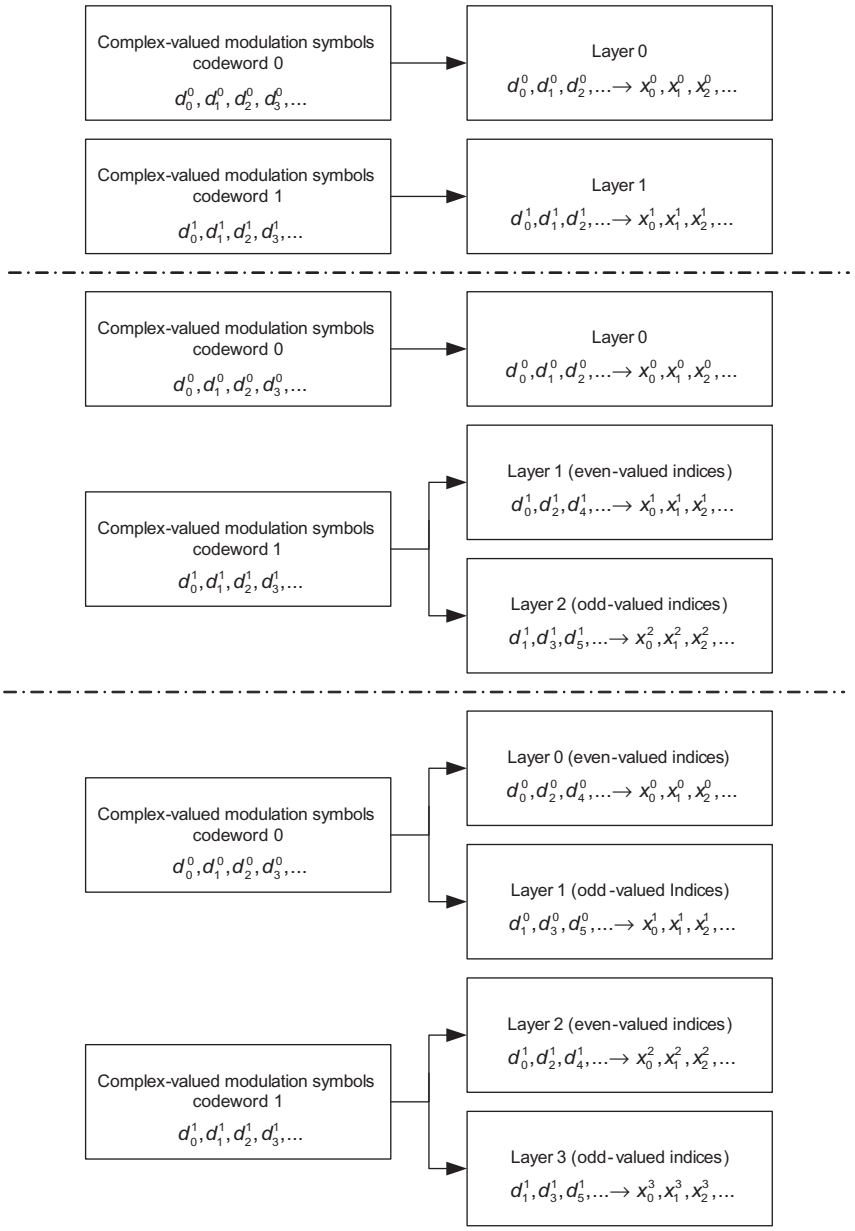


FIGURE 9.86

Layer mapping for spatial multiplexing with 2, 3, and 4 layers (dual codeword) [3,160].

Petitioners' Exhibit 1021
Nokia of America Corp., et al. v. KT Corporation, et al.
Case No. IPR2025-00036; U.S. Patent No. 11,627,631
Page 559 of 1122

The precoding function for spatial multiplexing without cyclic delay diversity (CDD) is defined as $(y_i^0, y_i^1, \ldots, y_i^{N_p-1})^{\mathrm{T}} = \mathbf{W}_i(x_i^0, x_i^1, \ldots, x_i^{N_l-1})^{\mathrm{T}}$ where the precoding matrix $\mathbf{W}_i$ is of size $N_p \times N_l$ and $i = 0, 1, \ldots, N_s^p - 1$, and $N_s^p = N_s^l$. The values of $\mathbf{W}_i$ are selected among the precoder elements in the codebook configured and stored in the eNB and the UE. The eNB can further restrict the precoder selection in the UE to a subset of the elements in the codebook.

In the case of precoding using large-delay CDD, the precoder for spatial multiplexing is defined as $(y_i^0, y_i^1, \ldots, y_i^{N_p-1})^{\mathrm{T}} = \mathbf{W}_i\mathbf{D}_i\mathbf{U}(x_i^0, x_i^1, \ldots, x_i^{N_l-1})^{\mathrm{T}}$, where the precoding matrix $\mathbf{W}_i$ is of size $N_p \times N_l$ and $i = 0, 1, \ldots, N_s^p - 1$ and $N_s^p = N_s^l$. The diagonal matrix $\mathbf{D}_i$ that is an $N_l \times N_l$ matrix which defines CDD, and the square matrix $\mathbf{U}$ is given in Table 9.18 for different numbers of transmission layers N_l. Similar to the previous scenario, the values of $\mathbf{W}_i$ are selected among the precoder elements in the codebook configured and stored in the eNB and the UE. The eNB can limit the precoder selection in the UE to a subset of the elements in the codebook.

Precoding for transmit diversity is only used in combination with layer mapping. The precoding operation for transmit diversity is defined for two and four antenna ports. For transmission on two antenna ports $p \in \{0, 1\}$, the output vector $\mathbf{y}_i = (y_i^0, y_i^1)^{\mathrm{T}}$ with $i = 0, 1, \ldots, N_s^p - 1$ is defined as follows:

$$\begin{bmatrix} y_{2i}^0 \\ y_{2i}^1 \\ y_{2i+1}^0 \\ y_{2i+1}^1 \end{bmatrix} = \frac{1}{\sqrt{2}} \begin{bmatrix} 1 & 0 & \mathrm{j} & 0 \\ 0 & -1 & 0 & \mathrm{j} \\ 0 & 1 & 0 & \mathrm{j} \\ 1 & 0 & -\mathrm{j} & 0 \end{bmatrix} \begin{bmatrix} \mathrm{Re}(x_i^0) \\ \mathrm{Re}(x_i^1) \\ \mathrm{Im}(x_i^0) \\ \mathrm{Im}(x_i^1) \end{bmatrix} \tag{9.50}$$

where $i = 0, 1, \ldots, N_s^l - 1$ and $N_s^p = 2N_s^l$.

For transmission on four antenna ports $p \in \{0, 1, 2, 3\}$ and for the purpose of CSI reporting based on antenna ports $p \in \{0, 1, 2, 3\}$ or $p \in \{15, 16, 17, 18\}$, the precoding matrix $\mathbf{W}_i$ is defined based on Householder codebook[19] $\mathbf{W}_n = \mathbf{I}_4 - 2\mathbf{u}_n\mathbf{u}_n^{\mathrm{H}}/\mathbf{u}_n^{\mathrm{H}}\mathbf{u}_n$ where $\mathbf{I}_4$ is a 4×4 identity matrix and the vector $\mathbf{u}_n$ is defined in Table 9.18.

[19]In linear algebra, a Householder transformation is defined as a linear transformation that performs a reflection about a plane or hyper-plane containing the origin. The reflection about the hyper-plane can be defined by a unit vector $\mathbf{u}_n$ which is orthogonal to the hyper-plane. The reflection of a vector $\mathbf{x}$ about this hyper-plane is defined as $\mathbf{x} - 2\langle\mathbf{u}_n, \mathbf{x}\rangle\mathbf{u}_n = \mathbf{x} - 2\mathbf{u}_n(\mathbf{u}_n{}^{\mathrm{H}}\mathbf{x})$ where $\mathbf{u}_n$ is given as a column unit vector. This is a linear transformation given by the Householder matrix $\mathbf{\Lambda} = \mathbf{I} - 2\mathbf{u}_n\mathbf{u}_n{}^{\mathrm{H}}$ in which $\mathbf{I}$ denotes the identity matrix. The Householder matrix has the following properties [31,32]:

1. It is a Hermitian matrix $\mathbf{\Lambda} = \mathbf{\Lambda}^{\mathrm{H}}$
2. It is a unitary matrix $\mathbf{\Lambda}^{-1} = \mathbf{\Lambda}^{\mathrm{H}}$ hence it is involutary $\mathbf{\Lambda}^2 = \mathbf{I}$. An involutary function is a function $f(x)$ that is its own inverse function, i.e., $f(f(x)) = x, \forall x$.
3. The eigenvalues of the Householder matrix are ± 1.
4. The determinant of a Householder reflector is $\det(\mathbf{\Lambda}) = -1$ given that the determinant of a matrix is the product of its eigenvalues.

Petitioners' Exhibit 1021
Nokia of America Corp., et al. v. KT Corporation, et al.
Case No. IPR2025-00036; U.S. Patent No. 11,627,631
Page 560 of 1122

Table 9.18 Codebook for Spatial Multiplexing with and without CDD [3]

N_l	U	D_i	W_i
2	$\frac{1}{\sqrt{2}}\begin{bmatrix}1 & 1\\ 1 & e^{-j2\pi/2}\end{bmatrix}$	$\begin{bmatrix}1 & 0\\ 0 & e^{-j2\pi i/2}\end{bmatrix}$	$N_{TX}=2$: $\mathbf{W}_i=\frac{1}{\sqrt{2}}\begin{bmatrix}1 & 0\\ 0 & 1\end{bmatrix}$ $N_{TX}=4$: $\mathbf{W}_n=\mathbf{I}_4-2\mathbf{u}_n\mathbf{u}_n^H/\mathbf{u}_n^H\mathbf{u}_n$ $n=12,13,14,15$
3	$\frac{1}{\sqrt{3}}\begin{bmatrix}1 & 1 & 1\\ 1 & e^{-j2\pi/3} & e^{-j4\pi/3}\\ 1 & e^{-j4\pi/3} & e^{-j8\pi/3}\end{bmatrix}$	$\begin{bmatrix}1 & 0 & 0\\ 0 & e^{-j2\pi i/3} & 0\\ 0 & 0 & e^{-j4\pi i/3}\end{bmatrix}$	$\mathbf{W}_n=\mathbf{I}_4-2\mathbf{u}_n\mathbf{u}_n^H/\mathbf{u}_n^H\mathbf{u}_n$ $n=12,13,14,15$
4	$\frac{1}{2}\begin{bmatrix}1 & 1 & 1 & 1\\ 1 & e^{-j2\pi/4} & e^{-j4\pi/4} & e^{-j6\pi/4}\\ 1 & e^{-j4\pi/4} & e^{-j8\pi/4} & e^{-j12\pi/4}\\ 1 & e^{-j6\pi/4} & e^{-j12\pi/4} & e^{-j18\pi/4}\end{bmatrix}$	$\begin{bmatrix}1 & 0 & 0 & 0\\ 0 & e^{-j2\pi i/4} & 0 & 0\\ 0 & 0 & e^{-j4\pi i/4} & 0\\ 0 & 0 & 0 & e^{-j6\pi i/4}\end{bmatrix}$	$\mathbf{W}_n=\mathbf{I}_4-2\mathbf{u}_n\mathbf{u}_n^H/\mathbf{u}_n^H\mathbf{u}_n$ $n=12,13,14,15$

Precoding for spatial multiplexing using antenna ports with UE-specific reference signals is only applicable in conjunction with layer mapping, and supports up to eight antenna ports where the set of antenna ports is given by $p = 7, 8, \ldots, N_l + 6$. For transmission on $N_p = N_l$ antenna ports, the precoding operation is defined by $(y_i^7, y_i^8, \ldots, y_i^{N_l+6})^{\mathrm{T}} = (x_i^0, x_i^1, \ldots, x_i^{N_l-1})^{\mathrm{T}}$, where $i = 0, 1, \ldots, N_s^p - 1$ and $N_s^p = N_s^l$.

For each antenna port used for transmission of the physical channels, the block of complex-valued symbols $y_0^p, \ldots, y_{N_s^p-1}^p$ must be sequentially mapped (starting with y_0^p) to resource elements (k, l) whose coordinates satisfy the following criteria: (1) these resource elements are in the PRBs corresponding to the designated VRBs; (2) these resource elements are not used for transmission of PBCH, synchronization signals, CRSs, MBSFN reference signals, or UE-specific reference signals; (3) the UE assumes that these resource elements are not used for transmission of CSI-RSs and the DCI associated with the downlink transmission using the C-RNTI or semi-persistent C-RNTI; and (4) index l in the first slot in a subframe satisfies $l \geq l_{\mathrm{DataStart}}$, where $l_{\mathrm{DataStart}}$ is the starting OFDM symbol index for corresponding downlink transmission. Therefore, for each antenna port used for transmission of PDSCH, the block of complex-valued symbols y_i^p are mapped in sequential order to resource elements that are not occupied by the PCFICH, PHICH, PDCCH, PBCH or synchronization, and reference signals. The number of resource elements involved in this mapping is controlled by the number of resource blocks allocated to PDSCH. The symbols are mapped by increasing the sub-carrier index and mapping all available resource elements within allocated resource blocks for each OFDM symbol, as shown in Figure 9.87.

9.12.1 Physical control format indicator channel

The PCFICH carries information about the number of OFDM symbols used for transmission of PDCCHs in a subframe. In other words, the PCFICH carries a control format indicator (CFI) which indicates the number of OFDM symbols, which is typically 1, 2, or 3, except for system bandwidth less than 5 MHz, used for transmission of control channel information in each subframe. In principle, the UE can intuitively deduce the value of the CFI without using PCFICH, e.g., by multiple attempts to blindly decode the control channels assuming each possible number of symbols, but this would result in significant additional processing complexity. Three different CFI values are used in LTE/LTE-Advanced. In order to make the CFI sufficiently robust, each codeword is 32 bits long and is mapped to 16 resource elements using QPSK modulation. These 16 resource elements are organized in groups of four resource elements, known as REGs. The resource elements occupied by reference signals are not included within the REGs, which means that the total number of REGs in a given OFDM symbol depends on whether cell-specific reference signals are present. The concept of REGs (i.e., mapping in groups of four resource elements) is also used for PHICH and

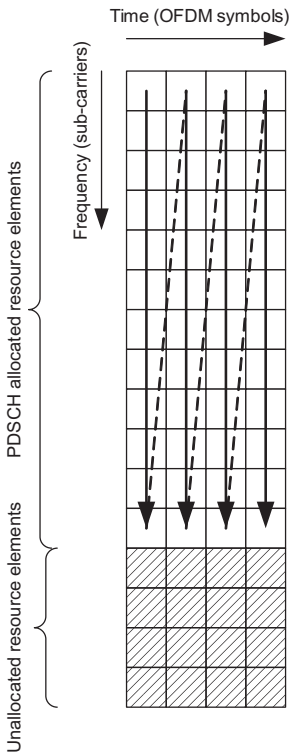


FIGURE 9.87

Resource element mapping [160].

PDCCH control channels. The PCFICH is transmitted on the same set of antenna ports as PBCH. The transmit diversity is applied if more than one antenna port is used. In order to achieve frequency diversity, the four REGs carrying the PCFICH are distributed across the frequency-domain. This is done according to a predefined pattern in the first OFDM symbol of each downlink subframe (Figure 9.88), so that the UEs can always locate the PCFICH information, which is a prerequisite for detection and decoding of the other control channels. To minimize the inter-cell interference, as well as the possibility of confusion with PCFICH information transmitted from neighboring cells, a cell-specific frequency offset is applied to the positions of the PCFICH resource elements. The offset value depends on the physical cell identity, which is derived from the primary and secondary synchronization signals. In addition, a cell-specific scrambling sequence is applied to the CFI codewords, so that the UE can preferentially receive PCFICH from the desired cell site.

Petitioners' Exhibit 1021
Nokia of America Corp., et al. v. KT Corporation, et al.
Case No. IPR2025-00036; U.S. Patent No. 11,627,631
Page 563 of 1122

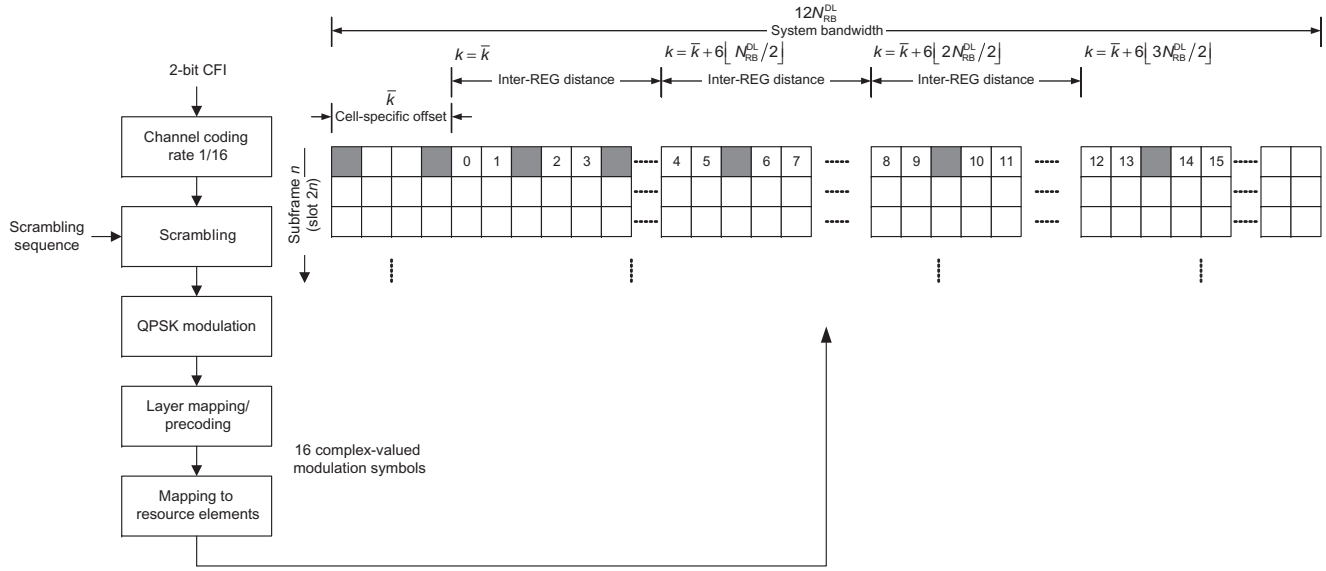


FIGURE 9.88

PCFICH physical layer processing [15,162].

Petitioners' Exhibit 1021
Nokia of America Corp., et al. v. KT Corporation, et al.
Case No. IPR2025-00036; U.S. Patent No. 11,627,631
Page 564 of 1122

As shown in Figure 9.88, the block of coded bits $(b_0, \ldots, b_{31})$ containing CFI information (i.e., 2 bits of information encoded at the rate 1/16) transmitted in one subframe are scrambled with a cell-specific sequence prior to modulation, resulting in a block of scrambled bits $(\tilde{b}_0, \ldots, \tilde{b}_{31})$, where $\tilde{b}_i = (b_i + c(i))\text{mod } 2$. The scrambling sequence $c(i)$ defined in previous sections is initialized with $c_{\text{init}} = \left(\lfloor n_s/2 \rfloor + 1\right)\left(2N_{\text{ID}}^{\text{cell}} + 1\right)2^9 + N_{\text{ID}}^{\text{cell}}$ at the start of each subframe. The block of scrambled bits $(\tilde{b}_0, \ldots, \tilde{b}_{31})$ is modulated using QPSK modulation, resulting in a block of complex-valued modulation symbols $(d_0, \ldots, d_{15})$ which are mapped to spatial layers using a transmit diversity transmission mode with $N_s^0 = 16$, i.e., 16 complex-valued modulation symbols per layer and are precoded, resulting in a block of vectors $\mathbf{y}_i = (y_i^0, y_i^1, \ldots, y_i^{N_p-1})^{\text{T}}$, $i = 0, \ldots, 15$, where y_i^p represents the signal for antenna port p and $p = 0, \ldots, N_p - 1$. The number of antenna ports for cell-specific reference signals $N_p \in \{1, 2, 4\}$. The PCFICH is transmitted on the same set of antenna ports that are used for transmission of PBCH. The mapping to resource elements is defined in terms of quadruplets of complex-valued symbols. Let $Z_i^P = (y_{4i}^P, y_{4i+1}^P, y_{4i+2}^P, y_{4i+3}^P)$ denote symbol quadruplet i for antenna port p. For each of the antenna ports, symbol quadruplets are mapped in increasing order of index i to four resource-element groups in the first OFDM symbol in a downlink subframe (assuming 12 sub-carriers per resource block) in the following manner:

$$\begin{aligned}
&Z_0^P \quad \text{is mapped to the resource-element represented by} \quad k = \overline{k} \\
&Z_1^P \quad \text{is mapped to the resource-element represented by} \quad k = \overline{k} + 6\lfloor N_{\text{RB}}^{\text{DL}}/2 \rfloor \\
&Z_2^P \quad \text{is mapped to the resource-element represented by} \quad k = \overline{k} + 6\lfloor 2N_{\text{RB}}^{\text{DL}}/2 \rfloor \\
&Z_3^P \quad \text{is mapped to the resource-element represented by} \quad k = \overline{k} + 6\lfloor 3N_{\text{RB}}^{\text{DL}}/2 \rfloor
\end{aligned} \tag{9.51}$$

where the additions are modulo $12N_{\text{RB}}^{\text{DL}}$, $\overline{k} = 6(N_{\text{ID}}^{\text{cell}} \bmod 2N_{\text{RB}}^{\text{DL}})$ and $N_{\text{ID}}^{\text{cell}}$ is the physical-layer cell identity. The above procedure is illustrated in Figure 9.88.

9.12.2 Physical broadcast channel

The essential system information which allows the other channels in the cell to be configured and operated is carried by PBCH. Therefore, the reliability and coverage of the PBCH is crucial for the successful operation of LTE/LTE-Advanced systems. The system information is divided into two categories: (1) the master information block as given in Table 9.19, which consists of a limited number of the most frequently transmitted parameters essential for initial access to the cell which is carried in PBCH; and (2) the other system information blocks (SIBs) which are multiplexed with unicast data and are transmitted in PDSCH. The design requirements for PBCH are as follows:

- The UE must be able to detect the PBCH without prior knowledge of the system bandwidth.
- The PBCH must have negligible impact on the total physical layer overhead.
- The PBCH must be reliably received by the cell-edge UEs.
- The PBCH must be decodable with low latency and complexity to reduce the impact on the UE battery life.

Petitioners' Exhibit 1021
Nokia of America Corp., et al. v. KT Corporation, et al.
Case No. IPR2025-00036; U.S. Patent No. 11,627,631
Page 565 of 1122

Table 9.19 Contents of the Master Information Block [9]

Parameter	Size (Bits)	Description
Downlink channel bandwidth	3	Selects one of the configured downlink system bandwidths in terms of the number of resource blocks (i.e., $N_{RB}^{DL} = 6, 15, 25, 50, 75, 100$)
PHICH configuration: PHICH Duration	1	Selects between two options "normal" and "extended" where normal refers to one OFDM symbol and extended refers to three OFDM symbols
PHICH configuration: PHICH Resource	2	Selects one of the values of PHICH group scaling factor $N_g \in \{1/6, 1/2, 1, 2\}$
System frame number (SFN)	8	Most significant bits of the 10-bit system frame number. The two least significant bits of the SFN are deducted by the UE from the position of the PBCH (i.e., within 40 ms PBCH TTI, the first radio frame: 00, the second radio frame: 01, the third radio frame: 10, the last radio frame: 11)
Unused bits	10	Null bits for future extensions

The overall PBCH structure is shown in Figure 9.89. The detectability of the PBCH without the UE's prior knowledge of the system bandwidth is achieved by mapping the PBCH to the center of the band using 72 sub-carriers, which corresponds to the minimum system bandwidth of six resource blocks, regardless of the actual system bandwidth. The UE will have to identify the system center frequency from the synchronization signals as described in earlier sections. Minimizing the impact on total overhead is achieved by deliberately keeping the amount of information carried by the PBCH to a minimum, since achieving stringent coverage requirements for a large quantity of data would result in a high system overhead. The size of MIB it is 24 bits and it is transmitted every 40 ms. In order to achieve reliable reception, time diversity, FEC, and antenna diversity mechanisms are used to transmit PBCH. Time diversity is introduced by spreading the transmission of the PBCH over a period of 40 ms with three retransmissions at 10 ms intervals. This significantly reduces the likelihood of missing/mis-detection of MIB due to multipath fading, interference, and noise in the radio channel, even when the mobile terminal is moving at high speeds.

The FEC coding for PBCH utilizes a tail-biting convolutional coder, considering that the number of information bits to be encoded is small and turbo codes are typically not suitable for small payloads. The basic code rate is 1/3, after which a high repetition factor is applied to the systematic and parity bits such that each MIB is coded at a very low code rate (1/48 over a 40 ms period) to provide strong error protection. Antenna diversity may be utilized at the eNB and the UE. The UE performance requirements specified for LTE/LTE-Advanced assume that all UEs can achieve a level of decoding performance proportional to dual-antenna

Petitioners' Exhibit 1021
Nokia of America Corp., et al. v. KT Corporation, et al.
Case No. IPR2025-00036; U.S. Patent No. 11,627,631
Page 566 of 1122

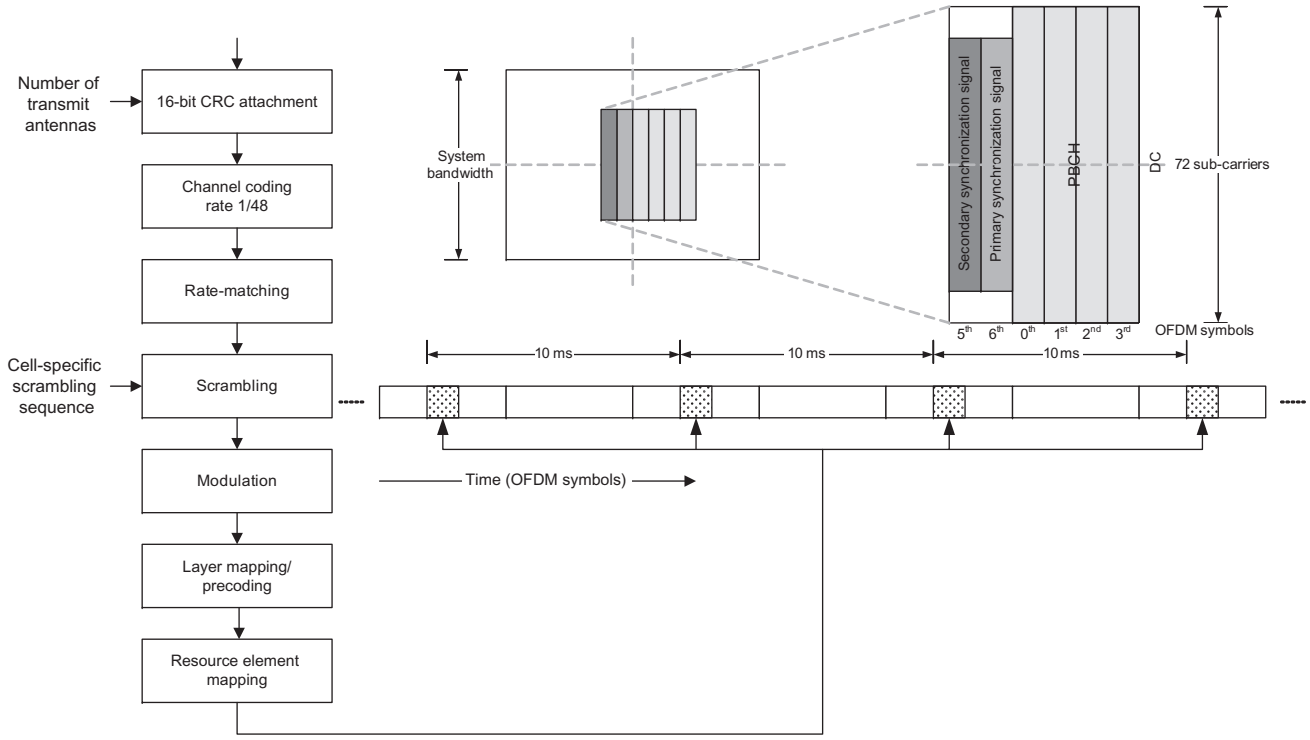


FIGURE 9.89

PBCH transmission and physical layer processing [162].

receive diversity, although it is understood that in low-frequency deployments, e.g., below 1 GHz, the advantage obtained from receive diversity is reduced due to the correspondingly higher correlation between the antennas. This enables wider or more reliable cell coverage to be achieved with fewer cell sites.

Transmit antenna diversity may be employed at the eNB to further improve coverage, depending on eNB implementation, eNB may transmit PBCH with two or four transmit antennas using an SFBC scheme. The set of resource elements designated to PBCH transmission is independent of the number of transmit antennas at the eNB, thereby any resource elements which may be used for cell-specific reference signals transmission are avoided by the PBCH, irrespective of the actual number of transmit antenna ports used by the eNB. The number of transmit antennas used by the eNB is blindly detected by the UE by decoding PBCH transmission corresponding to a different number of transmit antennas (i.e., one, two, or four). The detection of the number of transmit antennas is further facilitated by masking the CRC of each MIB with a unique masking sequence representing the number of transmit antenna ports. The 16-bit PBCH CRC masking sequence is $\langle 0,0,0,0,0,0,0,0,0,0,0,0,0,0,0,0\rangle$,$\langle 1,1,1,1,1,1,1,1,1,1,1,1,1,1,1,1\rangle$, or $\langle 0,1,0,1,0,1,0,1,0,1,0,1,0,1,0,1\rangle$ for one, two, or four transmit antennas, respectively.

Achieving low latency and minimal impact on UE battery life are facilitated through use of a low code rate with repetition wherein the set of coded bits are divided into four subsets, each of which is self-decodable. Each subset of the coded bits is transmitted in a different radio frame during the 40 ms transmission period, as shown in Figure 9.89. This means that if the SINR is sufficiently good to allow the UE to successfully decode the MIB in less than four radio frames, then the UE does not need to receive the other parts of the PBCH transmission in the remainder of the 40 ms period. On the other hand, if the SINR is low, the UE can take advantage of soft-combing of other parts of the MIB transmission until MIB is successfully decoded. The UE does not know in advance the timing of the 40 ms transmission interval for each MIB on the PBCH; therefore, this information is determined implicitly from the scrambling and bit positions, which are reinitialized every 40 ms. The UE can initially determine the 40 ms timing by performing four separate decodings of the PBCH using each of the four possible phases of the PBCH scrambling code and checking the CRC for each decoding.

When a UE initially attempts to select a cell by acquiring the PBCH, different approaches may be taken to perform the necessary blind decoding. A simple approach is to perform the decoding using soft combing of the PBCH instances over four radio frames, advancing a 40 ms sliding window one radio frame at a time until the sliding window aligns with the 40 ms period of the PBCH and the decoding succeeds. However, this would result in a 40−70 ms delay before the PBCH can be decoded. A faster approach would be to attempt to decode the PBCH from the first radio frame, which should be possible provided that the SINR is sufficiently high. If the decoding fails for all four possible scrambling sequences, the PBCH from the first frame could be soft-combined with the next

Petitioners' Exhibit 1021
Nokia of America Corp., et al. v. KT Corporation, et al.
Case No. IPR2025-00036; U.S. Patent No. 11,627,631
Page 568 of 1122

PBCH instances. It is evident that the latter approach may be much faster at the expense of slightly more complexity.

More specifically, the block of coded bits $(b_0, b_1 \ldots, b_{N_{\text{bit}}-1})$ are scrambled with a cell-specific scrambling sequence prior to modulation, resulting in a block of scrambled bits $(\tilde{b}_0, \tilde{b}_1, \ldots, \tilde{b}_{N_{\text{bit}}-1})$ in which $\tilde{b}_i = (b_i + c(i)) \bmod 2$ where the cell-specific scrambling sequence $c(i)$ was defined in the previous sections. The number of bits transmitted on PBCH $N_{\text{bit}} = 1920$ for a normal cyclic prefix and $N_{\text{bit}} = 1728$ for an extended cyclic prefix. The scrambling sequence is initialized with $c_{\text{init}} = N_{\text{ID}}^{\text{cell}}$ in each radio frame, provided that $n_f \bmod 4 = 0$.

The block of scrambled bits $(\tilde{b}_0, \tilde{b}_1, \ldots, \tilde{b}_{N_{\text{bit}}-1})$ is modulated using QPSK modulation, resulting in a block of complex-valued modulation symbols $(d_0, d_1, \ldots, d_{N_s-1})$. The block of modulation symbols $(d_0, d_1, \ldots, d_{N_s-1})$ is mapped to spatial layers with $N_s^0 = N_s$ and precoded, resulting in a block of vectors $\mathbf{y}_i = (y_i^0, y_i^1, \ldots, y_i^{N_p-1})^{\text{T}}$ where $i = 0, 1, \ldots, N_s - 1$ and y_i^p is the signal for antenna port $p = 0, 1, \ldots, N_p - 1$ and $N_p \in \{1, 2, 4\}$.

The block of complex-valued symbols $(y_0^p, y_1^p \ldots, y_{N_s-1}^p)$ for each antenna port is transmitted during four consecutive radio frames starting in the frame whose number satisfies $n_f \bmod 4 = 0$. The symbols are mapped sequentially starting with y_0^p to resource elements (k, l) that are not reserved for transmission of reference signals. The resource mapping is done in increasing order of sub-carrier index k (i.e., frequency first) and then index l (OFDM symbol number) in slot 1 of subframe 0 in each radio frame. The resource-element indices are given by $k = 6N_{\text{RB}}^{\text{DL}} - 36 + k'; k' = 0, 1, \ldots, 71;$ and $l = 0, 1, \ldots, 3$ where resource elements reserved for reference signals are excluded. The mapping procedure assumes that cell-specific reference signals for antenna ports 0−3 are used irrespective of the actual antenna configuration [3].

9.12.3 Physical hybrid-ARQ indicator channel

The PHICH carries the HARQ ACK/NACK, which indicates whether the eNB has correctly received a transmission on PUSCH. The HARQ indicator is set to "0" for a positive acknowledgment and is set to "1" for a negative acknowledgment. This information is repeated in each of three BPSK symbols. Multiple PHICHs are mapped to the same set of resource elements. These constitute a PHICH group, where different PHICHs within the same PHICH group are separated through different complex-valued orthogonal Walsh sequences. Each PHICH is uniquely identified by a PHICH index, which indicates both the group and the sequence. The sequence length is four for the normal cyclic prefix (or two for the extended cyclic prefix). As the sequences are complex-valued, the number of PHICHs in a group, i.e., the number of UEs receiving their acknowledgments on the same set of downlink resource elements, can be up to twice the sequence length. A cell-specific scrambling sequence is applied. A $3\times$ code repetition factor is applied for improved robustness, resulting in three instances of the orthogonal Walsh code being transmitted for each ACK or NACK. The error

Petitioners' Exhibit 1021
Nokia of America Corp., et al. v. KT Corporation, et al.
Case No. IPR2025-00036; U.S. Patent No. 11,627,631
Page 569 of 1122

rate on the PHICH is intended to be in the order of 0.01 for ACKs, and as low as 0.0001 for NACKs. The resulting PHICH construction, including repetition and orthogonal spreading, is shown in Figure 9.90.

The PHICH duration, in terms of the number of OFDM symbols used in the time-domain, is typically one or three OFDM symbols, which is configurable and the eNB broadcasts the configuration information via the PBCH (see Table 9.19). Since the PHICH cannot extend into the PDSCH transmission region, the duration configured for the PHICH puts a lower limit on the size of the control channel region at the start of each subframe. Each of the three instances of the orthogonal code of a PHICH transmission is mapped to a REG on one of the first three OFDM symbols of each subframe, so that each PHICH is partly transmitted on each of the available OFDM symbols. This mapping is illustrated in Figure 9.90 for an example PHICH duration. The PBCH also provides the number of PHICH groups that are configured in the cell, which enables the UEs to derive the resource elements in the control region where the PDCCHs are mapped.

In order to obviate the need for additional signaling to indicate which PHICH carries the ACK/NACK response for each PUSCH transmission, the PHICH index is implicitly associated with the index of the lowest uplink resource block used for the corresponding PUSCH transmission. This relationship is such that adjacent PUSCH resource blocks are associated with PHICHs in different PHICH groups, to enable some degree of load balancing. However, this mechanism alone is not sufficient to enable multiple UEs to be allocated in the same resource blocks for a PUSCH transmission, as occurs in the case of uplink MU-MIMO, in this case, different cyclic shifts of the uplink DM-RSs are configured for the different UEs which are allocated the same time−frequency PUSCH resources, and the same cyclic shift index is then used to shift the PHICH allocations in the downlink so that each UE receives its ACK/NACK on a different PHICH. The above procedures are illustrated in Figure 9.90 [13,14].

Each PHICH group consists of 12 complex-valued symbols which require three REGs and can carry up to four (extended cyclic prefix) or eight (normal cyclic prefix) ACK/NACKs, which are identified within a PHICH group by an orthogonal code. Each PHICH group is identified by a PHICH group number and one of the eight or four orthogonal spreading codes. The starting location of the first REG of the PHICH group is derived from the physical cell identity. The other two groups are equally spaced from the first group.

The PHICH may be configured with a normal or extended duration. In a normal duration, all three REGs of a PHICH group are mapped to the first OFDM symbol. In an extended duration, the three REGs are mapped to three different OFDM symbols, as shown in Figure 9.91. The extended duration PHICH mapping provides time diversity. The duration of the PHICH is signaled via RRC and carried in the PHICH configuration information element.

As mentioned earlier, multiple PHICHs are mapped to the same set of resource elements to create a PHICH group, where PHICHs within the same

Petitioners' Exhibit 1021
Nokia of America Corp., et al. v. KT Corporation, et al.
Case No. IPR2025-00036; U.S. Patent No. 11,627,631
Page 570 of 1122

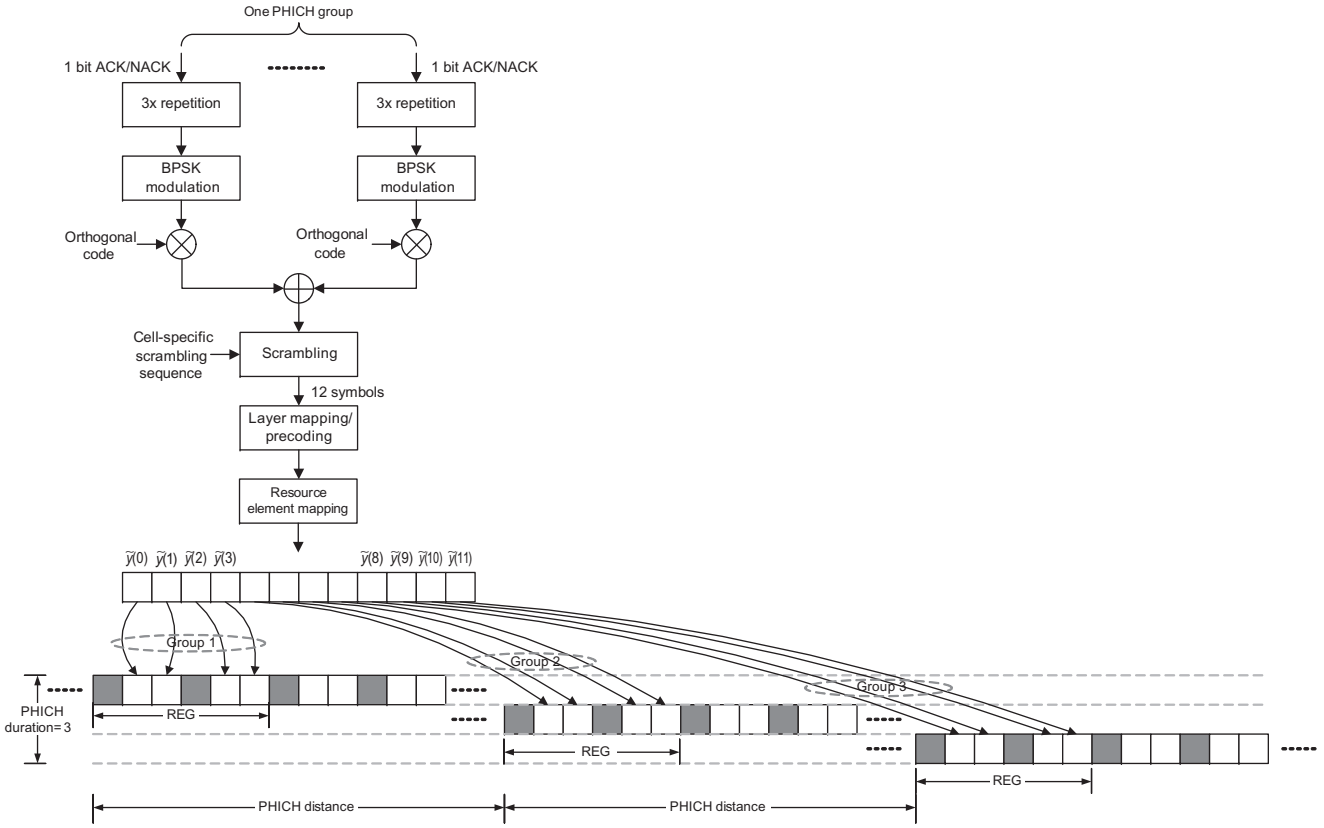


FIGURE 9.90

PHICH physical layer processing and mapping in time and frequency for an FDD system with normal cyclic prefix [15,162].

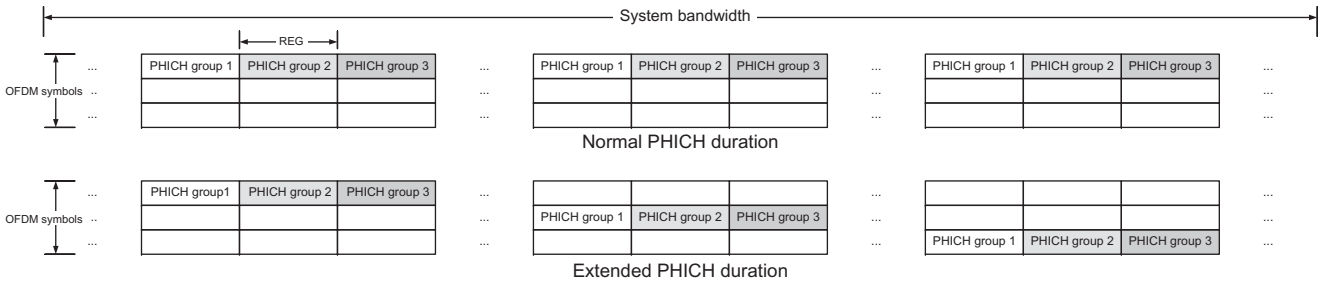


FIGURE 9.91

Illustration of normal and extended PHICH mapping.

PHICH group are separated by different orthogonal sequences. A PHICH resource is identified by the index pair $(n_{\text{PHICH}}^{\text{group}}, n_{\text{PHICH}}^{\text{sequence}})$, where $n_{\text{PHICH}}^{\text{group}}$ denotes the PHICH group number and $n_{\text{PHICH}}^{\text{sequence}}$ is the orthogonal sequence index within the group. For frame structure type 1, the number of PHICH groups $n_{\text{PHICH}}^{\text{group}}$ is constant in all subframes and is given by $N_{\text{PHICH}}^{\text{group}} = \lceil N_g(N_{\text{RB}}^{\text{DL}}/8) \rceil$ for a normal cyclic prefix and $N_{\text{PHICH}}^{\text{group}} = 2\lceil N_g(N_{\text{RB}}^{\text{DL}}/8) \rceil$ for an extended cyclic prefix, in which $N_g \in \{1/6, 1/2, 1, 2\}$ is a parameter configured by higher layers and transmitted in the form of two bits in the PBCH (see Table 9.19). The group index $n_{\text{PHICH}}^{\text{group}}$ assumes integer values between 0 and $N_{\text{PHICH}}^{\text{group}} - 1$. For frame structure type 2, the number of PHICH groups may vary from one downlink subframe to another and is given by $m_i N_{\text{PHICH}}^{\text{group}}$, where the value of parameter $m_i = 0, 1, 2$ depends on the TDD subframe configuration, e.g., $m_i = 1$ for the second subframe in TDD frame configuration 1. The group index $n_{\text{PHICH}}^{\text{group}}$ in a downlink subframe with non-zero PHICH resources assumes integer values between 0 and $m_i N_{\text{PHICH}}^{\text{group}} - 1$.

One may ask at this point how the UEs can find the PHICH corresponding to their earlier PUSCH transmissions. The UE searches for the PHICH in the fourth subframe $(n + 4)$ after an uplink transport block is transmitted in uplink subframe n. The PHICH group and sequence indices are calculated based on the lowest PRB index allocated for PUSCH transmission and the cyclic shift for the PUSCH DM-RS, both of which are associated with the uplink transmission and are provided to the UE in DCI format 0 or DCI format 4. The PHICH resource (N_g) is received in the MIB or in the PHICH configuration information element via dedicated RRC signaling. The ith UE selects its PHICH group and orthogonal sequence index $(n_{\text{PHICH}}^{\text{group}}(i), n_{\text{PHICH}}^{\text{sequence}}(i))$ according to the following rules in an FDD system [13]:

$$\begin{aligned} 1 - n_{\text{PHICH}}^{\text{group}}(i) &= (I_{\text{lowest}} + n_{\text{DM-RS}}) \bmod N_{\text{PHICH}}^{\text{group}} \\ 2 - n_{\text{PHICH}}^{\text{sequence}}(i) &= \left(\lfloor I_{\text{lowest}}/N_{\text{PHICH}}^{\text{group}} \rfloor + n_{\text{DM-RS}} \right) \bmod (2N_{\text{SF}}^{\text{PHICH}}) \end{aligned} \tag{9.52}$$

where $n_{\text{DM-RS}}$ denotes the PUSCH DM-RS cyclic shift signaled in DCI format 0 or 4, and I_{lowest} is the lowest PRB index allocated to the first slot of the PUSCH transmission. In the case of a TDD system with subframe configuration 0 and PUSCH transmission in subframes 4 or 9, the PHICH group index calculated in Eq. (9.51) must be incremented by $N_{\text{PHICH}}^{\text{group}}$ [13]. For a Rel-10 UE using two transport blocks within a subframe, the parameter I_{lowest} is incremented by one when calculating the PHICH group and sequence number for the second transport block.

As shown in Figure 9.90, the block of bits $(b_0, b_1, \ldots, b_{N_{\text{bit}}-1})$ transmitted on one PHICH in one subframe are modulated using BPSK modulation, resulting in a block of complex-valued modulation symbols $(z_0, z_1, \ldots, z_{N_s-1})$ where $N_s = N_{\text{bit}}$ given the type of modulation. The block of modulation symbols $(z_0, z_1, \ldots, z_{N_s-1})$ are symbol-by-symbol multiplied by an orthogonal

scrambling sequence, resulting in a sequence of scrambled modulation symbols $(d_0, d_1 ..., d_{N_{SF}^{PHICH} N_s - 1})$ where:

$$d_i = \underbrace{w(i \bmod N_{SF}^{PHICH})}_{\substack{\text{Orthogonal sequence symbol} \\ \text{with index } n_{PHICH}^{sequence}}} \quad \underbrace{(1 - 2c(i))}_{\substack{\text{Cell-specific scrambling} \\ \text{sequence symbol}}} \quad \underbrace{z\left(\left\lfloor i / N_{SF}^{PHICH} \right\rfloor\right)}_{\substack{\text{Modulated HARQ} \\ \text{indicator symbol}}} \quad i = 0, 1, \ldots, N_{SF}^{PHICH} N_s - 1 \tag{9.53}$$

The value of the spreading factor is $N_{SF}^{PHICH} = 4$ or 2 for a normal or extended cyclic prefix type, respectively [3]. The scrambling sequence $c(i)$ is a cell-specific scrambling sequence which was defined in the previous sections and is initialized by $c_{init} = \left(\lfloor n_s/2 \rfloor + 1\right)\left(2N_{ID}^{cell} + 1\right)2^9 + N_{ID}^{cell}$ at the beginning of each subframe. The orthogonal spreading sequence $(w_0, w_1, \ldots, w_{N_{SF}^{PHICH}-1})$ is defined in Table 9.20 where the sequence index $n_{PHICH}^{sequence}$ corresponds to the PHICH number within the PHICH group.

Since REGs contain four resource elements, each able to carry one modulation symbol, the blocks of scrambled symbols are aligned to create blocks of four symbols (Figure 9.92). In the case of a normal cyclic prefix, each of the original complex-valued modulated symbol is represented by four scrambled symbols, thus no alignment is required. In the case of an extended cyclic prefix, each of the original complex-valued modulated symbols is represented by two scrambled symbols. To create blocks of four symbols, zeros are added before or after blocks of two scrambled symbols, depending on whether the PHICH index is odd or even. This allows two groups to be combined during the resource mapping stage and mapped to one REG. Groups of four symbols are formed as illustrated in Figure 9.92.

The block of symbols $(d_0, d_1 \ldots, d_{N_{SF}^{PHICH} N_s - 1})$ are first aligned with REG size, and are then mapped to spatial layers and precoded, yielding a block of vectors $\mathbf{y}_i = (y_i^0, y_i^1, \ldots, y_i^{N_p - 1})^T$ where $i = 0, 1, \ldots, N_{SF}^{PHICH} N_s - 1$, and y_i^p represents the signal of antenna port $p = 0, 1, \ldots, N_p - 1$. The number of antenna ports with CRSs is chosen as $N_p \in \{1, 2, 4\}$. The layer mapping and precoding operation depend on the cyclic prefix type and the number of antenna ports used for transmission of the PHICH. The PHICH is transmitted on the same set of antenna ports that are used for transmission of the PBCH.

The number of OFDM symbols used to carry PHICH is configurable by PHICH duration. The PHICH duration is either normal or extended. A normal PHICH duration allows PHICH to present only in the first OFDM symbol of the subframe. In general, an extended PHICH duration allows PHICH to be located in the first three OFDM symbols of the subframe, with some exceptions. Under those exceptions, PHICH may present in the first two OFDM symbols of the subframe. Those exceptions are as follows: (1) within subframe 1 and 6 when frame structure type 2 (TDD) is used; and (2) within MBSFN subframes.

Petitioners' Exhibit 1021
Nokia of America Corp., et al. v. KT Corporation, et al.
Case No. IPR2025-00036; U.S. Patent No. 11,627,631
Page 574 of 1122

Table 9.20 Orthogonal Spreading Sequence for PHICH Processing [3]

Sequence Index	$(w_0, w_1, \ldots, w_{N_{SF}^{PHICH}-1})$	
$n_{PHICH}^{sequence}$	**Normal Cyclic Prefix** $N_{SF}^{PHICH} = 4$	**Extended Cyclic Prefix** $N_{SF}^{PHICH} = 2$
0	[+1 +1 +1 +1]	[+1 +1]
1	[+1 −1 +1 −1]	[+1 −1]
2	[+1 +1 −1 −1]	[+j +j]
3	[+1 −1 −1 +1]	[+j −j]
4	[+j +j +j +j]	–
5	[+j −j +j −j]	–
6	[+j +j −j −j]	–
7	[+j −j −j +j]	–

Given that CFI carried by PCFICH configures the number of OFDM symbols that are used for the control region, or alternatively the size of the PDSCH region, the extended PHICH duration must not exceed the size of the control region. For example, when using an extended PHICH in subframe zero of frame structure type 1 (FDD) with 10 MHz bandwidth, the first three OFDM symbols will contain the PHICH. Therefore, the CFI must be set to 3 so that the PDSCH is not mapped to OFDM symbols 0, 1, or 2, and thus does not collide with the PHICH. As shown in Figure 9.92, the corresponding elements of each PHICH sequence are summed to create the sequence for each PHICH group where the sum is over all PHICHs in the PHICH group, and $y_i^{(p)}(n)$ represents the symbol sequence from the ith PHICH in the PHICH group. As shown in Figure 9.92, the PHICH groups are mapped to PHICH mapping units, i.e., $\bar{y}_n^p = \sum_i y_i^p(n)$ where $y_i^p(n)$ is the nth element within the ith PHICH group on antenna port p. For a normal cyclic prefix, the mapping of PHICH group m to PHICH mapping unit m' is defined as $\tilde{y}_{m'}^p(n) = \bar{y}_m^p(n)$, where $m' = m = 0, 1, ..., m_i N_{PHICH}^{group} - 1$ for frame structure type 1, and $m' = m = 0, 1, \ldots, m_i N_{PHICH}^{group} - 1$ for frame structure type 2. In other words, the PHICHs are mapped to REGs using PHICH mapping units $\tilde{y}_{m'}^p(n)$, where m' is the index of the mapping unit. For a normal cyclic prefix, each PHICH group is mapped to a PHICH mapping unit. In the case of an extended cyclic prefix, two PHICH groups are mapped to one PHICH mapping unit. Due to the location of the padding zeros added during resource group alignment, when two consecutive groups are added, the zeros of one group overlap with the data of the other group.

Each mapping unit contains 12 symbols. In order to map these 12 symbols to REGs, the mapping units are split into three groups of four symbols, or

Petitioners' Exhibit 1021
Nokia of America Corp., et al. v. KT Corporation, et al.
Case No. IPR2025-00036; U.S. Patent No. 11,627,631
Page 575 of 1122

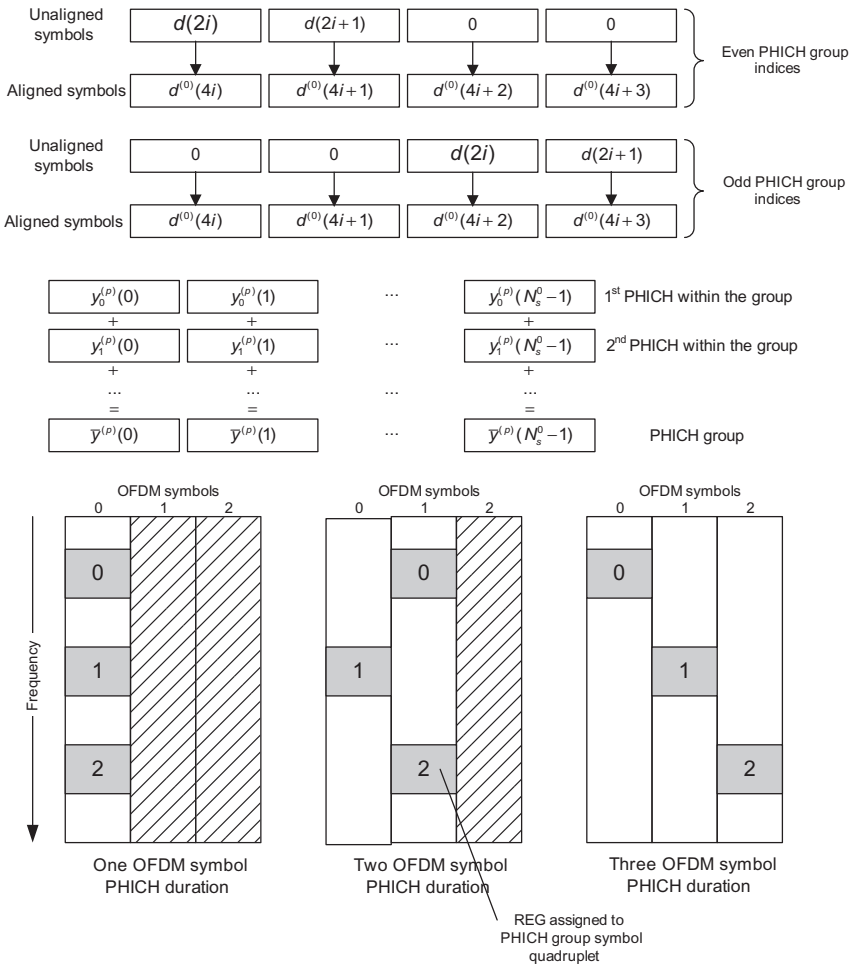


FIGURE 9.92

Illustration of PHICH symbol alignment, sequence combining, and mapping to REGs for normal and extended PHICH [160].

quadruplets. Each of the three symbol quadruplets $z^p(i) = (\tilde{y}^p(4i), \tilde{y}^p(4i+1), \tilde{y}^p(4i+2)$, and $\tilde{y}^p(4i+3))$ is mapped to REG (k'_i, l'_i) such that PHICH is spread over all available OFDM symbols and resource blocks. The OFDM symbol index l'_i is set so that adjacent quadruplets are spread among the available OFDM symbols as illustrated in Figure 9.90. The sub-carrier index k'_i of the REG is based on the cell identity $N_{\mathrm{ID}}^{\mathrm{cell}}$ and is chosen to spread the three symbol quadruplets over the entire system bandwidth.

Petitioners' Exhibit 1021
Nokia of America Corp., et al. v. KT Corporation, et al.
Case No. IPR2025-00036; U.S. Patent No. 11,627,631
Page 576 of 1122

9.12.4 Physical downlink control channel

The physical downlink control channel is used to carry the DCI, which contains downlink/uplink scheduling decisions and power-control commands. More specifically, the DCI includes downlink scheduling assignments, PDSCH resource allocation, transport format, HARQ related information, and control information related to spatial multiplexing. The downlink scheduling assignment further includes a command for power control of the PUCCH that is used for transmission of HARQ ACK/NACK in response to downlink scheduling assignments. The DCI further includes uplink scheduling grants, PUSCH resource indication, transport format, and other HARQ related information. The uplink scheduling grant also consists of a command for power control of PUSCH. Furthermore, it carries power-control commands for a set of terminals as complementary to the commands included in the scheduling assignments/grants. It must be noted that different types of control information correspond to different DCI message sizes. For example, supporting spatial multiplexing with non-contiguous allocation of resource blocks in the frequency-domain requires larger scheduling message in comparison to an uplink grant, only allowing frequency-contiguous allocations. The DCI is subsequently categorized to different formats where a format corresponds to a certain message size, content, and usage. The LTE/LTE-Advanced DCI formats are summarized in Table 9.21. The actual message size depends on, among other factors, the cell bandwidth, thus for larger bandwidths, a larger number of bits is required to indicate the resource-block allocation. The number of CRSs in the cell and whether cross-carrier scheduling is configured will also affect the size of most DCI formats. Hence, a given DCI format may have different sizes depending on the overall configuration of the cell.

9.12.4.1 PDCCH physical layer processing

As mentioned earlier, each PDCCH carries a message known as the DCI, which includes resource assignments and other control signaling information for a UE or a group of UEs. Each PDCCH is transmitted using one or more control channel elements (CCEs), where each CCE corresponds to nine REGs (Figure 9.93). The number of REGs that are not assigned to a PCFICH or PHICH is denoted by N_{REG}. The CCEs available in the system are numbered from 0 to $N_{CCE} - 1$, where $N_{CCE} = \lfloor N_{REG}/9 \rfloor$. The PDCCH supports multiple formats as listed in Table 9.21. A

Table 9.21 PDCCH Formats [3]

PDCCH Format	Number of CCEs (Aggregation Level)	Number of Resource Element Groups (REGs)	Number Of PDCCH Bits
0	1	9	72
1	2	18	144
2	4	36	288
3	8	72	576

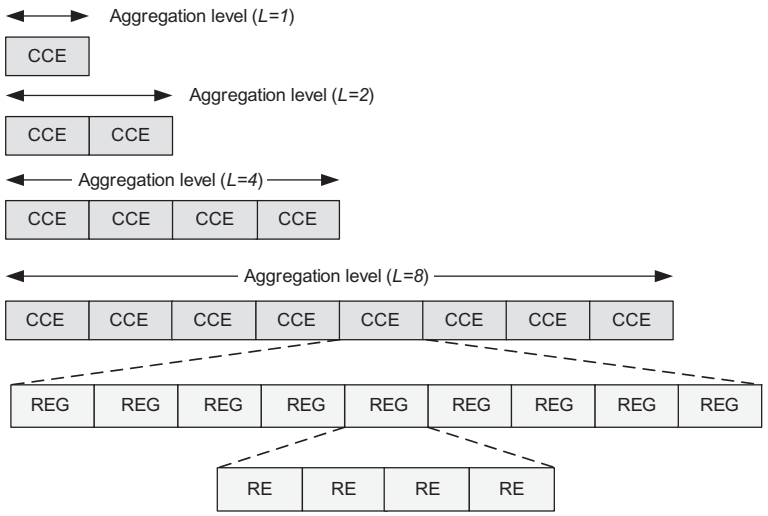


FIGURE 9.93

Illustration of various aggregation levels and CCE structure [162].

PDCCH consisting of L consecutive CCEs (aggregation level) may only start on a CCE that satisfies (n_{CCE} mod $L = 0$), where the parameter n_{CCE} denotes the CCE index. Multiple PDCCHs can be transmitted in a subframe. Four QPSK symbols are mapped to each REG. Four PDCCH formats are supported, as listed in Table 9.21.

A cyclic redundancy check is used for error detection in the DCI messages. The entire PDCCH payload is used to calculate a set of CRC parity bits. The PDCCH payload is divided by a cyclic generator polynomial to generate 16 parity bits. These parity bits are then appended to the end of the PDCCH payload. As multiple PDCCHs relevant to different UEs can be present in one subframe, the CRC is also used to specify to which UE a PDCCH is addressed. This is done by scrambling the CRC parity bits with the corresponding RNTI of the UE. The scrambled CRC is obtained by performing a bit-wise XOR operation between the 16-bit calculated PDCCH CRC and the 16-bit RNTI. Different RNTI can be used to scramble the CRC. Some examples include:

- A UE unique identifier in the RRC_CONNECTED mode (C-RNTI).
- A paging indication identifier (P-RNTI), if the PDSCH contains paging information.
- A system information identifier (SI-RNTI), if PDSCH contains system information.

When encoding a DCI format 0 payload, containing the UE UL-SCH resource allocation, and if the UE transmit-antenna selection is configured, the RNTI-scrambled CRC undergoes a bit-wise XOR operation with an antenna selection

Petitioners' Exhibit 1021
Nokia of America Corp., et al. v. KT Corporation, et al.
Case No. IPR2025-00036; U.S. Patent No. 11,627,631
Page 578 of 1122

mask. This informs the UE which transmit antenna must be used for uplink transmission. The antenna selection mask for UE antenna port 0 is $(0,0,0,0,0,0,0,0,0,0,0,0,0,0,0,0)$ and for UE antenna port 1 is $(0,0,0,0,0,0,0,0,0,0,0,0,0,0,0,1)$.

As shown in Figure 9.94, the DCI message with the attached CRC goes through tail-biting convolutional coding. LTE/LTE-Advanced uses a rate 1/3 tail-biting convolutional encoder with a constraint length $K = 7$. This means that one

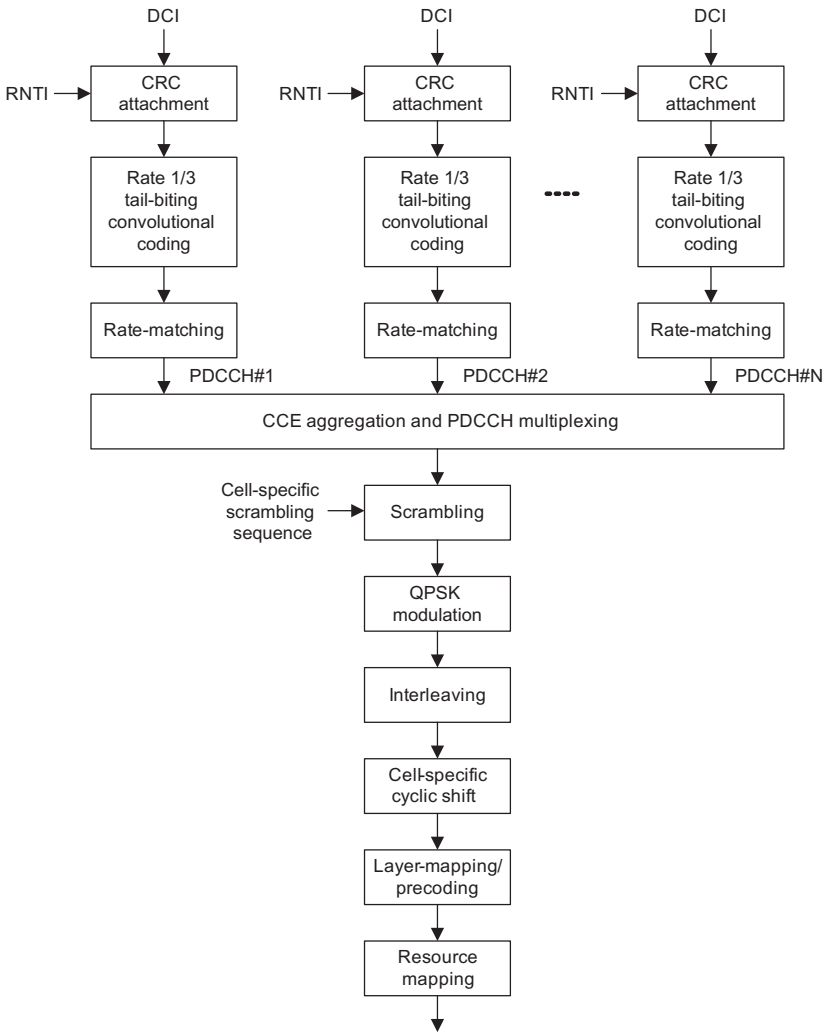


FIGURE 9.94

PDCCH physical layer processing stages [15].

Petitioners' Exhibit 1021
Nokia of America Corp., et al. v. KT Corporation, et al.
Case No. IPR2025-00036; U.S. Patent No. 11,627,631
Page 579 of 1122

in three bits of the output contain useful information while the other two add parity bits. Each output stream of the encoder is obtained by convolving the input with the impulse response of the encoder. The impulse responses are called the generator sequences of the encoder. Note that a conventional convolutional encoder initializes its internal shift register to the all-zero state and also ensures that the encoder finishes in the all-zero state, by padding the input sequence with K zeros at the end. Knowing the start and end states (i.e., all zeros) simplifies the design of the decoder (typically an implementation of the Viterbi algorithm). A tail-biting convolutional coder initializes its internal shift register to the last K bits of the current input block, rather than to the all-zero state. This means the starting and the ending states are the same, without the need to zero pad the input block. As the overhead of terminating the encoder has been eliminated, the output block contains fewer bits than a conventional convolutional coder. The drawback is that the decoder becomes more complicated, since the initial state is unknown; however, it does know the start and end states are the same. The rate-matching block creates an output bitstream with the desired code rate. The three bit streams from the convolutional encoder are interleaved, followed by bit collection to create a virtual circular buffer.

The three sub-block interleavers used in the rate-matching block are identical. Interleaving is a technique to reduce the impact of burst errors on a signal to ensure that consecutive data bits will not be corrupted. The bit collection stage creates a virtual circular buffer by concatenating the three interleaved encoded bit streams. The bits are then selected and pruned from the circular buffer to create an output sequence length which meets the desired code rate. The coded DCI messages for each control channel are multiplexed and scrambled before undergoing QPSK modulation, layer mapping, and precoding. The blocks of coded bits for each control channel are multiplexed in order to create a block of data as shown in Figure 9.96, where N_{bit}^{i} is the number of bits in the ith control channel and N_{PDCCH} is the number of control channels.

As shown in Figure 9.94, the block of coded and rate-matched bits $(b_0^i, b_1^i, \ldots, b_{N_{\text{bit}}^i-1}^i)$ on each of the control channels awaiting transmission in a subframe are multiplexed, resulting in a block of multiplexed bits $(b_0^0, b_1^0, \ldots, b_{N_{\text{bit}}^0-1}^0, b_0^1, b_1^1, \ldots, b_{N_{\text{bit}}^1-1}^1, \ldots, b_0^{N_{\text{PDCCH}}-1}, b_1^{N_{\text{PDCCH}}-1}, \ldots, b_{N_{\text{bit}}^{N_{\text{PDCCH}}-1}-1}^{N_{\text{PDCCH}}-1})$, where N_{bit}^{i} is the number of bits in the ith DCI, and N_{PDCCH} denotes the number of PDCCHs transmitted in one subframe. The block of multiplexed bits $(b_0^0, b_1^0, \ldots, b_{N_{\text{bit}}^0-1}^0, b_0^1, b_1^1, \ldots, b_{N_{\text{bit}}^1-1}^1, \ldots, b_0^{N_{\text{PDCCH}}-1}, b_1^{N_{\text{PDCCH}}-1}, \ldots, b_{N_{\text{bit}}^{N_{\text{PDCCH}}-1}-1}^{N_{\text{PDCCH}}-1})$ is scrambled with a cell-specific sequence prior to modulation (i.e., the multiplexed block of bits undergoes a bit-wise XOR operation with a cell-specific scrambling sequence), resulting in a block of scrambled bits $(\tilde{b}_0, \tilde{b}_1, \ldots, \tilde{b}_{N_{\text{total}}-1})$, in which $\tilde{b}_i = b_i \oplus c(i)$. The scrambling function provides more robustness through inter-cell interference randomization. When a UE descrambles the received bit stream with a known cell-specific scrambling sequence, interference from other cells will be descrambled

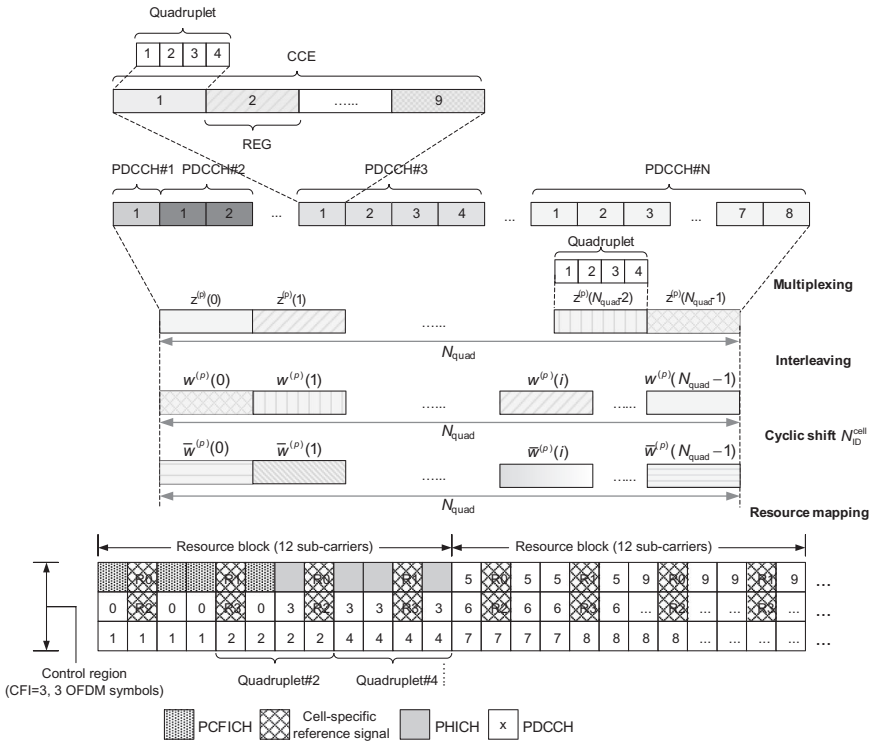


FIGURE 9.95

Example breakdown of CCE processing [162].

incorrectly and appear as uncorrelated noise. The cell-specific scrambling sequence $c(i)$ was defined in the previous sections and is initialized with $c_{\text{init}} = \lfloor n_s/2 \rfloor 2^9 + N_{\text{ID}}^{\text{cell}}$ at the start of each subframe. It must be noted that the CCE number n corresponds to bit array $(b_{72n}, b_{72n+1}, \ldots, b_{72n+71})$. If necessary, null elements are inserted in the block of bits prior to scrambling to ensure that the PDCCHs start at the permissible CCE positions, and to ensure that the length $N_{\text{total}} = 8N_{\text{REG}} \geq \sum_{i=0}^{N_{\text{PDCCH}}-1} N_{\text{bit}}^i$ of the scrambled block of bits matches the amount of REGs not assigned to the PCFICH or PHICH.

The block of scrambled bits $(\tilde{b}_0, \tilde{b}_1, \ldots, \tilde{b}_{N_{\text{total}}-1})$ is modulated using QPSK modulation, resulting in a block of complex-valued modulation symbols $(d_0, d_1, \ldots, d_{N_s-1})$. The block of modulated symbols $(d_0, d_1, \ldots, d_{N_s-1})$ are further mapped to $N_s^0 = N_s$ spatial layers and precoded, yielding the block of precoded vectors $\mathbf{y}_i = (y_i^0, y_i^1, \ldots, y_i^{N_p-1})^T$ with $i = 0, \ldots, N_s - 1$. The latter block of symbols are mapped to resources on the antenna ports used for transmission of PDCCH, where y_i^p represents the signal for antenna port p. Note that the PDCCH is transmitted on the same set of antenna ports that were used for PBCH transmission.

Petitioners' Exhibit 1021
Nokia of America Corp., et al. v. KT Corporation, et al.
Case No. IPR2025-00036; U.S. Patent No. 11,627,631
Page 581 of 1122

The mapping to resource elements are defined by operations on quadruplets of complex-valued symbols, as shown in Figure 9.95. Let $z_i^p = (y_{4i}^p, y_{4i+1}^p, y_{4i+2}^p, y_{4i+3}^p)$ denote the ith symbol quadruplet for antenna port p. The block of quadruplets $(z_0^p, z_1^p, \ldots, z_{N_{\text{quad}}-1}^p)$ where $N_{\text{quad}} = N_s/4$ are permuted (interleaved), resulting in a permuted quadruplet vector $(w_0^p, w_1^p, \ldots, w_{N_{\text{quad}}-1}^p)$. The permutation is performed similar to sub-block interleaving with the following exceptions: (1) the input and output to the interleaver are defined by symbol quadruplets instead of bits; and (2) interleaving is performed on symbol quadruplets instead of bits by substituting the bits with symbol quadruplets. The null elements at the output of the interleaver must be removed when constructing the permuted vector $(w_0^p, w_1^p, \ldots, w_{N_{\text{quad}}-1}^p)$. The block of interleaved quadruplets $(w_0^p, w_1^p, ..., w_{N_{quad}-1}^p)$ is then cyclically shifted, resulting in $(\overline{w}_0^p, \overline{w}_1^p, ..., \overline{w}_{N_{\text{quad}}-1}^p)$ where $\overline{w}_i^p = w_{(i+N_{\text{ID}}^{\text{cell}}) \bmod N_{\text{quad}}}^p$. The mapping of the block of quadruplets $(\overline{w}_0^p, \overline{w}_1^p, \ldots, \overline{w}_{N_{\text{quad}}-1}^p)$ is defined in terms of resource-element groups. Each symbol-quadruplet is sequentially mapped to an unallocated REG starting with REG $(k' = 0, l' = 0)$ such that symbol quadruplet $\overline{w}_{m'}^p$ is mapped to REG m'. The REG symbol index l' is then incremented until all the REGs at sub-carrier index $k' = 0$ have been allocated, provided that $l' < N_{\text{CFI}}$. The REG sub-carrier index k' is then incremented and the process is repeated until $k' < 12N_{\text{RB}}^{\text{DL}}$. This mapping continues until all symbol quadruplets have been allocated to REGs. The mapping is illustrated in Figure 9.95 for an example resource grid. Four transmit antenna ports and a control region size of three OFDM symbols are used to create the grid. The mapping is performed along symbols first, and then along frequency until the entire symbol quadruplets are mapped, in order to cause no significant power imbalance among the PDCCH symbols. If symbol-quadruplets were only mapped to the first OFDM symbol among OFDM symbols dedicated to the control region on a particular subframe, it would negatively impact the PA operation and performance.

Figure 9.97 shows an example mapping of CCEs in a subframe. In this example, REGs $(k' = 0, l' = 0)$ and $(k' = 6, l' = 0)$ were already allocated to PCFICH and PHICH, respectively, thus no symbol quadruplets are assigned to them. The symbol-quadruplets are first mapped to REG $(k' = 0, l' = 1)$, followed by REG $(k' = 0, l' = 2)$ and so on. The symbol-quadruplets are mapped in ascending order of index l'. As there are no REGs with $k' = 0$, the next REG allocated is REG $(k' = 4, l' = 2)$, as this REG has the lowest value of index l' that has not already been allocated. This process is repeated until all symbol quadruplets are assigned

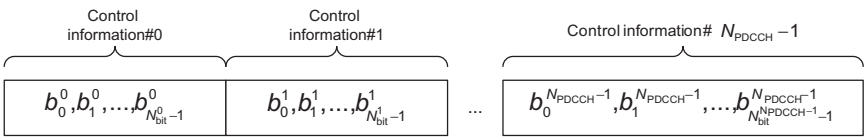


FIGURE 9.96

Illustration of PDCCH multiplexing function [160].

Petitioners' Exhibit 1021
Nokia of America Corp., et al. v. KT Corporation, et al.
Case No. IPR2025-00036; U.S. Patent No. 11,627,631
Page 582 of 1122

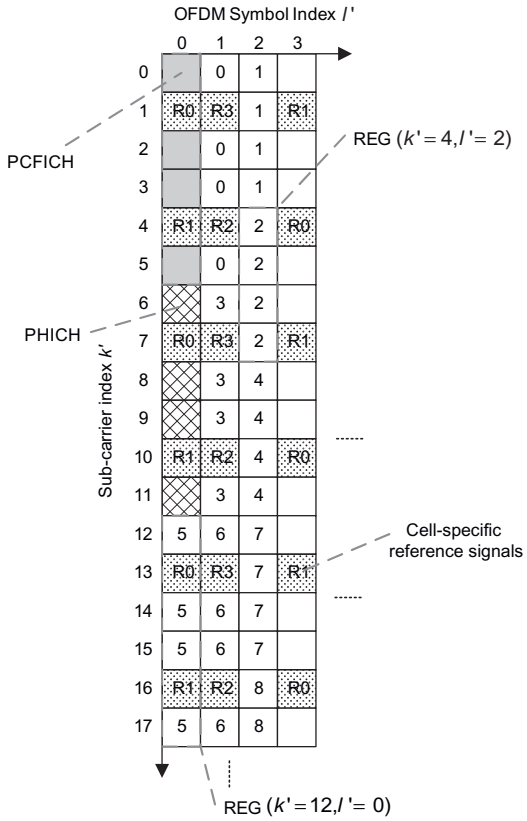


FIGURE 9.97

Example mapping of CCEs in the control region of a subframe [160].

to the available REGs [160]. Therefore, the CCE mapping process can be summarized as follows. Each symbol-quadruplet is sequentially mapped to an unallocated REG starting with REG $(k' = 0, l' = 0)$. This is described as symbol quadruplet $\overline{w}^{p}_{m'}$ being mapped to REG m'. The REG symbol index k' is then incremented until all the REGs at sub-carrier index $l' = 0$ have been allocated. The REG sub-carrier index k' is then incremented and the process is repeated. This mapping continues until all symbol quadruplets have been allocated REGs. The mapping is shown in Figure 9.97 for an example resource grid. Four transmit antenna ports and control region size of three OFDM symbols are used to create the grid.

9.12.4.2 DCI formats

One PDCCH carries one DCI message with one of the formats given in Table 9.21. Given that multiple terminals can be scheduled simultaneously on both downlink and uplink, there must be a possibility to transmit multiple

scheduling messages within each subframe. Each scheduling message is transmitted on a separate PDCCH, and consequently there are typically multiple simultaneous PDCCH transmissions within each cell. Furthermore, to support different radio channel conditions, link adaptation can be used, where the transmission format of the PDCCH (i.e., coding and modulation scheme, multi-antenna configuration) is adapted to cope with the severity of the radio channel conditions. For carrier aggregation, scheduling assignments/grants are transmitted individually per component carrier. Depending on the purpose of DCI message, different DCI formats are defined as follows [4]:

- Format 0: Transmission of uplink grants for PUSCH.
- Format 1: Transmission of PDSCH assignments with a single codeword.
- Format 1A: DCI Format 1A is used for compact signaling of resource assignments in single-codeword PDSCH transmissions using any PDSCH transmission mode. It is also used to allocate a dedicated preamble signature to a UE for the purpose of contention-free random access.
- Format 1B: DCI Format 1B is used for compact signaling of resource assignments in PDSCH transmissions using rank-1 closed-loop precoding. The information transmitted is the same as DCI Format 1A with the addition of an indicator for the precoding vector applied to PDSCH transmission.
- Format 1C: Transmission of PDSCH assignment using a very compact format. When format 1C is used, the PDSCH transmission is constrained to use QPSK modulation.
- Format 1D: Same as Format 1B with additional information for power offset (i.e., instead of one of the precoding vector indicator bits, there is a single bit to indicate whether a power offset is applied to the data symbols to indicate whether the transmission power is shared between two UEs) and PDSCH assignments for multi-user MIMO.
- Format 2: PDSCH assignments for closed-loop MIMO operation.
- Format 2A: PDSCH assignments for open-loop MIMO operation.
- Format 2B: PDSCH assignments for dual-layer beamforming.
- Format 2C: DCI Format 2C was introduced in Rel-10 and is used for signaling resource assignments for PDSCH transmissions using closed-loop single-user or multi-user MIMO with up to eight layers.
- Format 2D: DCI Format 2D was introduced in Rel-11 and is used for CoMP operations in conjunction with transmission mode 10.
- Format 3: Transmission of transmit power control (TPC) commands for multiple users and for PUCCH and PUSCH with 2-bit power adjustments.
- Format 3A: Transmission of TPC commands for multiple users and for PUCCH and PUSCH with 1-bit power adjustments.
- Format 4: DCI Format 4 was introduced in Rel-10 and is used for signaling resource grants for PUSCH when the UE is configured in PUSCH transmission mode 2 for uplink single-user MIMO. The information transmitted is similar to DCI Format 0, with the addition of MCS and new data indicator for a second transport block (TB) and precoding data.

Petitioners' Exhibit 1021
Nokia of America Corp., et al. v. KT Corporation, et al.
Case No. IPR2025-00036; U.S. Patent No. 11,627,631
Page 584 of 1122

Multiple UEs can be scheduled in one subframe; therefore, multiple DCI messages can be sent using multiple PDCCHs. The description, usage, and detailed information fields of various DCI formats for LTE/LTE-Advanced are given in Table 9.22.

As shown in Table 9.22, the number of bits required for resource allocation/assignment depends on the system bandwidth; therefore, the size of that information field also varies with the system bandwidth. The payload size for each DCI format including information bits and CRC are summarized in Table 9.23 for the E-UTRA supported system bandwidths. In addition, padding bits are added (if necessary) to ensure that DCI Formats 0 and 1A are of the same size, even in the case of different uplink and downlink bandwidths, in order to avoid additional complexity at the UE receiver. Furthermore, the padding bits may be added to ensure that DCI Formats 3 and 3A have the same size as DCI Formats 0 and 1A, to circumvent additional complexity at the UE receiver; to avoid potential ambiguity in identifying the correct PDCCH location; to ensure that DCI Format 1 has a different size than that of DCI Formats 0/1A, so that these formats can be easily distinguished at the UE receiver; to make sure that Format 4 has a different size from DCI Formats 1/2/2A/2B/2C, so that this format can be easily distinguished. As given in Table 9.22, in LTE Rel-10, some optional features were added that may be configured in some of the DCI formats; those bit counts are not included in Table 9.23. The DCI formats 1B/1D/2/2A/4 payload size calculations are based on two antenna ports [13]. The new DCI format 2D which has been added in Rel-11 includes the following information fields: Carrier indicator (0 or 3 bits); Resource allocation header for resource allocation type 0 or type 1 (1 bit), note that if downlink bandwidth is less than or equal to 10 resource blocks, there is no resource allocation header and resource allocation type 0 is assumed; Resource block assignment type 0/type 1 (variable number of bits depending on the system bandwidth); TPC command for PUCCH (2 bits); Downlink Assignment Index (TDD only) for uplink−downlink subframe configurations 1−6 (2 bits); HARQ process number (3 bits for FDD), (4 bits for TDD); Antenna port(s), scrambling identity and number of layers (3 bits); SRS request (0 or 1 bit) for TDD only; Modulation and coding scheme (5 bits), New data indicator (1 bit); Redundancy version (2 bits) for transport blocks 1 and 2; PDSCH resource element Mapping and Quasi Collocation Indicator (2 bits); HARQ-ACK resource offset (note that this field is present when this DCI format is carried by ePDCCH and is not present when this format is carried by PDCCH) (2 bits). The latter 2 bits are set to 0 when this format is carried by ePDCCH on a secondary cell. If both transport blocks are enabled; transport block 1 is mapped to codeword 0 and transport block 2 is mapped to codeword 1. In case one of the transport blocks is disabled; the transport block to codeword mapping is further specified [4].

9.12.4.3 Common and UE-specific search spaces and blind decoding

The PDCCH region consists of a number of CCEs which can be allocated to a PDCCH. The PDCCHs can be flexibly mapped to CCEs based on certain criteria.

Petitioners' Exhibit 1021
Nokia of America Corp., et al. v. KT Corporation, et al.
Case No. IPR2025-00036; U.S. Patent No. 11,627,631
Page 585 of 1122

Table 9.22 Descriptions, Usage, and Information Fields of Various DCI Formats [4,13]

DCI Format	Usage	Release	Information Fields	Size (Bits)	Description
Format 0	Scheduling of PUSCH in one uplink cell	10	Carrier indicator	0 or 3	Identifies the RF carrier to be used as the serving cell. A value of "0" implies the primary cell is used as the serving cell. This field only applies when carrier aggregation is enabled.
		10	Format 0/format 1A flag	1	Flag to differentiate between Format 0 and Format 1A.
		8	Frequency hopping flag	1	PUSCH frequency hopping flag for resource allocation type 0. This bit is used as the MSB of the resource block allocation in resource allocation type 1.
		8	Resource block allocation	7–13 variable	Resource block assignment/allocation. (In resource allocation type 0: 5, 7, 9, 11, 12, or 13 bits corresponding to 1.4, 3, 5, 10, 15, or 20 MHz system bandwidth). (In resource allocation type 1: 6, 8, 10, 12, 13, or 14 bits corresponding to 1.4, 3, 5, 10, 15, or 20 MHz system bandwidth).
		8	MCS and redundancy version	5	Modulation, coding scheme and redundancy version.
		8	New data indicator (NDI)	1	New data indicator.
		8	Transmit power control (TPC)	2	PUSCH TPC command.
		8	Cyclic shift for uplink DM-RS		Cyclic shift for uplink DM-RS (different look up tables are used for LTE Rel-8/9 and LTE Rel-10 UEs based on this value.
		10	Cyclic shift for uplink DM-RS and OCC index	3	

(*Continued*)

Table 9.22 (Continued)

DCI Format	Usage	Release	Information Fields	Size (Bits)	Description
		8	Aperiodic CQI request	1	Instructs the UE to provide a periodic CQI report.
		10	CSI request	1 or 2	Instructs the UE to send a CSI report, where one-bit case refers to a single cell and two-bit case applies to a UE which is configured with more than one downlink cell.
		10	SRS request	0 or 1	Instructs the UE to transmit an SRS for uplink channel measurements.
		10	Resource allocation type	1	Signals the type of uplink resource allocation.
		8	Uplink index (TDD only)	2	For TDD configuration 0, this field is the uplink index. For TDD configuration 1–6, this field is the downlink assignment index.
		8	Downlink assignment index (DAI) (TDD only)		
Format 1	Transmission of PDSCH assignments with a single codeword	10	Carrier indicator	0 or 3	Identifies the RF carrier to be used as the serving cell. A value of "0" implies the primary cell is used as the serving cell. This field only applies when carrier aggregation is enabled.
		8	Resource allocation header	0 or 1	Resource allocation header selects between resource allocation type 0 or type 1 (only exists if downlink bandwidth is greater than 10 RBs).
		8	Resource block allocation	6–25 variable	Resource block assignment/allocation (6, 8, 13, 17, 19, or 25 bits corresponding to 1.4, 3, 5, 10, 15, or 20 MHz system bandwidth).
		8	MCS	5	Modulation and coding scheme.

Petitioners' Exhibit 1021
Nokia of America Corp., et al. v. KT Corporation, et al.
Case No. IPR2025-00036; U.S. Patent No. 11,627,631
Page 587 of 1122

		8	HARQ process number	3 (FDD) 4 (TDD)	HARQ process number.
		8	New data indicator	1	HARQ new data indicator.
		8	Redundancy version	2	HARQ redundancy version.
		8	TPC command for PUCCH	2	PUCCH TPC command.
		8	Downlink assignment index (TDD only)	2	For TDD configuration 0, this field is not used. For TDD configurations 1−6, this field is interpreted as the DAI.
Format 1A	Compact signaling of resource assignments for single-codeword PDSCH transmissions for any PDSCH transmission mode	10	Carrier indicator	0 or 3	Identifies the RF carrier to be used as the serving cell. A value of “0” implies the primary cell is used as the serving cell. This field only applies when carrier aggregation is enabled.
		8	Format 0/format 1A flag	1	Flag to differentiate between Format 0 and Format 1A.
		8	Localized/ distributed VRB assignment flag	1	Selects between 0 (localized) or 1 (distributed) resource blocks.
		8	Resource block allocation	5−13 variable	Resource block assignment/allocation (5, 7, 9, 11, 12, or 13 bits corresponding to 1.4, 3, 5, 10, 15, or 20 MHz system bandwidth).
		8	MCS	5	Modulation and coding scheme.
		8	HARQ process number	3 (FDD) 4 (TDD)	HARQ process number.
		8	New data indicator	1	HARQ new data indicator.

(*Continued*)

Table 9.22 (Continued)

DCI Format	Usage	Release	Information Fields	Size (Bits)	Description
		8	Redundancy version	2	HARQ redundancy version.
		8	TPC command for PUCCH	2	PUCCH TPC command.
		8	Downlink assignment index (TDD only)	2	For TDD configuration 0, this field is not used. For TDD configurations 1–6, this field is interpreted as DAI.
		10	SRS request	0 or 1	Instructs the UE to transmit SRS for uplink channel measurements.
Format 1B	Compact signaling of resource assignments for PDSCH transmissions using closed-loop precoding with rank-1 transmission	10	Carrier indicator	0 or 3	Identifies the RF carrier to be used as the serving cell. A value of "0" implies the primary cell is used as the serving cell. This field only applies when carrier aggregation is enabled.
		8	Localized/ distributed VRB assignment flag	1	Selects between 0 (localized) or 1 (distributed) resource blocks.
		8	Resource block allocation	5–13 variable	Resource block assignment/allocation (5, 7, 9, 11, 12, or 13 bits corresponding to 1.4, 3, 5, 10, 15, or 20 MHz system bandwidth).
		8	MCS	5	Modulation and coding scheme.
		8	HARQ process number	3 (FDD) 4 (TDD)	HARQ process number.
		8	New data indicator	1	HARQ new data indicator.
		8	Redundancy version	2	HARQ redundancy version.

Petitioners' Exhibit 1021
Nokia of America Corp., et al. v. KT Corporation, et al.
Case No. IPR2025-00036; U.S. Patent No. 11,627,631
Page 589 of 1122

		8	TPC command for PUCCH	2	PUCCH TPC command.
		8	Transmitted PMI (TPMI)	2 (2 antenna ports) 4 (4 antenna ports)	Downlink PMI information, i.e., information about the codebook used for precoding PDSCH (codebook-based closed-loop MIMO).
		8	PMI confirmation for precoding	1	Indicates whether PDSCH has been precoded using the codebook indicated by TPMI or by the PMI sent by the UE.
		8	Downlink assignment index (TDD only)	2	For TDD configuration 0, this field is not used. For TDD configuration 1−6, this field is the downlink assignment index.
Format 1C	Transmission of PDSCH assignment using a very compact format	8	Gap value	0 or 1	DCI format 1C always signals resource allocation type 2 using a distributed mapping. Smaller bandwidths always use “gap1” and larger bandwidths greater than 10 MHz can select between “gap1” and “gap2.”
		8	Resource block allocation	3−9 variable	Resource block assignment/allocation (3, 5, 7, 7, 8, or 9 bits corresponding to 1.4, 3, 5, 10, 15, or 20 MHz system bandwidth).
		8	Transport block size	5	DCI format 1C does not use the general TBS table, rather it uses a smaller TBS table.
Format 1D	Same as format 1B with additional information for power offset (i.e., instead of one of the precoding vector indicator	10	Carrier indicator	0 or 3	Identifies the RF carrier to be used as the serving cell. A value of “0” implies the primary cell is used as the serving cell. This field only applies when carrier aggregation is enabled.
		8	Localized/ distributed VRB assignment flag	1	Selects between 0 (localized) or 1 (distributed) resource blocks.
		8		5−13 variable	

(*Continued*)

Table 9.22 (Continued)

DCI Format	Usage	Release	Information Fields	Size (Bits)	Description
	bits, there is a single bit to indicate whether a power offset is applied to the data symbols to indicate whether the transmission power is shared between two UEs) and PDSCH assignments for multi-user MIMO		Resource block allocation		Resource block assignment/allocation (5, 7, 9, 11, 12, or 13 bits corresponding to 1.4, 3, 5, 10, 15, or 20 MHz system bandwidth).
		8	MCS	5	Modulation and coding scheme.
		8	HARQ process number	3 (FDD) 4 (TDD)	HARQ process number.
		8	New data indicator	1	HARQ new data indicator.
		8	Redundancy version	2	HARQ redundancy version.
		8	TPC command for PUCCH	2	PUCCH TPC command.
		8	Transmitted PMI (TPMI)	2 (2 antenna ports) 4 (4 antenna ports)	Downlink PMI information, i.e., information about the codebook used for precoding PDSCH (codebook-based closed-loop MIMO).
		8	Downlink power offset	1	Downlink power offset is used in MU-MIMO to inform the UE of its downlink transmit power relative to single-user transmit power.
		8	Downlink assignment index (TDD only)	2	For TDD configuration 0, this field is not used. For TDD configuration 1–6, this field is the downlink assignment index.
Format 2	PDSCH assignments for closed-loop	10	Carrier indicator	0 or 3	Identifies the RF carrier to be used as the serving cell. A value of "0" implies the primary cell is used as the serving cell. This field only applies when carrier aggregation is enabled.

Petitioners' Exhibit 1021
Nokia of America Corp., et al. v. KT Corporation, et al.
Case No. IPR2025-00036; U.S. Patent No. 11,627,631
Page 591 of 1122

MIMO operation	8	Resource allocation header	0 or 1	Resource allocation header selects between resource allocation type 0 or type 1 (only exists if downlink bandwidth is greater than 10 RBs).
	8	Resource block allocation	6−25 variable	Resource block assignment/allocation (6, 8, 13, 17, 19, or 25 bits corresponding to 1.4, 3, 5, 10, 15, or 20 MHz system bandwidth).
	8	TPC command for PUCCH	2	PUCCH TPC command.
	8	HARQ process number	3 (FDD) 4 (TDD)	HARQ process number.
	8	Transport block to codeword swap flag	1	Defines the relationship between transport blocks 1 and 2 relative to codewords 0 and 1. If set to “0,” codeword 0 is generated from transport block 1 and codeword 1 is generated from transport block 2.
	8	MCS1	5	Modulation and coding scheme for transport block 1.
	8	New data indicator 1	1	HARQ new data indicator for transport block 1.
	8	Redundancy version 1	2	HARQ redundancy version for transport block 1.
	8	MCS2	5	Modulation and coding scheme for transport block 2.
	8	New data indicator 2	1	HARQ new data indicator for transport block 2.
	8	Redundancy version 2	2	HARQ redundancy version for transport block 2.
	8	Precoding information	3 (2-antenna ports) 6 (4-antenna ports)	Precoding information.
	8	Downlink assignment index (TDD only)	2	For TDD configuration 0, this field is not used. For TDD configuration 1−6, this field is the downlink assignment index.

(*Continued*)

Table 9.22 (Continued)

DCI Format	Usage	Release	Information Fields	Size (Bits)	Description
Format 2A	PDSCH assignments for open-loop MIMO operation	10	Carrier indicator	0 or 3	Identifies the RF carrier to be used as the serving cell. A value of "0" implies the primary cell is used as the serving cell. This field only applies when carrier aggregation is enabled.
		8	Resource allocation header	0 or 1	Resource allocation header selects between resource allocation type 0 or type 1 (only exists if downlink bandwidth is greater than 10 RBs).
		8	Resource block allocation	6–25 variable	Resource block assignment/allocation (6, 8, 13, 17, 19, or 25 bits corresponding to 1.4, 3, 5, 10, 15, or 20 MHz system bandwidth).
		8	TPC command for PUCCH	2	PUCCH TPC command.
		8	HARQ process number	3 (FDD) 4 (TDD)	HARQ process number.
		8	Transport block to codeword swap flag	1	Defines the relationship between transport blocks 1 and 2 relative to codewords 0 and 1. If set to "0," codeword 0 is generated from transport block 1 and codeword 1 is generated from transport block 2.
		8	MCS1	5	Modulation and coding scheme for transport block 1.
		8	New data indicator 1	1	HARQ new data indicator for transport block 1.
		8	Redundancy version 1	2	HARQ redundancy version for transport block 1.
		8	MCS2	5	Modulation and coding scheme for transport block 2.
		8	New data indicator 2	1	HARQ new data indicator for transport block 2.

Petitioners' Exhibit 1021
Nokia of America Corp., et al. v. KT Corporation, et al.
Case No. IPR2025-00036; U.S. Patent No. 11,627,631
Page 593 of 1122

		8	Redundancy version 2	2	HARQ redundancy version for transport block 2.
		8	Precoding information	0 (2 antenna ports) 2 (4 antenna ports)	Precoding information.
		8	Downlink assignment index (TDD only)	2	For TDD configuration 0, this field is not used. For TDD configuration 1−6, this field is the downlink assignment index.
Format 2B	PDSCH assignments for dual-layer beamforming	10	Carrier indicator	0 or 3	Identifies the RF carrier to be used as the serving cell. A value of “0” implies the primary cell is used as the serving cell. This field only applies when carrier aggregation is enabled.
		10	SRS request (TDD only)	0 or 1	Instructs the UE to transmit SRS for uplink channel measurements.
		9	Resource allocation header	0 or 1	Resource allocation header selects between resource allocation type 0 or type 1 (only exists if downlink bandwidth is greater than 10 RBs).
		9	Resource block allocation	6−25 variable	Resource block assignment/allocation (6, 8, 13, 17, 19, or 25 bits corresponding to 1.4, 3, 5, 10, 15, or 20 MHz system bandwidth).
		9	TPC command for PUCCH	2	PUCCH TPC command.
		9	HARQ process number	3 (FDD) 4 (TDD)	HARQ process number.
		9	Scrambling ID	1	Scrambling identity provides support for MU-MIMO by allowing separate users to reuse the same antenna port with different SCIDs.
		9	MCS1	5	Modulation and coding scheme for transport block 1.

(*Continued*)

Petitioners' Exhibit 1021
Nokia of America Corp., et al. v. KT Corporation, et al.
Case No. IPR2025-00036; U.S. Patent No. 11,627,631
Page 594 of 1122

Table 9.22 (Continued)

DCI Format	Usage	Release	Information Fields	Size (Bits)	Description
		9	New data indicator 1	1	HARQ new data indicator for transport block 1.
		9	Redundancy version 1	2	HARQ redundancy version for transport block 1.
		9	MCS2	5	Modulation and coding scheme for transport block 2.
		9	New data indicator 2	1	HARQ new data indicator for transport block 2.
		9	Redundancy version 2	2	HARQ redundancy version for transport block 2.
		9	Downlink assignment index (TDD only)	2	For TDD configuration 0, this field is not used. For TDD configuration 1–6, this field is the downlink assignment index.
Format 2C	Signaling resource assignments for PDSCH for closed-loop single-user or multi-user MIMO with up to 8 layers	10	Carrier indicator	0 or 3	Identifies the RF carrier to be used as the serving cell. A value of "0" implies the primary cell is used as the serving cell. This field only applies when carrier aggregation is enabled.
		10	SRS request (TDD only)	0 or 1	Instructs the UE to transmit SRS for uplink channel measurements.
		10	Resource allocation header	0 or 1	Resource allocation header selects between resource allocation type 0 or type 1 (only exists if downlink bandwidth is greater than 10 RBs).
		10	Resource block allocation	6–25 variable	Resource block assignment/allocation (6, 8, 13, 17, 19, or 25 bits corresponding to 1.4, 3, 5, 10, 15, or 20 MHz system bandwidth).
		10	TPC command for PUCCH	2	PUCCH TPC command.

Petitioners' Exhibit 1021
Nokia of America Corp., et al. v. KT Corporation, et al.
Case No. IPR2025-00036; U.S. Patent No. 11,627,631
Page 595 of 1122

		10	HARQ process number	3 (FDD) 4 (TDD)	HARQ process number.
		10	Antenna ports, scrambling ID and layers	3	Provides a pointer to a look-up table where the UE can find the number of layers, antenna ports, and the SCID. Scrambling identity provides support for MU-MIMO by allowing separate users to reuse the same antenna port with different SCIDs.
		10	MCS1	5	Modulation and coding scheme for transport block 1.
		10	New data indicator 1	1	HARQ new data indicator for transport block 1.
		10	Redundancy version 1	2	HARQ redundancy version for transport block 1.
		10	MCS2	5	Modulation and coding scheme for transport block 2.
		10	New data indicator 2	1	HARQ new data indicator for transport block 2.
		10	Redundancy version 2	2	HARQ redundancy version for transport block 2.
		10	Downlink assignment index (TDD only)	2	For TDD configuration 0, this field is not used. For TDD configuration 1−6, this field is the downlink assignment index.
Format 3	Transmit power control (TPC) commands for multiple users and for PUCCH and PUSCH with 2-bit power adjustment	8	TPC commands	20−28 variable	TPC commands for PUCCH and PUSCH are distinguished based the RNTI that is used to scramble CRC (20, 22, 24, 26, 26, or 28 bits corresponding to 1.4, 3, 5, 10, 15, or 20 MHz system bandwidth).

(*Continued*)

Table 9.22 (Continued)

DCI Format	Usage	Release	Information Fields	Size (Bits)	Description
Format 3A	Transmit power control (TPC) commands for multiple users and for PUCCH and PUSCH with one-bit power adjustment	8	TPC commands	21–28 variable	TPC commands for PUCCH and PUSCH are distinguished based the RNTI that is used to scramble CRC (21, 22, 25, 27, 27, or 28 bits corresponding to 1.4, 3, 5, 10, 15, or 20 MHz system bandwidth).
Format 4	Signaling resource grants for PUSCH when the UE is configured in PUSCH transmission mode 2 for uplink single-user MIMO	10	Carrier indicator	0 or 3	Identifies the RF carrier to be used as the serving cell. A value of "0" implies the primary cell is used as the serving cell. This field only applies when carrier aggregation is enabled.
		10	Resource block allocation	6–25 variable	Resource block assignment/allocation (6, 7, 10, 12, 13, or 14 bits corresponding to 1.4, 3, 5, 10, 15, or 20 MHz system bandwidth).
		10	TPC Command for Scheduled PUSCH	2	Interpretation of this command depends on whether absolute or accumulated power control is used.
		10	Cyclic shift for DM-RS and OCC		Provides a pointer to a look-up table at the UE for generation of DM-RS and OCC.
		10	Downlink Assignment Index (TDD Only)	2	For TDD configuration 0, this field is not used. For TDD configuration 1–6, this field is the downlink assignment index.

Petitioners' Exhibit 1021
Nokia of America Corp., et al. v. KT Corporation, et al.
Case No. IPR2025-00036; U.S. Patent No. 11,627,631
Page 597 of 1122

	10	CSI request	1 or 2	Instructs the UE to send a CSI report. 2 bits are used when the UE is configured with more than one downlink cell; otherwise, 1 bit is used.
	10	SRS request	2	Instructs the UE to transmit SRS for uplink channel measurement and selects between SRS configurations
	10	Resource allocation type	1	Selects the type of uplink resource allocation (type 0 or type 1).
	10	Precoding information and number of layers	3 (2 Antenna Ports) 6 (4 Antenna Ports)	Provides a pointer to a look-up table at the UE to obtain the number of layers and transmitted PMI (TPMI).
	10	MCS1	5	Modulation and coding scheme for transport block 1.
	10	New data indicator 1	1	HARQ new data indicator for transport block 1.
	10	MCS2	5	Modulation and coding scheme for transport block 2.
	10	New data indicator 2	1	HARQ new data indicator for transport block 2.

Table 9.23 DCI Formats' Payload Sizes Including 16-bit CRC and Padding Bits [13,14]

DCI Format	FDD System Payload Size (Bits)						TDD System Payload Size (Bits)					
	1.4 MHz	3 MHz	5 MHz	10 MHz	15 MHz	20 MHz	1.4 MHz	3 MHz	5 MHz	10 MHz	15 MHz	20 MHz
Format 0	37	38	41	43	43	44	39	41	43	45	46	47
Format 1	35	39	43	47	49	55	38	43	46	50	52	58
Format 1A	37	38	41	43	43	44	39	41	43	45	46	47
Format 1B	38	41	43	44	45	46	41	43	45	47	49	49
Format 1C	24	26	28	29	30	31	24	26	28	29	30	31
Format 1D	38	41	43	44	45	46	41	43	45	47	49	49
Format 2	47	50	55	59	61	67	50	53	58	62	64	70
Format 2A	44	47	52	57	58	64	47	50	55	59	61	67
Format 2B	44	47	52	57	58	64	49	51	57	61	62	68
Format 2C	46	49	54	58	61	66	50	53	58	62	64	70
Format 3	37	38	41	43	43	44	37	38	41	43	43	44
Format 3A	37	38	41	43	43	44	37	38	41	43	43	44
Format 4	46	48	50	52	53	54	48	49	52	54	55	56

Petitioners' Exhibit 1021
Nokia of America Corp., et al. v. KT Corporation, et al.
Case No. IPR2025-00036; U.S. Patent No. 11,627,631
Page 599 of 1122

The common and UE-specific PDCCHs are mapped to CCEs differently where each type has a specific set of search spaces associated with it. Each search space consists of a group of consecutive CCEs which can be allocated to a PDCCH, known as PDCCH candidate. The CCE aggregation level is given by the PDCCH format and determines the number of PDCCH candidates in a search space. The number of candidates and size of the search space for each aggregation level is given in Table 9.24.

The UE is only informed of the number of OFDM symbols which construct the control region of a subframe, and is not provided with the location of its corresponding PDCCH(s). The UE finds its PDCCH by monitoring a set of PDCCH candidates in every subframe. This process is referred to as blind decoding. The UE unmasks each control candidate's CRC using its C-RNTI. If no CRC error is detected, the UE considers that it as a successful decoding attempt and reads the control information within the candidate PDCCH. The serving eNB determines a PDCCH format to be transmitted to the UE, creates an appropriate DCI and attaches a CRC. The CRC is then masked with an RNTI corresponding to a specific user or users. If the PDCCH is meant for a specific UE, the CRC will be masked with a unique UE identifier, e.g., a cell-RNTI (C-RNTI). If the PDCCH contains paging information, the CRC will be masked with a paging indication identifier, i.e., paging-RNTI (P-RNTI). If the PDCCH contains system information, a system information identifier, i.e., a system information-RNTI (SI-RNTI), will be used to mask the CRC.

With the possibilities of different RNTIs, PDCCH candidates, DCI and PDCCH formats, a significant number of attempts may be required to successfully decode the PDCCH. To overcome this complexity, the UE first tries to blindly decode the first CCE in the control channel candidate set of a subframe. If the blind decoding fails, the UE tries to blindly decode the first 2, 4, then 8 CCEs sequentially, where the starting location is fixed for a common search space and is given by a hash function for a UE-specific search space. The UE first tries to decode PDCCHs in the common search space before trying in the UE-specific search space. When searching the common search space, it iterates for only two

Table 9.24 PDCCH Candidates Monitored by a UE [5]

Search Space $S_k^{(L)}$			Number of PDCCH Candidates N_L	DCI Format
Type	Aggregation Level L	Size (Number of CCEs)		
UE-specific	1	6	6	0, 1/1A/1B/1D, 2/2A/2B/2C
	2	12	6	
	4	8	2	
	8	16	2	
Common	4	16	4	1, 1A, 1C, 3, 3A
	8	16	2	

Petitioners' Exhibit 1021
Nokia of America Corp., et al. v. KT Corporation, et al.
Case No. IPR2025-00036; U.S. Patent No. 11,627,631
Page 600 of 1122

aggregation levels, i.e., 4 and 8, and tries to decode all PDCCH candidates for all possible common search space DCI formats (see Table 9.24). The UE-specific search is carried out on four aggregation levels, i.e., 1, 2, 4, and 8. If no CRC error is detected during a decoding attempt, the UE considers it a successful decoding and reads the decoded DCI message.

A perfect PDCCH scheduler would be able to continuously allocate resources to each UE that is chosen by the downlink and uplink schedulers up to the point where all resources for the PDCCH, PDSCH, and PUSCH simultaneously become exhausted. However, because of the mechanism used for allocating PDCCH resources, it is possible that we can no longer allocate PDCCH resources to a UE even if such resources are available. In such cases, the corresponding UE is said to be blocked, while the eNB is still able to serve subsequent UEs. As more UEs are blocked, the performance of the scheduler decreases because such UEs cannot be served. Hence, the blocking probability, together with the utilization efficiency of bandwidth and power resources, are suitable metrics to measure the performance of the system. We assume that the number of PDCCH resources (i.e., CCEs) and total PDCCH power are known for each subframe. Multiple CCEs (1, 2, 4, or 8) can be aggregated to achieve different coding rates. The aggregation level required for a particular UE depends on the channel conditions of the UE, and the size of the scheduling grant that must be used for the UE. Each UE is allocated a candidate set of PDCCH channels for each possible aggregation level. The UE must then conduct blind decoding of each of these possibilities for each of the feasible message formats to determine if it was allocated PDSCH or PUSCH resources. The starting point for the candidate set for each aggregation level varies for each UE in each subframe. However, the new starting point is always known by the eNB and the UE. For each scheduled UE, the eNB must determine a suitable aggregation level, and then must use an unallocated channel from the corresponding candidate set to signal the location and format of the transmitted data.

Let us summarize some underlying definitions concerning search spaces before proceeding to more detailed descriptions.

- *Common search space*: A common search space consists of the common control information and is monitored by all UEs in a cell. The number of CCE aggregation levels supported by the common search space is limited to four and eight, compared to the UE-specific search space where four CCE aggregation levels are possible. This reduces the burden on the UE for decoding common control information compared to decoding UE-specific control information. The common search space is used to carry important initial information including paging information, system information, and random access procedures. When searching the common search space, the decoder always starts decoding from the first CCE. This restriction further simplifies the common search space design. The decoding is done on every possible PDCCH candidate set for a given PDCCH format until it successfully decodes the PDCCH which can be present in the common search space. All

Petitioners' Exhibit 1021
Nokia of America Corp., et al. v. KT Corporation, et al.
Case No. IPR2025-00036; U.S. Patent No. 11,627,631
Page 601 of 1122

UEs monitor the common search space, which may carry paging, RACH response, system information, and uplink TPC commands. The common search space always corresponds to CCEs 0−15, i.e., four decoding candidates on aggregation level 4 (CCEs 0−3, 4−7, 8−11, 12−15), and two decoding candidates on aggregation level 8 (CCEs 0−7, 8−15). The common search space can be used for any PDCCH signaling not restricted to common PDCCH, it can be used to resolve blocking, as well. The UE may attempt a maximum of 12 blind decodings on the common search space.

- *UE-specific search space*: The UE-specific search space carries control information specific to a particular UE and is monitored by at least one UE in a cell. Unlike the common search space, the starting location of the UE-specific search space may vary for each subframe or UE. The starting location of the UE-specific search space is determined in every subframe using a hash function. In the UE-specific search space, the UE finds its PDCCH by monitoring a set of PDCCH candidates (i.e., a set of consecutive CCEs on which the PDCCH could be mapped) in every subframe. If no CRC error is detected when the UE uses its RNTI (i.e., a 16-bit value also referred to as C-RNTI) to unmask the CRC on a PDCCH, the UE determines that the PDCCH carries its own control information. The PDCCH candidate sets correspond to different PDCCH formats. There are four PDCCH formats, i.e., 0, 1, 2, or 3. If the UE fails to decode any PDCCH candidates for a given PDCCH format, then it attempts to decode candidates for other PDCCH formats. This process is repeated for possible PDCCH formats until all designated PDCCHs that can be present in the UE-specific search space are successfully decoded. A PDCCH can be transmitted on an aggregation of one or several CCEs depending on the target reliability and channel conditions. Each PDCCH carries one DCI message. The UE performs blind decoding on the received CCEs, assuming all four different aggregations of CCEs (Figure 9.98). The UE-specific search space indicates the starting offset for blind decoding; different UEs may have different offsets.

In LTE/LTE-Advanced, each scheduling grant is defined based on fixed size CCEs. Four different CCE aggregation levels are defined for the transmission of a control channel (see Table 9.21). The eNB scheduler schedules the PDCCH that should be mapped to the CCE size by applying different coding rates. For example, if the LTE scheduler uses DCI Format 1A which has a length of 28 bits, then a 16-bit CRC is added to the 28 bit information element, resulting in 44 bits. The 44 bits can be mapped to different CCE sizes depending on the desired coding rate, as follows (see Table 9.21):

- PDCCH Format 0: (CCE size = 72 bits) 44 bits are converted to 72 bits using coding rate 44/72.
- PDCCH Format 1: (CCE size = 144 bits) 44 bits are converted to 144 bits using coding rate 44/144.

Petitioners' Exhibit 1021
Nokia of America Corp., et al. v. KT Corporation, et al.
Case No. IPR2025-00036; U.S. Patent No. 11,627,631
Page 602 of 1122

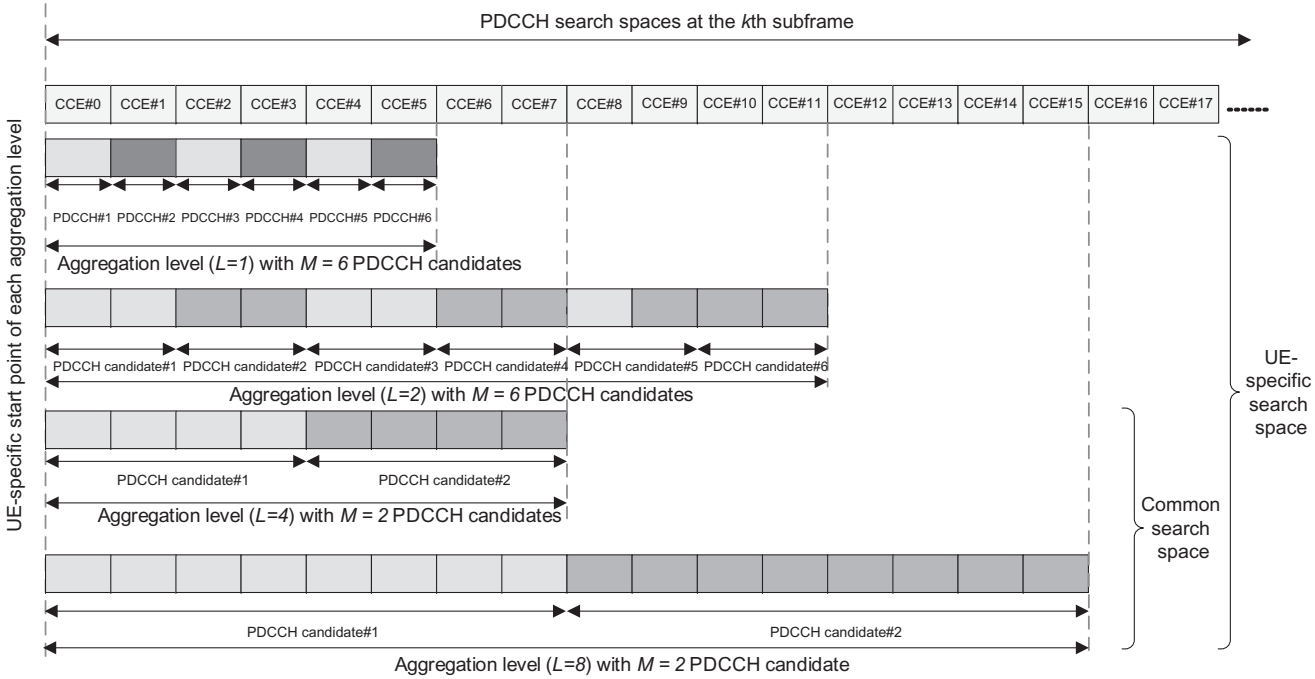


FIGURE 9.98

UE-specific/common search space (UE-specific search space starting offset is calculated based on RNTI) [15,162].

- PDCCH Format 2: (CCE size = 288 bits) 44 bits are converted to 288 bits using coding rate 44/288.
- PDCCH Format 3: (CCE size = 576 bits) 44 bits are converted to 576 bits using coding rate 44/576.

Note that the combination of PDCCH formats and CCE aggregation levels with coding rates greater than 3/4 is not supported. There are a maximum of 32 blind decoding attempts in the UE-specific search space. Assuming two payload sizes per aggregation level, the decoding attempts per payload size include six decoding attempts of 1-CCE aggregation, six decoding attempts of 2-CCE aggregation, two decoding attempts of 4-CCE aggregation, and two decoding attempts of 8-CCE aggregation. If the bandwidth is limited, then only some candidates may be available as the PDCCH region will be truncated. A PDCCH can be mapped to any candidate within its suitable search space as long as the allocated CCEs within the candidate do not overlap with a PDCCH already allocated.

The control region of each serving cell consists of a set of CCEs indexed from 0 to $N_{\mathrm{CCE}}^{k}-1$, where N_{CCE}^{k} denotes the total number of CCEs in the control region of the kth subframe. The UE monitors a set of PDCCH candidates on one or more activated serving cells configured for the UE for control information in every non-DRX subframe, where monitoring implies attempting to decode each of the PDCCHs in the set according to all the monitored DCI formats. The set of PDCCH candidates that a UE monitors are defined in terms of search spaces, where a search space S_k^L with aggregation level $L \in \{1, 2, 4, 8\}$ is defined by a set of PDCCH candidates. The starting point of the UE-specific search space to be monitored by the UE is determined through a hashing function.[20] For each serving cell on which the PDCCH is monitored, the starting point of the CCEs corresponding to the mth PDCCH candidate in search space S_k^L is given by $k' = [(Y_k + m') \mod \lfloor N_{\mathrm{CCE}}^{k}/L \rfloor]L + i$, where Y_k is defined as $Y_k = (AY_{k-1}) \mathrm{mod}\, D$ (i.e., the integer Y_k changes in each subframe, but it is deterministically determined from the value in the previous subframe) for the UE-specific search space S_k^L with aggregation level L or $Y_k = 0$ for common search space, and aggregation levels $L = 4$ or 8. In the latter equation $Y_{-1} = n_{\mathrm{RNTI}} \neq 0, A = 39827, D = 65537$, $k = \lfloor n_s/2 \rfloor$, and n_s is the slot number within a radio frame, and $i = 0, 1, \cdots, L-1$. For the UE-specific search space and the serving cell on which the PDCCH is monitored, if the monitoring UE is configured with a carrier indicator field (CIF), then $m' = m + M_L N_{\mathrm{CIF}}$, where N_{CIF} is the CIF value; otherwise $m' = m$, where $m = 0, 1, \ldots, M_L - 1$, and M_L is the number of PDCCH candidates to monitor in the given search space. In the case of common search space, it is assumed that

[20] A hash function is an algorithm that maps large data sets of variable length to smaller data sets of a fixed length. Hash functions are typically used to accelerate table lookup or data comparison tasks such as finding items in a database, detecting duplicates or similar records in a large file, etc. [31].

Petitioners' Exhibit 1021
Nokia of America Corp., et al. v. KT Corporation, et al.
Case No. IPR2025-00036; U.S. Patent No. 11,627,631
Page 604 of 1122